

ISTANBUL TECHNICAL UNIVERSITY ★ GRADUATE SCHOOL OF SCIENCE
ENGINEERING AND TECHNOLOGY

**DESIGN OF AN INTELLIGENT BOOST PRESSURE CONTROLLER
FOR A SERIES SEQUENTIAL TURBOCHARGED DIESEL ENGINE**

Ph.D. THESIS

Mustafa Engin EMEKLİ

Department of Mechanical Engineering

Mechanical Engineering Programme

JANUARY 2015

ISTANBUL TECHNICAL UNIVERSITY ★ GRADUATE SCHOOL OF SCIENCE
ENGINEERING AND TECHNOLOGY

**DESIGN OF AN INTELLIGENT BOOST PRESSURE CONTROLLER
FOR A SERIES SEQUENTIAL TURBOCHARGED DIESEL ENGINE**

Ph.D. THESIS

Mustafa Engin EMEKLİ
(503082030)

Department of Mechanical Engineering

Mechanical Engineering Programme

Thesis Advisor: Prof. Dr. Bilin AKSUN GÜVENÇ

JANUARY 2015

İSTANBUL TEKNİK ÜNİVERSİTESİ ★ FEN BİLİMLERİ ENSTİTÜSÜ

**SERİ BAĞLI AŞIRI DOLDURMA SİSTEMİNE SAHİP DİZEL MOTORLAR
İÇİN AKILLI MANİFOLD BASINCI KONTROLCÜSÜ TASARIMI**

DOKTORA TEZİ

**Mustafa Engin EMEKLİ
(503082030)**

Makina Mühendisliği Anabilim Dalı

Makina Mühendisliği Programı

Tez Danışmanı: Prof. Dr. Bilin AKSUN GÜVENÇ

OCAK 2015

Mustafa Engin Emekli, a Ph.D. student of ITU Graduate School of Science, Engineering and Technology student ID 503082030., successfully defended the dissertation entitled **”DESIGN OF AN INTELLIGENT BOOST PRESSURE CONTROLLER FOR A SERIES SEQUENTIAL TURBOCHARGED DIESEL ENGINE”**, which he/she prepared after fulfilling the requirements specified in the associated legislations, before the jury whose signatures are below.

Thesis Advisor : **Prof. Dr. Bilin AKSUN GÜVENÇ**
İstanbul Technical University

Jury Members : **Prof. Dr. Metin ERGENEMAN**
İstanbul Technical University

Prof. Dr. Levent GÜVENÇ
The Ohio State University

Assoc. Prof. Dr. Erdinç Altuğ
İstanbul Technical University

Asst. Prof. Dr. Erkin Dinçmen
Işık University

Date of Submission : 25 November 2014

Date of Defence : 06 January 2015

To my dear wife Betül and my lovely boy Aras,

FOREWORD

I wish to thank my advisor, Prof. Bilin Aksun Güvenç, for providing technical support throughout the course of this work.

Moreover, I would like to thank Prof. Metin Ergeneman and Prof. Levent Güvenç for accepting to be a member in thesis committee.

I would like to appreciate the support of entire colleagues from Ford Otosan, especially Didem Aydın during setting up the real time testing and Emre Özgül for providing technical support on WAVE RT models.

I would also like to thank Ford Otosan for providing support to my PhD thesis by supplying test engines, vehicles and engine dynamometer.

Finally, my thanks go to my parents and especially my dear wife whose support and encouragement made this thesis possible and completed.

January 2015

Mustafa Engin Emekli
(Mechanical Engineer)

TABLE OF CONTENTS

	<u>Page</u>
FOREWORD	ix
TABLE OF CONTENTS.....	xi
ABBREVIATIONS	xiii
LIST OF TABLES	xv
LIST OF FIGURES	xvii
SYMBOLS	xxi
SUMMARY	xxiii
ÖZET.....	xxvii
1. INTRODUCTION.....	1
1.1 Purpose of Thesis	2
1.2 Literature Review	4
1.3 Scope of the Thesis.....	10
2. DIESEL ENGINE AIR PATH	13
2.1 Main Components for Diesel Engine Air path.....	13
2.2 Supercharging the Diesel Engine	16
2.2.1 Basics of supercharging and turbocharging.....	17
2.2.2 Series Sequential turbocharging concept.....	25
3. ENGINE MODELING	27
3.1 System Layout.....	27
3.2 Nonlinear Engine Models	29
3.2.1 Mean value engine models (MVEM)	29
3.2.2 1D engine models	34
3.2.2.1 Ducts, flow splits/Junctions.....	37
3.2.2.2 Engine cylinders	39
3.2.2.3 Orifices, valves and actuators.....	39
3.2.2.4 Turbochargers (High/low pressure stages).....	41
3.3 1D Engine Model Calibration and Validation	45
3.3.1 Measurements	46
3.3.2 1D Model Calibration	49
3.3.3 Model validation.....	52
3.4 Control-Oriented Model	59
3.4.1 Prediction error based system identification	61
3.4.2 Subspace system identification	67
3.4.3 Application.....	70
3.4.3.1 SISO blackbox model	75
3.4.3.2 MIMO blackbox model.....	79
4. CONTROLLER DESIGN	85
4.1 MPC Concept.....	85
4.2 MPC Formulation.....	89
4.2.1 Predictive control with basic LTI model without MD	89

4.2.2 Predictive control with extended LTI model with MD and UD.....	100
4.3 Explicit MPC Formulation.....	103
4.4 Application.....	106
4.4.1 MIMO control design	106
4.4.1.1 Specification of signal properties	107
4.4.1.2 Control objectives	108
4.4.1.3 Specification of Prediction and Control horizons.....	110
4.4.1.4 Constraint definition	112
4.4.1.5 Controller Weights and Estimator tuning.....	114
4.4.1.6 Generation of polyhedral controller partitions for explicit MPC	117
4.4.2 SISO control design	119
4.4.2.1 Control objectives	120
4.4.2.2 Constraint definition	120
4.4.2.3 Controller Weights and Estimator tuning.....	120
4.4.2.4 Generation of polyhedral controller partitions for explicit MPC	121
5. SIMULATIONS	123
5.1 Offline Simulations with SISO Controller.....	124
5.1.1 Step Response Simulations with fixed engine speed.....	124
5.1.2 Simulations with mixed transient cycle in fixed engine speed	129
5.2 Offline Simulations with MIMO Controller	132
5.2.1 Step Response Simulations with fixed engine speed.....	132
5.2.2 Simulations in mixed transient cycle at fixed engine speed	137
6. REAL TIME TESTS.....	141
6.1 Vehicle Testing.....	141
6.2 Engine Dynamometer Testing.....	146
7. CONCLUSIONS	159
7.1 Conclusions.....	160
7.2 Recommendations	161
REFERENCES.....	163
APPENDICES.....	169
APPENDIX A: Nonlinear Engine model validation plots	170
APPENDIX B : Simulation results of SISO and MIMO MPC controllers	172
CURRICULUM VITAE	177

ABBREVIATIONS

API	: Application Programming Interface
BSR	: Blade Speed Ratio
CAC	: Charge Air Cooler
CBV	: Compressor Bypass Valve
CCP	: Can Calibration Protocol
ECU	: Engine Control Unit
EGR	: Exhaust Gas Recirculation
HP	: High Pressure
LP	: Low Pressure
LQG	: Linear Quadratic Gaussian
LTl	: Linear Time Invariant
MD	: Measured Disturbance
MIMO	: Multi Input Multi Output
MOESP	: Multivariable Output Error State Space Prediction
MPC	: Model Predictive Control
MV	: Manipulate Variable
MVEM	: Mean Value Engine Model
NEDC	: New European Drive Cycle
ODE	: Ordinary Differential Equations
PI	: Proportional-Integral
PID	: Proportional Integral-derivation
PM	: Particulate Matter
PRBS	: Pseudo Random Binary Sequence
SISO	: Single Input Single Output
SOC	: Start of Combustion
TBV	: Turbine Bypass Valve
WG	: Wastegate

LIST OF TABLES

	<u>Page</u>
Table 3.1 : Measurement signals from instrumentation and ECU.....	46
Table 3.2 : 1D engine model input data descriptions.....	50
Table 3.3 : Model identification candidate test points for local linear models	75
Table 3.4 : N4SID method and PEM accuracy.	78
Table 4.1 : Explicit MPC and Online computation optimization.	105
Table 4.2 : Specification of signal types.	107
Table 4.3 : Transient response time requirements for varying pressure steps.....	109
Table 4.4 : Control horizon and polyhedral regions.	118
Table 4.5 : Transient response requirements for varying pressure steps-SISO.....	120
Table 4.6 : Control horizon and polyhedral regions for SISO case.....	121

LIST OF FIGURES

	<u>Page</u>
Figure 1.1 : European exhaust emissions standards.	4
Figure 1.2 : Simulation results of CLF based robust nonlinear controller.....	5
Figure 1.3 : Nox and Smoke emissions results.	6
Figure 1.4 : Experimental results (green: Boost pressure setpoint, blue: control signal, red: actual boost pressure).	7
Figure 1.5 : HP turbine bypass vs. boost pressure for different VGT openings.	8
Figure 1.6 : Simulation results to step response.	10
Figure 2.1 : Diesel engine airpath layout	14
Figure 2.2 : CAC operation in Diesel engine	15
Figure 2.3 : Effect of EGR on NOx and PM emissions.	15
Figure 2.4 : Effect of supercharging in idealized engine process.....	19
Figure 2.5 : Effect of exhaust gas turbocharging in the idealized engine cycle.	20
Figure 2.6 : Basic exhaust gas turbocharger layout.....	21
Figure 2.7 : Typical compressor flow map	22
Figure 2.8 : Typical turbine map.	23
Figure 2.9 : Turbocharger matching	23
Figure 2.10 : Regulated two-stage turbocharger system layout	25
Figure 3.1 : Series Sequential turbocharged diesel engine layou	28
Figure 3.2 : Incompressible restriction tuning plot for air filter.	31
Figure 3.3 : Parametrization of HP compressor efficiency model.....	33
Figure 3.4 : Discretization of simple duct.....	35
Figure 3.5 : Representation of varying sub-volume length	36
Figure 3.6 : Discharge coefficients for orifice junction	39
Figure 3.7 : Compressor performance map and measured engine data (red dots: Measured engine data, blue contours: performance map).....	41
Figure 3.8 : Compressor performance map and measured engine data (black dots: Measured engine data, dashed contours: performance map).....	42
Figure 3.9 : Extrapolation of turbine efficiency vs. BSR.....	45
Figure 3.10 : Stationary measurement operating points.....	48
Figure 3.11 : Transient measurement operating points.....	49
Figure 3.12 : Engine core system parametrization overview.	51
Figure 3.13 : Duct-Junction-orifices parametrization overview.....	51
Figure 3.14 : LP/HP compressors parametrization overview.....	52
Figure 3.15 : LP/HP compressors parametrization overview.....	52
Figure 3.16 : Brake torque steady state validation result.	53
Figure 3.17 : Intake manifold pressure steady state validation result.	54
Figure 3.18 : Mass airflow steady state validation result.....	54
Figure 3.19 : LP compressor outlet temperature steady state validation result.....	55
Figure 3.20 : HP turbine inlet pressure steady state validation result.....	56
Figure 3.21 : Brake torque transient validation result.....	57

Figure 3.22 : Intake manifold pressure transient validation result.....	57
Figure 3.23 : HP turbocharger shaft speed transient validation result.	58
Figure 3.24 : LP turbocharger shaft speed transient validation result.....	58
Figure 3.25 : HP turbine outlet temperature transient validation result.	59
Figure 3.26 : Equation-error model family structure.	64
Figure 3.27 : LS method as Prediction error method.....	67
Figure 3.28 : System identification flow	72
Figure 3.29 : PRBS test signal generation.....	73
Figure 3.30 : Regions for local linear model across engine operating zone.....	74
Figure 3.31 : Offset removal of identification data.....	75
Figure 3.32 : SISO input signals for identification test in Region 4.....	76
Figure 3.33 : SISO model validation results for Region 4	77
Figure 3.34 : SISO input signals for identification test in Region 3.....	77
Figure 3.35 : SISO model validation results for Region 3	78
Figure 3.36 : Residual plots for N4SID and PEM methods used in Region 3	78
Figure 3.37 : Input signals for identification test in Region 4.....	79
Figure 3.38 : Input signals for identification test in Region 2.....	79
Figure 3.39 : Model validation results for Region 2.....	80
Figure 3.40 : Model validation results for Region 4.....	80
Figure 3.41 : Step response of Linear model 4 to a TBV step input.....	81
Figure 3.42 : Step response of Linear model 4 to a WG step input.....	82
Figure 3.43 : Bode magnitude and phase plots for linear model of region 4	82
Figure 3.44 : Pole zero mapping of linear model of region 4.....	83
Figure 4.1 : MPC strategy	86
Figure 4.2 : Main signals acting on the prediction model.	100
Figure 4.3 : Main signals acting on the prediction model.	103
Figure 4.4 : Transient response characteristics.....	108
Figure 4.5 : Effect of Prediction horizon tuning on controller operation.....	110
Figure 4.6 : Experiment to define control interval and Prediction horizon.....	111
Figure 4.7 : TBV and WG elektropneumatic actuator layout.	113
Figure 4.8 : Experiment for TBV rate constraint definition.....	114
Figure 4.9 : Effect of Output and input weights on controller response.	115
Figure 4.10 : Effect of Kalman gain matrix on disturbance rejection.....	117
Figure 4.11 : Effect of Kalman Gain matrix on Controller activity.....	117
Figure 4.12 : Polyhedral partition for region 1	119
Figure 4.13 : Polyhedral partition for region 3	119
Figure 4.14 : Effect of Output and input weights on SISO controller response.	121
Figure 4.15 : Polyhedral partition for region 1 in SISO case	122
Figure 4.16 : Polyhedral partition for region 3 in SISO case	122
Figure 5.1 : Overview of MATLAB-SIMULINK simulation model	123
Figure 5.2 : SISO small step response at 1500 rpm.....	125
Figure 5.3 : SISO medium step response at 1500 rpm.....	125
Figure 5.4 : SISO disturbance rejection with medium step setpoint applied at 1500 rpm.....	126
Figure 5.5 : SISO large step response at 1500 rpm.....	127
Figure 5.6 : SISO medium step response at 2000 rpm.....	128
Figure 5.7 : SISO large step response at 2000 rpm with injection disturbance.....	128
Figure 5.8 : SISO large step simulation at 2500 rpm with injection disturbance..	129
Figure 5.9 : Effect of Kalman filter gain on mixed transient cycle simulation at 1500 rpm.	130

Figure 5.10 : Effect of Prediction horizon on mixed transient cycle simulation at 1500 rpm.....	131
Figure 5.11 : Mixed transient simulation at 1500 rpm	131
Figure 5.12 : Large step simulation performed at 1500 rpm with MIMO controller	132
Figure 5.13 : Small step simulation performed at 1500 rpm with MIMO controller	133
Figure 5.14 : Comparison of MIMO MPC with WG control and WG fully closed setting	134
Figure 5.15 : Large step simulation performed at 2500 rpm with MISO controller	135
Figure 5.16 : Medium step simulation performed at 2000 rpm with MIMO control	136
Figure 5.17 : Medium step simulation performed at 2500 rpm.....	137
Figure 5.18 : Fine tuning of Kalman gain for MIMO controller at 1500 rpm.	138
Figure 5.19 : MIMO simulation performed at 2500 rpm.....	139
Figure 5.20 : MIMO simulation performed at 2500 rpm.....	140
Figure 6.1 : Vehicle testing setup	142
Figure 6.2 : On Road vehicle testing results	142
Figure 6.3 : On Road Vehicle Testing-Zoom.....	143
Figure 6.4 : On-Road test results-controller operation	144
Figure 6.5 : HP Compressor operation during On-Road vehicle testing	145
Figure 6.6 : HP Compressor operation during On-Road vehicle testing	145
Figure 6.7 : Engine Dynamometer test setup	146
Figure 6.8 : Transient test points	147
Figure 6.9 : Test results at 1800 rpm from %0 to %50.....	148
Figure 6.10 : Test results at 1800 rpm from %0 to %50-Actuator operation.....	148
Figure 6.11 : HP compressor map trace at 1800 rpm %0 to %50 load.....	149
Figure 6.12 : Test results at 2200 rpm from %0 load to %70 load.....	150
Figure 6.13 : Test results at 2200 rpm from %0 load to %70 load-actuator operation	151
Figure 6.14 : Boost pressure deviation distribution for 2200 rpm %0 to %70 testing	151
Figure 6.15 : Test results at 2200 rpm from %0 to %50 load.	152
Figure 6.16 : HP compressor map trace at 2200 rpm %0 to %50 load.....	152
Figure 6.17 : LP compressor map trace at 2200 rpm %0 to %50 load.....	153
Figure 6.18 : Sweep test (1000-2200 rpm) test results	154
Figure 6.19 : Sweep test (1000-2200) rpm detailed test results	154
Figure 6.20 : HP compressor map trace for sweep test(1000-2200 rpm)	155
Figure 6.21 : Sweep test 2 (1500-2500 rpm) test results	155
Figure 6.22 : Sweep test 2 (1500-2500 rpm) detailed test results	156
Figure 6.23 : HP compressor outlet temperature and LP turbine outlet temperatures at sweep test 1	157
Figure A.1 : HP compressor inlet pressure	170
Figure A.2 : LP turbine inlet Pressure	170
Figure A.3 : LP turbine outlet pressure.....	171
Figure A.4 : HP compressor outlet temperature.....	171
Figure B.1 : SISO medium step response at 2500 rpm.....	172
Figure B.2 : SISO small step response at 2500 rpm	172
Figure B.3 : MIMO small step response at 1500 rpm	173

Figure B.4 : MIMO small step response at 2500 rpm.....	174
Figure B.5 : MIMO small step response at 2000 rpm.....	175

SYMBOLS

P	Pressure (Pa)
ρ	Density (kg/m^3)
u_i	Mean axial velocity (m/s)
h	Specific enthalpy (J/kg)
τ_{ij}	Viscous wall stress (N/m^2)
Q_i	Heat Flux ($\text{J/m}^2\text{s}$)
\dot{Q}	External heat source (J/kgK)
\dot{W}_{ext}	Rate of change external work (J/s)
W	Work (J)
e	Internal energy (J/kg)
dx	Discrete control volume length (m)
B	Cylinder bore diameter (m)
C_f	Friction coefficient
Re	Reynolds number
ϵ	surface roughness
D	Pipe diameter (m)
Pr	Prandtl number
c_p	Specific heat at constant pressure (J/kgK)
c_v	Specific heat at constant volume (J/kgK)
u_{hpt}	Control signal (%)
A	Effective area of valves (m^2)
η	Efficiency
μ	Viscosity
ϕ	Fuel/Air equivalence ratio
k	Spring constant (N/m)
m	mass (kg)
ω	Rotational speed (rad/s)
q	Forward shift operator
n	Rotational speed (rpm)
\dot{m}_{fuel}	Fueling rate (l/h)
$x(t)$	State variable
$y(t)$	Output variable
$v(t)$	Measured disturbance variable
$d(t)$	Unmeasured disturbance variable
$e(t)$	Prediction error variable
T	Temperature (K)
λ	Air/fuel ratio
V	Volume (m^3)
\dot{m}	Mass Air flowrate (kg/s)
R	Specific gas constant (J/kgK)
θ_{soi}	Starting crank angle of injection ($^\circ$)

DESIGN OF AN INTELLIGENT BOOST PRESSURE CONTROLLER FOR A SERIES SEQUENTIAL TURBOCHARGED DIESEL ENGINE

SUMMARY

As a subsystem of automotive control field, engine control has evolved as one of the key research areas in control applications. Due to having highly nonlinear behaviour, relatively fast system dynamics and variety of constraints (emissions, Hardware limitations, performance requirements), engine controls softwares includes vast amounts calibrateable map and curves. Current methods in engine controls are mainly employing conventional PID-PI schemes with additional map based feedforward compensation with anti windup controllers.

With the increasing complexity of the engine control systems resulting from stringent emissions and customer performance requirements, control problem is becoming multi-dimensional and multi-variable. Moreover, as the system complexity increases, hardware limitations and constraints are increased proportionally.

Today, state of the art diesel engine airpath control is basically consists of two controller loops. First loop is controlling the amount of total air for EGR operation and the second loop is controlling the Boost pressure for performance requirement and efficient combustion. Main actuators for MAF control are intake throttle and low/high pressure EGR valve where for Boost pressure control Variable Nozzle Turbocharger(VNT) and Wastegate valves.

The term two-stage turbocharging described by system which involves 2 turbocharger units connected in series. This layout has several advantages.

- Higher boost pressure levels resulting in high mean effective pressures.
- Increased charging efficiency
- Higher engine out temperatures
- Better low-end torque

Below are the drawbacks of two-stage turbocharged system.

- Increased turbolag as two rotors needs to be accelerated
- Higher thermal inertia
- Bigger hardware package

Control and regulation of two stage system increases the effectiveness of turbocharger operation and results in wider flow range. The Boost level can be controlled via regulation of exhaust energy utilized by two stage turbines, using

actuators such as a Turbine Bypass Valve (TBV), wastegate (WG) or VNT. Two stage turbocharger system sometimes called as series sequential turbocharger system. As being one of the key elements of diesel engine airpath as well as multivariable control capability makes the two-stage turbocharged diesel engine control a challenging control application. Standard industrial boost pressure controllers for two-stage turbocharged diesel engine control employs gain-scheduled PI-PID controllers with boost pressure feedback. There are more than 500 parameters to be tuned which requires high level of engine dynamometer and vehicle testing. In addition, over-boost and under boost capability of the system should be considered separately by calibrating rate limitation or by means changing boost pressure setpoints.

In this thesis the main focus is to design an intelligent boost pressure controller which would reduce the time required to calibrate controllers as well as incorporating system pressure limits explicitly. Model predictive control stands as a candidate controller algorithm in terms of constrained optimal control formulation enables to handle input, output and state constraints via a online computation of optimal input trajectories. Big drawback of this method is the computational effort required. Explicit MPC method is based on the replacement of the online optimization with offline calculations with apriori knowloedge about system states, input and outputs. Quadratic cost function in optimal control formulation can be analyzed as a multi-parametric quadratic programme.

Modeling of the two-stage turbocharger system is a key milestone to achieve satisfactory control design. During this study, two-stage turbocharged system has been modeled in terms of nonlinear and linear models. Nonlinear model is used to simulate controller performance offline. Nonlinear model has been chosen as 1D model which incorporates 1-dimensional fluid flow across engine ducts. 1D engine model has been modeled in WAVE and then converted into MATLAB-SIMULINK environment by means of WAVE RT module. 1D engine offers several advantages over mean value engine models in terms of reduced parametrization, therefore data requirements. Linear model has been used to model system linear response to be used as a prediction model in MPC formulation. As nonlinear model includes complex fluid dynamics compared to mean value engine models, linearization would not be feasible. Therefore parameter identification methods has been used to derive linear models. It would not be feasible to define one local model for entire engine operating region, therefore engine operating region has been divided into 7 main sub-regions which have individual local linear models. The input-output data has been recorded during real-time engine dynamometer testing and post-processed in MATLAB-SIMULINK. The PEM and N4SID methods offered best fits and been used a black-box models.

Controller design has been performed separately for each of the local linear regions. Controller design has been performed by introducing Kalman filter, Prediction-Control horizon tuning as well as constraint and weighting definitions. Explicit MPC formulation has been calculated by using MATLAB Hybrid Toolbox offline. Two controllers has been designed. SISO controller employs TBV only control action in which WG is always set as zero. Whereas MIMO controller utilizes both TBV and WG. Controller objective are defines based on the experience in industrial boost pressure controller sign off criteria. Offline simulations are performed in MATLAB-

SIMULINK environment with the WAVE RT nonlinear model. 2 simulation sets are defined with mixed transient cycles and simulations at fixed engine speed with small-medium and large boost pressure setpoint applied. Simulation results shows that overall response of the system satisfied controller objective in terms of both overshoot and rise time. In addition MIMO and SISO controller shows close performance where in MIMO controller optimal control action is mostly calculated as fully closed.

As controllers are validated with offline simulations by using high fidelity nonlinear engine model, final validation has been performed by a series of in-vehicle and engine dynamometer testing. 2 different methods have been used for controller implementation. In vehicle testing has both been performed random testing on road for subjective evaluation as well as testing on chassis dynamometer. Test results shows that controller setpoint tracking performance is satisfactory. During the testing, compressor and turbine operation is observed to be inside hardware limits. Chassis dynamometer testing includes the replication of customer cycles and NEDC to compare conventional PID based controller and MPC performance. MPC performance shows close at some points even better against PIDs. Statistical analysis of boost deviation is also smaller in MPC operation compared to PIDs. Engine dynamometer testing consists of step response tests a fixed engine speed where load is changing. MPC performance satisfies the controller objectives in terms of rise time and overshoot.

During this study MPC proves to be succesfull candidate to replace conventional PID in terms of multivariable control capability and constraint handling. On the other hand it should be noted that MPC performance is strongly affected by prediction model accuracy. Further study, shall contain the inclusion of mean value 0D engine model with compressor speed estimation as well as effect of EGR operation.

SERİ BAĞLI AŞIRI DOLDURMA SİSTEMİNE SAHİP DİZEL MOTORLAR İÇİN AKILLI MANİFOLD BASINCI KONTROLCÜSÜ TASARIMI

ÖZET

Otomotiv kontrolü uygulamaları içerisinde içten yanmalı motorların kontrolü önemli bir araştırma ve geliştirme konusu olarak yer etmiştir. İçten yanmalı motorların yüksek düzeyde doğrusal olmayan davranış göstermesi, göreceli olarak daha hızlı bir sistem dinamiğine sahip olması ve sistem-donanım kısıtlarının (Emisyon, donanım-parça limitleri, performans gereklilikleri) çok çeşitli biçimlerde olmasından dolayı, motor kontrolü uygulamalarında Elektronik kontrol ünitesi yazılımında bir çok kalibrasyon parametresine ihtiyaç duyulmaktadır. Bu parametreler iki boyutlu- bir boyutlu tablolar veya sabitler şeklinde Elektronik kontrol ünitesi yazılımında mevcuttur. Endüstriyel anlamda kullanılan motor kontrolcülerinin genellikle PID-PI yapısında olmakta olup, kontrolcü saturasyonunu önleyici anti-windup ve ileribesleme kontrolcü yapıları ile beraber kullanılabilmektedir.

Günümüzde emisyon seviyelerinin artışı ve müşterilerin performans- yakıt tüketimi beklentileri, içten yanmalı motorların kontrolündeki kısıtları arttırmış ve motor kontrol problemi genel olarak daha çok boyutlu ve daha çok değişkenli bir hale gelmiştir. Buna ek olarak, sistemlerin karmaşıklığı arttıkça, donanım-parça kısıtları ve limitleri de doğru orantılı olarak artmıştır.

Günümüzde, modern dizel motorlarında kontrol çevrimleri temel olarak iki alt sistem üzerinden değerlendirilebilir. Dizel yanma çevrimine göre silindir içine püskürtülen yakıtın basıncı ve miktarının kontrolü yakıt hattının kontrol sisteminin temel görevini oluşturur. Common-Rail sistemlerdeki, ray basıncı geri beslemesi ile Elektronik kontrol ünitesi tarafından motorun çalışma koşullarına göre belirlenen ray basıncı kontrolü sağlanır. Yakıt sisteminden farklı olarak diğer temel kontrol çevrimi de silindir içine giren havanın miktarının ve basıncının kontrolüdür. Bu çevrim de kendi içerisinde iki temel kontrol çevrimine ayrılır. Birincisi, hava debisinin Egzoz Gazı geridönüşüm sistemi ve hava hattı giriş gaz keleşi ile kontrolüdür. Egzoz gazı geri çevrimi ile amaçlanan silindir içi yanma sonu sıcaklıklarının düşürölüp, Nox emisyonlarının azaltılmasıdır. Hava hattındaki bir diğer kontrol çevrimi ise hava basıncının kontrolüdür. Dizel motorlar atmosferik basınçlı olarak da çalışabileceğı gibi, günümüzde yüksek hızlı modern dizel motorları basınçlandırılmış emiş havası ile çalışmaktadır. Bu şartlandırma ise temel olarak aşırı doldurma üniteleri kullanılarak sağlanmaktadır. Aşırı doldurma üniteleri genel olarak egzoz gazı tahrikli veya mekanik tahrikli olarak iki temel tipte kullanılmaktadır.

Egzoz gazı tahrikli aşırı doldurma ünitelerinde manifold basıncı kontrolü, değişken geometrili türbinler kullanılarak veya atık havası tahliye valfleri kullanılarak sağlanmaktadır.

Seri bağılı aşırı doldurma sistemleri; birbiri ardınca bağlanmış iki farklı egzoz gazı tahrikli kompresör-türbin ünitelerinden oluşan aşırı doldurma sistemleri anlamına gelmektedir. Bu tip sistemlerin sahip olduğu avantajlar aşağıda sıralanmıştır.

- Yüksek aşırı doldurma basınçlarından kaynaklanan yüksek silindir içi ortalama efektif basınçlar
- Daha yüksek toplam aşırı doldurma verimi
- Daha yüksek silindir çıkışı-yanma sonun sıcaklıkları
- Düzeltilmiş düşük-yük tepkisi

Öte yandan bu sistemin sahip olduğu bazı dezavantajlar da aşağıda listelenmiştir.

- Turbo gecikmesindeki artış. (Bunun nedeni iki farklı aşırı doldurma sisteminin ivmelendirilmesidir.)
- Daha yüksek ısı sığası.
- Daha büyük paketleme ve mekanik tasarım kısıtları

Yukarıdaki dezavantajların büyük kısmı, Seri bağılı aşırı doldurma sisteminin kontrolü ve regülasyonu ile önemli ölçüde düzeltilmektedir. Böylelikle, daha yüksek motor hava debisi aralığında sistemin efektif çalışması sağlanmaktadır. Bu tip sistemlerde manifold basıncı kontrolü, iki ayrı türbine paralel olarak bağılı bypass ve atık havası tahliye valfleri ile sağlanabilir. Bazı sistemlerde, türbinlerden bir tanes değişken geometriye de sahip olabilir. Seri bağılı aşırı doldurma sistemleri, iki kademelei aşırı doldurma sistemleri olarak da isimlendirilmektedir. Dizel motorlarda hava hattının önemli bir alt sistemi olmasının yanı sıra, çok değişkenli kontrol imkanı ve iki kademeli aşır doldurma sistemleri motor kontrol uygulamaları için örnek bir uygulama haline getirmektedir. İki kademeli aşırı doldurma sistemlerinde mevcut endüstriyel kontrolcüler, kazanç- değişimli genişletilmiş PID-PI kontrolcü yapısına sahiptir. Bu tip kontrolcülere ait yazılım, elektronik kontrol ünitesinde 500'den fazla parametre ile uygulamaya dönüştürülmektedir. Tüm bu parametrelerin kalibrasyonu için motor dinamometresi ve araç testleri gerçekleştirilmektedir. Bunlara ek olarak, Sistem limitleri ve kısıtları için ayrıca testler yapılmaktadır.

Bu tez kapsamında gerçekleştirilen çalışmanın kapsamı; sistem basınç limitlerini ve parça kısıtlarını tasarım sırasında içeren ve daha hızlı bir şekilde kalibre edilebilen manifold basınç kontrolcüsü tasarımı ve uygulaması gerçekleştirmektir. Bu amaçla yapılan literatür araştırması sonucunda, Model tahmini kontrolcü (MPC) yapısı kullanılacak kontrolcülerin ana yapısı olacak şekilde seçilmiştir. Kısıtlı optimal kontrol yapısının kullanılması, giriş- çıkış kısıtlarının tasarım sırasında hesaba katılması ve çevrimiçi optimizasyon gibi noktalar MPC yapısının seçilmesindeki temel ölçütler olarak belirlenmiştir. Tüm bu noktalara rağmen, MPC kontrol algoritmasının temel kısıtı, çevrimiçi optimizasyon için gereken mikroişlemci gücüdür. Bu kısıtı ortadan kaldırmak için, explicit MPC metodu uygulanmıştır. Böylelikle, belirli bir aralıkta çevrimdışı olarak belirlenen kontrolcü katsayıları, kontrolcünün gerçek zamanlı çalışması sırasında doğrudan sisteme uygulanmış ve çevrimiçi optimizasyon sırasına gereken mikroişlemci gücünden tasarruf sağlanmıştır.

Kontrolcü tasarımından önceki temel aşama olarak sistem modelleme aşaması belirlenmiştir. Bu çalışmada, iki kademeli aşırı doldurma sistemi doğrusal ve doğrusal olmayan model olarak iki farklı biçimde modellenmiştir. Doğrusal olmayan modelin temel kullanım amacı, kontrolcü performansını çevrimdışı simülasyonlarda test etmektir. Bu nedenle gerçek motora mümkün olduğunca yakın sonuçlar vermesi

için, doğrusal olmayan motor modellenmesi sırasında bir boyutlu gaz dinamiği bazlı modeller tercih edilmiştir. Dizel motorlarda meydana gelen termodinamik ve kinetik prosesler milisaniyeler mertebesinde tamamlanmaktadır. Akışkan hareketinin mikroskobik yapısı ve türbülansından dolayı, motorun çevrimleri arasında değişkenlik kaçınılmazdır. Gerçekte, motordaki akışkan hareketi, ortalama değer modellerindeki gibi sabit değil, darbeli bir karakteristik gösterir. Bu tip darbeli akışın modellenmesi, motor modelinin simülasyon ortamında gerçek motora çok yakın bir davranış göstermesini sağlar. Bir boyutlu modelleme metodolojisindeki boyut kavramı, akışkanın hareketinin temsil edildiği boyutu ifade eder. Bu modelleme metodunda, akışkan hareketi bir boyutlu, boyuna veya eksenel yönde ifade edilmektedir. Akış alanı içerisinde birden fazla durum değişkeni için kütle ve enerjinin korunumu denklemlerinin çözülmesi ile akış alanı hakkında daha detaylı bir bilgiye erişilmektedir. Bu çalışmada bir boyutlu motor modeli, WAVE paket programında gerçekleştirilmiş ve WAVE RT yardımı ile MATLAB-SIMULINK ortamına aktarılmıştır. Doğrusal olmayan motor modelinin doğrulanması ise, sürekli rejim ve geçici rejim test verilerine göre gerçekleştirilmiştir. Doğrulanma sonuçlarında birçok temel fiziksel değişkenler maksimum %10 hata görülmüştür. Bu hassasiyet seviyesi motor modelinin kontrol uygulamalarında kullanılabileceğini doğrulamıştır. Doğrusal model ise iki kademeli aşırı doldurma sisteminin doğrusal tepkisini veren bir model olarak, MPC tasarımında tahmin modeli olarak kullanılmıştır. Yukarıda bahsedilen bir boyutlu gaz dinamiğine göre modellenmiş motor modelinin doğrusallaştırılması mümkün olmadığı için, doğrusal modelin oluşturulmasında sistem tanıma metodolojisi kullanılmıştır. Yapılan çalışmalarda motorun tüm çalışma bölgesinde tek bir doğrusal modelin yeterli miktarda hassasiyete sahip olmadığı görülmüştür. Bu nedenle, motorun çalışma bölgesi temel olarak 7 farklı bölgeye ayrılmış ve her bölge ayrı bir lokal doğrusal model oluşturulmuştur. Sistem tanıma işlemi gereken giriş-çıkış testleri ve verileri, motor dinamometresinde gerçekleştirilmiştir. Alınan bu veriye göre N4SID ve PEM metodlarına göre oluşturulan modeller, nonlinear sisteme yakın sonuçlar vermiştir.

Kontrolcü tasarımı her bir lokal doğrusal bölge için ayrı ayrı gerçekleştirilmiştir. Kontrolcü tasarımında temel olarak dikkat edilen noktalar, Kalman filtresi tasarımı ve kalibre edilmesi, Tahmin ve kontrol ufukları ve Sistem kısıtları ile ağırlandırmasının yapılmasıdır. Explicit MPC'e ait kontrolcü kurallara ve formülasyonu Hybrid Toolbox kullanılarak MATLAB-SIMULINK ortamında gerçekleştirilmiştir. Kontrolcü tasarımında iki adet kontrolcü tasarlanmıştır. İlki, sadece TBV valfi ile kontrolün sağlandığı ve WG valfinin sürekli kapalı olduğu ve kontrol edilmediği tek giriş ve tek çıkışlı (SISO) kontrolcü. İkinci kontrolcü ise, TBV ve WG'in ikisini de giriş olarak hesaba katan çok-giriş- çok çıkışlı MIMO kontrolcü. Kontrolcülerin testleri sırasındaki performans metrikleri olarak, endüstriyel manifold basıncı kontrolcülerinde kullanılan ölçütler kullanılmıştır. Çevrimdışı benzetimler, MATLAB-SIMULINK ortamında gerçekleştirilmiş ve yukarıda bahsedilen doğrusal olmayan motor modeli kullanılmıştır. Simülasyonlar sırasında 2 farklı veri kümesi kullanılmıştır. İlk kümede, sabit motor hızında yüke verilen basamak sinyallerinde kontrolcünün tepkisi ölçülmüştür. İkinci benzetim kümesinde, birçok basamak ve rampa sinyalini içinde barındıran karışık dinamik test çevrimleri kullanılmıştır. Yapılan benzetim sonuçlarında, gerek maksimum aşım gerekse tırmanma zamanı olarak, performans metriklerinin üzerinde sonuçlar alınmıştır. Ayrıca benzetim sonuçlarında bir diğer önemli nokta da, MIMO ve SISO kontrolcülerin birbirine yakın sonuçlar vermesidir. Bunun sebebi, MIMO kontrolcünün optimal WG çıkışını genellikle tamamen kapalı olarak hesaplamasıdır.

Kontrolcülerin çevrimdışı doğrulanmasından sonra, son doğrulanma gerçek araç ve motor üzerinde yapılan testler ile icra edilmiştir. Araç testleri ile motor dinamometresinde yapılan testlerde farklı metodlar kullanılmıştır. Ancak her iki metodta da hesaplanan kontrol sinyalleri doğrudan ECU tarafından iletilmiştir. Araç testleri daha çok subjektif değerlendirme amacıyla kullanılmıştır. Yapılan testlerde kontrolcülerin referans takibi yeterli olarak gözlemlenmiştir. Testler sırasında, kompresör ve türbinlerin çalışması gerek sıcaklık gerekse de hızlar açısından limitlerin içerisinde. Şasi dinamometresinde ve motor dinamometresinde yapılan testlerde ise tekrarlanabilirlik yüksek olduğu için MPC'nin performansı, endüstriyel kontrolcüler ile karşılaştırılmıştır. Test sonuçlarında, MPC'nin genellikle PID'ye yakın, bazı noktalarda ise daha iyi bir referans takibi performansı gösterdiği gözlemlenmiştir. Bununla birlikte, istatistiksel olarak MPC daha düşük bir manifold basıncı sapması göstermiştir.

Bu çalışmada alınan sonuçlarda, MPC'nin çok değişkenli kontrol ve sistem kısıtlarını içermesi bakımından, iki kademeli aşırı doldurma sistemi basınç kontrolcüsü olarak endüstriyel PID'lerin yerini alabilecek alternatif bir kontrolcü olduğu gösterilmiştir. Öte yandan MPC'nin hassasiyetinin doğrudan kullanılan modellere bağlı olduğu unutulmamalıdır. Bu nedenle ileriki çalışmalarda, fiziksel bir model kullanarak daha fazla sistem kısıtı ve EGR sisteminin modele dahil edilmesinin kontrolcü tasarımındaki etkileri değerlendirilecektir.

1. INTRODUCTION

Customer performance and fuel economy requirements as well as environmental concerns (reduction of gaseous and particulate emissions, CO₂) lead progressive development in the field of Automotive Control. Although the challenges are valid for most of the subsystems, powertrain control is emerged thanks to high nonlinear behavior, fast system dynamics and complexity. Stringent emissions legislations requires extensive control loops with more sensors and actuators added. This phenomena makes the control problem multi-dimensional and multi-variable.

Diesel engine management consists of controlling of fuel, air and exhaust paths. Coordinated control of fuel and air path results in efficient diesel combustion. The amount of fresh inside cylinders is controlled by boost pressure . Increased boost leads to increased air density therefore higher mean effective pressure which increases power output from the engine. Supercharging increases the amount of boost by employing exhaust-gas turbochargers and/or mechanical supercharging units. Modern diesel engines use exhaust gas supercharging (turbocharging) for better utilization of exhaust energy. This results in high power densities with better fuel consumption and emissions. Turbocharging by single stage charging may be effective but the increased power density demand with stringent EU6 emissions requirements limits results in further research in the field of alternative boosting methods. Two stage turbocharging is achieved by introducing two compressor turbine units connected in series. The advantages of two stage turbocharging are excessive boost pressures and, thus, mean effective pressures, improved charging efficiency, wider compressor maps in adaptation of engine operating points.

Considering the system complexity; control design and application is becoming critical to achieve desired performance targets. Standard industrial control mainly employs gain-scheduled PI-PID controllers for boost pressure control. This requires high effort in terms of calibration of the controller maps and validation of the system behavior.

Hardware limitations (i.e. turbocharger speeds) and system constraints (over boost capability) should be considered individually in map based control systems. These limitations are calibrated as set point limitations by performing numerous steady state and transient engine dyno tests. In two stage turbocharged engine applications, additional hardware constraints and system states make conventional control even harder and more complex. In order to increase controller performance and decrease the effort required for design, intelligent control design schemes shall be used.

Although its performance has been proven in the process industry in the early 90s, MPC has recently re-gained interest in the automotive controls community. Model Predictive Control is widely accepted design tool for process control engineer in early 80's. Due to computation availability at that era, MPC is only applicable to process industry where low sampling rates are sufficient. In addition, MPC was more successful for systems with slow dynamics such as Petrochemical industry. As the Electronic Control Unit (ECU) computation capacity is increased recently, it has become more attractive to Automotive control community. Its ability to handle multivariable control and its ease of tuning make the MPC method attractive for automotive control. With the growing computational capacity of microprocessors and ECUs, MPC has become suitable for high-sample rate applications such as internal combustion engine control. In addition, explicit MPC method is based on the replacement of the online optimization with offline calculations with prior knowledge about system states, input and outputs. Quadratic cost function in optimal control formulation can be analyzed as a multi-parametric quadratic program..

1.1 Purpose of Thesis

The main objective of this research is to design an intelligent and optimal boost pressure controller that would satisfy industrial boost pressure controller objectives for two stage turbocharged diesel engine employing two separate fixed geometry turbochargers. The research processes and specific objectives were listed below;

1. Model 2.0L EU6 two-stage turbocharged diesel engine by using RICARDO-WAVE high fidelity non-linear engine model according to 1D gas dynamics

- a. Conduct steady state engine dynamometer testing
 - b. Conduct transient engine dynamometer testing
2. Develop control-oriented model by using system identification methods supporting multiple operating zones in entire engine operation region
3. Define system-hardware constraints by a series of dynamometer testing
4. Design Model predictive controller both for SISO and MIMO configurations.
5. Define multi-parametric programming rule for Explicit MPC controller.
6. Conduct controller performance simulations for step response and mixed transient cycles on RICARDO WAVE RT.
7. Implement controller in real time control environment.
 - a. Testing on engine dynamometer for load step response testing
 - b. Testing on vehicle for general driving and subjective evaluation.

Current industrial boost pressure controllers for series sequential diesel engines consists of map-based strategies which requires extensive amount of calibration workload and testing hours in vehicle and engine dynamometer. Conventional ECU controllers includes PI-PID controller with anti-windup strategies consists of gain-scheduled P, I and D gain maps as well as set point limitations to consider hardware-system limitations. As the controller cannot guarantee constraints explicitly, validation tests should be performed in a series of engine dynamometer and vehicle testing.

As mentioned in section 1.2, model predictive controller for two stage turbocharged diesel engine boost pressure control, which has proven its performance in real time applications and has never been applied before in research and industrial community. There have been some promising research but none of them have been implemented in real time environment and compared with conventional industrial controllers. In addition, MPC offers constraint handling and multivariable control framework integrated into controller design which enables decreased development time and effort compared to conventional ECU controllers. As proposed controller eliminates manual tuning for constraints and optimize the control signals, in terms of

automotive context, it can be termed as “Intelligent”. The rationale outlined here is justifying the novelty of the research performed in this thesis and its contribution to the field of Automotive control.

1.2 Literature Review

Modeling and control of diesel engines has been subjected to research since 1990s. By introducing electronic engine controls by 1980s, thanks to increasing environmental regulations, internal combustion engine control has gained interest among control engineering community. Figure 1.1 shows the evolution of European exhaust emissions standards. It is clear that the control window is narrowed from Euro3 to Euro 6, which drives innovations in base engine technology such as Exhaust gas recirculation, Fuel Injection equipment systems. In time, as the base engine development technology is advanced, control schemes are following in parallel.

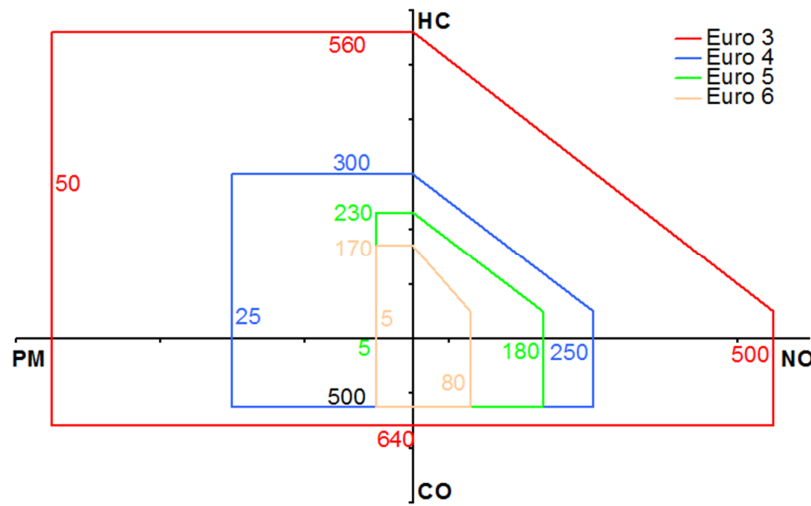


Figure 1.1 : European exhaust emissions standards.

In order satisfy emissions requirements, This results in more precise fuel injection and pressure control which would dramatically reduce particulate and gaseous emissions. Diesel engine controls has made an outstanding pace as the common rail direct injection is introduced to market by mid-1990's. Due to nature of diesel combustion, air control is required to optimize fuel-air mixture. This resulted in development of Variable Geometry Turbocharging (VGT) concept which would utilize the closed loop control of boost pressure. In order compensate the effect of high fuel pressures and combustion temperatures, Exhaust Gas recirculation system

is introduced for reducing NO_x emissions by lowering oxygen concentration inside combustion chamber.

Previous research on boosting control mostly focused on single stage turbocharging and specifically on Variable Nozzle Turbocharger (VNT) control and the interaction with Exhaust Gas Recirculation (EGR). Stefanopoulou et.al (2000) investigated the interaction of VNT and EGR control in terms of emission control problem. Main research includes the design of a multivariable feedback control, which utilizes VNT and EGR simultaneously to achieve emission control targets. The controller is based on nonlinear feed forward and a gain-scheduled multivariable feedback controller. The controllers are designed to achieve optimal Air-fuel Ratio (AFR) and burned mass fraction by controlling VGT and EGR in a multivariable controller structure.



Figure 1.2 : Simulation results of CLF based robust nonlinear controller.

In contrast to previous research, nonlinear control scheme have been designed and tested by Jankovic and Kolmanovsky (1998), in terms of control Lyapunov function (CLF) based design method. CLF is explained as smooth, positive definite, and radially unbounded function. Model of the diesel engine includes multiplicative uncertainty to accommodate parametric uncertainty as well as modeling errors. Design objective of the controller is defined as regulating the AFR and EGR flow fraction to the reference values. The simulations are performed by using seventh order nonlinear engine model. Model of the engine is generated by using 0D principles and mean value approach.

Plianos and Stobart (2010) which introduces a control strategy for a multivariable control of EGR and VGT perform another interesting research on EGR-VGT control. Basically, fuzzy estimator has been used to identify engine-turbocharger dynamics and update the control law online. Controller design has been based on feedback linearization and trajectory planning. Validation has been performed with promising simulation results although real time implementation has not been shown.

Wahlström et.al (2005) studied the PID controller tuning for coordinated EGR-VGT control for heavy duty engine. Similar to the previous researches, controller objective is control AFR and EGR ratio. In addition, turbocharger speed is controlled against over speed issues. The controller has been tested in European Transient cycle (ETC).

Ortner and Del Re (2007), has presented a model based approach for multivariable control of Diesel engine air path. Model based controller utilizes MPD framework. Performance objectives are defined as minimizing NOx and particulate emissions where fixing fuel consumption. During their research, comparison with conventional ECU controller has been performed on real engine, which proves the superiority of MPC controller over ECU controller. Figure 1.3 shows the snapshot of the test result performed on NEDC emissions cycle.

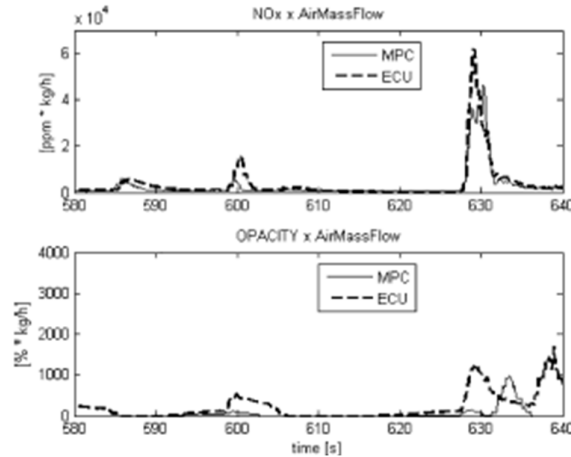


Figure 1.3 : Nox and Smoke emissions results.

Another research about using MPC on diesel engine controls have been presented by Perez et.al (2006). Generalized Predictive control scheme have been used by introducing nonlinear black-box model defined by as Wiener-Hammerstein model. Black-box model have been used as prediction model during MPC design.

Ferreau et.al (2007) demonstrated the performance of modified optimization algorithm, which introduces online active set strategy for Diesel engine predictive control. The aim of the study is to present a optimization algorithm which will be accomplished real time with cheap controller hardware. Performance of the active set strategy has been tested on real engine by using black-box engine model as MPC prediction model.

As the performance objectives and customer requirements demanded higher power densities, researches focused on boost pressure control not only with coordinated with EGR but standalone. Thomasson et.al, (2009), presented a study on model based boost pressure applied to fixed geometry turbocharger with waste gate. During this research, complete engine model is constructed based on MVEM methodology where models of waste gate actuator and position dynamics models are found as sub models. Validation of the model has been performed on engine test bench. Model based controller includes the IMC control scheme with identified model. Figure 1.3 shows the experimental results presented. The rise time and settling time are promising which allows rapid boost pressure build up thanks to feed forward controller.

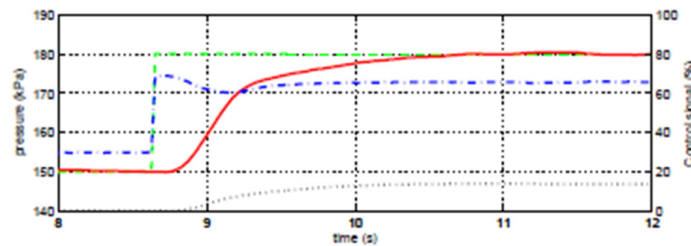


Figure 1.4 : Experimental results (green: Boost pressure setpoint, blue: control signal, red: actual boost pressure).

Kristofferson (2006), demonstrates the model predictive control structure to control the turbocharged SI engine equipped with Waste gate. The objective function used includes the fuel consumption and torque error. Basically, controller is trying to regulate WG position to achieve requested torque set points. The results have been validated in simulations. No real time implementation has been performed.

Although the two-stage turbocharger concept has a long history, control, utilization and application of the system has been recently developed. Due to high complexity and number of components, modeling of two stage turbocharger system is itself subjected to research. Leufven (2010) has presented a detailed compressor models

including surge and choke characteristics. Compressor is developed as a parametric model in which parameters can be tuned automatically by using a compressor map.

Shu and Nieuwstadt (2007) presented a modeling method, which incorporates total compressor efficiency. Two compressor model is connected by means of a new variable called as compressor temperature ratio. Model validation has been performed on FTP cycle.

Canova et.al (2010) describes a modeling and a characterization study on two stage turbocharged medium duty diesel engine equipped with passive LP bypass valve and HP VGT turbocharger with bypass valve. Research is mostly focused on the operation of HP bypass valve with VGT by means of MVEM modeling methodology. Model validation has been carried out on steady-state engine data. Transient validation of the model has not been performed.. Figure 1.4 shows the HP turbine bypass opening vs. boost pressure plotted for different VGT configurations.

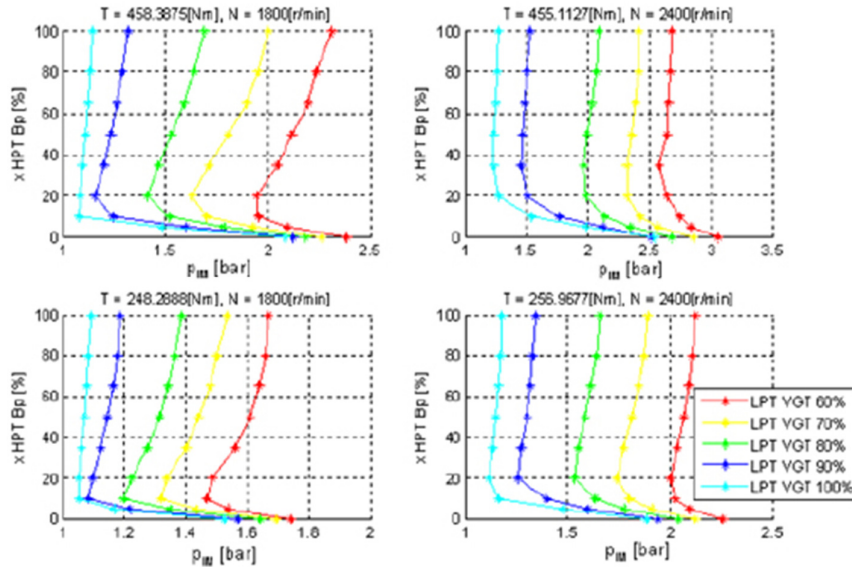


Figure 1.5 : HP turbine bypass vs. boost pressure for different VGT openings.

Yang and Zhu, (2010) has presented a modeling method for two-stage turbocharged SI engine by introducing a mixed discrete event and mean value approaches. In this case, HP and LP waste gate models, engine mass flow, intake manifold, crankshaft dynamics and turbine-compressor models are modeled based on MVEM. Gasoline wall wetting dynamics as well air-fuel ratio calculation and in-cylinder pressure-temperature models are designed as crank-angle based discrete event model. The model has been integrated and tested in Real-time HIL simulation. Integrated model

has been compared with GT-Power model by a series of steady-state and transient simulations.

There is a scarcity of papers that focus on two stage turbocharger control. Kotmann et.al, (2010) mentioned a study in which control design is achieved by employing the flatness based feed forward method. The study includes the model based control method which utilizes inversion based feed forward controller similar to IMC approach. Effort is mostly on model reduction and to create a controller which is differentially flat. Air system model is constructed based on ideal gas law and MVEM methodology. Full order MVEM model has been reduced to reduced order model to be used in control design. Although, the proposed control structure includes Feedback and feed forward designs, focus was to design and validate feed forward controllers. Simulation results include the effect of EGR on the controller operation.

Moreover, model based PI+Feedforward control has been designed and successfully implemented by Moulin et.al, 2009. Proposed controller structure has been extended from single stage application. The controller objective has been selected as boost pressure set point tracking. Controller structure utilized cascaded controller structure. System limitation including turbocharger over speed and exhaust manifold pressure limits have been considered under set point definitions rather than controller explicitly. Cascaded controller structure employs PI controllers for Feedback controller.

One way of controller improvement is to use the LQG method. In their research, Plianos and Stobart (2008), implemented a SISO LQG controller for two stage turbocharger application with HP stage is charged with VNT. Nonlinear model has been designed based on MVEM methodology. Compressor and turbine maps have been matched by using the method suggested by Jensen et.al (1991).

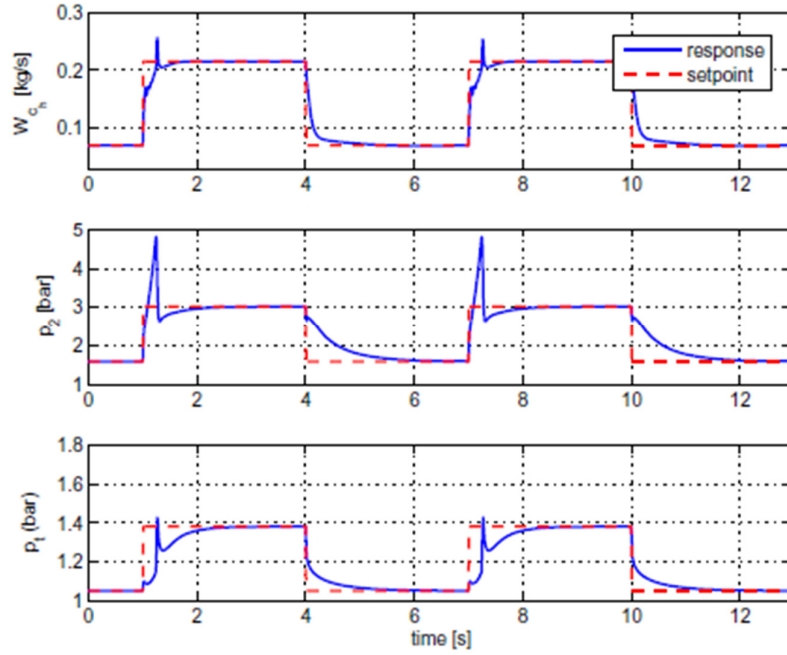


Figure 1.6 : Simulation results to step response.

Parameter estimation for turbine and compressor maps have been performed by using engine data rather than turbocharger supplier map. LQG control objective is defined as regulating AFR, EGR ratio as well LP and HP turbines against fuelling set points. Linear model identification is performed by using black-box methods rather than direct linearization of MVEM due to its increase complexity. Figure 1.4 shows the simulation results performed under step set point signals.

Schwarzmann et.al (2006) presented a nonlinear IMC approach for two stage turbocharged diesel engine control. Control variables are set as boost pressure, exhaust backpressure as well as interstage pressure between turbines. The target engine application includes controllable High Pressure compressor bypass valve. EGR flow is not considered under this study.

1.3 Scope of the Thesis

The organization of rest of the thesis is outlined as follows. In Chapter 2, diesel engine air path operation is summarized by mentioning supercharging-turbocharging basics as well as main components of the diesel engine air path. Thermodynamic aspects of supercharging is explained. Moreover, two stage turbocharging operation is mentioned by focusing the goals and benefits. In Chapter 3, modeling steps and formulation is mentioned. First, the system layout is explained in addition to brief

information given about different modeling schemes (MVEM and 1D models). Furthermore, 1D modeling methodology is mentioned by focusing on the subsystems such as valves, ducts-junctions, combustion models and turbocharger models. The Chapter 2 also includes the detailed information about control oriented black-box model and validation results for both 1D model and black box model. In Chapter 4, focus is to mention Model Predictive Controller formulation. Receding horizon control concept is explained as well as detailed design steps for constraint definition, prediction&control horizon selection and Kalman filter tuning. Design steps are detailed by focusing on MIMO and SISO controller separately. Controller objective are defined by considering industrial controller signoff criteria specified as basic time-domain properties. In Chapter 5, simulation results performed by nonlinear WAVE RT model are mentioned. Simulations are performed in terms of step-response tests and mixed transient cycles. System response has been assessed by taking into account of controller objectives mentioned in Chapter 4. In Chapter 5, real time tests are explained. Real time tests have been performed in terms of engine dyno testing and in-vehicle testing. Brief information about test setups performed in both cases is given in this chapter. As engine dyno testing provide repeatable testing environment, comparison results with conventional ECU controller have been shown. The improvements in system response and remarks have been mentioned. Turbocharger operation have been compared both in time-domain and compressor phase plots. In Chapter 6, conclusions about the research and contributions are presented. Further research opportunities and recommended subjects are finally mentioned.

2. DIESEL ENGINE AIR PATH

Diesel engines utilize compression-ignition base combustion in which, there is no a single ignition source as a spark ignition engines. Ignition occurs at multiple sites due to the high pressure and temperature associated with the higher compression ratios of the compression ignition engine. In order to operate in this manner, Compression ignition engine runs lean in which there is more O₂ than necessary to burn the fuel stoichiometrically. In conventional diesel engine combustion, fuel is not mixed with the air entering the cylinder during the intake stroke. Only air enters the cylinder during induction phase. This method of injection in fuel-air cycles allows high compression ratios to be used increasing the efficiency of the engine, decreasing fuel consumption. Gas-exchange(Intake) systems, which is also called Air path, are responsible to deliver desired amount of fuel in predefined pressures, temperatures and flowrates. As mentioned in Heywood (1988), the purpose of gas exchange system is to deliver required amount of air in order to satisfy required indicated power from the engine. Therefore, maximum air mass will be inducted at full load and retained in the cylinder. In addition, gas exchange processes are responsible to setup a flow field inside cylinders which will provide fast-enough combustion process.

2.1 Main Components for Diesel Engine Air path

As shown in Figure 2.1, Diesel engine Air path include but not limited to turbochargers/superchargers, charge air coolers, exhaust gas recirculation (EGR), valves and cooler, intake manifold and throttle plate. Turbochargers/superchargers are used to boost the air flowing through the intake ports. More information can be found below at section 2.1.

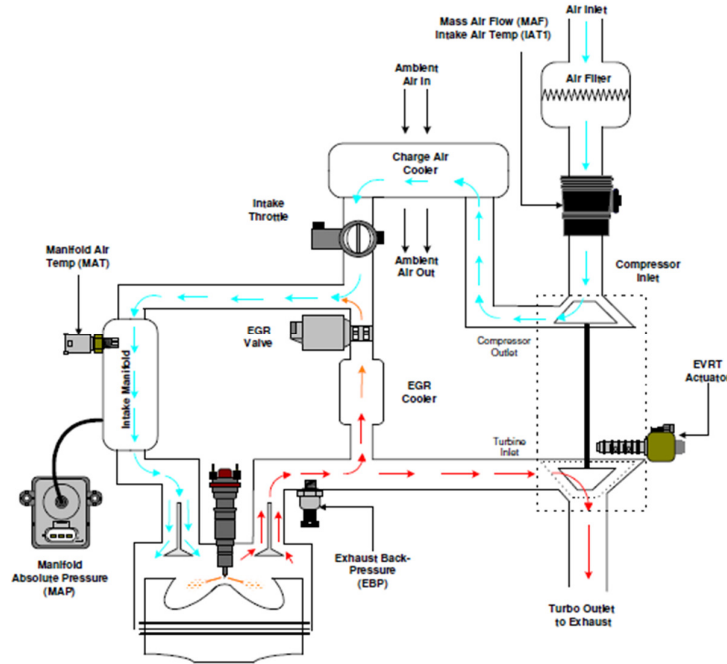


Figure 2.1 : Diesel engine airpath layout.

Charge air coolers (CAC) are usually used in combination with turbochargers/superchargers to reduce the temperature of the boosted air. This would result in improvement in emissions and performance while enhancing the effect of boosted air within the cylinders. CACs are a specific form of a heat exchanger that can be either air-air or air-water (coolant) heat exchangers. As standard heat exchangers, CACs are characterized by effectiveness, which is defined as the actual heat transfer rate that can occur based on the entry conditions of the fluids in the boundary conditions. Mollenhauer and Tschoeke (2010) mentioned that the CAC effectiveness determine the potential reduction of temperature in the CAC. Figure 2.2 shows the effect of CAC to two stage turbocharged diesel engine operation. As the ambient air inducted to LP compressor, the air compressed and its temperature is increased. Similar step occurs during HP stage also. Post HP turbocharger, CAC cools down the compressed air before inducting to the intake manifold and cylinders.

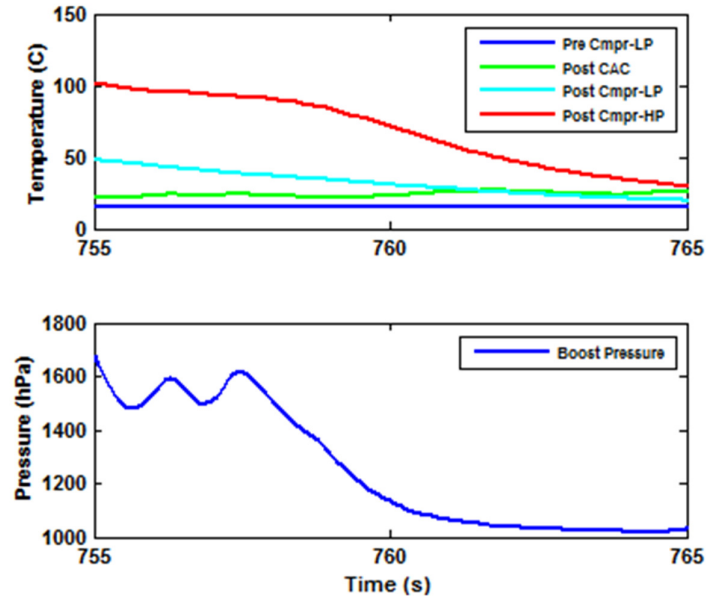


Figure 2.2 : CAC operation in Diesel engine.

Exhaust Gas Recirculation (EGR) system's primary purpose is to control the NO_x emissions by limiting peak combustion temperatures. EGR flow into the cylinders increases the burnt mass fraction and decrease the O_2 in the cylinders. The heat energy is absorbed by this increased burnt mass fraction therefore, N_2 disassociation is decreased. In contrast to decrease in NO_x emissions, increased EGR flow will increase HC and CO emissions. Particulate (PM) emissions and engine-out soot is also increase due to switching to degraded combustion mode. Figure 2.3 shows the NO_x and PM tradeoff for different values of EGR and air/fuel ratio.

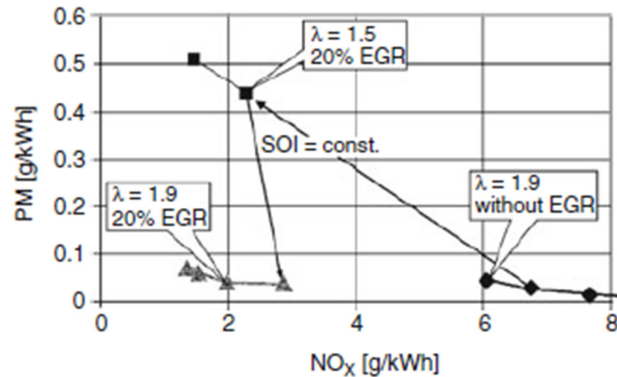


Figure 2.3 : Effect of EGR on NO_x and PM emissions.

Moulin (2010) states that there is an interaction between EGR and turbocharger system as pressure difference between intake and exhaust manifolds affects EGR operation directly especially in steady state operation. EGR systems are classified under the general terms of high pressure and low pressure EGR. High Pressure EGR systems utilizes the exhaust flow upstream of turbine where Low pressure EGR flow is taken downstream of the DPF.

The purpose of Intake throttle in Diesel engines is entirely different than the gasoline engines. Throttle valve on diesel engines are exclusively used to increase intake manifold vacuum upstream the EGR valve to achieve higher EGR levels in the intake manifold where in gasoline applications, it is used a main torque actuator to increase air mass flow. This increase of the vacuum increases the exhaust gas return rate by up to %60. In addition, it is used to accomplish below operations as well,

- Reducing the shut-off shake of engine
- Reducing warm-up times when closed during over-runs
- Control of exhaust temperatures during DPF regeneration
- Controller air flow to adjust air/fuel ratio < 1 during NO_x storage catalysts' s regeneration
- Used in idle to optimize noise by lowering the peak cylinder temperatures.

Intake manifolds in diesel engines are mainly designed for cylinder charge distribution, EGR distribution, charge swirl and dynamic response of a boosted engine. Swirl requirements are typically handled through intake port design to achieve desired swirl characteristics.

2.2 Supercharging the Diesel Engine

During engine design process, the air induction capacity of each engine is fixed. The maximum amount of air inducted depends on air filter restriction, intake manifold, intake ports and valves. The amount of induction air can be increased by compressing to higher densities before sending to cylinders. In this case more fuel can be injected to overcome increased amount of air. This results in increase in power output. This process is simply called as supercharging or boosting the internal combustion engine. Diesel engines are especially suitable for boosting as only air

and EGR is flowing into the engine during intake stroke. The manifold air charge density can be increased by boosting in order to achieve improved volumetric efficiency. This would result in performance improvement.

2.2.1 Basics of supercharging and turbocharging

As mentioned above, supercharging is basically a method to improve power density of the internal combustion engine. Net power produced by engine is increased with the amount of total injected fuel per time. Equation (2.1) shows the formula to calculate engine net power.

$$P_e = \frac{H_u}{L_{min}} \cdot \frac{V_H}{\alpha} \cdot \lambda_l \cdot n_M \cdot \rho_L \cdot \mu_e \quad (2.1)$$

As mentioned in Mollenhauer and Tschoeke (2010), Air density flowing into the cylinders depends on the pressure and temperature which are calculated in terms of thermal equation of state of a gas as shown in (2.2).

$$\rho_L = \frac{1}{R} \cdot \frac{P_L}{T_L} \quad (2.2)$$

In order to increase density, either temperature should be dropped or pressure should be increased. T_L might not be below environment temperature therefore P_L is increased by boosting methods. P_L is called as boost pressure. In an application basis, boosting can be performed by means variety of methods and systems. Hiereth and Prenninger (2007) listed non-exhaustive list of supercharging methods.

■ Supercharging by gasdynamic effects

- Systems that are using pressure waves occurred in the intake and exhaust systems.
- Supercharging by Helmholtz resonator intake manifold layouts
- Supercharging by using pressure wave charging method via direct pressure exchange between exhaust gas and charge air.(Comrpex)

■ Supercharging with mechanically driven chargers

- Displacement or rotary piston chargers (Roots)
- Displacement of screw-type charger with internal compression

- Turbo compressors (radial-axial compressor units)
- Supercharging systems with exhaust gas energy recovery
 - Coupling a turbo compressor with a turbine- exhaust gas turbochargers
 - Coupling of a displacement compressor with expander located on the same shaft. (Wankel)
- Supercharging via combination of the components mentioned above
 - Turbocompound system, exhaust gas turbocharger with downstream energy recovery turbine.
 - Combined systems with resonance charger and exhaust gas turbocharger
 - Combination of a mechanical charger with an exhaust gas turbocharger

The comparison of exhaust gas turbocharging and supercharging is can be well understood by illustrating their effects on thermodynamic cycle. Figure 2.4 and 2.5 shows the effect of mechanical supercharging and turbocharging in idealized engine process.

When mechanical supercharger, which is driven by the engine by pulley or chain drive, supplies cylinders a fresh air with pressure P_L . This pressure is similar to pressure values at the intake stroke which is higher than the naturally aspirated engines. The compression starts with higher initial values at point 1 shown in Figure 2.4. At the end of the expansion stroke at point 5, exhaust valve actuation makes the cylinder charge out of the cylinder against environmet pressure P_1 . This produces extra positive gas exchange work shown as W_{LDW} against the engine. The isentropic supercharger work, which is shown as W_L , is greater than engine's gas exchange work. The perpendicular hatched area is the loss of work from point 5 to environment pressure.



In the case exhaust gas turbocharging, the supercharger work is also similar at the same boost pressure P_2 . However, supercharger work is handled by turbine work W_T , which is drawn from the exhaust gases. As the exhaust gases hitting turbine blades at a temperature T_3 , at the end of the turbine expansion, the temperature drops down to T_2 . When $W_T = W_L$, the exhaust pressure P_3 before the turbine is lower than P_2 . Therefore gas exchange work, W_{LDW} is also positive as in supercharger case. In addition, higher exhaust back pressure at the exhaust valve, results in loss of work than the mechanical supercharger due to incomplete expansion of the cylinder charge.

19

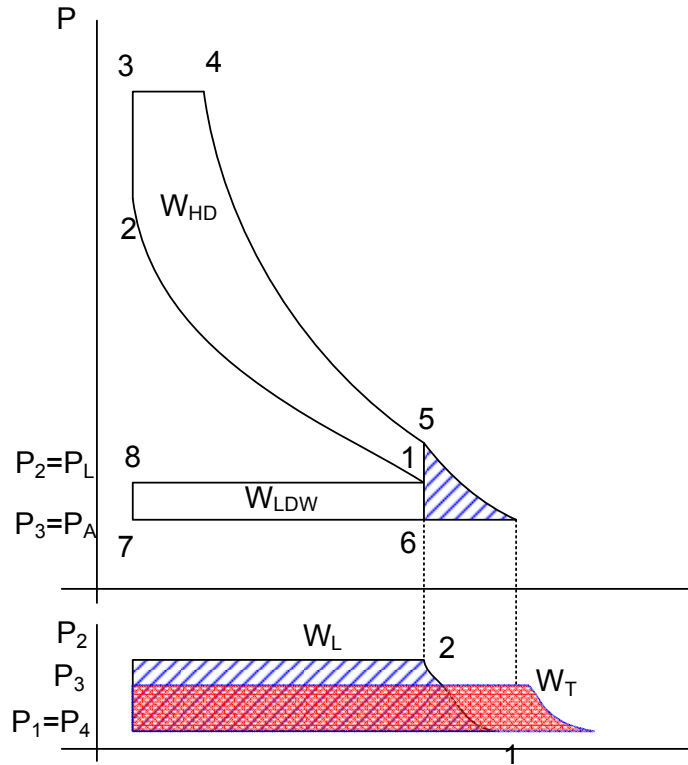


Figure 2.5 : Effect of exhaust gas turbocharging in the idealized engine cycle.

Exhaust gas turbochargers consists for compressor and turbine units which are connected with a shaft. Due to the high rotational speeds up to 230000 rpm, the shaft should be lubricated to prevent failures. The lubrication is carried out by feeding oil from engine lubrication system. Figure 2.6 shows the very basic diagram of turbocharger unit. Exhaust gas flows through the diffuser which allows the increase the expansion ratio in the turbine by means of recovering the pressure downstream of the turbine, thus increases the turbine efficiency. As the exhaust gas hits the turbine blades, turbine blades extract kinetic energy from the exhaust gases. Kinetic energy is transferred to the rotor which is accelerated and rotating the compressor at the air side. In practical applications, axial compressors are used. As the inlet gases enters to compressor, kinetic energy of the turbine shaft speed is transferred to inlet gases by centrifugal effect of rotating impeller. Again diffuser on the compressor side helps to recover static pressure.

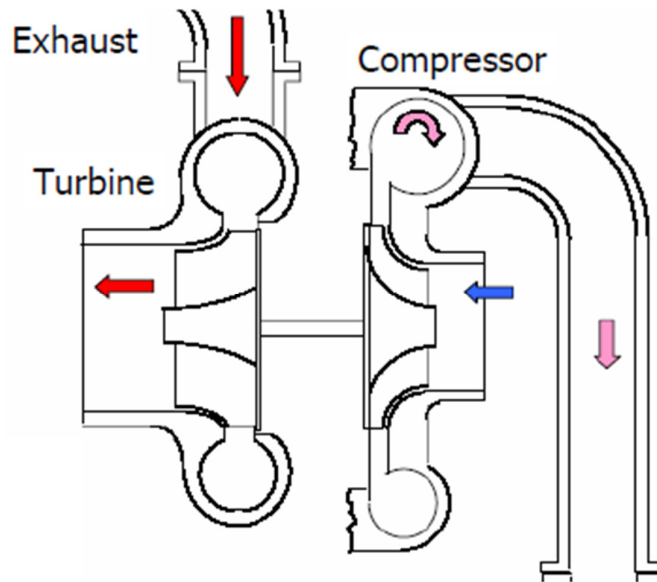


Figure 2.6 : Basic exhaust gas turbocharger layout.

The performance of the exhaust gas turbocharger can be investigated by means of compressor and turbine performance maps. Typical compressor performance map is shown in Figure 2.7 which is shown by Prenninger and Hiereth, 2010. This is basically the flow maps showing the isentropic efficiency and flow vs. Pressure ratio at various turbocharger shaft speeds. It should be noted that two limits are introduced on compressor performance maps. When the pressure ratio is high but the mass flow is small, there is a risk of instability in the gas flow. This is called surge limit. As mentioned in Prenninger and Hiereth (2010), the compressor flow in the impeller is stalling thus resulting in pressure waves in the charger as well as charger air manifold upstream of compressor. Challen and Baranescu (1999), although the dynamics and detailed explanation of surge has yet to be fully accepted, it is induced when the mass flow rate through the compressor is reduced whilst maintaining a constant pressure ratio, at the point where local flow reversal are occurring. The surge line shown in the compressor performance maps are different in every engine application as surge behaviour is influenced by complete intake and exhaust system layout.

Another important limits illustrated on the compressor performance map is the choke limit. It is characterized by very high mass flows occurring on the compressor inlet. As the gas flow reaches sonic speeds, it would be impossible to increase the volumetric flow even if the compressor speed is increased. In theory, compressor speed can be increased but due to mechanical stress occurred on the turbocharger

shaft, there is a hard limit. Moreover, at higher shaft speeds, lubrication of shaft would not be sufficient enough.

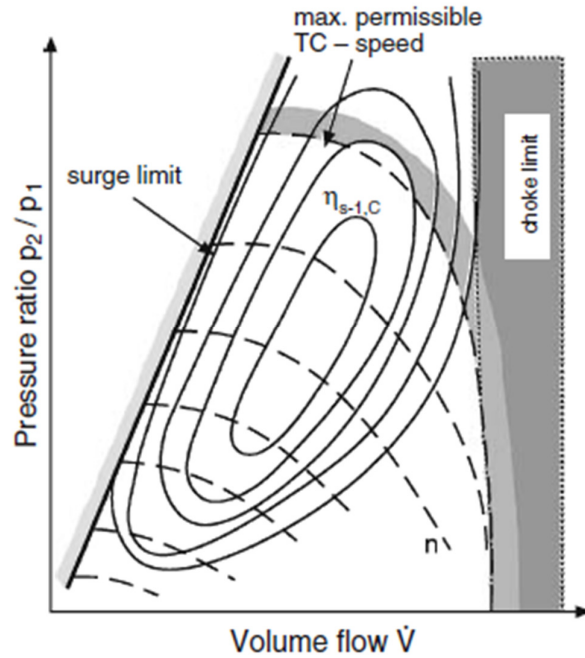


Figure 2.7 : Typical compressor flow map.

The circular contours shown in figure 2.7 are related to constant isentropic lines where dashed dotted contours are related to constant turbocharger speed.

Similar to compressors, turbines also represented by means of performance maps. The turbine maps are represented as turbine expansion and pressure ratio against the flow rate reduced by inlet pressure and temperature as wells as the total turbine efficiency. Figure 2.8 shows the typical turbine map. Here the X-axis is defined as reduced flow rate which is shown in (2.3).

$$\dot{m}_{redT} = \dot{m}_T \cdot \frac{\sqrt{T}}{P_{03}} \quad (2.3)$$

One of the key aspects that can be extracted from turbine map is, constant speed lines are converging to a single line of almost constant flow parameter. When the inlet gases reaches sonic velocity, they are choking the inlet casing of the turbine thus resulting in this phenomenon.

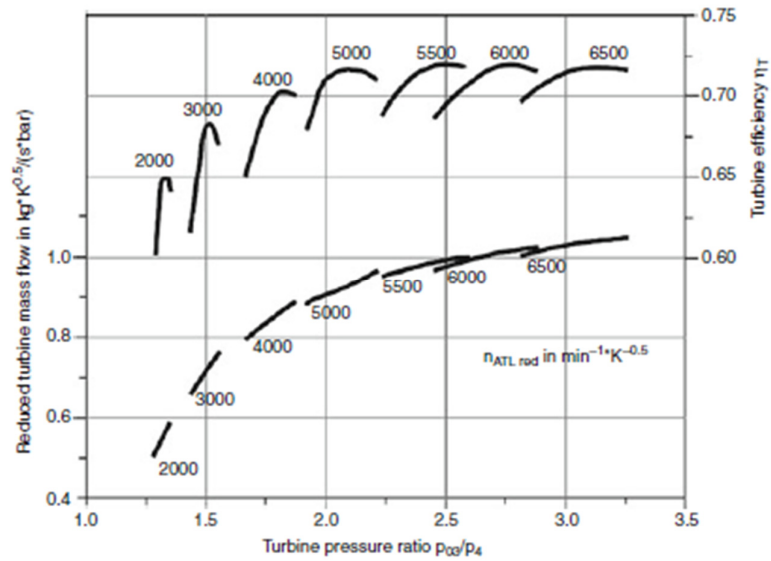


Figure 2.8 : Typical turbine map.

In order to match the flow and pressure characteristics of turbocharger with the engine power requirements, it is extremely important to choose best combination of turbine and compressor across engine speed-load range. Figure 2.9 shows the behaviour of the mis-selected compressors on the compressor map. If the turbine is chosen as too small, it will make compressor to hit the choke limit too frequent. This would result in lack of full-load power in the engine as turbocharger will cause excessive exhaust backpressure at high speeds.

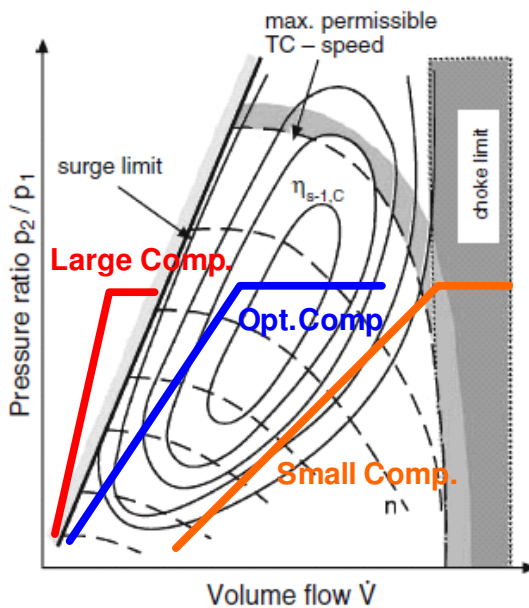


Figure 2.9 : Turbocharger matching.

If the turbine is chosen to be large in impeller diameter, this would have some adverse effect as the flow characteristics of the compressor which is triggering surge too often. In addition poor turbocharger matching will result in poor driveability, higher fuel consumption as well as higher emissions. Larger turbine will be more efficient at higher speeds as they will create less exhaust back pressure.

Turbocharger matching should be completed in the early phases of the engine design and development. It can be considered as empirical and iterative process. Required boosting for engine can be calculate by engine's peak fire pressure (maximum cylinder pressure) which would satisfy power requirements. Several combination of turbine and compressors are tested to satisfy the maximum design limits on the cylinder pressure, exhaust temperature, turbocharger speed, exhaust backpressure as well as vehicle's altitude performance.

Turbocharger operation affects engine operation. During boost pressure build-up, turbocharger is accelerating to provide boost to the cylinders. Turbocharger acceleration depends on the power balance between turbine and the compressor. At low engine speeds, engine power available for turbine acceleration is low. Hence, turbine blades are acting as a throttle valve resisting to flow. There is a significant time to move between low speed points to more efficient point. This phenomenon is called as Turbo lag.

There are several solution to overcome Turbo lag in engine application. Below are the non-exhaustive list of possible solutions available in state of the art turbocharger technology.

- Reducing the turbine inertia
- Optimizing turbine blade and nozzle design, Variable Geometry Turbocharger designs
- Reducing exhaust manifold heat losses
- Fuelling strategies to increase exhaust energy
- Series sequential turbocharging (two-stage turbocharging)
- Electrically assisted turbocharging (E-boosting)

2.2.2 Series Sequential turbocharging concept

The series sequential turbocharging can be named as two stage turbocharging also. It refers to a turbocharger layout in which two separate turbocharger units are connected in series. In series configuration, the boosted air at the outlet of one compressor is the inlet of another compressor. One should note that it is different than the parallel sequential configuration in which two separate turbochargers are connected in parallel and two compressor are boosting the air two the same manifold. Parallel sequential configuration is mostly used in V-engines.

Regardless of being parallel or series, the primary goal of sequential turbocharging is to improve transient response at low engine speed. Transient response of the engine is improved in case of sequential boosting due to utilization of lower inertia compared to single turbocharger (Bjungchan, 2009).

Figure 2.10 shows the passenger car application of regulated two-stage turbocharger layout.

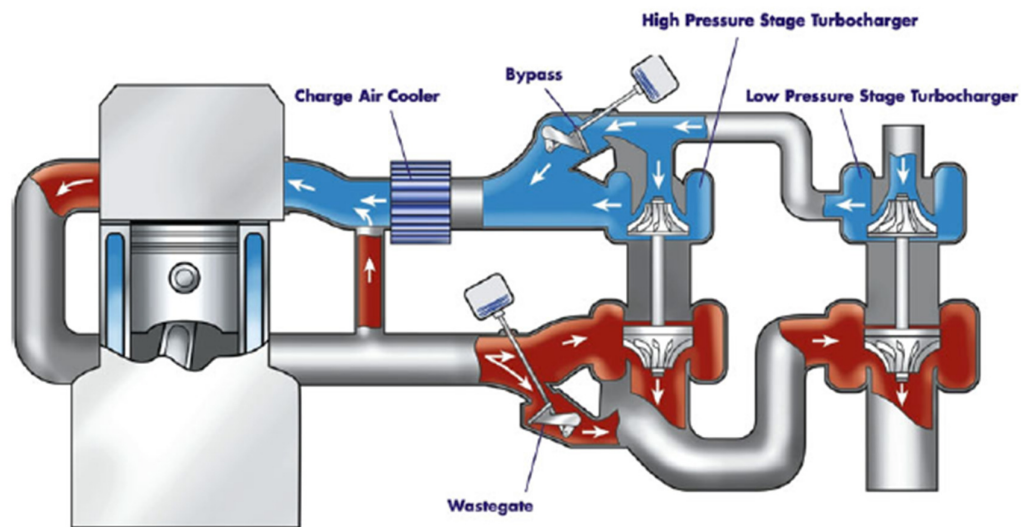


Figure 2.10 : Regulated two-stage turbocharger system layout.

Two-stage turbocharger system may be designed in several different architectures. These architectures are differed with respect to the type actuators and bypass valves. High pressure stage turbocharger is matched to provide high boost at lower engine speeds. The boost pressure is controller by means of HP bypass valve or VNT turbine. As the HP compressor/turbine choke is approached, HP bypass valve or VNT is opened. At this point, HP compressor bypass valve is also bypassed to

prevent HP compressor becoming a restriction. As the engine speed is increased, low pressure stage contributes much to the boost pressure as it has larger diameter. Low pressure stage is matched for the rated power air mass flow. Low pressure bypass valve is used to control the flow across the low pressure turbine. As mentioned in Matterelli et.al (2009), matching of LP compressor has an effect on HP compressor as well. Minimum flow rate for LP compressor at medium speeds is the maximum flow rate that should be delivered by HP compressor. Therefore HP compressor cannot be too small due to the transition between LP and HP compressor operation. So matching of two separate units are related to each other.

Series sequential boosting offers many advantages to single-stage turbocharging as listed below (Prenninger and Hiereth, 2010);

- Higher boost levels thus higher mean effective pressures
- An improved charging efficiency.
- Wider compressor and turbine maps, improved flexibility to adapt turbocharger operation to desired engine operation range.
- When using uncontrolled series sequential system, transient response is worse as two turbocharger units should be accelerated. But this turned into an advantage in case of utilizing actuators and bypass valves.

3. ENGINE MODELING

3.1 System Layout

The test engine system layout can be seen in Figure 3.1. The aforementioned engine is 2L, 4 cylinder, two stage turbocharged diesel engine. The turbocharger system consists of two units named as High Pressure stage and Low-pressure stage turbochargers. Naming convention is based on the turbine inlet pressures of each turbocharger. HP stage turbine is subject to exhaust backpressure. After the thermodynamic expansion occurred in HP turbine, LP turbine is rotating with low inlet pressures compared to HP stage. In principle, turbocharging matching is based on the low-end and high-end torque characteristics of the engine. LP turbocharger is more efficient at high load-speed points therefore Turbocharger size is matched according to the rated power. HP turbocharger matching is performed according to satisfy better transient characteristics and low-end torque performance only. Compared to VNT applications, HP turbine can be selected relatively smaller size (Schmitt and Sweetland, 2004).

Boost pressure control is achieved via two valves connected to each turbocharger. Turbine Bypass Valve (TBV) controls HP stage and Waste gate (WG) controls LP stage. Both of the valves are of electro-pneumatic solenoid valve controlled by Engine Control Unit (ECU). When TBV is fully opened and it is bypassing the exhaust flow, HP compressor will apply restriction to the mass airflow on the intake side. In order to prevent this phenomenon, Compressor Bypass Valve (CBV) is utilized. CBV is a passive valve, which works with respect to pressure difference across the valve.

The engine is equipped with high Pressure Exhaust Gas Recirculation system, which is used to recirculate burned exhaust gases back into the intake line. This process is used to lower the in-cylinder temperatures in order reduce the NO_x emissions. Moreover, Air Cooled charge air cooler, which is similarly named as Intercooler, is

used in test engine. The purpose of the intercooler is to cool the compressed intake air thus result in increase in the air density and volumetric efficiency.

The states of the system can be summarized as follows;

$$[P_{exh} P_{boost} P_{intt} P_{intc} n_{hp} n_{lp}]^T \quad (3.1)$$

As realized, system states are mainly pressures and turbocharger shaft speeds. This is due to having been represented by dynamic equations rather than static maps. The inputs to the system can be divided into 2 groups. Manipulated variables (MV) are the main actuator inputs in which we apply the control. These group mainly includes TBV control signal (%) and WG control signal (%). CBV cannot be considered as MV as it is working passive without any control intervention.

$$x_{mv} = [u_{hpt} u_{lpt}]^T \quad (3.2)$$

Second group is the exogenous inputs or measured disturbances (MD) which can affect the system behaviour but there is no control applied. These are mainly the engine speed (rpm), total amount of injection (mg/stk), start of main injection (deg).

$$x_{md} = [n_{eng} \dot{m}_{fuel} \theta_{soi}]^T \quad (3.3)$$

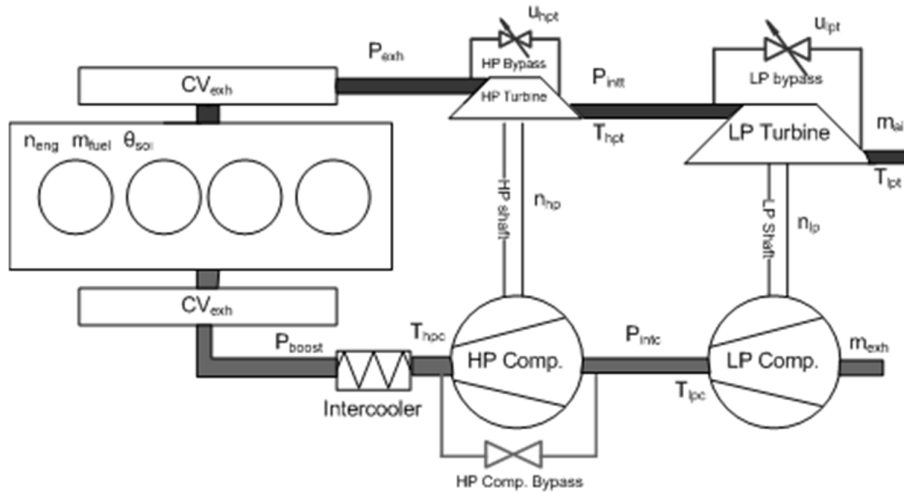


Figure 3.1 : Series Sequential turbocharged diesel engine layout.

The exhaust after-treatment parts such as Diesel oxidation catalyst and Diesel Particulate filter have not been considered in this study. Therefore, the LP turbine outlet pressure is assumed equal to atmospheric pressure. Moreover, the air filter restriction is not taken into account.

3.2 Nonlinear Engine Models

Designs of model based diesel engine controllers require generation of suitable models to achieve satisfactory performance criteria. Models should be capable of representing the transient behavior of the diesel engine.

Thermodynamics and kinetic processes occurred in Diesel engines are highly fast which is completing in milliseconds. Due to the microscopic effect of fluid flow and turbulence, cycle-to-cycle variations are inevitable. Moreover, actual fluid flow is not constant rather it has a pulsation characteristic. As mentioned in Guzzella and Onder (2010), the reciprocating behavior of the engine systems results in different modeling schemes.

In this study, the engine modeling scheme are investigated in terms of two different sections. In the following section, Mean Value Engine Models (MVEM) which are usually called as 0D engine models, are mentioned. MVEM use lumped parameter modeling approach to express the physical behavior of the system. In the section 3.3.2, 1D models are investigated and explained in which the fluid are formulated in terms of one directional flow characteristics. Moreover 3rd party SW package modeling is mentioned.

3.2.1 Mean value engine models (MVEM)

Mean Value Engine Modeling scheme basically models the Internal combustion engine behavior physically in time frame rather than consideration of crank angle as independent variable (Guzzella and Onder , 2010). The term “Mean Value” refers to using average value of some number of cycles in a time interval. MVEM scheme refers to family models, which utilizes lumped parameter modeling in which system dynamics, are expressed as Ordinary Differential Equations (ODE). During the formation of the ODEs, changes that took place faster than 1 engine cycle are expressed by static relations. Physical phenomena that occur slower than 1000 cycles are expressed by constants.

Methodology for MVEM modeling is to separate the system into several components and define each component behavior by an aid of physical and thermodynamic relations (Eriksson, 2007).

1. Control Volumes
2. Restrictions

Control volumes are basically the mass storing elements. One of the acronyms for control volumes are reservoirs (Guzzella and Onder, 2010). Intake and exhaust manifolds, ducts, connecting pipes are considered as control volumes. The dynamics of the mass stored in control volumes are expressed in terms of conversation of mass and energy. As mentioned in Eriksson et al. (2010), control volumes can expressed by isothermal assumption or adiabatic. When using isothermal approach, only the pressure dynamics is captured as temperature changes are assumed to be zero across the control volume. (3.4) shows the differential equation for isothermal approach.

$$\frac{dp}{dt} = \frac{RT}{V}(\dot{m}_{us} - \dot{m}_{ds}) \quad (3.4)$$

R is the ideal gas constant, \dot{m}_{us} is the upstream mass flow and \dot{m}_{ds} is the downstream massflow through the control volume.

In case of heat transfer occurred in the control volumes, the temperature change would be non-zero. Therefore temperature is added to system states. See Hendricks (2010) for detailed formulation. If it is assumed that the heat transfer is adiabatic process, the temperature and pressure dynamics can be expressed as a series of ODEs as shown in (3.5).

$$\begin{aligned} \frac{dP}{dt} &= \frac{\kappa R}{V}(\dot{m}_{us}T_{us}(t) - \dot{m}_{ds}T(t)) \\ \frac{dT}{dt} &= \frac{TR}{PVc_v}(c_p\dot{m}_{us}T_{us} - c_p\dot{m}_{ds}T - c_v(\dot{m}_{us} - \dot{m}_{ds}).T) \end{aligned} \quad (3.5)$$

The parameters used above are defined as below;

c_p specific heat at constant pressure, units J/(kg K)

c_v specific heat at constant volume, units J/(kg K)

κ ratio of specific heats, $\kappa = \frac{c_p}{c_v}$

R gas constant, units J/(kg K)

Restrictions are basically transporting the mass and energy stored in the control volumes. This transport phenomenon is occurred by means of energy and mass flows between control volumes (Guzzella and Onder, 2010).

The fluid flow can between control volumes are modeled as a flow from an orifice, which utilizes pressures upstream and downstream of the restriction. The components such as air filter, intercooler, exhaust gas catalysts are examples of restrictions. Those components can be modelled by using incompressible and turbulent flow equation as shown in (3.6).

$$P_{us} - P_{ds} = \Delta P$$

$$\Delta P = K_{fr} \left(\frac{RT_{us}}{P_{us}} \right) \cdot \dot{m}^2 \quad (3.6)$$

K_{fr} is the restrictor constant depending on the area, wall friction etc. This is used to tune the model to fit the measured data as shown on Figure 3.2. The accuracy of fitting of the model to measured data is below %5 percent.

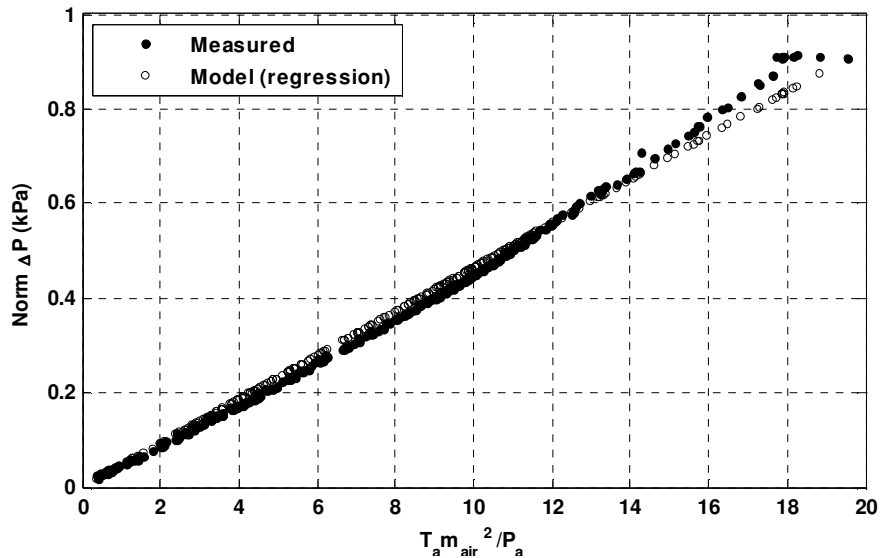


Figure 3.2 : Incompressible restriction tuning plot for air filter.

Actuator valves used in engines to control the fluid flow should be expressed in different formulation due to higher pressure losses and flow velocities (Eriksson, 2007). This results in necessity to use compressible flow formulation shown in (3.4).

$$\begin{aligned}\dot{m}(u, P_{us}, P_{ds}, T_{us}) &= \frac{P_{us}}{\sqrt{RT_{us}}} A_e(u) \psi(\Pi_{vl}) \\ \psi(\Pi_{vl}) &= \sqrt{\frac{2\gamma}{\gamma-1} \left(\Pi_{vl}^{\frac{2}{\gamma}} - \Pi_{vl}^{\frac{\gamma+1}{\gamma}} \right)} \\ \Pi_{vl} &= \max \left(\frac{P_{ds}}{P_{us}}, \left(\frac{2}{\gamma+1} \right)^{\frac{\gamma}{\gamma-1}} \right)\end{aligned}\tag{3.7}$$

In (3.3), $A_e(u)$ is the effective opening area of the valve or orifice which is expressed as a function of control input u . $A_e(u)$ is the main parameter that is used to tune the valve model by using several parametrization techniques. Compressible flow model mostly represents the dynamics of Throttle valve, Waste gate valve, turbine bypass valve, EGR valve well.

Final components in MVEM is the models for turbocharger. Compressor and turbine modeling is a challenging task as the models should define the mass flows and efficiencies inside engine operating regions well (Moraal and Kolmanovsky, 1999). Compressor and turbine is modeled separately and connected via energy transport between each components. This relation basically defines the rotational dynamics of the turbocharger shaft. Turbocharger shaft speed is the main state variable for turbocharger model which is shown in (3.8).

$$\frac{d\omega_{tc}}{dt} = \frac{1}{J_{tc}} \left(\frac{P_{trb}}{\omega_{tc}} - \frac{P_{cmp}}{\omega_{tc}} - M_{fric}(\omega_{tc}) \right)\tag{3.8}$$

Where P_{trb} is the turbine power and P_{cmp} is the compressor power consumed. M_{fric} is the shaft friction which damps the system.

Compressor models should model the corrected mass flow accurately in order to calculate the power consumption P_{cmp} of the compressor well. P_{cmp} can be formulated as shown in (3.9).

$$P_{cmp} = W_c c_p (T_{c2} - T_{c1}) \quad (3.9)$$

Considering that the compression process is isentropic, actual power consumption would be different than ideal consumption. Therefore compressor efficiency term can be introduced to overcome.

$$\eta_{cmp} = \frac{P_{cmp,ideal}}{P_{cmp}} = \frac{\left(\left(\frac{P_{c2}}{P_{c1}} \right)^{\frac{\gamma-1}{\gamma}} - 1 \right)}{\frac{T_{c2}}{T_{c1}} - 1} \quad (3.10)$$

(3.9) and (3.10) shows that compressor mass flow and efficiency should be known in order to model compressor dynamics. By using different parametrization methods, massflow and efficiency can be fitted to real data. There are several interpretations in the literature. Figure 3.3 shows the parametrization of HP compressor efficiency model in terms of different turbocharger shaft speeds. In the literature, there are several methods for parametrization techniques of compressor and turbine models (Moraal and Kolmanovsky, 1999).

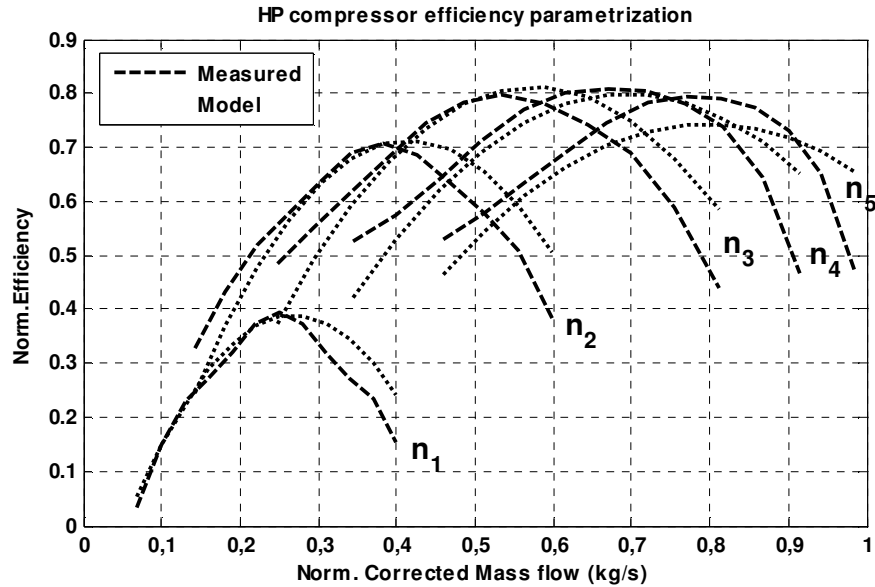


Figure 3.3 : Parametrization of HP compressor efficiency model.

MVEM models have several advantages to use such as, being directly used in control design and having physical understanding as it is based on first principles, it has some drawbacks as well. First, MVEM models are modeled as grey box models, which can be considered as combination of physics and tuning parameters. Tuning of MVEM models requires considerable amount of time and effort (Ortner and Del Re, 2007). In addition, linearization is cumbersome due to having several local linear models.

Due to those disadvantages, under the content of this study, nonlinear simulation model has been selected as 1D engine model and control oriented modeling method is based on the system identification methods. The advantages of using this method is due to providing high fidelity simulation environment for engine control system synthesis (Wu, 2011). Gas dynamics occurred on air path and exhaust path can be represented accurately while covering heat transfer effects in the piping and other components (Ricardo Wave, 2013). Furthermore, 1D modeling approach reduced the efforts for parameterization.

3.2.2 1D engine models

The term 1D is due to the calculation of the fluid flow in one direction, which is usually along the pipe or duct. Before going in detail with the subcomponents, one needs to mention the principles of fluid dynamics that is used to formulate 1D models.

Fluid flow is derived from principles of conservation of mass, momentum and energy. The fluid flow in the engine can be considered as unsteady, 3D, compressible flow. 1D modeling scheme is derived by an assumption that the flow varies only in one direction, which is the axial direction along the stream (Renberg, 2008). The three conservation equations (mass, momentum and energy) are shown for 1D scheme in (3.11), (3.12), (3.13) and (3.14) respectively.

$$\frac{\partial \rho}{\partial t} + \frac{\partial}{\partial x}(\rho u_x) = 0 \quad (3.11)$$

$$\frac{\partial}{\partial t}[\rho \cdot h] + \frac{\partial}{\partial x}[\rho \cdot u_x \cdot h] = \frac{\partial p}{\partial t} + u_x \frac{\partial p}{\partial x} + \tau_{xx} \frac{\partial u_x}{\partial x} - \frac{\partial q_x}{\partial x} + \dot{Q} + \dot{W}_{ext} \quad (3.12)$$

$$h = e + \frac{p}{\rho} \quad (3.13)$$

$$u_x \frac{\partial}{\partial x} [\rho \cdot u_x] + \frac{\partial}{\partial t} [\rho \cdot u_x] = -\frac{\partial p}{\partial x} + \frac{2}{3} \cdot \mu \left(2 \frac{\partial^2 u_x}{\partial x^2} \right) \quad (3.14)$$

The flow fields characterized by governing equations are discretized into a series of small volumes. Above governing equations are solved by using finite difference techniques utilizing the finite-volume approach to the discretization of the partial differential equations. The reason behind discretization is to model the pulsation and propagative properties of the fluid. Generally a staggered grid approach is used in which the scalar variables are calculated at the center of the small volume and vector variables such as velocity and mass flux are calculated at the boundaries. In other words, conservation of mass and energy equations is solved at the center in contrast, conservation of momentum is solved at the volume boundaries. Basically 1D engine modeling scheme is some sort of distributed parameter modeling rather than lumped parameter modeling in MVEM. Figure 3.4 shows the simple discretization of the duct.

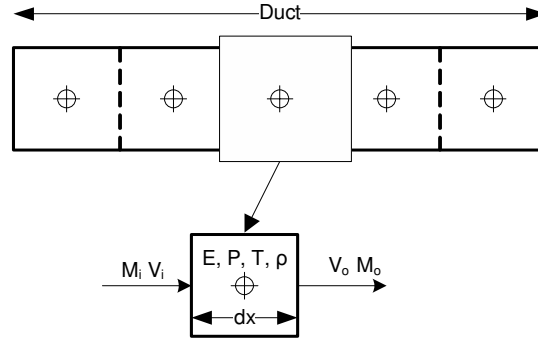


Figure 3.4 : Discretization of simple duct.

In Figure 3.4, the length of the sub-volume dx , is defined during modeling stage. Typically, 30-40 mm is the recommended values for length of the sub volume segments (Renberg, 2008). On the other hand, Ricardo Wave, 2013 suggests experimentally defined relations for sub-volume length as shown in (3.15) and (3.16).

$$dx = 0.45 \cdot B \quad (3.15)$$

$$dx = 0.55.B \quad (3.16)$$

B is the engine bore diameter. (3.15) is suggested for ducts used in air intake side where (3.16) is for ducts used in exhaust side.

Depending on the number of segments, the model's accuracy for pressure wave representation is changing. As a rule of thumb, longer lengths results in faster simulation times due to the necessity of solving less equations at boundary locations. Similarly, decreasing the sub-volume length will result in more accurate representation of flow pulsation and pressure waves as shown on Figure 3.5.

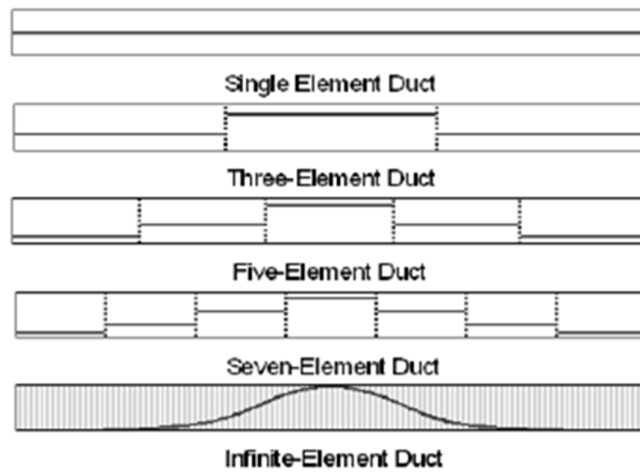


Figure 3.5 : Representation of varying sub-volume length.

The discretization and solution of the flow network can be accomplished by manual coding by using programming languages such as FORTRAN. However, due to intense coding effort, it would be standalone study just for modeling. In order focus more on control design, third party commercial Software package (WAVETM) has been used to form nonlinear high-fidelity engine model.

The general 1D model structure of the two stage turbocharged engine system consists of different components. We can analyze the components in 4 groups.

- Ducts, flow splits, junctions
- Engine Cylinders
- High Pressure and Low Pressure stage Turbochargers
- Actuator valve-orifices (TBV, CBV and WG)

3.2.2.1 Ducts, flow splits/Junctions

Ducts are the main components for modeling of pipe network. Flow is considered in one directional due to the reasons outlined in section 3.2.3 with varying or constant diameter at beginning and ends. Discretization length is also defined during modeling for solver. The cross section of the pipe can be calculated either rectangular or circular depending on the real component design. WAVETM includes the parameters for heat transfer multipliers, friction multipliers and pressure loss coefficients, which affects the fluid flow across straight pipe. During this study all ducts are modeled as circular ducts with constant diameter therefore relations for rectangular ducts are not mentioned.

The friction occurred inside duct is due to the viscosity of gas mixture. Gas mixture includes fresh air, combustion products and fuel vapor. Heywood, 1988 derived the viscosity of the aforementioned combustion products as shown in (3.17).

$$\mu_{comb} = \frac{\mu_{air}}{1 + 0.027\phi} \quad (3.17)$$

Where ϕ is the fuel/air equivalence ratio. By using (3.17), total viscosity of the gas mixture can be calculated by taking into account of mass ratios of the mixture.

$$\mu = (r_{air} + r_{fvap})\mu_{air} + r_{comb}\mu_{comb} \quad (3.18)$$

The friction coefficient C_f is calculated as shown in (3.19) and (3.20). One need to note that, the friction is changing according to the flow characteristics (laminar or turbulent).

For Laminar flow;

$$\frac{C_f}{2} = \frac{4}{Re} \quad (3.19)$$

For turbulent flow where;

$$\frac{C_f}{2} = 0.027Re^{-0.25} \quad (3.20)$$

Where Re is the Reynolds number.

The roughness due to material characteristics used in duct design is important, as it would result in friction in turbulent flows. As mentioned in Swamee and Jain, 1976, the effect of roughness can be expressed as shown in (3.21).

$$C_{rough} = \left(\frac{\log \frac{5.74}{Re^{0.9}}}{\log \left(\frac{\epsilon}{3.7} + \frac{5.74}{Re^{0.9}} \right)} \right)^2 \quad (3.21)$$

Where ϵ is the surface roughness changing according to material. Because of (3.21), we can modify the friction coefficient for turbulent flow as shown in (3.22).

$$\left(\frac{C_f}{2} \right)_{rough} = C_{rough} \left(\frac{C_f}{2} \right) \quad (3.22)$$

As mentioned in Ricardo Wave, 2013, the heat transfer effects is calculated via the empirical relation shown in (3.23).

$$h_g = \frac{C_f}{2} \rho U c_p Pr^{-\frac{2}{3}} \quad (3.23)$$

Where Pr is the Prandtl number, c_p is the gas heat capacity, U is the gas velocity.

In order to take into account of dimensional nonuniformity of the real engine ducts, pressure losses should be modeled as well. Those pressure losses can be occurred due to irregular cross sections or increasing-decreasing pipe diameter or bends (Renberg, 2008). The Pressure loss is defined as dimensionless pressure loss shown in (3.24).

$$C_p = \frac{P_{us} - P_{ds}}{0.5 \rho_{us} U_{us}^2} \quad (3.24)$$

Flow junctions or splits are used to model the flow elements, which has several opening to several ducts. They are simulating the Y-T junctions in the engine systems. As mentioned in section 3.2.3, again, scalar variables are calculated at the center but conservation of momentum needs to be solved separately in each flow opening. Wall friction and heat transfer effects are calculated similar to circular ducts as mentioned above. During modeling of two-stage turbocharged system, all

the air-intake and exhaust system hoses, pipes are modeled as ducts. In addition, Intake and Exhaust manifolds, Intercooler and EGR coolers as well as cavities like Air filter are modeled as Flow splits.

3.2.2.2 Engine cylinders

Cylinders are modeled to accommodate the combustion dynamics. Due to high nonlinear and complex behavior of combustion, some level of simplification needs to be done. The cylinder model should represent the energy release at the end of the combustion event. Conservation of mass is used to model changes in in-cylinder mass due to flow through valves and products of combustion (Heywood, 1988).. Using first law of thermodynamics, we can write the relationship between in-cylinder internal energy, the sum of enthalpy fluxes in and out of chamber and heat transfer as shown in (3.25).

$$\Delta U = \sum_{i=1}^{n_{valves}} m_i h_i - Q_{ht} + \Delta W \quad (3.25)$$

WAVETM includes the various inputs and parameters for combustion modeling, namely from scavenging effect to burned/unburned combustion phenomenon. Due to the content of this study, we will go into the details of combustion modeling.

3.2.2.3 Orifices, valves and actuators

Orifices are mainly the volume less boundary elements between two ducts. As gas flow from one duct to another, as the cross sectional area changes, one need to modify the area change by a discharge coefficient which is the ratio of effective are of orifice to geometrical area. This phenomenon is shown in Figure 3.6.

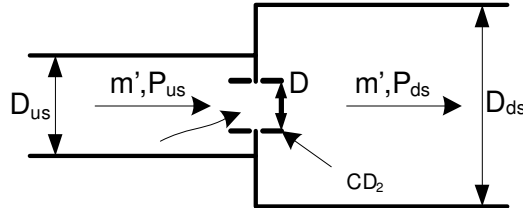


Figure 3.6 : Discharge coefficients for orifice junction.

Similar to orifices, valves are represented as orifices with variable area. Valves are placed in between two ducts. The valve models can be either passive or active.

Passive valve characteristics and opening are modeled by using pressure and flow dynamics for example one-way check valve. On the other hand, active valve behavior are modeled as actuator valve in which the valve motion is defined by electrical or pneumatic actuator. WAVETM includes 2 different valve models. Inline valve models are mostly used to model check ball valves or reed valves. Throttle valves are used to model butterfly type valves.

Inline valves are modeled as spring-mass-damper element, which is responding against pressure ratio across the valve. Effective flow area, which is a function of valve lift, is controlling the total flow across the valve.

The spring preload distance can be defined as shown in (3.26).

$$X_{pre} = \frac{\left(\Delta P \cdot ARD \cdot \frac{\pi D^2}{4} \right)}{k} \quad (3.26)$$

Where ΔP is the pressure difference across the valve which is needed to close the valve, ARD is the valve multiplier in the relevant direction, D is the valve reference diameter, k is the valve spring constant.

Valve's effective mass is required to model valve as spring-mass-damper element. As valve is modeled as elastic element, we can use the formula of free oscillations at natural frequency.

$$\omega = \sqrt{\frac{k}{m}} \quad (3.27)$$

Here, ω is the natural frequency of the valve, m is the effective mass.

The force acting on the valve as result of pressure ratio can be shown as (3.28).

$$F = \Delta P \cdot ARD \cdot \frac{\pi D^2}{4} \quad (3.28)$$

During the modeling of the two-stage turbocharged system, as shown in Figure 3.1, three valves are modeled. Compressor Bypass Valve (CBV), which is a one-way check valve, is modeled as passive inline valve.

On the other hand, TBV and WG are modeled as active valve in which the effective area of the valve is determined by electro pneumatic actuator. Electropneumatic actuators consist of vacuum valves and solenoid actuators..

3.2.2.4 Turbochargers (High/low pressure stages)

In 1D modeling scheme, modeling of turbochargers are handled by orifice junction elements which has no volume but effect on the flow conditions. In other words, compressor and turbine units are adding or subtracting the energy from the gas as the gas crosses the orifice junction. Those junction elements are connected each other via turbo-shaft element which represents the energy flow between compressor and turbine therefore the dynamics of the turbocharger unit. Generally, turbine and compressor are modeled by parameters, which are based on turbocharger performance data in which steady-state flow conditions are used in gas stand with moderate temperature (Renberg, 2007).

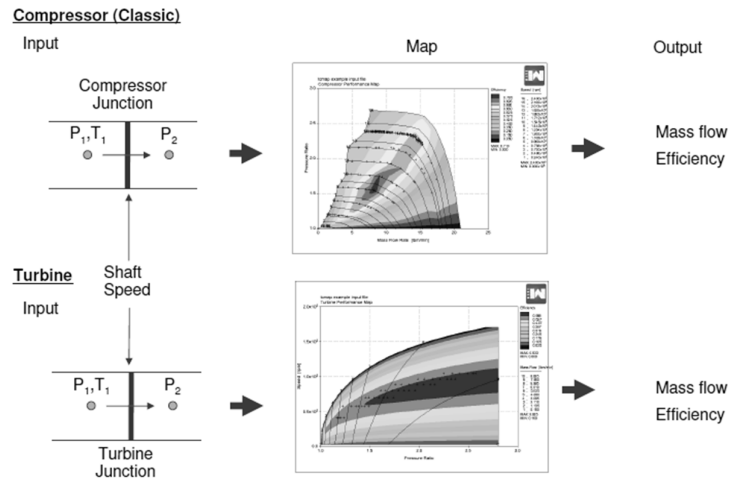


Figure 3.7 : Compressor and turbine 1D modeling methodology.

Figure 3.7 shows the methodology of 1D turbocharger modeling. Compressor and turbine are modeled as volume less junctions and with performance maps entered as inputs. Mass flow and efficiencies are the main outputs from sub-models.

Turbocharger manufacturers usually provide performance maps. They include different operating points in which compressor and turbine are subjected to varying mass flow rate, pressures, temperatures and turbocharger rotational speed. Map data does not include every point in engine operating points. As mentioned by Moraal and Kolmanovsky, 1999, turbocharger characteristics are mostly mapped to points

where the turbocharger speeds and pressure ratios are relatively higher. Figure 3.8 includes the steady state engine mapping data and the compressor performance map for Low Pressure stage turbocharger of two stage-turbocharged system.

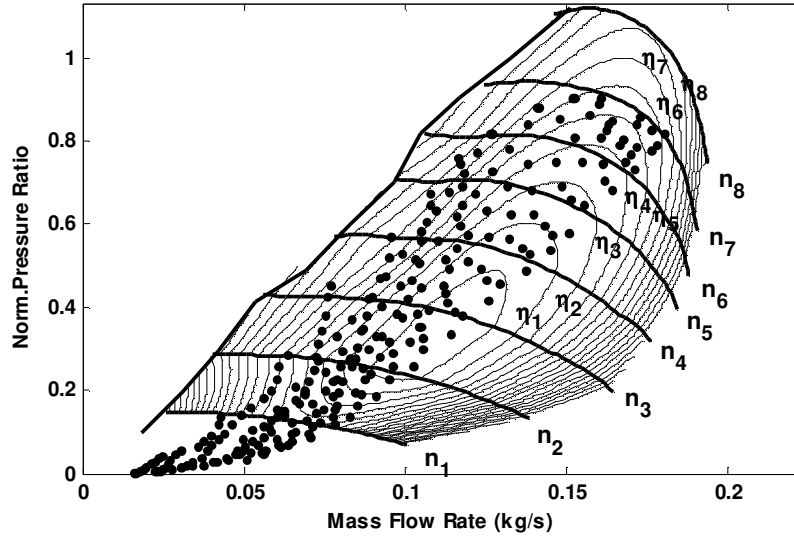


Figure 3.8 : Compressor performance map and measured engine data (black dots: Measured engine data, dashed contours: performance map).

It is clear that there are some operating points, which are not covered by turbocharger performance maps. Standard interpolation methods are not effective to use as they produce unacceptable performance during simulations. We have already mentioned about the curve fitting methods in section 3.2.2.

The turbocharger shaft is modeled as rigid body, which has its own rotational inertia. As mentioned in Hiereth and Prenninger (2007), the angular velocity of the shaft is defined as a power balance between compressor and turbine as shown in (3.8).

During modeling of compressors, two basic performance maps are used. First map shows the dimensionless mass flow as function of dimensionless shaft speed and compressor pressure ratio. Efficiency as function of pressure ratio and dimensionless speed is used in second map. (3.29) and (3.30) are used

$$N^* = \frac{(\pi N D_{ref})}{30 \sqrt{RT_{us}}} \quad (3.29)$$

$$\dot{m}^* = \frac{\dot{m} \sqrt{RT_{us}}}{P_{us} D_{ref}^2} \quad (3.30)$$

Pressure ratio and dimensionless speed is calculated in each time step. Interpolation is carried out to calculate dimensionless mass flow and efficiency from the maps.

In order to model compressor surge, the model suggested by Greitzer, 1976 is used. Compressor surge behavior is predicted by assuming a system consisting of a compressor discharging into a manifold. There are 2 components: first one is the planar rotor element and the second one is output duct with length L and cross sectional area A . With the help of conservation of momentum as shown in (3.31), we can derive the change of mass flow rate.

$$\frac{d\dot{m}}{dt} = \frac{A}{L} (P_{dsr} - P_{ds}) = \frac{A}{L} \left(PR - \frac{P_{ds}}{P_{usr}} \right) \quad (3.31)$$

Where P_{dsr} is the pressure at rotor outlet, P_{ds} is the pressure at the compressor outlet and P_{usr} is the pressure at rotor inlet. $\frac{A}{L}$ is the compressor inductance. Compressor inductance affects the surge stability of the compressor. As it increases, surge ability is decreased. As the compressor inductance increases, pulsations in the mass flow through the compressor will also decrease (Ricardo Wave, 2013).

As mentioned above, when the operating points exceeds the boundary of compressor performance maps, there should be special extrapolation routines apply. Below is the method that is used to apply to compressor performance maps when using WAVE™.

- When the angular velocity of the turbocharger shaft (N) exceeds the maximum velocity (N_{max}) defined in compressor map, the value is not extrapolated and maximum velocity curve will be used.
- When the pressure ratio (Γ) is smaller than 1, the functions shown in (3.32) will be used to extrapolate pressure ratio vs. mass flow curves.

$$\dot{m} = \dot{m}^* + \alpha(1 - e^{\beta(\Gamma-1)}) \quad (3.32)$$

Where \dot{m}^* is the mass flow when $\Gamma = 1$, β is taken empirically as 10.01, Γ is the pressure ratio.

When the compressor efficiency is equal to 0 if $\Gamma = 1$, then enthalpy rise will be extrapolated using the following equation;

$$\Delta h^* = \left(\Gamma^{\frac{\gamma-1}{\gamma}} - 1 \right) + \Delta h_0^* \quad (3.33)$$

$$\Delta h_0^* = \frac{\Delta h_0}{C_p T_i} = \frac{\gamma - 1}{\gamma} \frac{1}{\frac{d\eta}{d\Gamma_0}} \quad (3.34)$$

Where γ is the ratio of specific heats and η is the compressor efficiency.

- If the efficiency is greater than 0 when $\Gamma = 1$, then (3.35) will be used for extrapolation;

$$\Delta h^* = \left(\Gamma^{\frac{\gamma-1}{\gamma}} - 1 \right) \eta_0 \quad (3.35)$$

Similar to compressor modeling, performance maps are used to model turbine characteristics. There are basically two maps; first one representing the dimensionless mass flow as a function of pressure ratio and Blade Speed Ratio (BSR), and the second one representing efficiency as a function of pressure ratio and BSR. Performance maps and BSR can be defined as shown in (3.36), (3.37) and (3.38) respectively.

$$BSR = \frac{\pi D_{ref} N}{60 \sqrt{2 C_p T_{us} \left(1 - \left(\frac{P_{us}}{P_{ds}} \right)^{\frac{1-\gamma}{\gamma}} \right)}} \quad (3.36)$$

$$\dot{m}^* = \frac{\dot{m} \sqrt{R T_{us}}}{P_{us} D_{ref}^2} \quad (3.37)$$

$$\tau^* = \frac{\eta_t}{BSR} \sqrt{\frac{1}{8}} \quad (3.38)$$

When the operating points exceed the boundary of turbine performance maps, there should be special extrapolation routines apply. Below is the method that is used to apply to compressor performance maps when using WAVE™.

- BSR is substituted as 0 if the real value is smaller than zero. When BSR is zero, then the efficiency would be zero as well. This would result in no turbine power.

- During turbine operation, if the levels of pulsations are high, then there might an excessive increase in the turbine speed. This would name as “runaway” speed in which turbine produce no power. In this case, the efficiency is linearly extrapolated beyond BSR_{max} as shown in Figure 3.9.

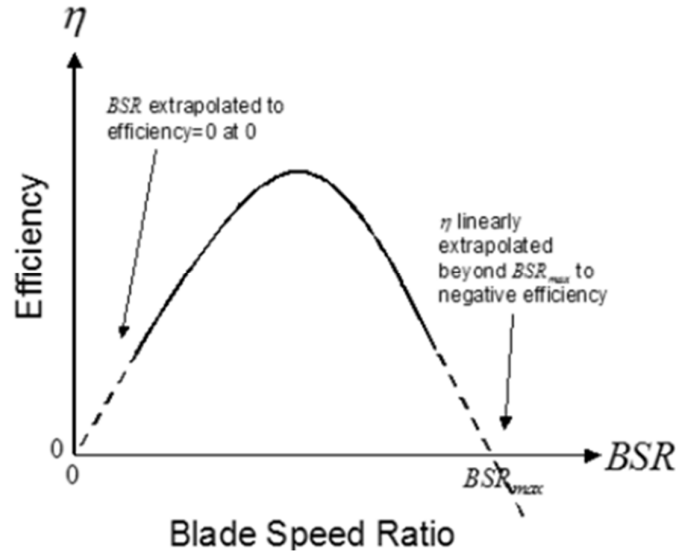


Figure 3.9 : Extrapolation of turbine efficiency vs. BSR.

3.3 1D Engine Model Calibration and Validation

The first part of this section includes the calibration of the model and input data requirements. Second part includes the validation results for steady state (stationary) and transient measurements with WAVE™ 1D engine model output. All of the steady state and transient measurements were performed in Ford Otosan Engine Testing facility.

During calibration and validation of the 1D engine model following assumptions has been made.

- Exhaust Gas Recirculation (EGR) valve is completely closed.
- Emissions model is not included as the primary focus is to control the boost pressure.
- Pilot injections and post injections are assumed to be zero. This is due to the fact that main injection has a main torque generating capability
- The flow content through the duct is assumed fresh air only. Amount of burned gas is assumed zero.

3.3.1 Measurements

Both for validation and calibration of the model stationary and transient measurements are required. Stationary measurements have been performed on an engine dyno with the specific test called, “fuel loop” testing. All of the engines operating points including part load points are scanned during fuel loop testing. During the tests, there were 390 operating points, which consists of two consecutive fuel loop tests. Measurement value is recorded after 30 seconds is elapsed at each operating to cover steady state behavior of the engine. This means engine speed and indicated torque values should be fixed to constant values to observe the steady state intake and exhaust temperatures, turbocharger speeds and pressures. Stationary points include the operating points in which New European Drive Cycle is operated as well (NEDC). The engine is equipped with thermocouples and instrumented pressure sensors for model validation. Table 3.1 includes the list of instrumentation signals required for measurement.

Table 3.1 : Measurement signals from instrumentation and ECU.

Signal	Source-Type	Unit
LP compressor upstream temperature	Instrumentation Thermocouple K – Type (max 1000 °C)	°C
LP compressor downstream temperature	Instrumentation Thermocouple K – Type (max 1000 °C)	°C
HP compressor upstream temperature	Instrumentation Thermocouple K – Type (max 1000 °C)	°C
HP compressor downstream temperature	Instrumentation Thermocouple K – Type (max 1000 °C)	°C
LP compressor upstream pressure	Instrumentation 0-4bar (gauge)	Pa
LP compressor downstream pressure	Instrumentation 0-4bar (gauge)	Pa
HP compressor upstream pressure	Instrumentation 0-4bar (gauge)	Pa
HP compressor downstream pressure	Instrumentation 0-4bar (gauge)	Pa
Mass air flow	Dyno ABB SensyFlow measurement	kg/h

LP turbine upstream temperature	Instrumentation Thermocouple K – Type (max 1000 °C)	°C
LP turbine downstream temperature	Instrumentation Thermocouple K – Type (max 1000 °C)	°C
HP turbine upstream temperature	Instrumentation Thermocouple K – Type (max 1000 °C)	°C
HP turbine downstream temperature	Instrumentation Thermocouple K – Type (max 1000 °C)	°C
LP turbine upstream pressure	Instrumentation 0-4bar (gauge)	Pa
LP turbine downstream pressure	Instrumentation 0-4bar (gauge)	Pa
HP turbine upstream pressure	Instrumentation 0-4bar (gauge)	Pa
HP turbine downstream pressure	Instrumentation 0-4bar (gauge)	Pa
LP turbine speed	Instrumentation Hall effect	Rpm
HP turbine speed	Instrumentation Hall effect	Rpm

Pressure and temperature sensor instrumentation were performed separately on the engine. Turbocharger supplier has done the turbine speed instrumentation, which is coming as built-in with turbo units.

Figure 3.10 shows the stationary tests point on brake torque axis and data points. The y-axis has been normalized for confidentiality reasons. As stated above full load, curve and part load curves are scanned during fuel loop testing.

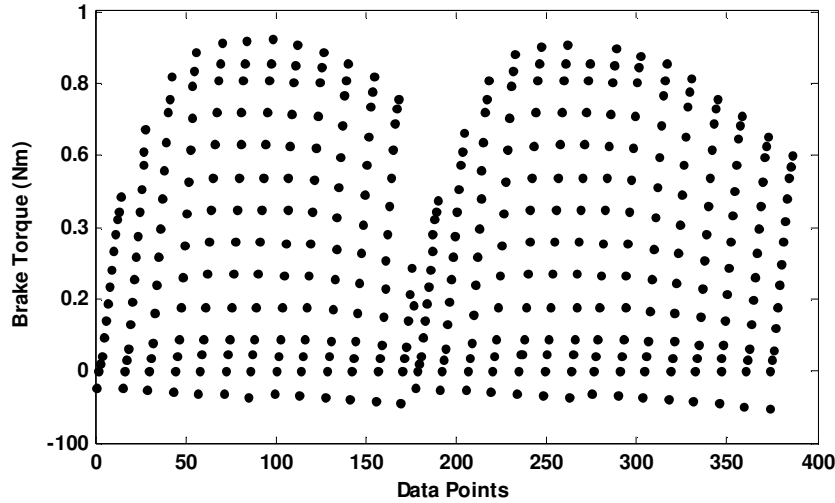


Figure 3.10 : Stationary measurement operating points.

Transient measurements were performed as applied load steps at constant engine speeds. Engine speeds are selected as 1500 rpm and 2000 rpm so as to capture the low-end torque dynamics of engine and turbocharger acceleration. This simulates the real world operation of ECU. In conventional engine control systems, fuel and air set points are given together in order to optimize the combustion process. The cycle consists of three sections.

- Small steps: Applied load steps are in the range of $\pm 10\%$ in order to simulate disturbances which would occur in small amplitudes.
- Medium steps: Applied load steps are in the range of $\pm 20\%$.
- Large steps: Applied load steps are in the range of $\pm 50\%$ in order to capture the turbocharger dynamics during high boost pressure set points close to full load torque demand which occurred especially during vehicle launch and sudden acceleration.

As load is applied through engine dynos, it is impossible to apply delay-free step signal. Therefore, step signal is approximated as ramp signal in which the ramp time is 2 seconds. In order to capture settling times, the final value of the step signal is taken as 15 seconds.

Transient cycle is also used in validation of System Identification based control-oriented model.

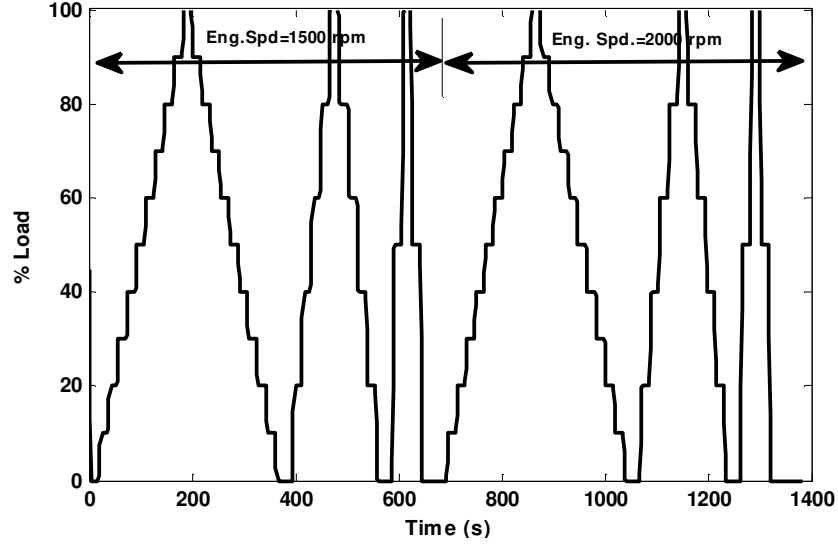


Figure 3.11 : Transient measurement operating points.

3.3.2 1D Model Calibration

During 1D engine modeling, data is required to structure the model itself. Engine data consists of dimensions and material properties of engine components, turbocharger performance maps and valve- actuator's maximum and minimum opening diameter&areas. Due to using 1D modeling principles shown in Section 3.2, the level of parameterization and calibration is not as much as MVEM grey box models.

WAVETM includes exhaustive list of input data requirements but most of the data is not required in this study due the fact that main focus is engine control purpose. Table 3.2 includes the critical 1D model data requirements.

Main inputs to the 1D model are shown in (3.39). This is the combination of measured disturbances such as engine speed, n_{eng} , total amount of injected fuel, \dot{m}_{fuel} , start of main injection, θ_{soi} as well as the manipulated variables as TBV command, u_{hpt} , WG command, u_{lpt} .

$$U = [u_{hpt} \ u_{lpt} \ n_{eng} \ \dot{m}_{fuel} \ \theta_{soi}]^T \quad (3.39)$$

Each of the above inputs has contribution to main engine control loops. Start of injections and injected fuel mass are the main inputs fuelling thus triggering combustion event. On the other hand, TBV and WG valves control the manifold

pressure. As EGR and throttle affects the mass airflow to the engine, together with manifold pressure, they define the air set point for combustion and torque generation.

Table 3.2 : 1D engine model input data descriptions.

Data	Description
Geometrical inputs	CAD geometry of the pipes, manifolds, coolers.
Material properties	Wall thickness, conductivity, thermal inertia
Engine-Piston dimensions	Bore-Stroke-compression ratio, engine friction
Heat exchangers	Efficiency maps, pressure drop
Valves	Valve reference diameters, valve lift vs effective area, discharge coefficient

In order to increase the accuracy of the engine model, model parameters should be calibrated rather than imposing dynamometer measurements on the model directly. Methodology is the tune parameters critical sub-components with steady state measurements. Below are the lists of tuned sub-components.

- Engine core system: Cylinders, Combustion event and heat release
- Intake and exhaust manifold junction
- Ducts between HP and LP compressors
- Duct between LP and HP turbines
- Heat exchangers
- Air Intake system
- Compressor and turbine

Engine core system consists of cylinders, intake and exhaust valves and combustion model. As shown in Figure 3.12, intake manifold pressure&temperature and exhaust manifold pressures (can be assumed as HP turbine inlet temperatures) are fed as inputs. Main output is the torque that is the product of combustion event. Engine torque is assumed brake torque, as friction and pumping losses are taken into account. In order to match engine output torque, cylinder pressure and exhaust flow rate, valve timing, start of combustion (SOC) and cylinder heat transfer multipliers are tuned.

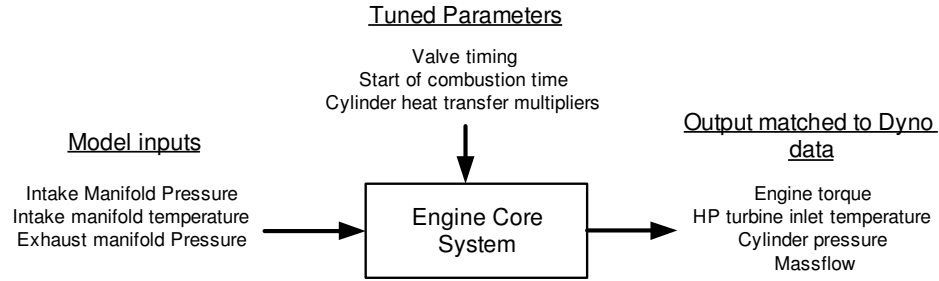


Figure 3.12 : Engine core system parametrization overview.

In each of the ducts, orifices and junctions, main characteristics variables are pressure drop, temperature and mass flow rate. As WAVE™ includes geometrical data, mostly duct models are fitted accurately in %5-10 accuracy band without further tuning. On the other mass flow rate based multipliers can be used to tune pressure drop in order to match with dyno measurement. Figure 3.13 shows the workflow for duct-junction parameterization.

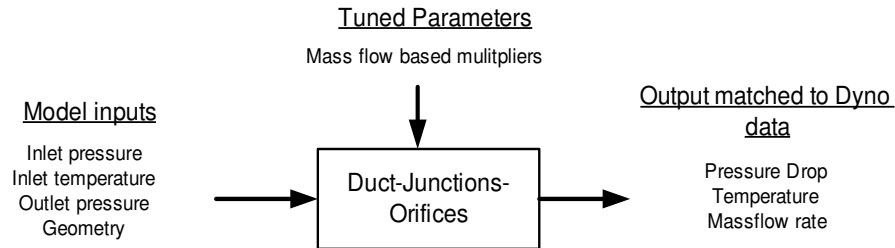


Figure 3.13 : Duct-Junction-orifices parametrization overview.

For heat exchangers such as EGR cooler and intercooler, heat transfer and friction loss multipliers are used to tune. These multipliers are tuned to match different pressure drops due to the 3D effects. Basically they are multiplying the calculate friction losses. During this study only intercooler model is tuned as EGR is assumed to be closed during turbocharger operation.

The last part of the tuning is the turbochargers. HP and LP turbocharger are connected separately. What follows is the procedure for LP compressor and turbine but same procedure applies to HP turbocharger as well. First LP compressor is added to the model, with LP compressor inlet pressure and temperature, LP turbine inlet pressure and shaft speed is applied to the LP compressor. WAVE™ options for compressor should be set as “Fixed compressor speed”. The aim is to match mass

flow across the compressor with steady state dyno measurement. Figure 3.14 shows the workflow.

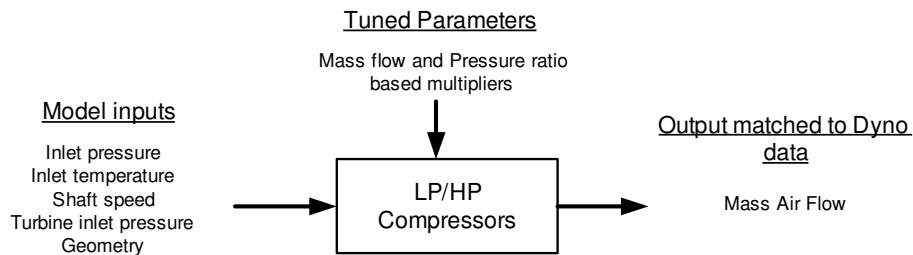


Figure 3.14 : LP/HP compressors parametrization overview.

Last part of the tuning procedure is to add LP and HP turbine to the engine model and close the loop. Turbine models are added to the exhaust system connected with compressor models via turbocharger shaft speed model.

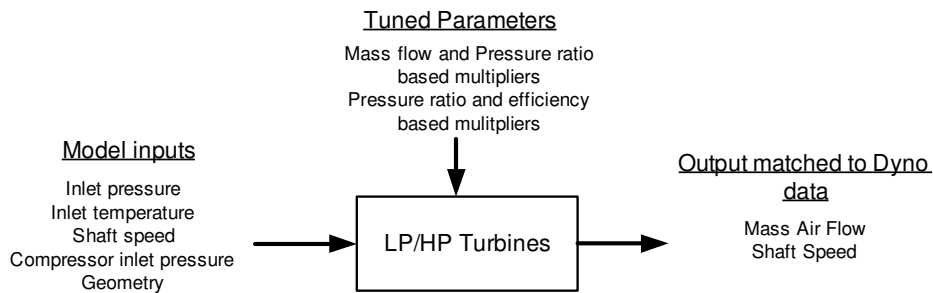


Figure 3.15 : LP/HP turbines parametrization overview.

Keep in mind that, until turbine mass flow matches with dyno measurements, shaft speed is hold at fixed speed. After a satisfactory accuracy level is achieved during turbine mass flow tuning, turbocharger speed is matched by imposing pressure ratio vs. efficiency multiplier. Figure 3.15 shows the basic workflow for LP/HP turbine tuning.

3.3.3 Model validation

As the model calibrated with steady state dyno measurements, complete engine model is simulated for both steady state and transient data. Model simulation has been performed by using WAVE RT[™] in SIMULINK[™]. Steady state measurements has been imposed on the model by feeding the inputs shown in (3.39). Each state input has been applied 20 samplings to simulate steady state conditions. During the

analysis of validation results, relative error, mean relative error and maximum relative error calculations are used in the form as shown in (3.40), (3.41) and (3.42).

$$Relative\ error = \frac{y_{meas}(i) - y_{mod}(i)}{y_{meas}(i)} \times 100 \quad (3.40)$$

$$Mean\ relative\ error = \frac{1}{N} \sum_{i=1}^N \frac{y_{meas}(i) - y_{mod}(i)}{y_{meas}(i)} \times 100 \quad (3.41)$$

$$Max.\ relative\ error = \max \left(\frac{y_{meas}(i) - y_{mod}(i)}{y_{meas}(i)} \right) \times 100 \quad (3.42)$$

The relative error calculation method suggested by Wahlström and Eriksson (2011) is not used here, as it would create inconsistent information about model accuracy. Figure 3.16 shows the validation results for brake torque. It has small absolute relative errors with a mean and absolute relative errors of %0.75 and %5.86.

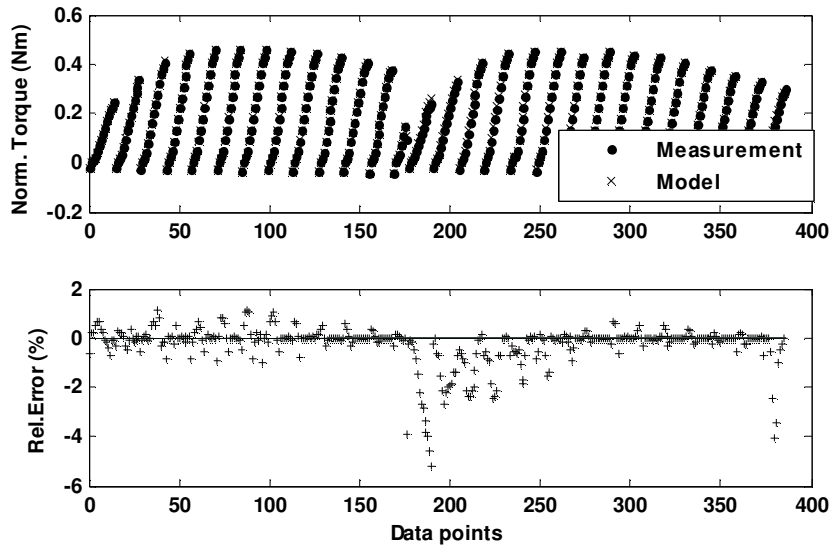


Figure 3.16 : Brake torque steady state validation result.

Intake manifold pressure validation result is shown in Figure 3.17. Mean and maximum absolute relative errors are %1.06 and %16 respectively. Maximum error occurs operating points in which turbocharger speed are relatively low. Compressor mass flow rate estimation accuracy is lower in those points that correspond to reduction in volumetric efficiency thus manifold pressure. On the other hand, during the operating points in which there are part load conditions, overall error of intake

manifold pressure is very small. This is critical in order to support validation test of intelligent boost pressure controller.

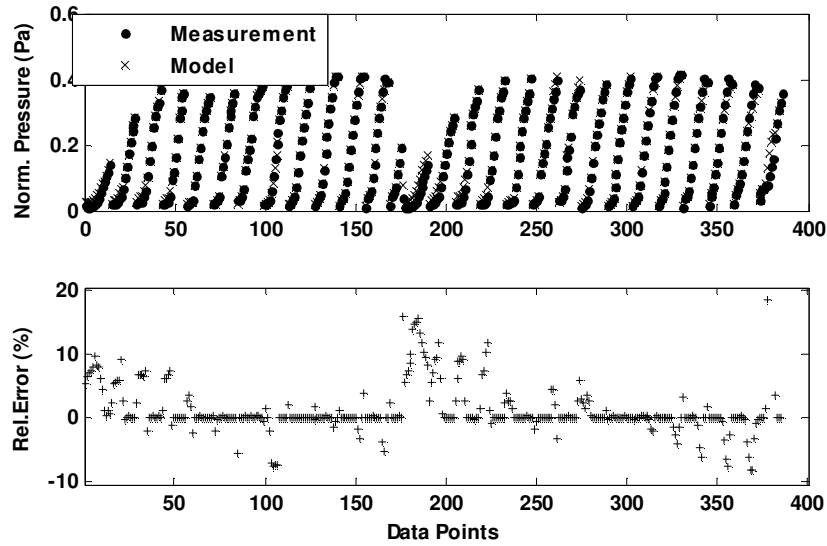


Figure 3.17 : Intake manifold pressure steady state validation result.

Figure 3.18 shows the validation results for mass airflow. Mean relative error is %4,56 and maximum relative error is %12. Mass airflow fit of model is inside +/- %5 accuracy band during part load region. Mass airflow model accuracy increases the overall accuracy of the engine model, as it is one of the main inputs to subcomponents of 1D engine model.

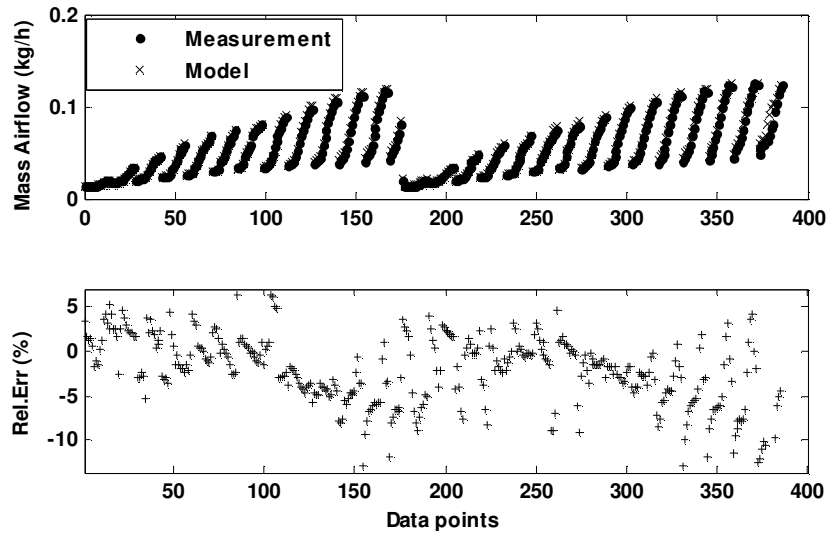


Figure 3.18 : Mass airflow steady state validation result.

Figure 3.19 shows the result of LP compressor outlet temperature vs. measurement data. Absolute relative mean error is %2.75 and maximum absolute relative error is %18. It is clear that the high modeling errors are inevitable during low load&speed conditions where the turbine&compressor efficiencies are extrapolated. On the other hand, during part load conditions, where the engine air flow requirements are matched with compressor delivery, compressor efficiencies are estimated accurately which results in accurate compressor outlet temperature (+/-%5).

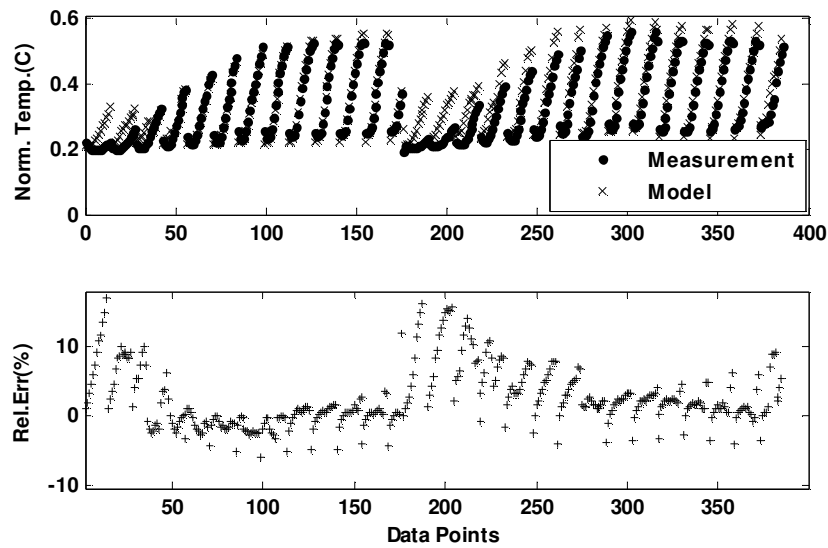


Figure 3.19 : LP compressor outlet temperature steady state validation result.

Figure 3.20 shows the validation result of HP turbine inlet pressure. This is mainly the exhaust manifold pressure, which is driving the HP turbine thus accelerating the turbocharger system. Absolute relative mean error is %2.34 and maximum absolute relative error is %12.3. It is visible that exhaust manifold pressure accuracy is getting worse during low load&speed section when mass air flow estimation is degraded. On the other hand, the contribution of this phenomenon is relatively low as during low load speed conditions, no boost pressure control is applied.

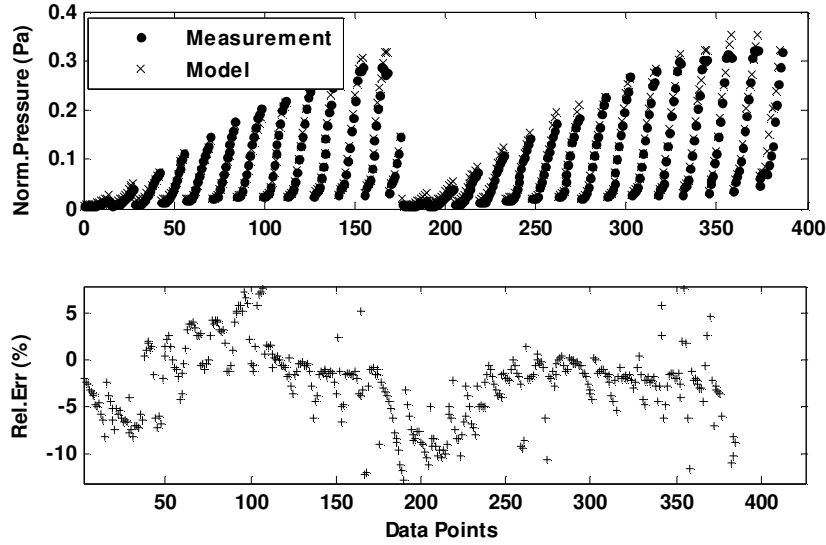


Figure 3.20 : HP turbine inlet pressure steady state validation result.

Remaining validation results for pressures and temperatures of turbine and compressors may be found at Appendix A.

In order to design and test successful controller, the engine model needs to capture essential dynamic behavior and nonlinear effects. Therefore, transient validation is must to ensure correct model behavior. During transient validation, small portion of transient cycle defined in section 3.3.1, has been used. This is due to capturing the engine operation points in which both WG and TBV are fully closed and mass flow are flowing across turbines. Throttle is assumed to be fully open and there is no EGR flow.

Figure 3.21 shows result of brake torque. Relative errors are small as absolute relative mean error is % 2.86 and absolute maximum relative error is % 4.82.

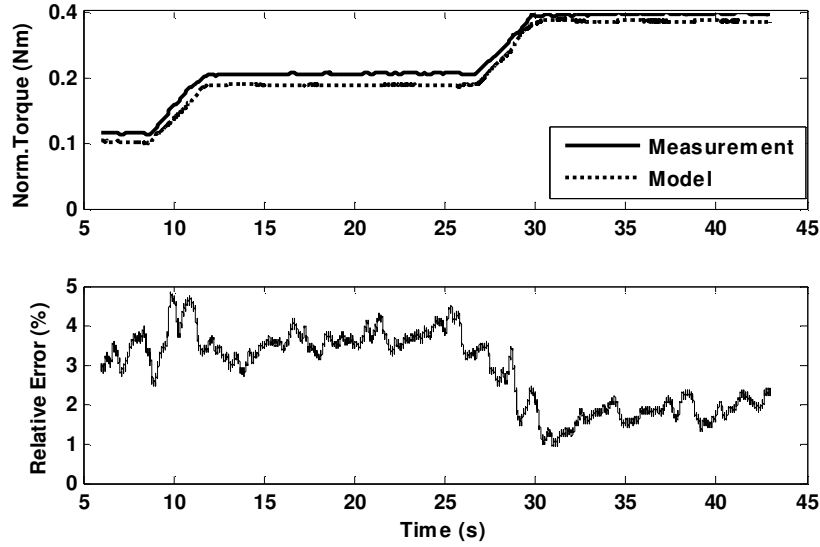


Figure 3.21 : Brake torque transient validation result.

Intake manifold pressure transient validation result is shown in Figure 3.22. It has absolute mean relative error of % 4.45 and maximum absolute relative error of % 6.64. It is essential to mention that model has steady state error, which can be prioritized as low because steady-state error can be eliminated by controller design.

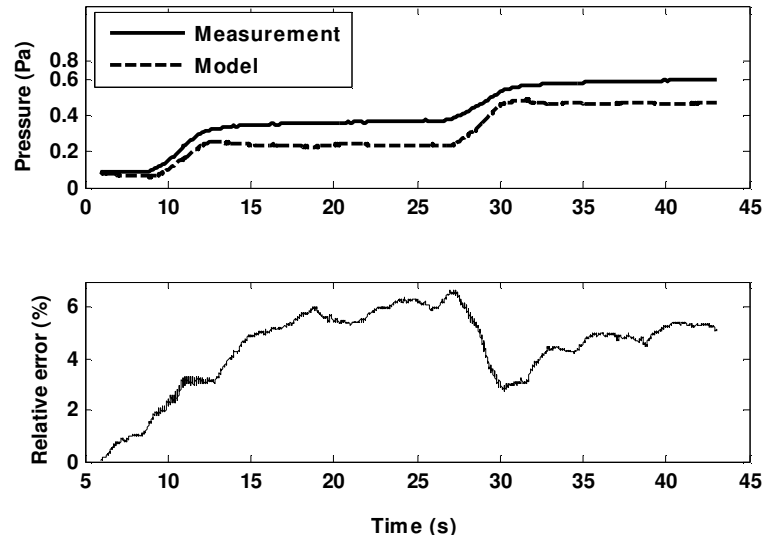


Figure 3.22 : Intake manifold pressure transient validation result.

In contrast to steady state validation, it will be worth mentioning about turbocharger shaft speed estimations. Figure 3.22 shows the turbocharger speed estimation for HP turbocharger. Absolute mean relative error is % 3.10, and maximum absolute relative error is % 4.44.

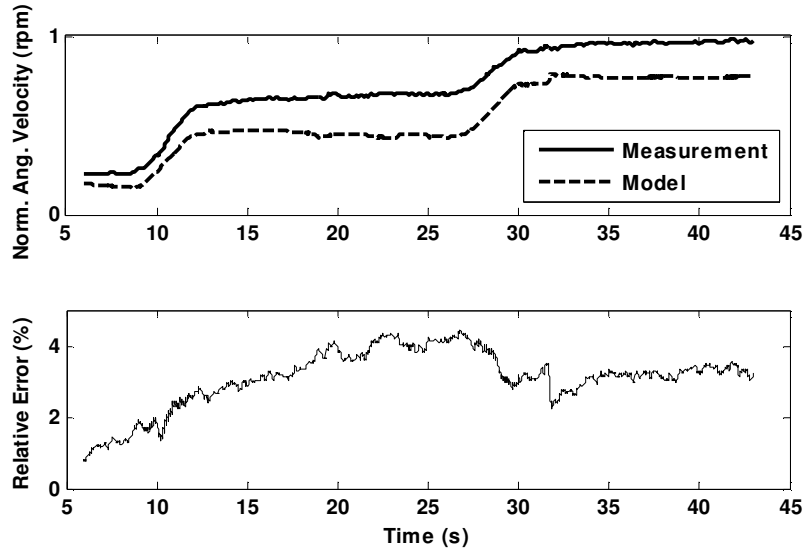


Figure 3.23 : HP turbocharger shaft speed transient validation result.

LP turbocharger speed validation result is shown in Figure 3.24. It has small relative errors such as absolute maximum relative error %7.3 and absolute mean relative error %2.85. Both of the HP and LP turbocharger speed models have mean errors below % 5 which means shaft balance and energy transfer model is accurate.

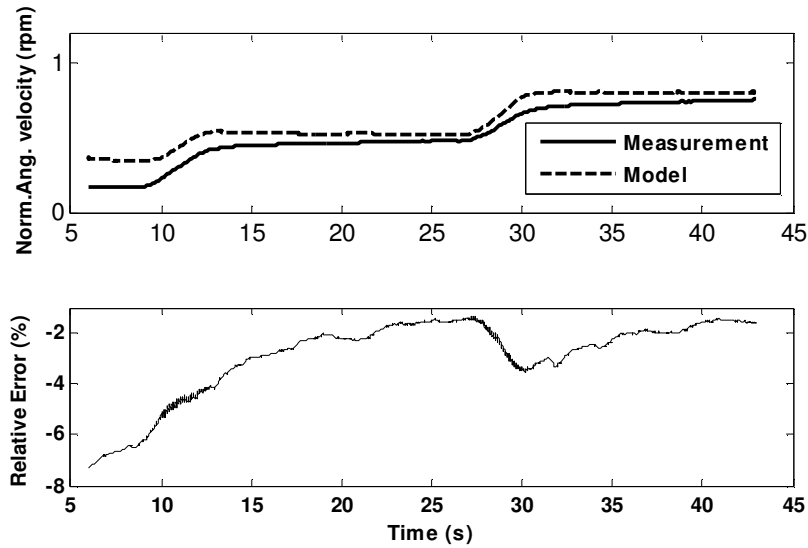


Figure 3.24 : LP turbocharger shaft speed transient validation result.

Figure 3.35 shows the validation of HP turbine outlet temperature model. It has mean absolute relative error of % 0.23 and maximum absolute relative error of % 1.82.

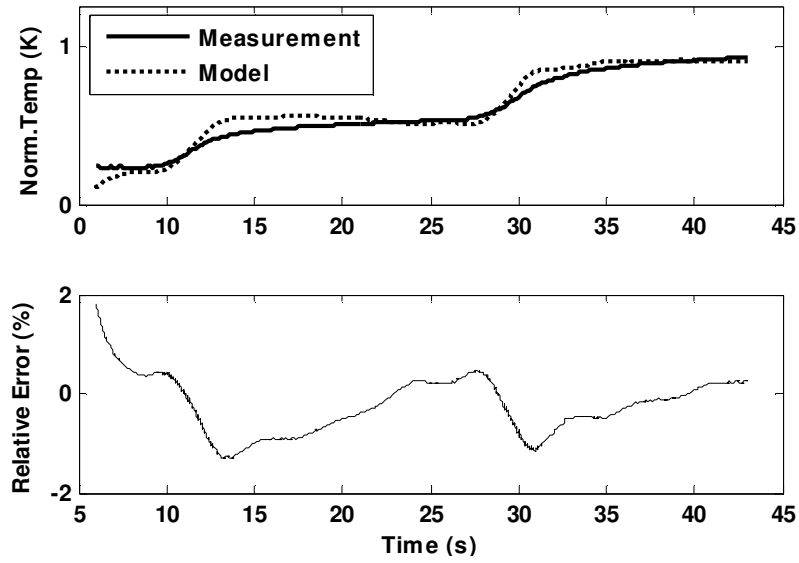


Figure 3.25 : HP turbine outlet temperature transient validation result.

3.4 Control-Oriented Model

In order to design linear control system, the controlled plant should be represented in linear system formulation. This can be achieved by 2 methods.

- Linearization of nonlinear Gray box models: Gray box models might be utilized to represent linear engine models for specific application (i.e. SI engine throttle control). On the other hand, Linearization of MVEM is cumbersome and tough that is not preferable in boost pressure controller design (Thomasson et.al, 2009). Therefore it is not preferred method for two stage turbocharged engine system
- Second method is to use black-box modeling scheme: In this case, linear system is identified by using input and output data. Unlike, gray box models, there is no physical relation of black-box model to real engine system but only mathematical relations (Houska et.al, 2012). Moreover, as mentioned by Isermann and Münchhof (2011), black-box model derivation can take shorter times, which would be less than theoretical, gray-box modeling method.

During this study, black box modeling methods has been chosen for controller design due to several reasons. First of all, number of states increased in two stage turbocharged system. There will be 2 more states included which are additional shaft speed and interstage pressure. Therefore degree of model will increase. Secondly,

nonlinear engine model is based on 1D engine modeling which is complex than MVEM but more accurate also. Due to the compromise made here, black box modeling is chosen as control oriented modeling method.

Generally, there are parametric and non-parametric methods used in system identification. Non-parametric methods are so-called data-based identification. Non-parametric methods are useful when the prior system knowledge is not clear but the data sets are in good quality. According to Keesman, 2011, model representation in this method is given by convolution integral shown in (3.43).

$$y(t) = \int_{-\infty}^t g(t - \tau)u(\tau)d\tau, \quad t \in \mathbb{R} \quad (3.43)$$

Please keep in mind that (3.40) is shown in continuous time domain. The discrete variant is shown in (3.44).

$$y(t) = \int_{k=-\infty}^t g(t - k)u(k), \quad t \in \mathbb{Z}^+ \quad (3.44)$$

Example model types as non-parametric models are step response models, impulse response models, Sine-wave models, frequency response models as well as correlation type models. Interested reader might look at Keesman, 2011, and Ljung, 1999.

LTI system identification in state-space form by using parametric methods is much more easier and convenient than using non-parametric data-based methods. There are number of parametric methods but during this study, Prediction Error Minimization (PEM) methods and Sub-Space identification methods are used due to being compatible with state-space identification. In either method, final form of the model is described in terms of state space realization shown in (3.45).

$$\begin{aligned} x(t + 1) &= Ax(t) + Bu(t) + Ke(t) \\ y(t) &= Cx(t) + e(t) \end{aligned} \quad (3.45)$$

3.4.1 Prediction error based system identification

There are many other advantages and drawbacks of using PEM as mentioned in Ljung, 2001.

- It is compatible with many model parameterization schemes (LTI models, Linear Regression models and nonlinear models)
- Asymptotic properties of PEM generated models are excellent.
- During data collection, there may be outputs, which is determined partially by inputs. Those systems can be handled directly in PEM.

To make an introduction to PEM based identification method, identification of dynamic system with least square method should be analyzed. In identification literature, Least square method is also called as linear regression or equation error method. Basic idea behind least squares method is to estimate the unknown parameters of a mathematical model by such a process that the sum of the squares of some chosen error is minimized. Assume a continuous mathematical model is given as (3.46).

$$y(t) = x_1(t)\theta_1 + x_2(t)\theta_2 + \dots + x_n(t)\theta_n \quad (3.46)$$

Where $y(t)$ is the output variable, θ_n is the parameter vector and x_n is the known functions. We can assume that measurements are made for N samples for time values corresponds to $t = 1, 2, 3, \dots, N$

By limiting the measurements by number of samples N , (3.46) can be simplified in matrix form as in (3.47) where Φ and θ shown in (3.48)

$$\mathbf{y} = \Phi \theta \quad (3.47)$$

$$\mathbf{y} = \begin{bmatrix} y(1) \\ y(2) \\ \vdots \\ y(N) \end{bmatrix}, \quad \Phi = \begin{bmatrix} x_1(1) & x_2(1) & \dots & x_n(1) \\ x_1(2) & x_2(2) & & x_n(2) \\ \vdots & \vdots & \ddots & \vdots \\ x_1(N) & x_2(N) & \dots & x_n(N) \end{bmatrix}, \quad \theta = \begin{bmatrix} \theta_1 \\ \theta_1 \\ \vdots \\ \theta_n \end{bmatrix} \quad (3.48)$$

By using matrix algebra when $\geq n$, the unique solution of (3.47) is;

$$\hat{\theta} = \Phi^{-1} \mathbf{y} \quad (3.49)$$

Where Φ^{-1} is the inverse of square matrix Φ and $\hat{\theta}$ corresponds to estimate of parameter vector, θ . Direct fit of data samples is not feasible due to high possibility of misfit. This can be caused by contaminated data or noise. Least square error method may eliminate the misfit.

Assume that an error is shown as in (3.50);

$$\varepsilon(t) = y(t) - \hat{y}(t) = y(t) - \varphi(t)\theta \quad (3.50)$$

Estimated parameter vector, $\hat{\theta}$ is chosen such that the loss function in (3.51) is minimized.

$$V_{LS} = \frac{1}{N} \sum_{t=1}^N \varepsilon(t)^2 = \frac{1}{N} \sum_{t=1}^N |y(t) - \varphi(t)\theta|^2 = \frac{1}{N} \varepsilon^T \varepsilon \quad (3.51)$$

Where error is represented as vector;

$$\varepsilon = \begin{bmatrix} \varepsilon(1) \\ \varepsilon(2) \\ \vdots \\ \varepsilon(N) \end{bmatrix} \quad (3.52)$$

In order to complete minimization process, loss function should be expressed in terms of Φ and θ

$$\begin{aligned} V_{LS} &= \frac{1}{N} (y - \Phi\theta)^T (y - \Phi\theta) \\ &= \frac{1}{N} [y^T y - \theta^T \Phi^T y - y^T \Phi \theta - \theta^T \Phi^T \Phi \theta] \end{aligned} \quad (3.53)$$

Minimization is taken place when first derivative of the loss function with respect to θ . Then the derivative is equalized to zero.

$$\left. \frac{\partial V_{LS}(\theta)}{\partial \theta} \right|_{\theta=\hat{\theta}} = \frac{1}{N} [-2\Phi^T y + 2\Phi^T \Phi \hat{\theta}] = 0 \quad (3.54)$$

The solution is given by in (3.55).

$$\Phi^T \Phi \hat{\theta} = \Phi^T y \quad (3.55)$$

Finally, one can derive the formulation for least square estimator of θ as shown in (3.56).

$$\hat{\theta} = [\Phi^T \Phi]^{-1} \Phi^T y \quad (3.56)$$

Least square estimation can easily be applied to transfer functions models such as, ARX, ARMAX, Output Error and Box-Jenkins models.

Consider an input and output relation of a discrete time system as shown in (3.57).

$$y(t) = \sum_{k=1}^{\infty} g(t)u(t-k), \quad t = 1, 2, \dots \quad (3.57)$$

We can introduce a forward shift operator q and unit delay operator accordingly q^{-1} .

$$qu(t) = u(t+1), \quad q^{-1}u(t) = u(t-1) \quad (3.58)$$

It is known that discrete time LTI system can be shown by employing zero-order hold as shown in (3.58).

$$\begin{aligned} y(t) + a_1 y(t-1) + \dots + a_{n_a} y(t-n_a) \\ = b_1 u(t-1) + \dots + b_{n_b} u(t-n_b) \end{aligned} \quad (3.59)$$

The representation is done by using the notation of difference equations where d is the delay of number of samples.

$$G(q) = \frac{b_1 q^{-1} + \dots + b_{n_b} q^{-n_b}}{1 + a_1 q^{-1} + \dots + a_{n_a} q^{-n_a}} q^d \quad (3.60)$$

(3.57) is the model of the form of impulse response, mainly non-parametric model. On the other hand, the representation in form of difference equations or transfer function as shown in (3.60), are called as a parametric models. One can derive the state-space realization of transfer function models.

$$\begin{aligned} x(t+1) &= Ax(t) + Bu(t) \\ y(t) &= Cx(t) + Du(t) \end{aligned} \quad (3.61)$$

As mentioned above least square methods can be applied to transfer function models, which are mainly equation error type models. However, before, introduction to equation-error type models should be made. Equation (3.59) can be extended by white noise error term $e(t)$ to derive general equation-error type model structure. Please note that in general equation-error model structure, moving average of error term is calculated.

$$\begin{aligned} y(t) + a_1 y(t-1) + \dots + a_{n_a} y(t-n_a) \\ = b_1 u(t-1) + \dots + b_{n_b} u(t-n_b) + e(t) \\ + c_1 e(t-1) + \dots + c_{n_c} e(t-n_c) \end{aligned} \quad (3.62)$$

Figure 3.25 shows the general structure of equation error model family. Model families are separated according to the existence of polynomial $A(q)$, $B(q)$ and $C(q)$. If the moving average is not taken into account then model structure is represented as shown in (3.63)

$$y(t) = \frac{B(q)}{A(q)} u(t) + \frac{1}{A(q)} e(t) \quad (3.63)$$

This model is called as ARX (Auto Regressive with eXogenous input). When the model family is represented as general structure as shown in (3.62), it is called as ARMAX (Auto Regressive with Moving Averaged eXogenous input). ARMAX model can be shown simply as in (3.64).

$$y(t) = \frac{B(q)}{A(q)} u(t) + \frac{C(q)}{A(q)} e(t) \quad (3.64)$$

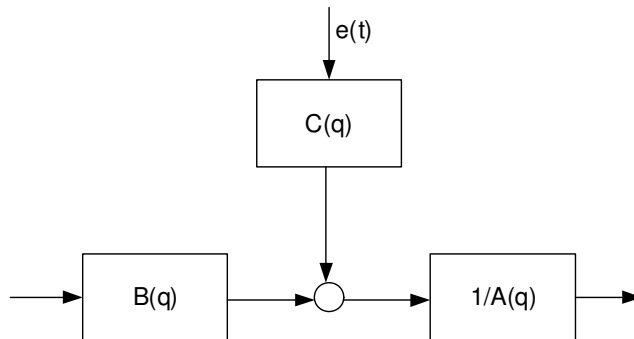


Figure 3.26 : Equation-error model family structure.

In case of models when the linear difference equation does not have errors but only measurement error exists, we have the following representation available.

$$\begin{aligned}\xi(t) + f_1\xi(t-1) + \dots + f_{n_f}\xi(t-n_f) \\ = b_1u(t-1) + \dots + b_{n_b}u(t-n_b) \\ y(t) = \xi(t) + e(t)\end{aligned}\tag{3.65}$$

Where $\xi(t)$ is the noise-free output. This model structure is called as output-error model which can simply represented as (3.66).

$$y(t) = \frac{B(q)}{F(q)}u(t) + e(t)\tag{3.66}$$

Similar to ARMAX model, if the moving average calculation is added to Output error structure then we will have Box-Jenkins model structure.

$$y(t) = \frac{B(q)}{F(q)}u(t) + \frac{C(q)}{D(q)}e(t)\tag{3.67}$$

Above equation can be summarized to simpler form to cover whole class of transfer function models. This generalized transfer function model is shown in (3.68). Please note that $G(q)$ and $H(q)$ are referred to rational transfer functions.

$$y(t) = G(q)u(t) + H(q)e(t)\tag{3.68}$$

Now we have completed the equation-error model structure, we can formularize the least squares estimation of equation error models.

First of all, rewriting the equation (3.59) will give below formulation.

$$\begin{aligned}y(t) = -a_1y(t-1) - \dots - a_{n_a}y(t-n_a) - b_1u(t-1) - \dots \\ - b_{n_b}u(t-n_b) + e(t) \\ y(t) = \varphi(t)\theta + e(t)\end{aligned}\tag{3.69}$$

Where $\varphi(t)$ is the data vector, which is taken from the measurement data.

$$\varphi(t) = [-y(t-1), \dots, -y(t-n_a), u(t-1), u(t-2), \dots, u(t-n_b)] \quad (3.70)$$

For $n_a \geq n_b$, elements of (3.69) will become as follows for N number of data samples;

$$\Phi = \begin{bmatrix} -y(n_a-1) & \dots & -y(0) & u(n_a-1) & \dots & u(n_a-n_b) \\ -y(n_a) & \dots & -y(1) & u(n_a) & \dots & u(n_a-n_b+1) \\ -y(n_a+1) & \dots & \vdots & \vdots & \vdots & \vdots \\ \vdots & \dots & \vdots & \vdots & \vdots & \vdots \\ -y(N-1) & \dots & -y(N-n_a) & u(N-1) & \dots & u(N-n_b) \end{bmatrix} \quad (3.71)$$

By using the loss function defined in (3.51), we will have;

$$V_{LS} = \sum_{t=n_a+1}^N \varepsilon(t)^2 = \sum_{t=n_a+1}^N |y(t) - \varphi(t)\theta|^2 \quad (3.72)$$

The estimation of parameters which minimized loss function in (3.72) is;

$$\hat{\theta} = [\Phi^T \Phi]^{-1} \Phi^T y = \left[\sum_{t=n_a+1}^N \varphi^T(t) \varphi(t) \right]^{-1} \left[\sum_{t=n_a+1}^N \varphi^T(t) y(t) \right] \quad (3.73)$$

This solution exists only if matrix shown in (3.74) is nonsingular;

$$\Phi^T \Phi = \sum_{t=n_a+1}^N \varphi^T(t) \varphi(t) \quad (3.74)$$

According to Zhu, 2001, the advantage of parametric identification by the least squares method, is the numerical simplicity. When the model order $[n_a \ n_b \ n_c]$ is correctly defined and the noise level is low, the minimization will eliminate misfit and convergence will be satisfactory. If the noise level increases, this will cause some accuracy problems especially in low and middle frequencies.

After constructing base information about equation-error/output-error models as well as least squares estimation, formulation for PEM can be derived.

Consider an ARX model as shown in (3.63). If equation error is neglected, the output at time t can be predicted both by using input $u(t)$ and output y at $t-1, t-2 \dots$. Thus, the equation error in (3.75) can be considered as one-step ahead prediction error.

$$e(t) = y(t) - \hat{y}(t|t-1) \quad (3.75)$$

By using the generalized transfer function model shown in (3.68), above expression can be modified.

$$y(t) = -H^{-1}(q)G(q)u(t) + H^{-1}(q)y(t) \quad (3.76)$$

The basis of the PEM method is to use the least squares algorithm to find the optimal parameter set that minimize the one-step ahead prediction error.

$$V_{LS} = \frac{1}{N} \sum_{t=1}^N \varepsilon(t)^2 = \frac{1}{N} \sum_{t=1}^N (D(q)[A(q)y(t) - B(q)u(t)])^2 \quad (3.77)$$

Figure 3.27 shows the block diagram for PEM method.

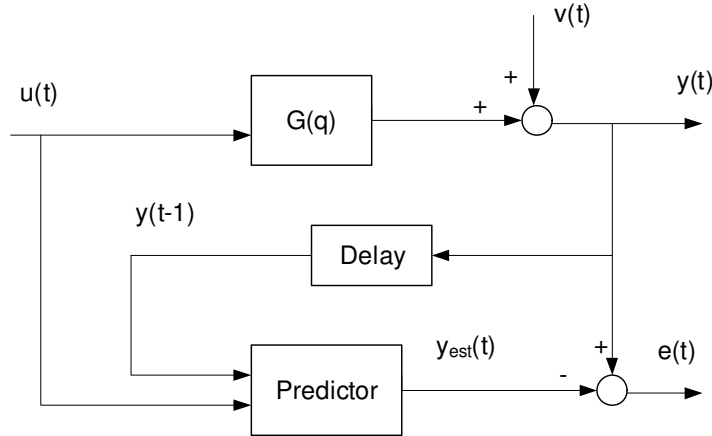


Figure 3.27 : LS method as Prediction error method.

3.4.2 Subspace system identification

Although PEM method is being developed for decades, there are some drawbacks. Main problem is the case of state-space systems where the system has multiple inputs and outputs. In this case PEM method's reliability poor especially for large system orders (Viberg, 1995).

In contrast, Subspace-based state-space system identification methods (4SID) result in numerically feasible solutions for state space identification. They are used to identify state-space models directly if input and output measurements are available only. As mentioned in Viberg, 1995, computational complexity is relatively low compared to PEM method especially when the number of inputs, outputs and states is large. There are several subspace identification methods in the literature, see Qin, 2006 for an overview and Haverkamp, 2001 for detailed formulations. In addition, Chiuso and Picci, 2005, mentioned the difference of PEM and 4SID methods in closed loop identification process. In this study N4SID (Numerical algorithms for Subspace State Space identification) and MOESP methods are used. What follows are the basic formulation and understanding of N4SID algorithm.

First of all, it should be mentioned that N4SID method is direct and non-iterative method compared to PEM. Basic idea is to derive minimal state-space realization of the system using noisy input-output data.

Assume that the system is represented by process form in discrete time as shown in (3.61) and (3.57). The aim is to determine the matrices A, B, C, and D by taking into account of the relation shown in (3.78)

$$g(t) = \begin{cases} 0 & t < 0 \\ D & t = 0 \\ CA^{t-1}B & t > 0 \end{cases} \quad (3.78)$$

Based on this relationship, the parameters A, B and C can be determined based on Hankel matrix representation.

$$H = \begin{bmatrix} g(1) & g(2) & \dots & g(n+1) \\ g(2) & g(3) & \dots & g(n+2) \\ \vdots & \vdots & \ddots & \vdots \\ g(n+1) & g(n+2) & \dots & g(2n+1) \end{bmatrix} \quad (3.79)$$

Hankel matrix can be expressed as the product of controllability and observability matrices as shown in (3.80). Γ is the observability matrix and Ω is the controllability matrix.

$$H = \Gamma_{n+1}\Omega_{n+1} \quad (3.80)$$

$$\Gamma_n = \begin{bmatrix} C \\ CA \\ \vdots \\ CA^{n-1} \end{bmatrix}$$

$$\Omega = [B \quad BA \quad \dots \quad A^{n-1}B]$$

Rank of the Hankel, observability and controllability matrices are n . The matrices B and C are cut out of observability and controllability matrices in such a way that upmost rows and leftmost columns of factors are resulting in. By using this property, we can further decompose the observability matrix with system matrix A .

$$\Gamma_{2:n+1} = \Gamma_{1:n}A \quad (3.81)$$

If the first and last rows of Γ_{n+1} are deleted, $\Gamma_{2:n+1}$ and $\Gamma_{1:n}$ are derived. By using the relationship in (3.81), finally we can express the A matrix in below form.

$$A = \Gamma_{1:n}^* \Gamma_{2:n+1} \quad (3.82)$$

The term $\Gamma_{1:n}^*$ is called as Moore-Pseudo-inverse of $\Gamma_{1:n}$. And it is basically defined as;

$$\Gamma_{1:n}^* = (\Gamma_{1:n}^T \Gamma_{1:n})^{-1} \Gamma_{1:n}^T \quad (3.83)$$

Above the system is defined in noiseless process form. If the system includes noisy inputs and outputs, the formulation will change. Consider an LTI system which has system noise term $w(t)$ added. System states are perturbed by the addition of noise term

$$\begin{aligned} x(t+1) &= Ax(t) + Bu^0(t) + w(t) \\ y^0(t) &= Cx(t) + Du^0(t) \end{aligned} \quad (3.84)$$

Where y^0 and u^0 are noise free input and output signals. Assume the input and output signals are perturbed by noise;

$$\begin{aligned} u(t) &= u^0(t) + z(t) \\ y(t) &= y^0(t) + v(t) \end{aligned} \quad (3.85)$$

Substituting (3.85) in (3.84) we will have;

$$\begin{aligned} x(t+1) &= Ax(t) + Bu^0(t) + Bz(t) + w(t) \\ y^0(t) &= Cx(t) + Du^0(t) + Dz(t) + v(t) \end{aligned} \quad (3.86)$$

It is clear that by substituting $Bz(t) + w(t)$ with $Ke(t)$ and $Dz(t) + v(t)$ with $e(t)$ we will have the state space realization in the form of (3.45). We can organize the output, input and error vector by length equals to $m-1$.

$$Y(t) = [y(t) \quad y(t+1) \quad \dots \quad y(t+m-1)] \quad (3.87)$$

$$U(t) = [u(t) \quad u(t+1) \quad \dots \quad u(t+m-1)] \quad (3.88)$$

$$E(t) = [e(t) \quad e(t+1) \quad \dots \quad e(t+m-1)] \quad (3.89)$$

$$Z(t) = [z(t) \quad z(t+1) \quad \dots \quad (t+m-1)] \quad (3.90)$$

Hankel matrix can be used to express output vector in the form shown in (3.91)

$$Y(t) = \Gamma_m x(t) + H_m^u U(t) - H_m^u Z(t) + H_m^e E(t) \quad (3.91)$$

$$\begin{aligned} \Gamma_n &= \begin{bmatrix} C \\ CA \\ \vdots \\ CA^{m-1} \end{bmatrix} \\ H_m^u &= \begin{bmatrix} D & 0 & \dots & 0 \\ CB & D & \dots & \vdots \\ \vdots & \vdots & \ddots & \vdots \\ CA^{m-2}B & CA^{m-3}B & \dots & D \end{bmatrix} \\ H_m^e &= \begin{bmatrix} 1 & 0 & \dots & 0 \\ CK & 1 & \dots & \vdots \\ \vdots & \vdots & \ddots & \vdots \\ CA^{m-2}K & CA^{m-3}K & \dots & 1 \end{bmatrix} \end{aligned} \quad (3.92)$$

3.4.3 Application

During the modeling process, workflow shown in Figure 3.28 has been followed. Isermann, 2011, recommends this process. System identification process should start with selection of appropriate input and output signals as well as planning of

experiments&data collection. This would result in the selection of manipulated variables (MV), measured disturbances (MD) and output variables(OV). Boost pressure is selected as only OV. Sensor noise and model-plant error is taken into account as unmeasured disturbances (UD). Manipulated variables are basically the process inputs which have the strong effect on the OV. In two stage turbocharged diesel engine application MV's would be TBV and WG. In this study, MD's are selected as injection quantity and engine speed as they can be measured but cannot be manipulated. As mentioned by Zhu, (2001), disturbance effect on the OV caused by MD are compensated by feedforward control. It will be mentioned further in section 4 that MD are treated internally during Model predictive control setup. (3.93) shows the structure of Linear time invariant model with MD and UD included.

$$\begin{aligned}x_{k+1} &= Ax_k + Bu_k + B_v v(t) + B_d d(t) \\y_k &= Cx_k + D_v v(t) + D_d d(t)\end{aligned}\tag{3.93}$$

Where $d(t)$ is the measured disturbances and $v(t)$ is the unmeasured disturbances expressed as;

$$v(t) = [n_{eng} \dot{m}_{fuel}]^T\tag{3.94}$$

States of the linear model need not be physically realizable variables as mentioned in Plianios and Stobart, (2008). They are linear combinations of several physical variables found in the system. States are selected by identifier in order to achieve optimum system performance and enable the system both controllable and observable.

After defining the signals, excitation test signal types should be assigned to each MV and MD to characterize the boost pressure dynamics of two stage turbocharged system. Here, it should be notes that signal waveform and power spectrum is important. In order to capture the high frequency dynamics of two-stage turbocharged system, Pseudo Random Binary Sequence (PRBS) signal has been used. PRBS test signal is recommended signal in the literature as they excite the dynamics of all frequencies uniformly, and relatively easy and safe to implement (Sung and Lee, 2003). The term pseudo refers to the fact that the PRBS signal is actually deterministic signal and its autocorrelation function is the same as a white

random noise. PRBS signal is applied for MVs where MDs are fixed constant but excited zero mean white noise only.

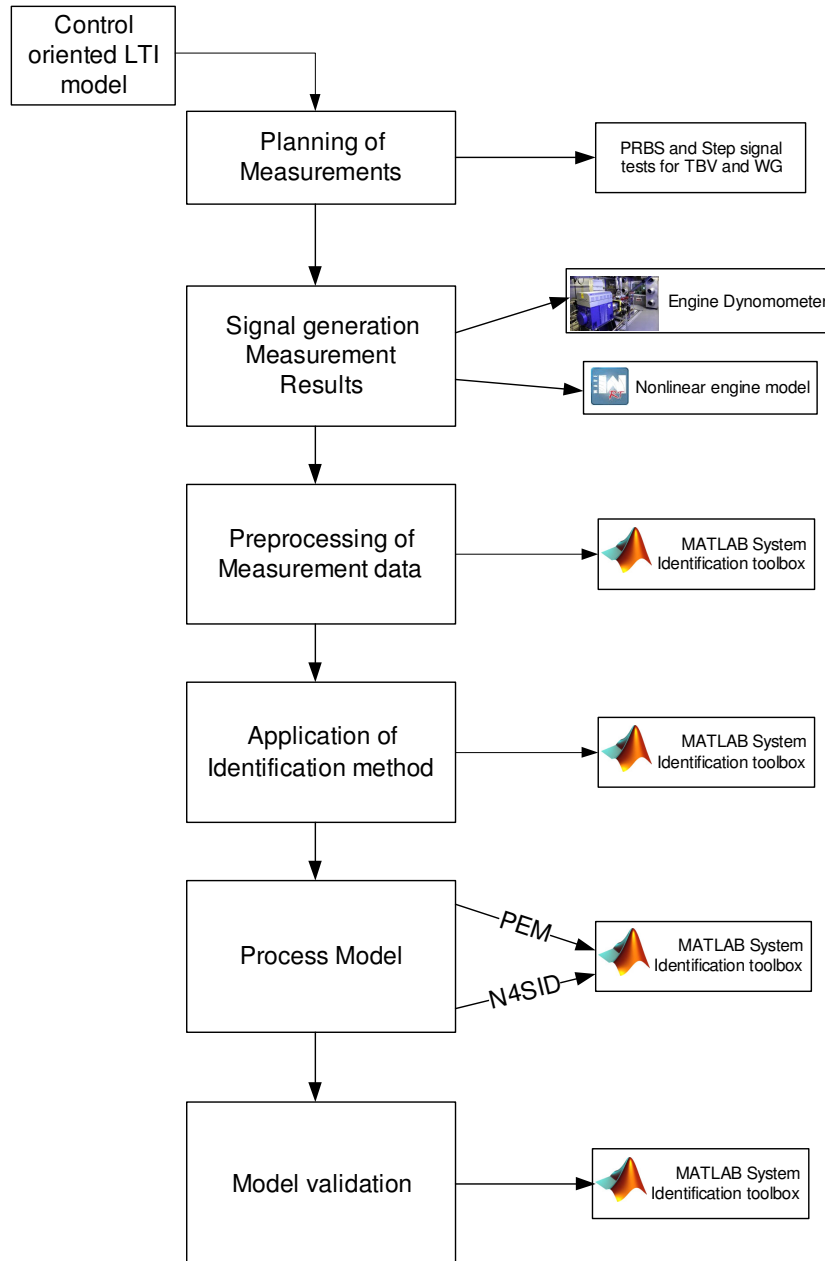


Figure 3.28 : System identification flow.

PRBS signal model is constructed in MATLAB. PRBS can be generated by using feedback shift register as shown in Figure 3.29. It is a two state signal. Here n means the number of registers. The registers are fed with 1 or 0. As the clock is triggered, The value of k^{th} state will equal to $(k+1)^{\text{th}}$ state and the first value determined by feedback path. The feedback coefficients will be equal to either 1 or 0. Hence, this

method will generate ones and zeros in sequence (Zhu, 2001). As the test signal sent directly to ECU drivers as PWM duty cycle, scaling has been applied as min %15 and Max %85.

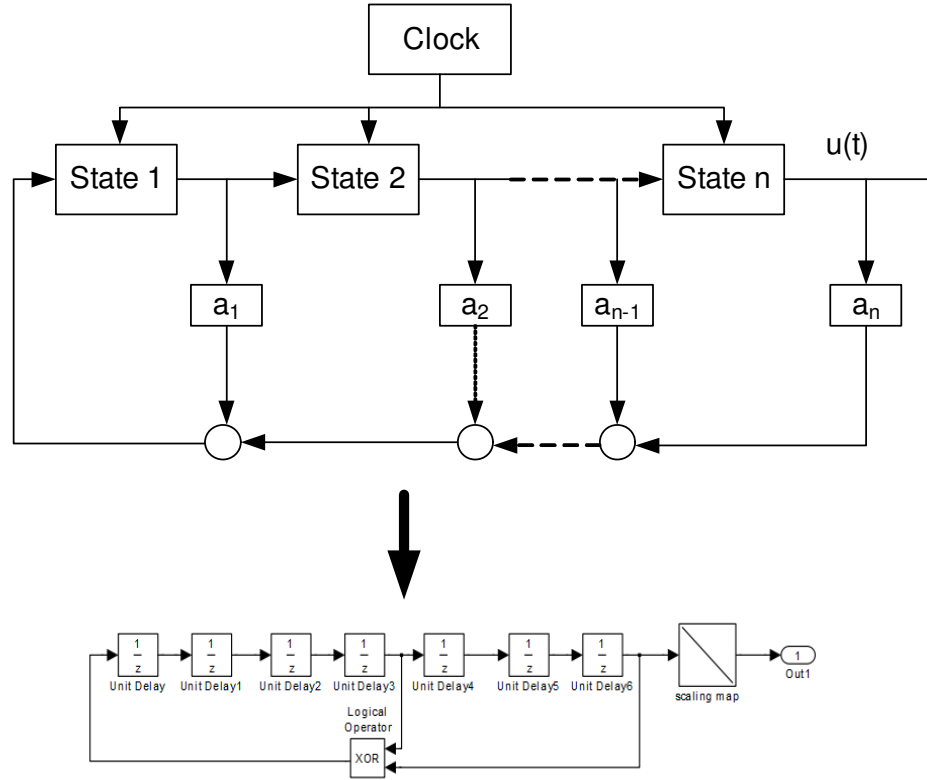


Figure 3.29 : PRBS test signal generation.

Identification test has been carried out engine dynamometer mainly by using API connection between MATLAB and ATI-VISION as shown in Figure 3.29. Calculated test signals are modeled in SIMULINK and by using API connection, excitation signals are sent to calibration tool interface, ATI VISION. This methodology is applied for both SISO and MIMO cases.

As the control oriented model will be used for MPC design, SISO and MIMO models are designed separately. During the model identification, it is not feasible to use single linear model as no linear model covers entire engine-operating region. Therefore as suggested by Ortner and del Re, (2007), engine-operating region is separated into 4 sub-regions by engine speed and indicated torque separations. Methodology is to select a candidate test point in each region and perform the PEM or N4SID identification method mentioned in the previous section. For each of the regions, one local linear model is found.

Figure 3.30 shows the separation of engine operating and relevant model regions. Regions have been selected according to turbocharger operation and hardware capabilities. Region 2 and region 1 denotes the operating conditions where engine speed is low but the low-end torque is high. It is quite likely that during acceleration, turbocharger will operate in this region. Region 2 and region 4 is coinciding with NEDC, emissions cycle. Region 3 is the intermediate region, which is critical in boost pressure control. Corrected mass flows and compressor/turbine efficiencies are high in this section. It should be noted that due to turbocharger matching HP turbocharger is only effective in region 1 to 4. Outside this region, it is likely that HP turbocharger might be over speed. Therefore, in order to protect HP turbocharger from failure, HP bypass should be fully open outside predefined regions. It should be noted that there is no control zone in which controller is not activated. It is quite unlikely that transient conditions are occurred in this zone as the engine speed is high but the torque is low. Engine operation is more likely to work in steady-state conditions. Please note that full load curve visualization not describing actual curve due to confidentiality reasons.

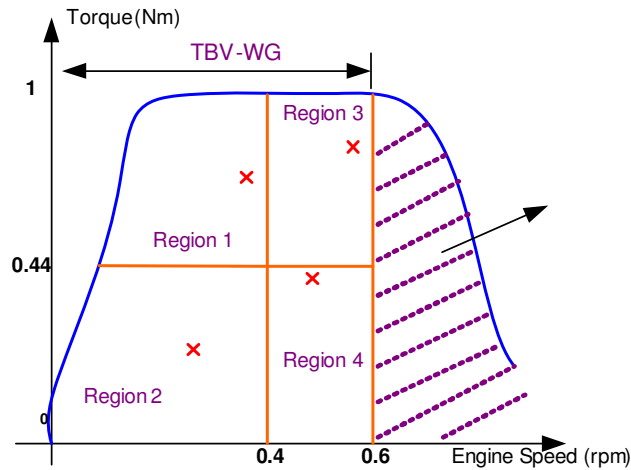


Figure 3.30 : Regions for local linear model across engine operating zone.

Table 3.3 shows the locations of candidate test points. Test points are defined in terms of normalized torque and engine speed values. Locations of candidate points are shown with red crosses on Figure 3.30.

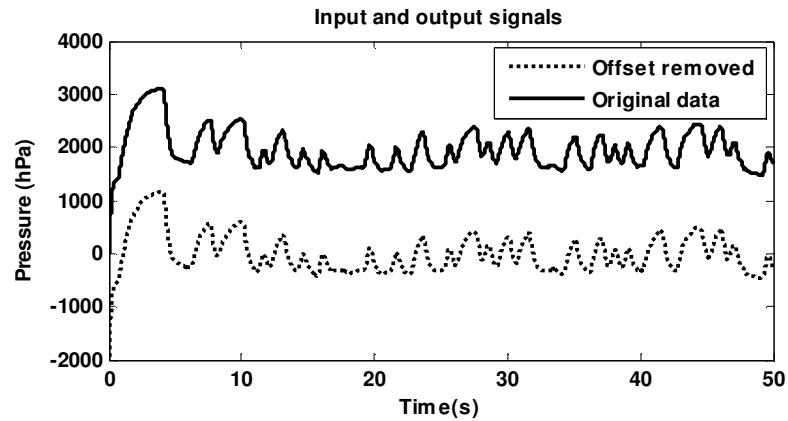
Table 3.3 : Model identification candidate test points for local linear models

Region	Norm. Engine Speed	Norm. Torque
Region 1	0.37	0.66
Region 2	0.33	0.33
Region 3	0.53	0.77
Region 4	0.44	0.44

It is not suitable to use the data for identification directly. The identification data might contain,

- Measurement noise
- Outliers
- Drift and offset which would act as nonlinearity.

Drifts and offsets are observed during testing. During stationary operation in candidate test points, inputs and outputs are applied with offsets. As mentioned in Zhu, (2001), trends and offsets have bad effects on estimation because they do not average out due to their low frequency behavior and they will cause model errors at low frequencies. Linear models cannot estimate arbitrary differences between input and outputs. Thus, the offset should be removed the test data. The offset removal process and pretreatment has been applied via “detrend” function in MATLAB System Identification toolbox. It should be noted that offset removal have been applied offline once after the identification test. Figure 3.31 shows the differences between detrended and original data.

**Figure 3.31 :** Offset removal of identification data.

3.4.3.1 SISO blackbox model

During SISO model identification, we assume that TBV is the only MV where no control applied to WG. It is fully closed in entire operating range. As the model will

be used for controller synthesis, identification region should be selected accordingly. The boost pressure control during low-speed points is critical to minimize turbocharger lag and achieve faster transient response. Therefore, regions are limited to 4 in SISO case. Due to turbocharger over speed issues, TBV is fully opened in high engine speed load regions. This leads to control limitation after region 4 and region 3. It is assumed that, no SISO control is applied when the normalized engine speed exceeds 0.6.

Figure 3.32 shows the identification signals for region 4. PRBS signal is applied to TBV and filtered white noise signal is applied to injection quantity.

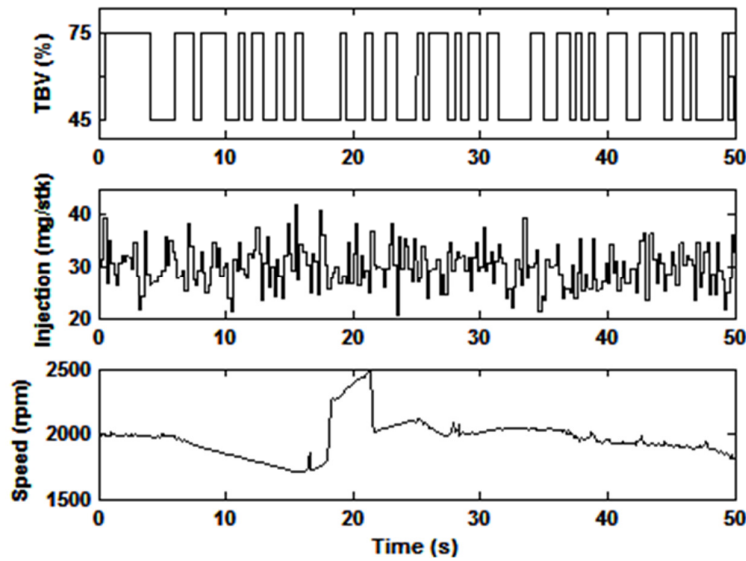


Figure 3.32 : SISO input signals for identification test in Region 4.

Identification results for region 4 are shown in Figure 3.33. N4SID identification is superior to PEM based model in terms of amplitude of residuals and prediction accuracy. Therefore N4SID based state space model is used for this model. The dynamics of boost pressure is well captured by N4SID model. The accuracy is overall below %10 percent.

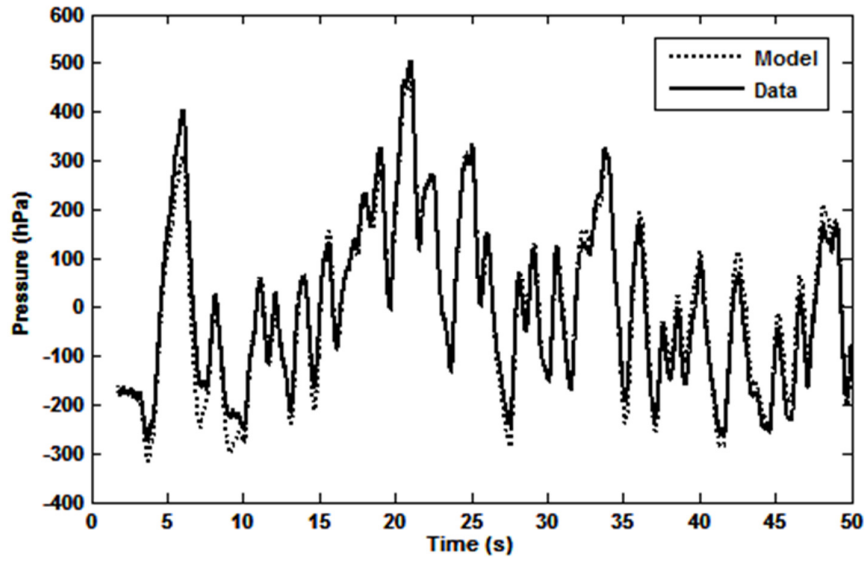


Figure 3.33 : SISO model validation results for Region 4.

Figure 3.34 also shows the input signals applied for identification test in Region 3. Similar signal patterns are used except the mean value of injection quantity and engine speed is changed to match with candidate test points as shown in Table 3.3.

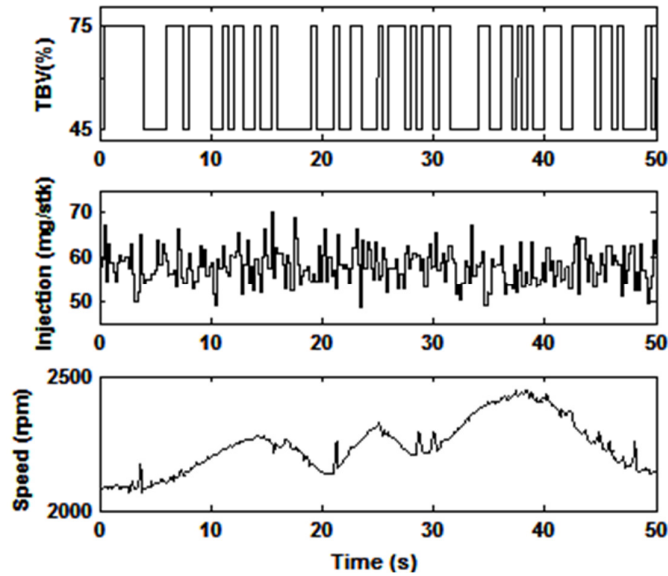


Figure 3.34 : SISO input signals for identification test in Region 3.

The identification result for Region 3 is shown in Figure 3.35. Although the model fit performances are similar between N4SID and PEM methods, N4SID method is slightly better than PEM. This is clear in Figure 3.35 where the residual plots for N4SID and PEM is shown. Residuals are calculated as the difference between measured output and simulated model output. Main statistical variables are shown in

Table 3.4. N4SID shows better performance as the 3σ (3 times standard deviation) separation is 80.23 hPa where PEM shows 141 hPa separation.

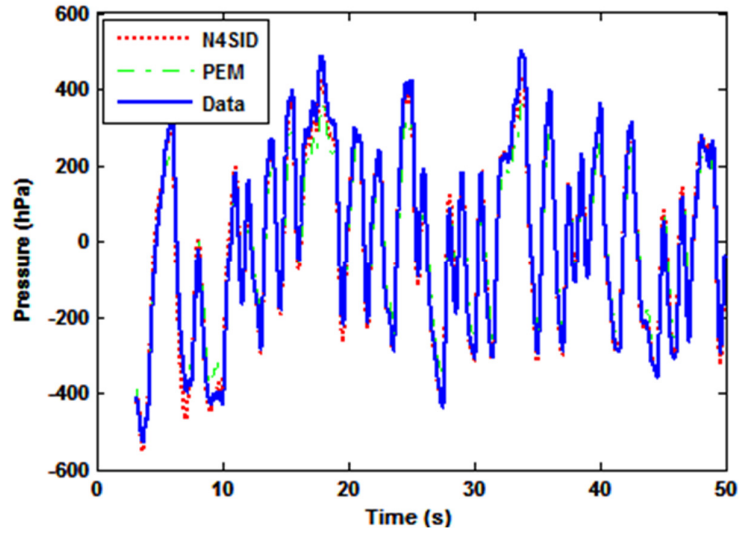


Figure 3.35 : SISO model validation results for Region 3.

Table 3.4 : N4SID method and PEM accuracy

Identification method	Std.Dev.(hPa)	3xStd.dev.(hPa)	Mean (hPa)	Min (hPa)	Max(hPa)
N4SID	26.79	80.37	5.43	-61.17	96.17
PEM	47.03	147	6.334	-89.87	139.3

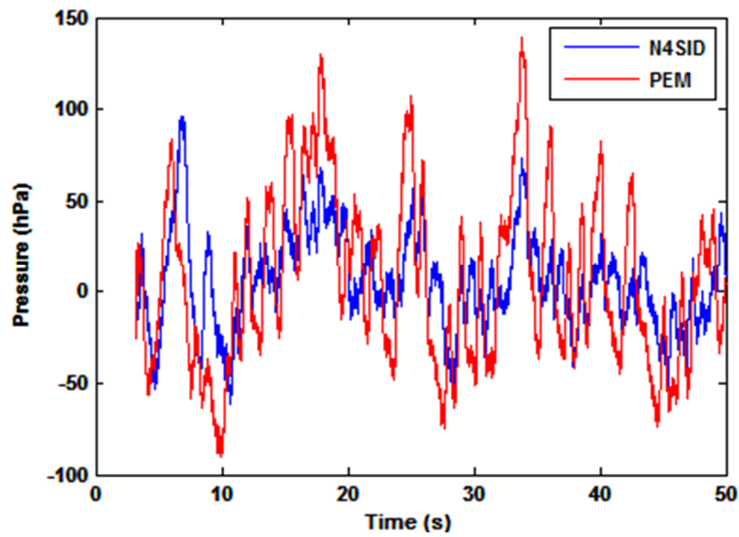


Figure 3.36 : Residual plots for N4SID and PEM methods used in Region 3.

3.4.3.2 MIMO blackbox model

MIMO identification model is used for MIMO model predictive control design. Multivariable inputs includes TBV and WG as MVs and engine speed, injection quantity as MDs. Figure 3.37 and 3.38 shows the identification test signals for region 2 and region 4. Basically PRBS signal is used to excite the inputs. The identification test duration is limited to 50 seconds. PWM limits for WG and TBV duty cycles are changed between %45 and %75.

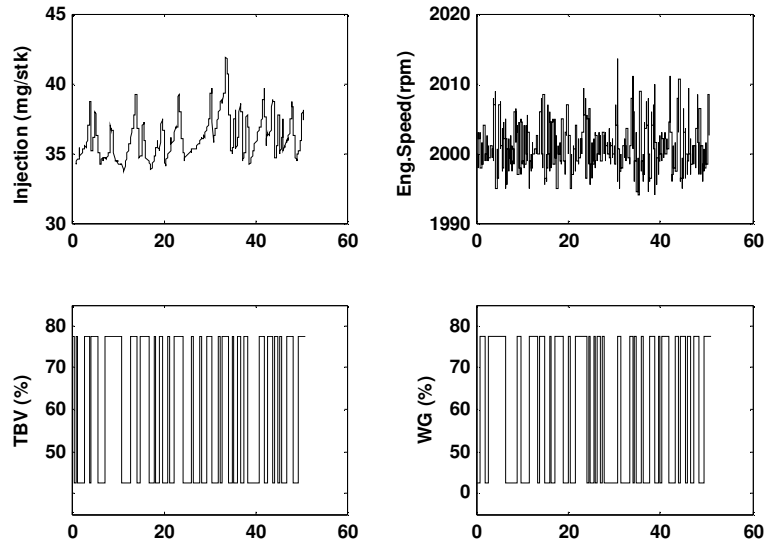


Figure 3.37 : Input signals for identification test in Region 4.

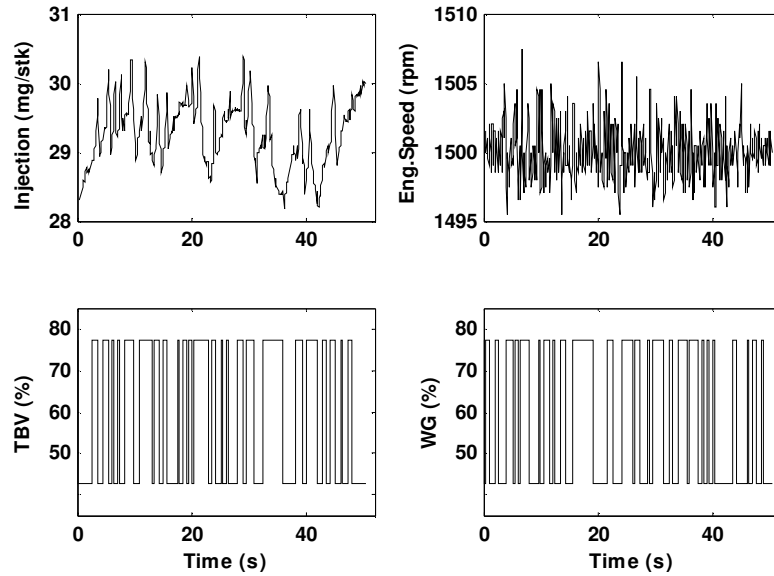


Figure 3.38 : Input signals for identification test in Region 2.

As the identification test completed and pre-treatment have been performed, PEM or N4SID identification methods are applied. Figure 3.39 shows the validation plot for identification model. N4SID based model performance was not satisfactory therefore resulting model structure is PEM based 4th order state space model.

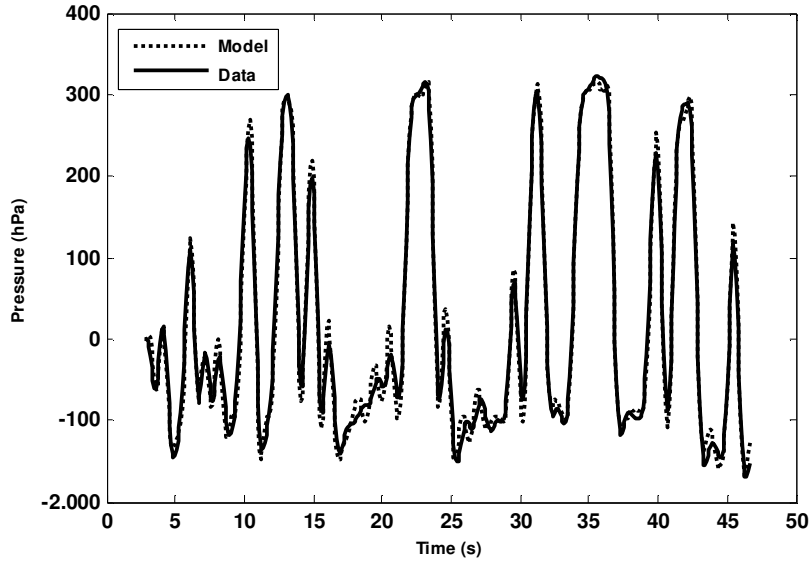


Figure 3.39 : Model validation results for Region 2.

It is quite clear that the model captures the dynamics for boost pressure well, although in some regions high frequency behavior of the data and the model is above %20. Please note that data the steady state offset has been removed from the data thus resulting boost pressure is assumed to be fluctuating around zero mean.

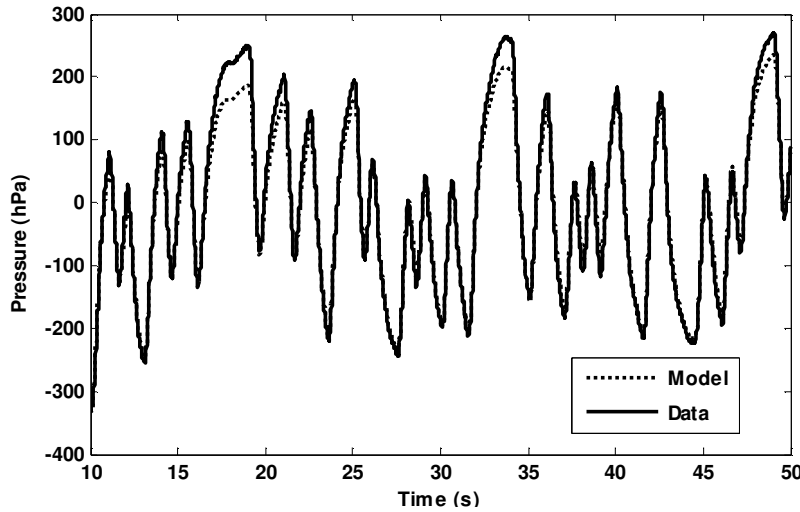


Figure 3.40 : Model validation results for Region 4.

Figure 3.40 shows the validation plots for Region 4. Similar to the local linear model in region 2, resulting model is found as 4th order State space model and the identification method is PEM. Here not all the local model will be shown. Appendix B shows the validation results for remaining regions.

In conclusion, resulting model structure for all local linear models are 4th order state space model. The state variables are not physically realizable due to using identification model but they are the combination of physical states.

As the model identification has been completed, analysis of linear models should be performed in terms of their transient behavior and pole-zero placements. Here, results of linear model for region 4 is presented. Similar analysis has been carried out for remaining models as well.

The transient response analysis of local linear models is shown in Figures 3.41 and Figure 3.42. It is clear that, the sensitivity of boost pressure to TBV input is higher than the WG input.

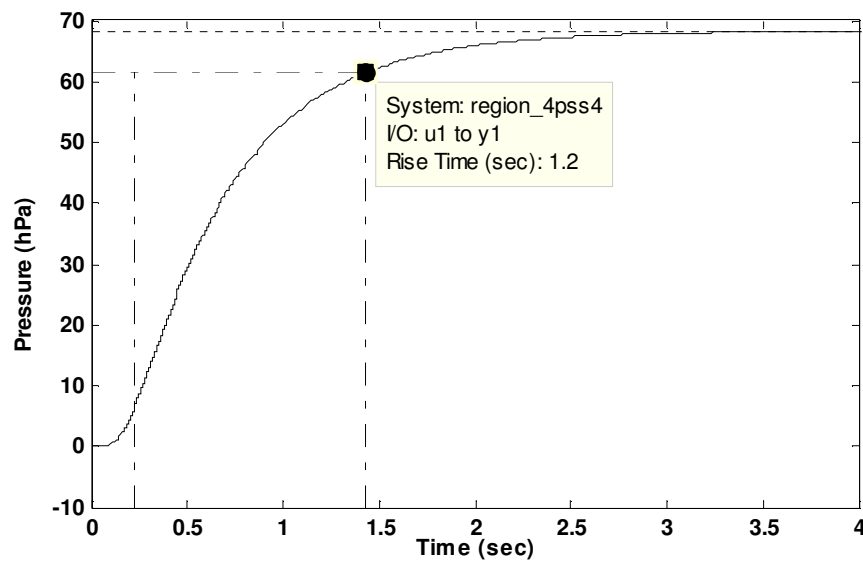


Figure 3.41 : Step response of Linear model 4 to a TBV step input.

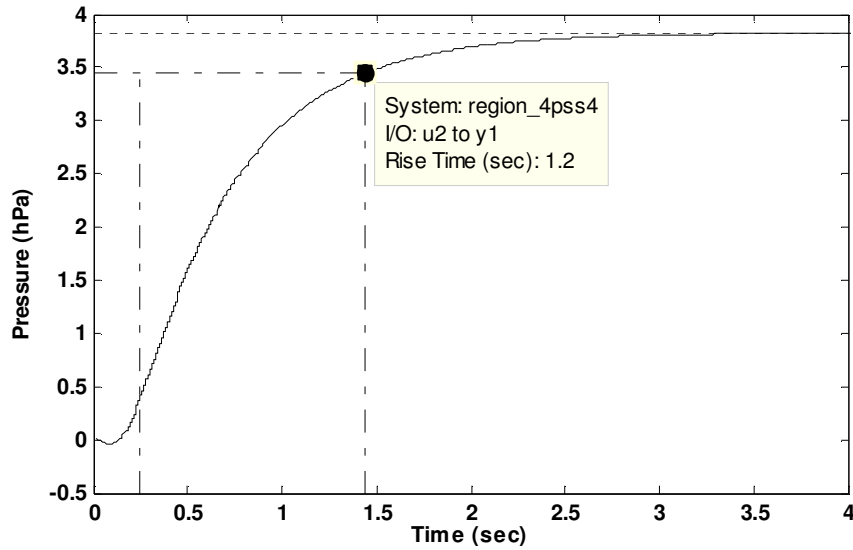


Figure 3.42 : Step response of Linear model 4 to a WG step input.

It can also be observed that system exhibits relatively slight non-minimum phase behavior. The opening of the Waste gate valve initially reduces the boost pressure slightly.

The Bode gain and magnitude plots for the transfer function of TBV to Boost pressure and WG to Boost Pressure are shown in Figure 3.343.

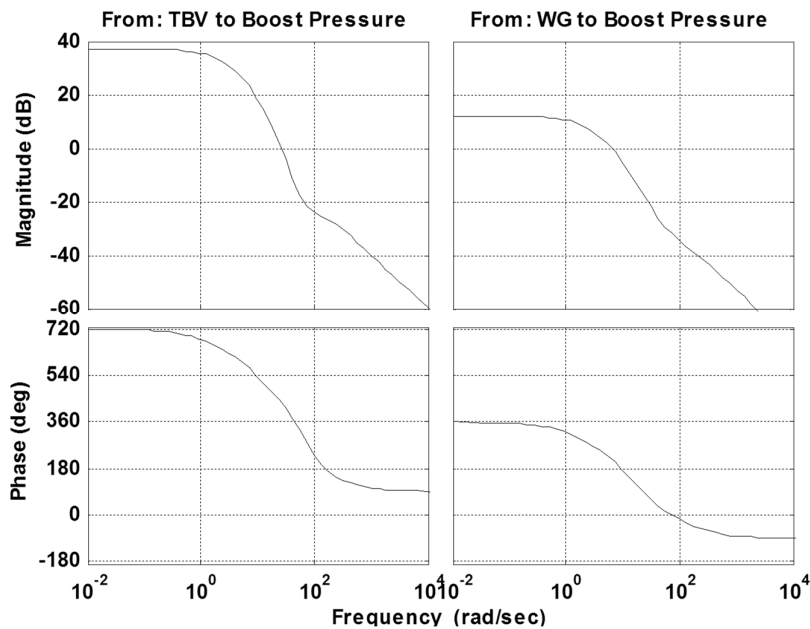


Figure 3.43 : Bode magnitude and phase plots for linear model of region 4.

Finally, the pole-zero mapping of the linear system is shown on Figure 3.44. Both of the transfer functions employs open-loop stable systems. In addition, due to the

additional right half plane zeros, systems show non-minimum phase behaviors shown above.

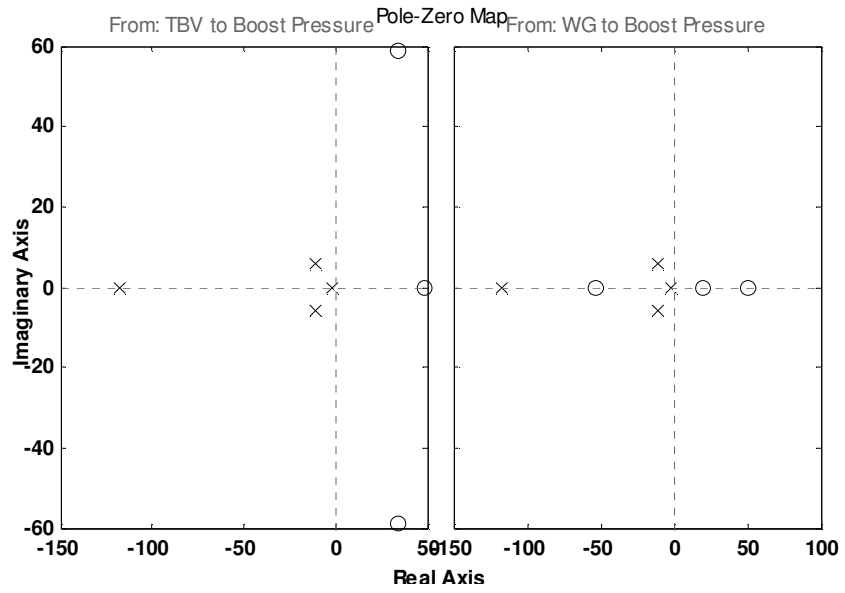


Figure 3.44 : Pole zero mapping of linear model of region 4.

4. CONTROLLER DESIGN

In order to design intelligent boost pressure controller for two stage turbocharged can be performed by utilizing explicit use of models. At each sampling instants the optimization routine is performed application, search have been focused on model-based controller schemes due to ability to incorporate system dynamics to controller synthesis. In the literature, there are variety of model based controllers but during this study, research have been focused on Explicit Model Predictive Controller (MPC) design. First, MPC concept and basics of Receding Horizon Control is mentioned in section 4.1. MPC control problem and formulation is mentioned in section 4.2 as well as state estimation, Quadratic Programming (QP) problem and optimization. Section 4.3 includes the detailed explanation about explicit formulation of MPC. Finally, application to boost pressure control and control design is highlighted in section 4.4. Control design is performed separately for SISO and MIMO cases.

4.1 MPC Concept

Online computation of future manipulated variables to optimize the future behavior of the outputs is the MPC's main design objective (Liuping, 2009). The term "Prediction" in MPC definition denotes the prediction of future output trajectories. This objective can be performed by utilizing explicit use of models. At each sampling instants the optimization routine is performed for predefined duration online to find the optimum control trajectory. This predefined duration is called as Prediction Horizon (PH). At each sampling instants, predefined number of optimum control sequence is applied to system. This predefined number is called as Control Horizon (CH). During practical MPC design, Receding Horizon Control (RHC) scheme is used in which only first control signal of optimum control sequence is applied at each step. For details on RHC, see Kwon and Han (2005),. At each time step, finite horizon open-loop optimal control problem is solved online. Optimization yields an optimal control sequence. Please keep in mind that MPC is family of

controller. It is not designating a specific controller but explains the range of methods. As mentioned in Camacho and Bordons (1999), various MPC controllers are separated according to the plant model types, noises and cost function used in optimization.

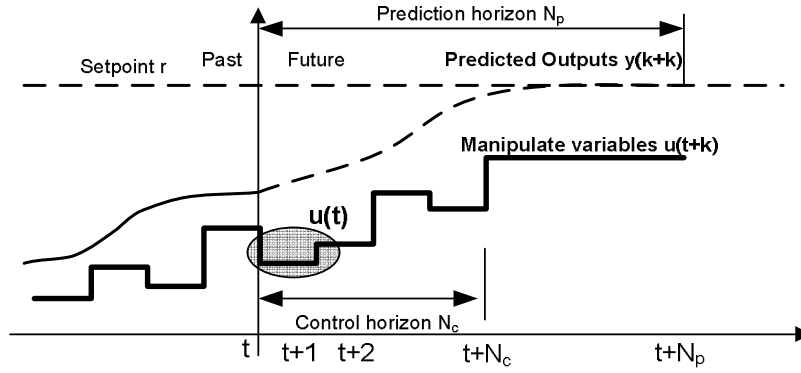


Figure 4.1 : MPC strategy.

Figure 4.1 shows MPC strategy. The methodology followed can be outlined as follows;

- Moving horizon window can be defined as time dependent window from arbitrary time t to $t + N_p$. N_p is the Prediction horizon which defines the prediction window for output variables. By using fixed N_p , future output variables, $y(t + k|t)$, are predicted at each time instant. These future output variables are depending on the current, known values (past inputs and outputs).
- The optimal control sequence $u(t)$, is the output of the optimization routine calculated at each time instant. This optimization is based on the cost function which aims to minimize tracking error between set point r and $y(t + k|t)$. The cost function is mostly defined as quadratic function with control effort, tracking error considered.
- At each time instants, first of the control signals is applied while rest of them are neglected. This is due to using RHC approach. If RHC is not used, Control signal is applied with respect to predefined sampling instants (CH)

It is important to note that, process models are critical in MPC design. First, they are key to calculate predicted outputs. Secondly, they should be simple and easy to

implement considering computational concerns for optimization. The models used in MPC are varying from transfer function models to Impulse response models as well as identified black box models. A good dynamics model will result in consistent and accurate prediction.

On the other hand, optimization routine and algorithm is another factor which defined MPC performance. Optimizer complexity is drastically increasing via constraints (equality or inequality) and cost function (linear or quadratic). In addition, numbers of state and output variables on the PH are effecting the computation resources required to solve finite horizon optimal control problem. Considering online optimization requirement for MPC, computational requirement is becoming one of the key design criteria.

Based on the information outlined here, one can list the advantages of MPC as follows;

- It is suitable to handle multivariable problems.
- It has relatively easy and intuitive tuning process compared to other complex controllers (i.e. H_∞ optimal control). The basic tuning variables are easy to understand by engineers and non-control staff.
- Great span of application from chemical industry to Automotive. It can be applied to non-minimum phase or long-delayed system.
- It has a feed forward compensation taking into account of measured disturbances.

In contrast to advantages listed above, there are some drawbacks, which should be considered during design process.

- Control law derivation is complex compared to standard PID based controllers.
- Computational requirement to solve optimal control problem might be cumbersome depending on the cost function, constraints and system complexity. Due to recent advances in microprocessor capacities and parallel

computing capabilities, this case is more likely to disappear in the following decades.

- Need for an appropriate model to represent system dynamics.

Based on the general idea of the MPC operation outlined above, design steps can be summarized as follows. During this study, controller synthesis and design has been carried out by following these steps.

1. Model the open-loop process, which represents the main system dynamics.
2. Add the constraints for in the form of input (amplitude of the control signal), output(physically realizable output range) and rate constraints(constraints on the control variable incremental variation).
3. Cost function should be defined which shows the performance specification by considering different weights on tracking errors, and input energy (actuator efforts).

As above steps are completed, the rest of the MPC design is automatic. Optimal control problem is constructed based on the model information constraints and weighting on the cost function (Bemporad, 2006). Then, as mentioned above, at each sampling instance, the optimization problem is solved.

MPC has become attractive especially for linear processes. Linear model are used in Linear MPC family in order to represent the system dynamics although the real dynamics of the system is non-linear. Linear MPC formulation is well addressed across industry, research community, and proved its performance in terms of performance, stability and online-computation requirements. In contrast to linear MPC, in order to increase performance and better representation of system dynamics, nonlinear models can be employed in MPC formulation. This motivates the use of nonlinear MPC (NMPC) scheme (Findensen and Allgöwer, 2002). In NMPC, system representation can be described by set of nonlinear differential equations shown in (4.1).

$$\dot{x}(t) = f(x(t), u(t)), \quad x(0) = x_0 \quad (4.1)$$

Due to incorporating nonlinear model in MPC formulation, online optimization with long finite horizons will lead unfeasible results even cannot be suitable for online computation. Moreover, when using shorter horizons, the predicted and actual trajectories will be different, thus closed loop system stability will not be guaranteed. Due to the numerous advantages, there are still some issues related to real time applicability and stability issues in NMPC. Hence, during this study, Controller synthesis is based on Linear MPC formulation. Interested reader might refer to Findensen et.al (2007) and Kouvaritakis and Cannon (2008) for detailed information on NMPC.

4.2 MPC Formulation

Model predictive control systems are designed based on a mathematical model of the plant. The plant models are taken as a state-space model. Before dealing with MPC formulation in detail, one might need to address plant formulation and input-output definitions. This would be analyzed in two sub sections. In section 4.2.1, we mentioned the basic MPC formulation for simple LTI model with constrained and unconstrained cases. In section 4.2.2, detailed and extended formulation for MD, UD, MV and OV are mentioned with constraints and state estimation. During this study, Model predictive control toolbox and Hybrid toolbox has been used to design and implement MPC controllers, thus the latter formulation is aligned with the formulations used in the toolboxes.

4.2.1 Predictive control with basic LTI model without MD

We can start by representing the very basic SISO LTI model as shown in (4.2) and (4.3).

$$\dot{x}_m(k+1) = A_m x_m(k) + B_m u(k) \quad (4.2)$$

$$y(k) = C_m x_m(k) \quad (4.3)$$

Where u is the manipulated variable (MV), y is the Output Variable (OV) and x_m is the the state vector. In order to modify the model to accommodate future control

inputs and outputs, integrator should be added. Thus (4.2) and (4.3) should be modified accordingly.

Taking one-step difference on both sides of (4.2) yields;

$$\begin{aligned} x_m(k+1) - x_m(k) \\ = A_m(x_m(k) - x_m(k-1)) + B_m(u(k) - u(k-1)) \end{aligned} \quad (4.4)$$

MV can be modified as shown in (4.5).

$$\Delta u(k) = u(k) - u(k-1) \quad (4.5)$$

The Δ variables are indicating the incremental change in $x_m(k)$ and $u(k)$. We can modify (4.4) and (4.3) by transformation.

$$\Delta x_m(k+1) = A_m \Delta x_m(k) + B_m \Delta u(k) \quad (4.6)$$

Next, $\Delta x_m(k)$ should be connected to OV, $y(k)$. The new state variable vector will be constructed as follows.

$$x(k) = [\Delta x_m(k)^T \ y(k)^T]^T \quad (4.7)$$

Taking the one-step difference of (4.3) will result in (4.4).

$$y(k+1) - y(k) = C_m(x_m(k+1) - x_m(k)) = C_m A_m \Delta x_m(k) \quad (4.8)$$

By combining (4.8) and (4.7), we will have the final formulation of state-space model with embedded integrator.

$$\begin{aligned} \begin{bmatrix} \Delta x_m(k+1) \\ y(k+1) \end{bmatrix} &= \begin{bmatrix} A_m & 0_m^T \\ C_m A_m & 1 \end{bmatrix} \begin{bmatrix} \Delta x_m(k) \\ y(k) \end{bmatrix} + \begin{bmatrix} B_m \\ C_m B_m \end{bmatrix} \Delta u(k) \\ y(k) &= [0_m \quad 1] \begin{bmatrix} \Delta x_m(k) \\ y(k) \end{bmatrix} \end{aligned} \quad (4.9)$$

Where,

$$\begin{aligned}
x_{k+1} &= \begin{bmatrix} \Delta x_m(k+1) \\ y(k+1) \end{bmatrix} \\
x(k) &= \begin{bmatrix} \Delta x_m(k) \\ y(k) \end{bmatrix} \\
A &= \begin{bmatrix} A_m & 0_m^T \\ C_m A_m & 1 \end{bmatrix} \\
B &= \begin{bmatrix} B_m \\ C_m B_m \end{bmatrix} \\
C &= [0_m \quad 1]
\end{aligned} \tag{4.10}$$

The Augmented LTI model with (A,B,C) will be used in MPC formulation below.

Assume that at the sampling instant k_i , the state vector $x(k_i)$ is measured. Future control trajectory can be represented as,

$$\Delta u(k_i), \Delta u(k_i + 1), \dots, \Delta u(k_i + N_c - 1) \tag{4.11}$$

Where N_c is the control horizon as mentioned in section 4.1. Considering the measured states available at sampling instant k_i , future state variables are predicted for N_p number of samples where N_p is the prediction horizon. In addition, at each sampling instant, optimization is taking place for N_p . Future state variables can be defined as follows.

$$x(k_i + 1|k_i), x(k_i + 2|k_i), \dots, x(k_i + m|k_i), \dots, x(k_i + N_p|k_i) \tag{4.12}$$

Where $x(k_i + m|k_i)$ is the predicted state variable at $k_i + m$ with given plant information $x(k_i)$. Augmented state space model in (4.9) can be updated sequentially using future control parameters.

$$\begin{aligned}
x(k_i + 1|k_i) &= Ax(k_i) + B\Delta u(k_i) \\
x(k_i + 2|k_i) &= Ax(k_i + 1|k_i) + B\Delta u(k_i + 1) \\
x(k_i + 3|k_i) &= A^2x(k_i) + AB\Delta u(k_i) + B\Delta u(k_i + 1) \\
&\vdots \\
x(k_i + N_p|k_i) &= A^{N_p}x(k_i) + A^{N_p-1}B\Delta u(k_i) + A_{N_p-2}B\Delta u(k_i + 1) \\
&\quad + \dots + A^{N_p-N_c}B\Delta u(k_i + N_c - 1) \\
y(k_i + 1|k_i) &= CAx(k_i) + CB\Delta u(k_i) \\
\\
y(k_i + 2|k_i) &= CA^2x(k_i + 1|k_i) + CAB\Delta u(k_i) + CB\Delta u(k_i + 1) \\
y(k_i + 3|k_i) &= CA^3x(k_i) + CA^2B\Delta u(k_i) + CAB\Delta u(k_i + 1) \\
&\quad + CB\Delta u(k_i + 2) \\
&\vdots \\
x(k_i + N_p|k_i) &= CA^{N_p}x(k_i) + CA^{N_p-1}B\Delta u(k_i) \\
&\quad + CA^{N_p-2}B\Delta u(k_i + 1) + \dots + CA^{N_p-N_c}B\Delta u(k_i + N_c - 1)
\end{aligned}$$

In order to simplify the formulation for matrix definition, we can define vectors for output variables and incremental future control inputs.

$$\begin{aligned}
Y &= [y(k_i + 1|k_i) \quad y(k_i + 2|k_i) \quad y(k_i + 3|k_i) \quad \dots \quad y(k_i + N_p|k_i)] \quad (4.13)
\end{aligned}$$

$$\Delta U = [\Delta u(k_i) \quad \Delta u(k_i + 1) \quad \Delta u(k_i + 2) \quad \dots \quad \Delta u(k_i + N_c - 1)]^T \quad (4.14)$$

Equations (4.13) and (4.14) can be combined in a matrix form as shown in (4.15).

$$Y = Fx(k_i) + \phi\Delta U \quad (4.15)$$

$$F = \begin{bmatrix} CA \\ CA^2 \\ CA^3 \\ \vdots \\ CA^{N_p} \end{bmatrix} \quad (4.16)$$

$$\phi = \begin{bmatrix} CB & 0 & 0 & \dots & 0 \\ CAB & CB & 0 & \dots & 0 \\ CA^2B & CAB & CB & \dots & 0 \\ \vdots & \vdots & \vdots & \dots & \vdots \\ CA^{N_p-1}B & CA^{N_p-2}B & CA^{N_p-3}B & \dots & CA^{N_p-N_c}B \end{bmatrix}$$

Based on the formulation and the matrices shown in (4.16), details on the optimization can be briefly mentioned. Thus, definition of cost function would be crucial. Assume that the main objective of the controller is to track the setpoint signal $r(k_i)$ with minimal tracking error between the output and setpoint. While satisfying this tracking objective, controller effort should be as small as possible. This objective can be represented mathematically as shown in (4.18). Assuming the setpoint is given in vector form.

$$R_s^T = [1 \ 1 \ 1 \ \dots \ 1]_{1 \times N_p} r(k_i) \quad (4.17)$$

The cost function is represented as follows.

$$J = \min_U ((R_s - Y)^T (R_s - Y) + \Delta U^T \bar{R} \Delta U) \quad (4.18)$$

Where $(R_s - Y)$ denotes the tracking error and $\Delta U^T \bar{R} \Delta U$ is referring to input energy. \bar{R} is the weighing vector which is used to tune the closed loop performance of the controller. It is shown in (4.19).

$$\bar{R} = r_w I_{N_c \times N_c} (r_w \geq 0) \quad (4.17)$$

Please keep in mind that (4.18) is an example performance criteria for setpoint tracking. Other performance criteria considering terminal state and state regulation can be derived as well. In that case main performance criteria will be “Find the optimal control law that would drives the states to the origin”

The quadratic performance index will be defined as shown in 4.18. Here the first term is to terminal state cost, second term is state tracking cost and final term is the input energy cost.

$$J = \min_U x^T(N_p)Px(N_p) + \sum_{i=0}^{N_p-1} x^T(k_i)Qx(k_i) + u^T(k_i)Ru(k_i) \quad (4.18)$$

Continuing from tracking problem as shown in (4.18), in order to find the optimal control input which will minimize cost functions, J will be expressed as;

$$J = (R_s - Fx(k_i))^T (R_s - Fx(k_i)) - 2\Delta U^T \phi^T (R_s - Fx(k_i)) + \Delta U^T (\phi^T \phi + \bar{R}) \Delta U \quad (4.19)$$

The first derivative of the cost function will be as follows.

$$\frac{\partial J}{\partial \Delta U} = -2\phi^T (R_s - Fx(k_i)) + 2(\phi^T \phi + \bar{R}) \Delta U \quad (4.20)$$

The necessary condition for minimum J is $\frac{\partial J}{\partial \Delta U} = 0$, then the optimal control input will be;

$$\Delta U = (\phi^T \phi + \bar{R})^{-1} \phi^T (R_s - Fx(k_i)) \quad (4.21)$$

Above formulation is to show how control law and cost function is obtained for SISO case. As mentioned before, one of the key advantages of MPC is, it can handle multivariable MIMO processes straightforward.

Let us consider a MIMO process with n outputs and m inputs as defined in the following model which is similar to SISO case.

$$x_m(k+1) = A_m x_m(k) + B_m u(k) + B_w w(k) \quad (4.22)$$

$$y(k) = C_m x_m(k) \quad (4.23)$$

Where $w(k)$ is the input disturbance or mainly the noise affecting the process assumed to be a white stationary random processes with $E[w(k)] = 0$. In other words, $w(k)$ can be expressed by zero mean, white noise $\epsilon(k)$ as below.

$$w(k) - w(k-1) = \epsilon(k) \quad (4.24)$$

Equation 4.22 can be expressed in a different form as following expression.

$$x_m(k) = A_m x_m(k-1) + B_m u(k-1) + B_w w(k-1) \quad (4.25)$$

The incremental variables for state and input variables are defined as $\Delta u(k) = u(k) - u(k-1)$ and $\Delta x(k) = x(k) - x(k-1)$. Substracting (4.25) from (4.22) yields,

$$\Delta x_m(k+1) = A_m \Delta x_m(k) + B_m \Delta u(k) + B_w \epsilon(k) \quad (4.26)$$

From (4.23), in order to derive a relationship between the output $y(k)$ and incremental state variable $\Delta x(k)$, we will have the following expression.

$$\begin{aligned} \Delta y(k+1) &= C_m \Delta x_m(k+1) \\ &= C_m A_m \Delta x_m(k) + C_m B_m \Delta u(k) + C_m B_d \epsilon(k) \end{aligned} \quad (4.27)$$

Then the final form of augmented model for MIMO systems will be;

$$\begin{aligned} \begin{bmatrix} \Delta x_m(k+1) \\ y(k+1) \end{bmatrix} &= \begin{bmatrix} A_m & 0_m^T \\ C_m A_m & I_{n \times n} \end{bmatrix} \begin{bmatrix} \Delta x_m(k) \\ y(k) \end{bmatrix} + \begin{bmatrix} B_m \\ C_m B_m \end{bmatrix} \Delta u(k) \\ &\quad + \begin{bmatrix} B_w \\ C_m B_w \end{bmatrix} \epsilon(k) \end{aligned} \quad (4.28)$$

$$y(k) = [0_m \quad I_{n \times n}] \begin{bmatrix} \Delta x_m(k) \\ y(k) \end{bmatrix}$$

After finding the augmented model, formulation for optimal control law would be straightforward. Based on the augmented model shown in (4.28), future state variables will be found as follows.

$$\begin{aligned}
x(k_i + 1|k_i) &= Ax(k_i) + B\Delta u(k_i) + B_w\epsilon(k_i) \\
x(k_i + 2|k_i) &= Ax(k_i + 1|k_i) + B\Delta u(k_i + 1) + B_w\epsilon(k_i + 1|k_i) \\
x(k_i + 3|k_i) &= A^2x(k_i) + AB\Delta u(k_i) + B\Delta u(k_i + 1) + AB_w\epsilon(k_i) + B_w\epsilon(k_i \\
&\quad + 1|k_i) \\
&\vdots \\
x(k_i + N_p|k_i) &= A^{N_p}x(k_i) + A^{N_p-1}B\Delta u(k_i) + A^{N_p-2}B\Delta u(k_i + 1) \\
&\quad + A^{N_p-N_c}B\Delta u(k_i + N_c - 1) + A^{N_p-1}B_w\epsilon(k_i) \\
&\quad + A^{N_p-2}B_w\epsilon(k_i + 1|k_i) + \dots + B_w\epsilon(k_i + N_p - 1|k_i) \\
y(k_i + 1|k_i) &= CAx(k_i) + CB\Delta u(k_i)
\end{aligned}$$

Equation (4.15) is still valid considering F and ϕ matrices as follows,

$$\begin{aligned}
F &= \begin{bmatrix} CA \\ CA^2 \\ CA^3 \\ \vdots \\ CA^{N_p} \end{bmatrix} \\
\phi &= \begin{bmatrix} CB & 0 & 0 & \dots & 0 \\ CAB & CB & 0 & \dots & 0 \\ CA^2B & CAB & CB & \dots & 0 \\ \vdots & \vdots & \vdots & \dots & \vdots \\ CA^{N_p-1}B & CA^{N_p-2}B & CA^{N_p-3}B & \dots & CA^{N_p-N_c}B \end{bmatrix}
\end{aligned} \tag{4.29}$$

Incremental control sequence will be found as (4.21),

$$\Delta U = (\phi^T\phi + \bar{R})^{-1}\phi^T(R_s - Fx(k_i)) \tag{4.30}$$

Where $\phi^T\phi$ has dimension $mN_c \times mN_c$, ϕ^TF has dimension of $mN_c \times n$ and ϕ^TR_s equals to the n last columns of ϕ^TF .

It should be noted that optimal control sequence calculated in (4.21) and (4.30), is only applicable when the control problem is not constrained. However, most of the applications include constraints on the input, input rates and outputs. Optimization routine will be changed accordingly to accommodate constrained optimal control problem. Beforehand, we need to outline the constraints types briefly. Please note

that there are various types of constraints but here we will mention 3 types which are used during this study.

- Output (band) constraints

When it is desired that output variables are to follow a trajectory within a band, one shall use the output constraints.

$$y_{\min} \leq y(k) \leq y_{\max} \quad (4.31)$$

- Input constraints

These type of constraints limit the amplitude of the control signal. This is required due to physical behaviour of the actuator acting on the system. Hard maximum and minimum limits on the actuator valves are an example to input constraints. In case of not considering input rate constraints, cost function might result in high values. Violation of input constraint might lead to critical even dangerous situation on the real system.

$$u_{\min} \leq u(k) \leq u_{\max} \quad (4.32)$$

- Input rate(slew) constraints

Slew constraints basically limits the speed or rate of change of control variable. Similar to input constraints, input rate constraints are directly related to physical system and actuator behaviour.

$$\Delta u_{\min} \leq \Delta u(k) \leq \Delta u_{\max} \quad (4.33)$$

As the constraints definition completed, we need to define the constrained optimal control problem. As part of the MPC design, constraints should be formulated in terms of linear inequalities. In this case, it is essential to define constraints in a set of linear equations based on parameter vector ΔU . By using receding horizon principle, optimal control input calculated at each sampling will be;

$$\Delta u_{\min} \leq \Delta u(k_i) \leq \Delta u_{\max} \quad (4.34)$$

$$\Delta u_{\min} \leq \Delta u(k_i + 1) \leq \Delta u_{\max}$$

$$\Delta u_{\min} \leq \Delta u(k_i + 2) \leq \Delta u_{\max}$$

As the constraints are embedded as linear inequalities in the input vector ΔU , next we need to combine with cost function J. We can express (4.34) in a matrix form by means of two inequalities.

$$\begin{aligned} -\Delta U &\leq -\Delta U^{\min} \\ \Delta U &\leq \Delta U^{\max} \end{aligned} \quad (4.35)$$

In a more simpler form;

$$\begin{bmatrix} -I \\ I \end{bmatrix} \Delta U \leq \begin{bmatrix} \Delta U^{\min} \\ \Delta U^{\max} \end{bmatrix} \quad (4.36)$$

By considering the constraint on the manipulated variables, future control variables can be written as shown in (4.36).

$$\begin{bmatrix} u(k_i) \\ u(k_i + 1) \\ u(k_i + 2) \\ \vdots \\ u(k_i + N_c - 1) \end{bmatrix} = \begin{bmatrix} I \\ I \\ I \\ \vdots \\ I \end{bmatrix} u(k_i - 1) + \begin{bmatrix} I & 0 & 0 & \dots & 0 \\ I & I & 0 & \dots & 0 \\ I & I & I & \dots & 0 \\ \vdots & \vdots & \vdots & \ddots & \vdots \\ I & I & \dots & I & I \end{bmatrix} \begin{bmatrix} \Delta u(k_i) \\ \Delta u(k_i + 1) \\ \Delta u(k_i + 2) \\ \vdots \\ \Delta u(k_i + N_c - 1) \end{bmatrix} \quad (4.37)$$

By organizing (4.37) in a more compact matrix form, constraint definition in (4.35) can be modified as shown in (4.38).

$$\begin{aligned} -(C_1 u(k_i - 1) + C_2 \Delta U) &\leq -U_{\min} \\ -(C_1 u(k_i - 1) + C_2 \Delta U) &\leq U_{\max} \end{aligned} \quad (4.38)$$

Above formulation is given for input amplitude constraints, but similar formulation might be derived for output and rate constraints as well. The output constraints are expressed in terms of ΔU .

$$Y_{\min} \leq Fx(k_i) + \phi \Delta U \leq Y_{\max} \quad (4.39)$$

Finally, combining all constraint definitions to find optimum control movement that minimizes cost function.

$$J = (R_s - Fx(k_i))^T (R_s - Fx(k_i)) - 2\Delta U^T \phi^T (R_s - Fx(k_i)) + \Delta U^T (\phi^T \phi + \bar{R}) \Delta U \quad (4.40)$$

Subject to inequality constraints

$$\begin{bmatrix} M_1 \\ M_2 \\ M_3 \end{bmatrix} \Delta U \leq \begin{bmatrix} N_1 \\ N_2 \\ N_3 \end{bmatrix} \quad (4.41)$$

The data matrices M_i and N_i are defined as below.

$$M_1 = \begin{bmatrix} -C_2 \\ C_2 \end{bmatrix}; N_1 = \begin{bmatrix} -U_{\min} + C_1 u(k_i - 1) \\ U_{\max} - C_1 u(k_i - 1) \end{bmatrix}; M_2 = \begin{bmatrix} -I \\ I \end{bmatrix}; N_2 = \begin{bmatrix} -\Delta U_{\min} \\ \Delta U_{\max} \end{bmatrix}$$

$$M_3 = \begin{bmatrix} -\phi \\ \phi \end{bmatrix}; N_3 = \begin{bmatrix} -Y_{\min} + Fx(k_i) \\ Y_{\max} - Fx(k_i) \end{bmatrix}$$

Here we can conclude that, with the quadratic cost function and linear constraints, the MPC problem is standard constrained quadratic programming problem where $\phi^T \phi + \bar{R}$ is the Hessian matrix. In order to solve the standard quadratic programming problem, It is assumed that the cost function is convex. This would leads to convex optimization in which very efficient numerical numerical methods exists (Bemporad, 2013). We can replace the cost function by using weighting matrices (Q and R), as shown in (4.42).

$$J = \sum_{i=0}^{N-1} (y(k_i) - r(k_i))' Q_y (y_k - r(k_i)) + \Delta u(k_i)' R \Delta u(k_i) \quad (4.42)$$

Considering Q and P are positive semidefinite matrices, (4.42) can be treated as convex optimization problem. Detailed information on convex optimization can be found in Boyd and Vandenberghe (2009).

4.2.2 Predictive control with extended LTI model with MD and UD

As the basic MPC scheme has been outlined in previous section, the formulation can be extended to cover measured disturbances as well as unmeasured disturbances such as noise and model uncertainty.

One should start with modifying the plant definition. Figure 4.2 shows the main signals in the extended prediction model. Generally, plant inputs are now classified as measured disturbances, unmeasured disturbances and manipulated variables. There is also additional measurement noise signal which is acting on the plant output.

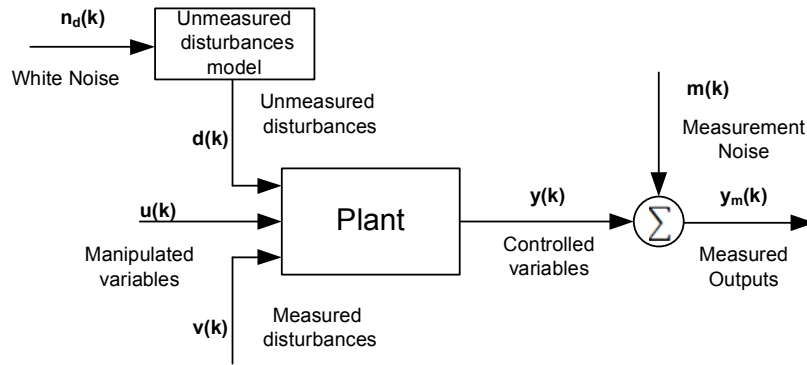


Figure 4.2 : Main signals acting on the prediction model.

Based on the signals above, prediction model of the extended LTI system can be described by following equations.

$$\begin{aligned} x(k+1) &= Ax(k) + B_u u(k) + B_v v(k) + B_d d(k) \\ y_m(k) &= C_m x(k) + D_{vm} v(k) + D_{dm} d(k) \end{aligned} \quad (4.43)$$

Where $v(k)$ is the measured disturbances, $d(k)$ is the unmeasured disturbances which covers both state disturbances defined by B_d and output disturbances D_d . Disturbance model is totally application dependent. During this study, disturbance model suggested by Bemporad et.al (2004) has been implemented. It is basically modeled as shown in 4.44.

$$\begin{aligned}
x_d(k+1) &= \bar{A}x_d(k) + \bar{B}n_d(k) \\
d(k) &= \bar{C}x_d(k) + \bar{D}n_d(k)
\end{aligned}
\tag{4.44}$$

Where $n_d(k)$ is zero-mean, unit variance, random Gaussian input and $x_d(k)$ is the input disturbance states. Basically, unmeasured disturbances are also representing modeling errors. Measurement noise model also implemented in a similar way.

By combining (4.44) and (4.43) we will have the extended state vector $[x'(t) \ x_d'(t)]$ described in (4.45) below.

$$\begin{aligned}
\begin{bmatrix} x(k+1) \\ x_d(k+1) \end{bmatrix} &= \begin{bmatrix} A & B_d\bar{C} \\ 0 & \bar{A} \end{bmatrix} \begin{bmatrix} x(k) \\ x_d(k) \end{bmatrix} + \begin{bmatrix} B_u \\ 0 \end{bmatrix} u(k) + \begin{bmatrix} B_v \\ 0 \end{bmatrix} v(k) + \\
\begin{bmatrix} 0 & B_u & B_v \\ \bar{B} & 0 & 0 \end{bmatrix} \begin{bmatrix} n_d(k) \\ n_u(k) \\ n_v(k) \end{bmatrix} & \\
y(k) &= [C \ \bar{C}] \begin{bmatrix} x(k) \\ x_d(k) \end{bmatrix}
\end{aligned}
\tag{4.45}$$

It should be noted that \bar{D} , D_{du} , D_{dv} is assumed to be zero through the formulations. In addition $n_u(k)$ and $n_v(k)$ are the unmeasured disturbances applied to manipulated variables and measured disturbances which are also modeled as zero-mean, unit covariance white noise signals. Some of the states cannot be measured depending on the model information. System identification based models includes some states which combination of physical states. These states cannot be measured but rather are estimated. In this case, linear state observer should be used for state estimation. Please note that the necessary and sufficient condition for observer design is that, combined state space model in (4.45) should be observable. Linear state estimator is used to estimate combined state vector $[x_d(k+1) \ x(k+1)]^T$ by using measured output values. During this Kalman filter is designed as a state estimator. State estimation of Discrete time Kalman filter is generic with linear state estimation formulation.

$$\hat{x}(k+1|k) = A\hat{x}(k-1|k) + B\Delta u(k) + L(y(k) - Cx(k-1|k))
\tag{4.46}$$

Where L is the observe gain matrix. The gain matrix L is derived by solving a discrete Riccati equation.

During Kalman filter operation first of all output estimate is calculated by using previously estimated states and measured disturbances as shown in (4.47).

$$\begin{aligned}\hat{y}_m(k) = & C_m \hat{x}(k-1|k) + D_{vm} v(k) + D_{dm} \bar{C} \hat{x}_d(k-1|k) \\ & + \bar{C} \hat{x}_d(k-1|k)\end{aligned}\quad (4.47)$$

Where m corresponds to the rows of C,D matrices. As output is estimated during each sampling, Estimation of current states are carried out by using observer gain matrix.

$$\begin{bmatrix} \hat{x}(k|k) \\ \hat{x}_d(k|k) \end{bmatrix} = \begin{bmatrix} \hat{x}(k|k-1) \\ \hat{x}_d(k|k-1) \end{bmatrix} + M(y_m(k) - \hat{y}_m(k)) \quad (4.48)$$

Last step is to estimate future state information by using the relation shown in (4.49) below.

$$\begin{bmatrix} \hat{x}(k+1|k) \\ \hat{x}_d(k+1|k) \end{bmatrix} = \begin{bmatrix} A\hat{x}(k|k) + B_u u(k) + B_v v(k) + B_d \bar{C} \hat{x}_d(k|k) \\ \bar{A} \hat{x}_d(k|k) \end{bmatrix} \quad (4.49)$$

As the state estimation is included to the MPC formulation, we can rearrange the quadratic cost function for reference tracking control.

$$\begin{aligned}\min_{\Delta U} \sum_{k=0}^{N_p-1} & (y(k) - r(k))^T Q_y (y(k) - r(k)) + \Delta u(k)^T R \Delta u(k) \\ & + (u(k) - u_{target}(k))^T S (u(k) - u_{target}(k))\end{aligned}\quad (4.50)$$

Where $Q_y = Q_y^T \geq 0$ is the weighting matrix for output tracking and R is the weighting matrix for input increments and S is the weighting matrix for input signal amplitude. The vector $u_{target}(k)$ is the setpoint for input vector. Both Q_y, R and S are diagonal and nonnegative matrices.

Figure 4.3 shows the final MPC layout for implementation. MPC controller design includes the modeling of prediction model as well as computation of the cost function by means of quadratic programming.

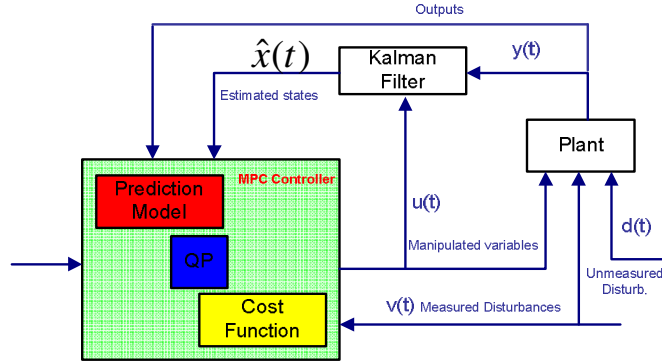


Figure 4.3 : Main signals acting on the prediction model.

4.3 Explicit MPC Formulation

As mentioned in section 4.2, online computation is the key element of standard MPC formulation. Although there are efficient QP solvers based on active set and interior point methods, significant amount of computational requirement is demanded in order calculate optimum value of $u(t)$. Therefore complexity and model scaling is limited in MPC applications in which applications are rather slow such as chemical processes. Bemporad et.al (2002) proposed an alternative approach to overcome the computational effort to solve online optimization. Basic idea of the proposed approach is to represent online control computation in a simple explicitly defined piecewise linear functions. This method is known as explicit MPC.

Assume that the cost function is defined as a quadratic cost function defined for constrained regulation problem.

$$J^*(x) = \min x_{t+N}^T P x_{t+N} + \sum_{k=0}^{N-1} x_{t+k|t}^T Q x_{t+k|t} + u_{t+k}^T R u_{t+k} \quad (4.51)$$

Subject to;

$$\begin{aligned} x_0 = x, \quad x(t+1) &= Ax(t) + Bu(t), \quad y(t) = Cx(t) \\ y_{\min} \leq y(t) &\leq y_{\max}, \quad u_{\min} \leq u(t) \leq u_{\max} \\ u_{t+k} &= Kx_{t+k|t} \end{aligned} \quad (4.52)$$

In (4.51), Q,P and R matrices are positive semi-definite weighting matrices. as mentioned in Bemporad et.al (2002), if we substitute $x_{t+k|t}$ by the expression below, we will have the equivalent representation of (4.51) and (4.52) as shown in (4.54).

$$J^*(x) = A^k x(t) + \sum_{j=0}^{k-1} A^j B u_{t+k-1-j} \quad (4.53)$$

$$V(x(t)) = \frac{1}{2} x^T(t) Y x(t) + \min_U \left\{ \frac{1}{2} U^T H U + x^T(t) F U \right. \\ \left. \text{subject to } GU \leq W + Ex(t) \right\} \quad (4.54)$$

Where $U = [u_t^T, \dots, u_{t+N-1}^T]$ and H is the optimization vector. In conventional MPC approach, optimization problem defined in (4.53) need to be solved online a finite horizon. Therefore control sequence U will be computed implicitly as a function of x. In explicit MPC formulation, the basic idea is to treat x(t) as a function of parameters and solve (4.53) offline explicitly. This leads to parametric programming approach in which the solution of control problem is found for a range of parameters. If the programs are depending on more than one parameter, than the case will be multi- parametric programming. Solution of multi-parametric programming will come up with the result that the optimizer U is a piecewise affine and continuous function represented explicitly as;

$$u(x) = \begin{cases} F_1 x + g_1 & \text{if } H_1 x \leq k_1 \\ \vdots & \vdots \\ F_M x + g_M & \text{if } H_M x \leq k_M \end{cases} \quad (4.55)$$

The set of states thus parameters for which the problem is feasible ,is a polyhedral set. Basically, the polyhedral sets $(H_M x \leq k_M)$ shown in (4.55) are a partition of the given set of states X.

The cost function defined in (4.51) is covering the regulation problem. The controller can be extended to support offset-free reference tracking of setpoint signals. Assume that r(t) is the reference signal and the goal is to keep y(t) following r(t). (4.51) can be modified as follows.

$$\begin{aligned}
& \min \sum_{k=0}^{N-1} [y_{t+k|t} - r(t)]^T Q [y_{t+k|t} - r(t)] + \delta u_{t+k|t}^T R \delta u_{t+k|t} \\
& \quad s. t. \\
& \quad y_{\min} \leq y_{t+k|t} \leq y_{\max}, \quad k = 1, \dots, N_c \\
& \quad u_{\min} \leq u_{t+k} \leq u_{\max}, \quad k = 1, \dots, N_c \\
& \quad \delta u_{\min} \leq \delta u_{t+k} \leq \delta u_{\max}, \quad k = 1, \dots, N_u - 1 \\
& \quad x_{t+k+1|t} = A x_{t+k|t} + B u_{t+k}, \quad k \geq 0, \\
& \quad y_{t+k|t} = C x_{t+k|t}, \quad k \geq 0, \\
& \quad u_{t+k} = u_{t+k-1} + \delta u_{t+k}, \quad k \geq 0, \\
& \quad \delta u_{t+k} = 0, \quad k \geq N_u
\end{aligned} \tag{4.56}$$

We can express (4.56) in a similar form defined in (4.54).

$$\begin{aligned}
V(x(t)) &= \min_{\mathbf{u}} \left\{ \frac{1}{2} U^T H U + [x^T(t) u^T(t-1) r^T(t)] F U \right. \\
&\quad \left. \text{subject to } G U \leq W + E \begin{bmatrix} x(t) \\ u(t-1) \\ r(t) \end{bmatrix} \right\}
\end{aligned} \tag{4.57}$$

Please note that, the controller type is in state-feedback form as shown in (4.52). In case of using output feedback controller scheme, one need to use state estimator to compute the control law as a function of states.

Basically, the control actions computed by multi-parametric programming are expressed in terms of look-up tables by using gains F_i and g_i . The polyhedral partition M defines the number of operations and size of lookup table gains. During real-time applications computer code is used to generate pre-defined lookup tables. Lookup tables are then stored in real-time operating computer. Therefore, storage is more important than the computation as the whole computation process is taken place offline.

Table 4.1 : Explicit MPC vs Online computation optimization (Bemporad, 2006).

$2N_u$	Online QP(ms)	Explicit MPC(ms)	Regions	Storage (Kb)
4	1.1[1.5]	0.005[0.1]	25	16
8	1.3[1.9]	0.023[1.1]	175	78
20	2.5[2.6]	0.038[3.3]	1767	811
30	5.3[7.2]	0.069[4.4]	5162	2465
40	10.9[13.0]	0.239[15.6]	11519	5598

Table 6.1 shows the performance comparison for different values of control horizon (N_u) which is mentioned in Bemporad (2006). The brackets shows the worst case values.

There are several tools for multi-parametric programming computation and explicit MPC formulation. Hybrid toolbox for MATLAB has been developed and presented in Bemporad (2004) which allows users to design and explicit and online MPC both for linear and hybrid systems. Tool is also used to generate piecewise affine controller code to be implemented directly as a C-Code for real-time applications. Herceg et.al (2013) presented the Multi-parametric toolbox. MPT toolbox is also used to design explicit MPC controller for high-speed implementation of MPC in real time applications.

4.4 Application

During this study, controller design have been performed both SISO and MIMO cases. In SISO case, controller design is based on where TBV is the only manipulated variable. In MIMO case, both TBV and WG are taken into account as manipulated variables. As similar design steps are used for MIMO and SISO controller design, the details are first mentioned in section 4.4.1 for MIMO control, then same steps are followed in SISO control as mentioned in section 4.4.2.

Controller design is relatively simple compared to frequency domain controller design and PIDs. Please note that controller design is repeated for each region by using the representative local linear model as shown in section 3.4.3. During this study, MPC design with online optimization has been performed by using MATLAB Model Predictive Control toolbox and explicit MPC design has been performed with Hybrid Toolbox.

4.4.1 MIMO control design

In MIMO control design, MPC design steps consist of following steps.

- Specification of signal properties
- Control objectives

- Specification of Prediction horizon and Control horizon
- Constraint definition
- Controller weights and estimator tuning

4.4.1.1 Specification of signal properties

Specification of signal types is essential for MPC design. By using the system model shown in (4.44), we can specify the signals as manipulate variables, measured disturbances and unmeasured disturbances. The selection of signals is similar to the signal types used in control-oriented modeling mentioned in section 3.4.3. Table 6.2 summarizes the signal specifications.

Table 4.2 : Specification of signal types.

Signal name	Definition	Unit	Type
Turbine Bypass Valve control	HP stage bypass valve control signal	%	Manipulated variable
Waste gate control	LP stage bypass valve control signal	%	Manipulated variable
Engine Speed	Engine rotational Speed	rpm	Measured Disturbance
Injection quantity	Quantity of main injection	mg/stk	Measured Disturbance
Boost Pressure	Pressure at intake manifold	hPa	Output variable
Boost Pressure noise-error	Error and noise signal for boost pressure	hPa	Unmeasured disturbance

4.4.1.2 Control objectives

Two-stage turbocharged system should satisfy certain performance criteria. Here the performance criteria can be defined in terms of the transient response of the system and the tracking of optimized steady state set points.

As mentioned in Lezhnev et.al (2002), Diesel engine torque response is proportional to intake manifold pressure gradient. Due to combustion characteristics of Diesel engine, overshoot observed in the boost pressure may be accepted. The primary focus is to reduce the response time of boost pressure. During controller design, system's performance should be assessed by using prespecified transient response criteria. During this study, the transient performance criteria are based on the load acceptance test suggested by Lezhnev et.al, 2002. The details of the test are explained below.

1. Primary goal is to track the desired boost pressure shown as red line in Figure 4.4 at constant engine speed.

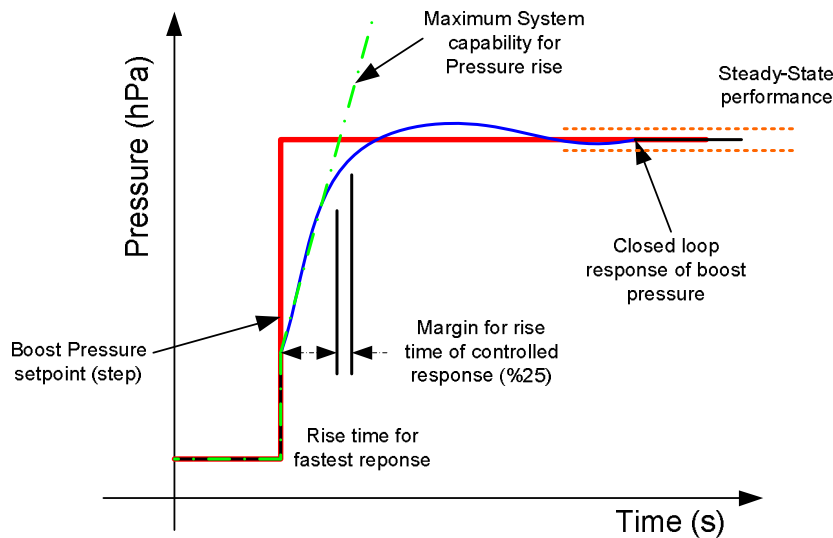


Figure 4.4 : Transient response characteristics.

2. The maximum system characteristics to increase the boost pressure is experimented by setting both TBV and WG to fully closed positions. This will give us the physical limitation of the system. This is shown in green dash-dot line in Figure 3.48. The response of the closed loop control system must be inside the boundary in which %25 additional time is added to

maximum boosting capability. Based on the experiments performed with state of the art boosting hardware, Response time criteria can be found in Table 6.3.

3. The boost pressure response of the two-stage turbocharged system will have a slower response compared to the maximum response line shown as blue line.
4. The overshoot of boost pressure should be limited to the values shown in Table 6.2 according to the varying steps in intake pressure.

As the increase in boost pressure is directly affecting brake torque characteristics, drivability attribute is also affected. Although load acceptance tests were performed in engine dyno and high fidelity simulation model, fine tuning of the controller is performed upon vehicle testing.

Table 4.3 : Transient response time requirements for varying pressure steps.

Step	Rise/Fall Time (ms)	Nominal Over/Undershoot	Robustness (for aged HW)	Steady-State Accuracy
150-200 hPa	1500	%5	%5	%2.5
300-350 hPa	2000	%6	%8	%2.5
450-500 hPa	2500	%7	%12	%2.5

The controller should exhibit satisfactory steady-state performance in which the steady state set points are optimized for fuel economy and full-load performance. The fuel and Air set points are defined in steady-state dyno testing. During set point optimization, 2D lookup tables are populated with optimum steady state values for intake manifold pressure as well as fuelling set points. Controller should keep the boost pressure inside the margin, which is defined as %2.5 as shown in Table 6.3. During this study, boost pressure set points are already optimized for production validated vehicle and satisfying EU6 emissions.

4.4.1.3 Specification of Prediction and Control horizons

As mentioned in section 4.1, prediction horizon and control horizon are the key tuning parameters for MPC control design. Prediction horizon defines the optimization window therefore, system response is affected directly. Under the situation in which sufficiently longer prediction horizon is used, potential constraints can well be considered and avoided. In addition, if the plant includes pure time delay, then the prediction horizon will have minimum limit such as it is greater than the delay of the system. Also increasing the Prediction horizon will have positive effects on controller performance when the plant shows non-minimum phase-behavior. In this case, MPC will compute the control action based on the longer behavior of the system. Figure 4.5 shows the comparison of different prediction horizons. First simulation is performed with Prediction horizon set to five samplings and latter was set to 50 samplings. The rise time of boost pressure response is higher when PH is set to 50. However, the disturbance rejection and robustness is better than smaller PH's.

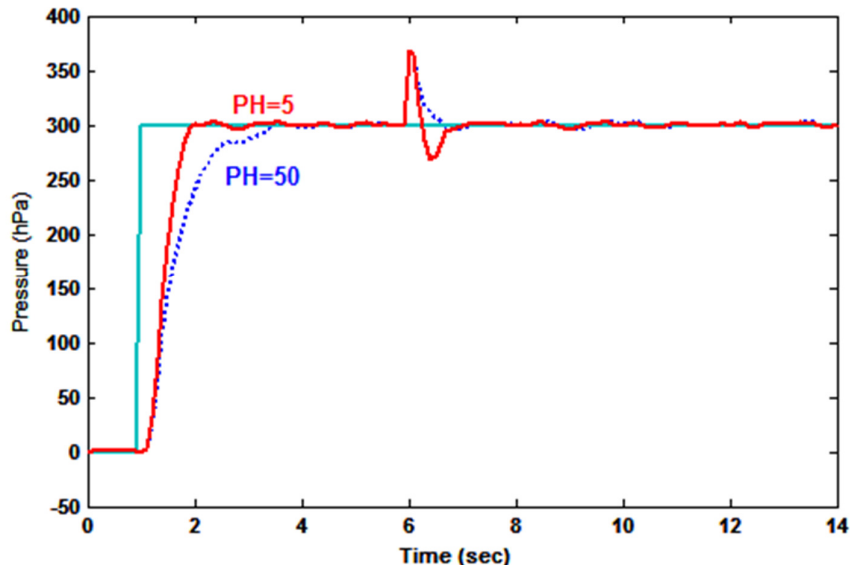


Figure 4.5 : Effect of Prediction horizon tuning on controller operation.

There are some examples from literature, which includes the tuning strategy for prediction and control horizons. Shridhar and Cooper, (1997), suggest defining the prediction horizon as the process settling time in samples, which is rounded to the next integer. In order to calculate the process settling time in samples, we need to

define the controller interval in which the controller runs. Control horizon is suggested to be set as some values in between 1 and 6.

During this study, the methodology suggested by Bemporad et.al, (2004) has been used.

1. We have defined the control interval based on the system's settling time. Figure 4.6 shows the results of engine dyno experiment to define control interval. Maximum TBV step command has been applied to observe system's settling time. It was recorded as 4 seconds approximately. Therefore, control interval is selected as 0.1 seconds.
2. Prediction horizon is set as number of sampling periods used in step 1 as 30. Decreasing this value should be avoided considering the system has pure time delay and exhibits non-minimum phase behavior.
3. Control horizon is set as 3. Increasing control horizon will have a relaxation on number of free moves thus explicit MPC computation. Therefore, control horizon should be selected as small as possible.

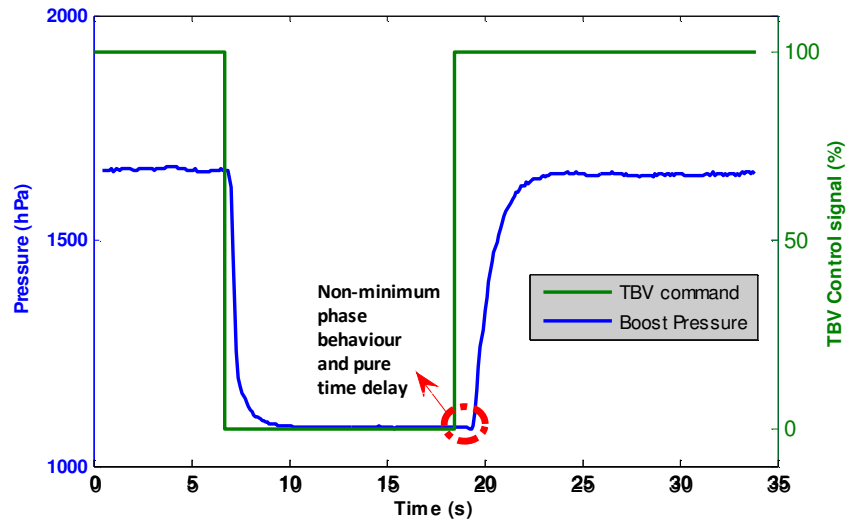


Figure 4.6 : Experiment to define control interval and Prediction horizon.

4.4.1.4 Constraint definition

As critical part of the finite horizon optimal control problem, constraint definition should be clearly determined during controller design process. Constraints are mostly related with physical system. As mentioned in section 4.2.1, constraints are investigated under 3 main types.

Output constraints are considered as 1st type which are directly related with the system dynamics. During this study, the single output and the controlled variable is the boost pressure. Constraint definition for boost pressure is required especially for maximum values in order to prevent cylinder failure. Hiereth and Prenninger, (2010) mentioned that the dynamics of thermal and mechanical stress induced by boost pressure. As the boost pressure increases the fuel quantity is also increased which resulting in increase in heat dissipation on cylinders and pistons. This would add additional thermal stress on the aforementioned engine components. In addition to thermal stress, mechanical stress should be investigated. As the boost pressure increased, there should be increase in the peak fire pressure and compression end pressure. These would increase the mechanical strength applied on the connecting rod, piston, cylinder head and bearings. There should be design limit for over boost, which would prevent the engine component's failure. During this study, the upper limit for boost pressure is set as 3500 hPa, which slightly lower than the design limit. There is not any lower limit for boost pressure. Therefore, it is set a 0 as shown in 4.58.

$$\begin{bmatrix} y_{\max} \\ y_{\min} \end{bmatrix} = \begin{bmatrix} 3500 \\ 0 \end{bmatrix} \quad (4.58)$$

The second type of constraints is the input constraints. Here, we need to analyze the TBV and WG actuators and their characteristics mostly. During this study, TBV and WG valves are driven with electro pneumatic valve actuators (EVRV). The schematics for working principles are shown in Figure 4.7.

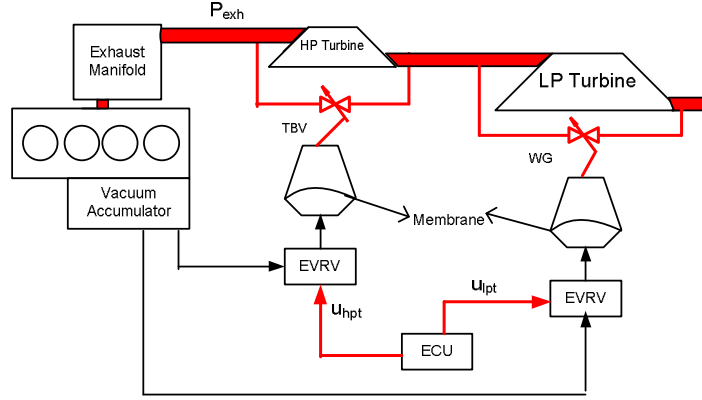


Figure 4.7 : TBV and WG elektropneumatic actuator layout.

Both TBV and WG are actuated by vacuum pressure actuator which is mechanically connected to the bypass valves. The source of the pressure inside the actuator is the vacuum pressure blender solenoid. This solenoid is controlled by PWM signal sent by ECU. As the Duty cycle of the PWM signal increases the amount of vacuum applied by solenoid is decreases so the valve is more likely to close. Closed valve results in increase in the turbocharger activity and boost pressure. There is a linear relationship between valve's output vacuum and the PWM duty cycle. PWM is sent by ECU using internal low-side drivers. Thus input signal constraints are taken directly as the maximum and minimum realizable PWM limits sent by the driver.

$$\begin{bmatrix} u_{\max tbv} \\ u_{\min tbv} \end{bmatrix} = \begin{bmatrix} 90 \\ 0 \end{bmatrix}, \begin{bmatrix} u_{\max wg} \\ u_{\min wg} \end{bmatrix} = \begin{bmatrix} 90 \\ 0 \end{bmatrix} \quad (4.59)$$

Same input constraints are valid both for TBV and WG as the ECU low-side drivers are identical.

Third and the last type of constraints are the input rate constraints. Basically they are related with speed of the actuator. During this study the maximum and minimum rate of the TBV and WG actuators are defined by using engine dyno experiment. Maximum rise of actuators are defined by sending PWM signal by applying maximum Duty Cycle. This would allow observing the rate of change of actuator control signal. Figure 4.8 shows the test sequence and signals.

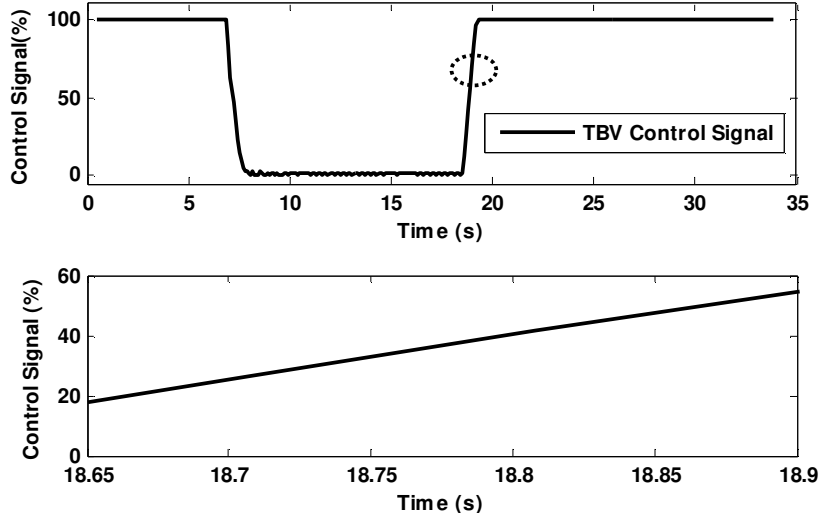


Figure 4.8 : Experiment for TBV rate constraint definition.

4.4.1.5 Controller Weights and Estimator tuning

As a last step in the MPC design process, controller weights should be defined and the estimator tuning should be performed. Please note that only key critical points are mentioned here. Simulation results are mentioned in Section 5.

As shown in (4.56), Q and R matrices are used for weighing the cost function for output set point tracking as well as satisfying input rate constraints to prevent drastic changes in the control signal. Boost pressure output tracking is adjusted by matrix Q and controller adjustments are weighted by matrix R. Please note that the effect of output and input rate weights are contradicting with each other. Increasing R matrix will result in smaller TBV and WG valve's controller actions, which would increase the controller robustness to Boost pressure prediction inaccuracies while degrading set point tracking. On the other, increasing Q will have positive effect on boost pressure tracking but will lead to excessive TBV and WG movement thus controller wear and instability. During the simulations, default values of Q and R matrices are used initially.

The effect of weights is shown in Figure 4.9 below. The simulation were performed on linear model for region 4 with 300 hPa step set point signal applied to boost pressure. Zero mean Gaussian white noise is applied to output signal as well as step disturbance of 50 hPa is applied at time 6 seconds. The rise time and disturbance rejection is affected from weighting due to consideration of input rate and ranges.

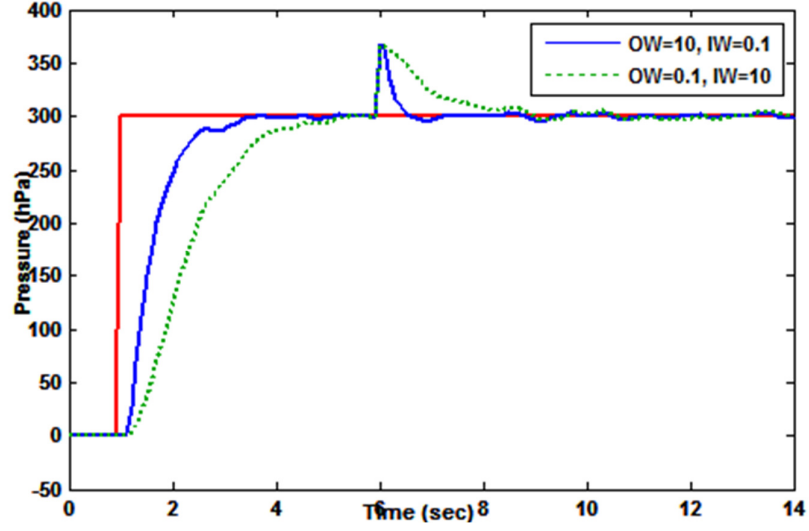


Figure 4.9 : Effect of Output and input weights on controller response.

As mentioned in Section 3, the system models are unmeasured signal as they have no physical significance because the model is generated as black box model. So the system states should be estimated using a linear state estimator to generate a control law. During this study, Linear Kalman Filter is used as state estimator. The necessary and sufficient condition for estimator design is to check whether the linear system is observable. (4.60) shows the observability matrix, which is calculated for Region 1.

$$AC_{region4} = 1 \times 10^8 \begin{bmatrix} 0.0001 & 0 & 0 & 0 \\ 0.0002 & -0.0003 & 0 & 0.0002 \\ -0.0015 & 0.0006 & 0.0001 & -0.0425 \\ 0.0703 & -0.2912 & -0.8634 & 6.3134 \end{bmatrix} \quad (4.60)$$

The observability condition is satisfied for all regions the observability matrix has a full rank.

The complete linear system for Region 1, which is used during estimator design, is shown in (4.61), (4.62) and (4.63).

$$\begin{aligned} & \hat{y}_m(k|k-1) \\ &= 1 \times 10^4 [1.7892 \quad -0.0177 \quad 0.0004 \quad -0.0007 \quad 0.0402 \quad 0.3311] \\ & \hat{x}(k|k-1) \end{aligned} \quad (4.61)$$

$$\begin{aligned}
& \hat{x}(k|k) \\
& = \hat{x}(k|k-1) \\
& + [0 \quad -0.0009 \quad 0.0007 \quad -0.0069 \quad 0.0002 \quad 0](y_m(k) \\
& - \hat{y}(k|k-1))
\end{aligned} \tag{4.62}$$

$$\begin{aligned}
& \hat{x}(k+1|k) \\
& = \begin{bmatrix} 0.9966 & -0.0213 & 0.0006 & -0.0016 & 0.0398 & 0 \\ 0.0369 & 0.9780 & -0.0425 & 0.0559 & -0.7834 & 0 \\ -0.0075 & -0.0037 & -0.8940 & -0.4096 & -6.2978 & 0 \\ 0.0207 & -0.1229 & -0.2938 & 0.7452 & 16.2813 & 0 \\ 0 & 0 & 0 & 0 & 1 & 0 \\ 0 & 0 & 0 & 0 & 0 & 1 \end{bmatrix} \hat{x}(k|k) \\
& + 1 \times 10^3 \begin{bmatrix} 0.0001 & 0 \\ 0.0081 & 0.0008 \\ -0.1480 & -0.0435 \\ -0.1616 & -0.0117 \\ 0 & 0 \\ 0 & 0 \end{bmatrix} \Delta u(k)
\end{aligned} \tag{4.63}$$

Estimator tuning is based on the adjustment of Kalman gain matrix, M . Estimator tuning is as much critical as controller design, as it defines the controller sensitivity to unmeasured disturbances (prediction errors). During controller design, estimator tuning is performed in MATLAB Model predictive control toolbox. Figure 4.10 shows the effect of Kalman gain matrix on MPC's disturbance rejection capability. Overall gain of estimator is changed from 0.44 to 0.56. 50 hPa unmeasured disturbances is applied on boost pressure at 4 sec. with boost pressure set point value is stepped to 300 hPa. In addition, Gaussian white noise signal is applied as input disturbances. As the Kalman estimator gain is increased, controller becomes much more sensitive to disturbances. Any Kalman gain matrix is increased, controller is responding less aggressively on the unexpected changes in the output, because it assumes that they are measurement noise rather than a disturbance. On the other hand, this phenomenon is resulting in the increased controller activity as shown in Figure 4.11.

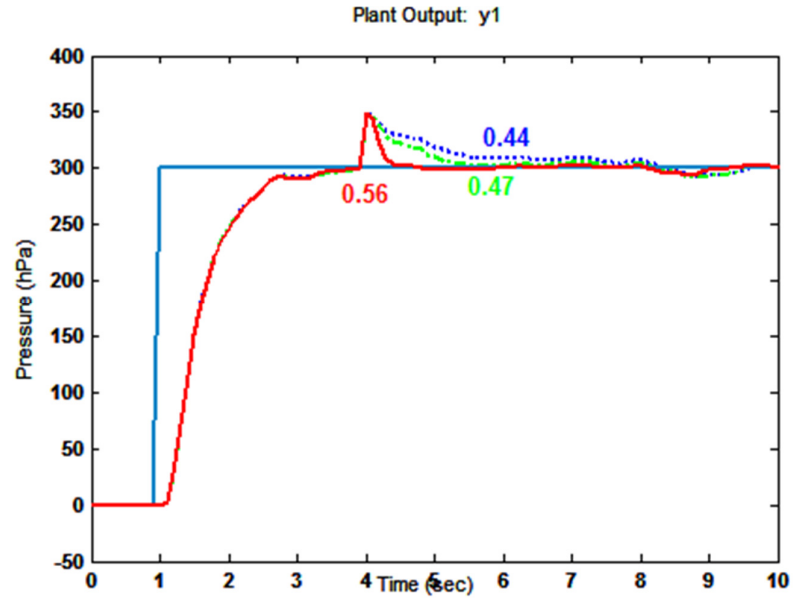


Figure 4.10 : Effect of Kalman gain matrix on disturbance rejection.

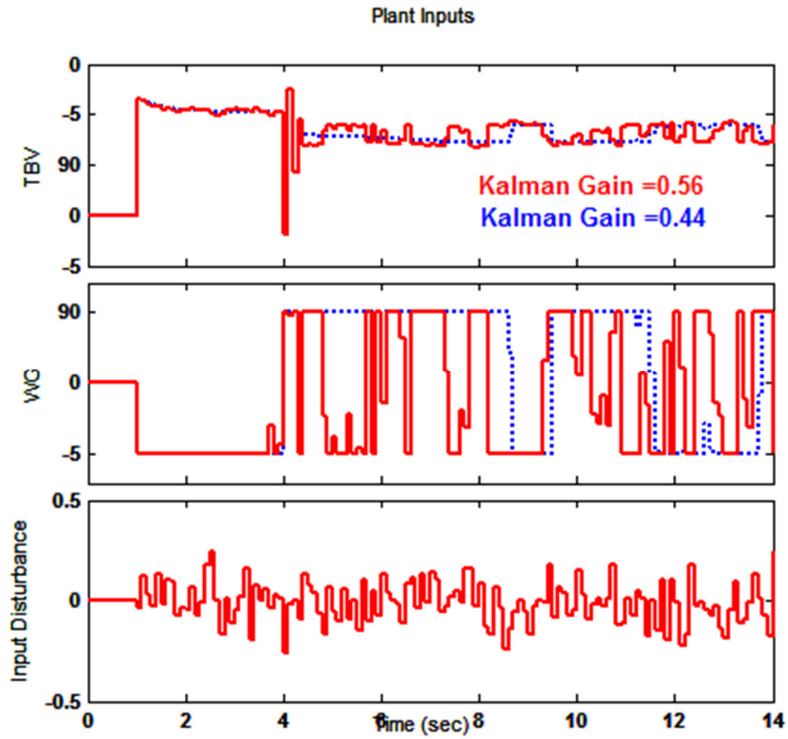


Figure 4.11 : Effect of Kalman Gain matrix on Controller activity.

4.4.1.6 Generation of polyhedral controller partitions for explicit MPC

As mentioned in section 4.3, in order to use explicit formulation of MPC during controller implementation, polyhedral controller regions should be determined. During this study, 4 different explicit MPC controllers are generated corresponding

to 4 local linear regions mentioned in section 3. Therefore, multi parametric programming has been calculated 4 times for each controller.

As mentioned in section 4.3, number of controller regions is critical for explicit MPC real time operation as it defines the storage of controller code in real time processor. Main item increasing the number of regions is controller horizon. Table 6.4 shows the relationship between Control horizon and the number of controller regions. The calculation is performed by using the model and linear MPC controller for local linear region 1 and local linear region 3. Throughout the calculations, prediction horizon is kept at 30.

Table 4.4 : Control horizon and polyhedral regions

Controller region	Control horizon	# of controller regions
Region 1	1	24
Region 1	2	244
Region 1	3	879
Region 3	1	19
Region 3	2	213
Region 3	3	1619

Increasing the control horizon, which is mainly describing the free control moves, are increasing the number of polyhedral partitions in explicit MPC computation. This would result in excessive processor storage. As there is already 4 different multi-parametric programs for each local linear regions, increasing the controller partitions more may result in issues during real time operation. Therefore, control horizon is set as 1 for all regions.

Figure 4.12 and Figure 4.13 show the polyhedral partition for region 1 and region 3 respectively.. The plot shows the partition for input space (TBV and WG). Originally, controller is function of system states therefore, it is four dimensional. But for visualization purposes, 4 states and reference boost pressure set point is fixed and resulting partitions are shown in input space.

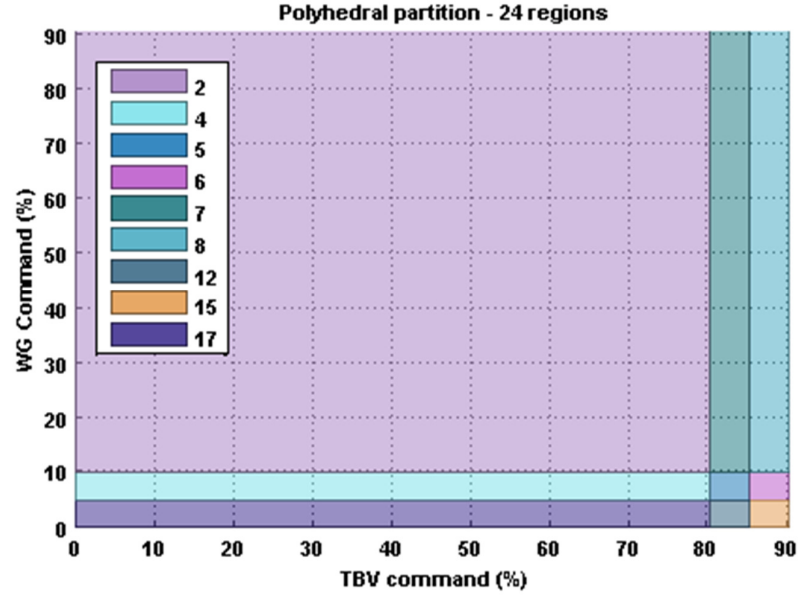


Figure 4.12 : Polyhedral partition for region 1.

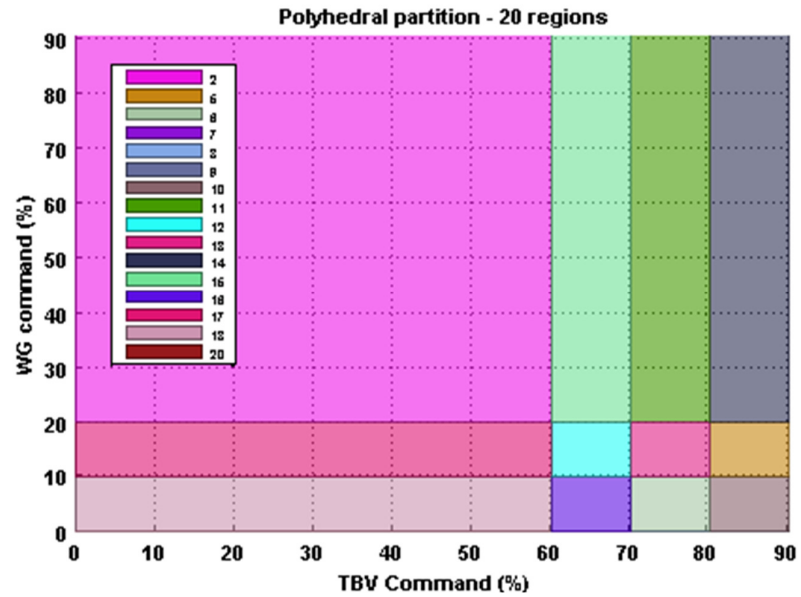


Figure 4.13 : Polyhedral partition for region 3.

4.4.2 SISO control design

SISO controller design steps are similar to those mentioned in section 4.4.1. Below are just the incremental design changes performed during SISO design. Validation results which shows the comparison with MIMO controller is mentioned in section 5.

4.4.2.1 Control objectives

Control objectives are similar to MIMO control. But, target rise/fall time of the system needs to be modified to be aligned with single actuator case. As WG is fully closed, all the flow would be directed to low pressure stage turbocharger, which would add additional inertia to the system during turbocharger acceleration. Therefore, target rise/fall times would be longer than MIMO targets.

Table 4.5 shows the modified target parameters for SISO control in terms of rise-fall time, nominal over/undershoot and steady-state accuracy.

Table 4.5 : Transient response time requirements for varying pressure steps-SISO.

Step	Rise/Fall Time (ms)	Nominal Over/Undershoot	Robustness (for aged HW)	Steady-State Accuracy
150-200 hPa	1700	%4	%5	%2.5
300-350 hPa	2300	%5	%8	%2.5
450-500 hPa	2700	%6	%12	%2.5

4.4.2.2 Constraint definition

Output constraints are similar as shown in (4.58) as well as input and input rate constraints shown in (4.59).

4.4.2.3 Controller Weights and Estimator tuning

The effect of weights and estimator is same as mentioned in section 4.4.1.5. Figure 4.12 shows the effect of Output and input weightings on the controller performance. During simulations, 50 hPa unmeasured disturbances is applied on boost pressure at 5 sec. with boost pressure set point value is stepped to 300 hPa. In addition, 50 mg/stk injection quantity is applied as measured disturbance at time 3 sec.

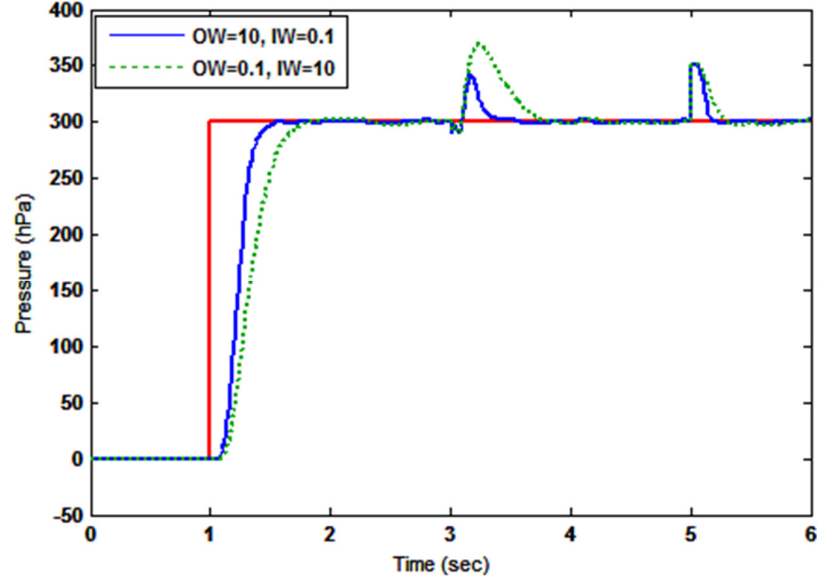


Figure 4.14 : Effect of Output and input weights on SISO controller response.

4.4.2.4 Generation of polyhedral controller partitions for explicit MPC

Similar methodology has been carried out as in section 4.4.1.6. Table 6.6 shows the relationship of Control horizon and number of controller regions for SISO case. Due absence of WG input, number of controller regions for same Control horizon is lesser than MIMO case. In addition, number of local linear regions is 4 rather than 7. Therefore, Control horizon is selected as 3 in SISO case. Figure 4.15 and Figure 4.16 shows the polyhedral partitions for regions 1 and 3.

Table 4.6 : Control horizon and polyhedral regions for SISO case.

Controller region	Control horizon	# of controller regions
Region 1	1	5
Region 1	2	17
Region 1	3	45
Region 3	1	5
Region 3	2	21
Region 3	3	87

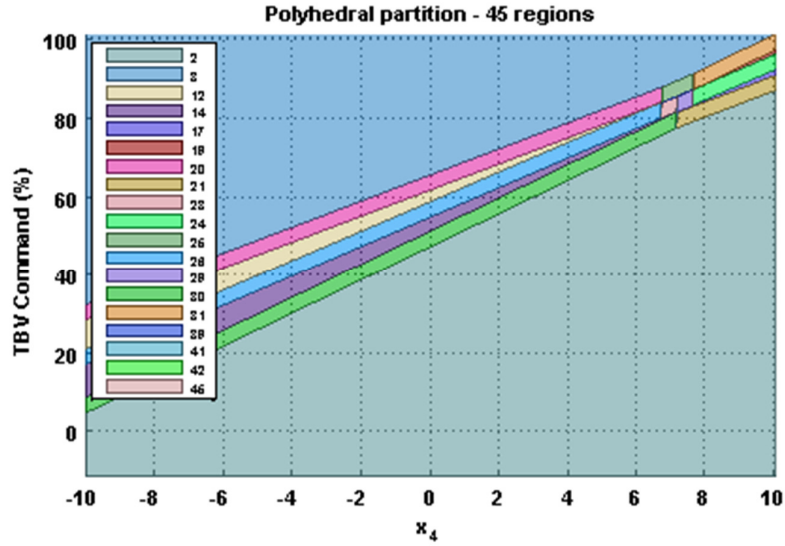


Figure 4.15 : Polyhedral partition for region 1 in SISO case.

Similar to MIMO case, Figure 4.15 and 4.16 is plotted when remaining 3 states and reference boost pressure set point signal is fixed to constant values. During the calculation of Multi-parametric programming for explicit MPC, Hybrid toolbox has been used.

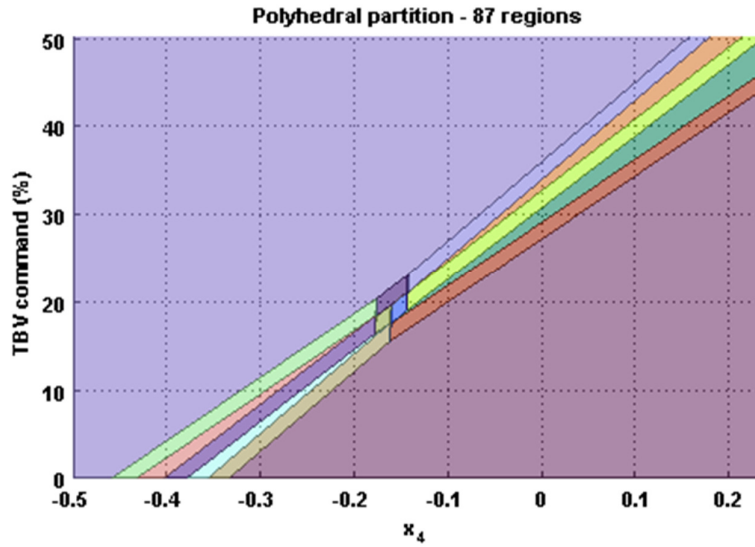


Figure 4.16 : Polyhedral partition for region 3 in SISO case.

5. SIMULATIONS

As controller design completed, performance of the MPC controller is tested by a series of offline simulations. Nonlinear engine model mentioned in Section 3 has been used during offline simulations. Simulations were performed in MATLAB-SIMULINK. Controller generated in Hybrid toolbox and Model Predictive Control toolbox have been combined with WAVE RT model as shown in Figure 5.1

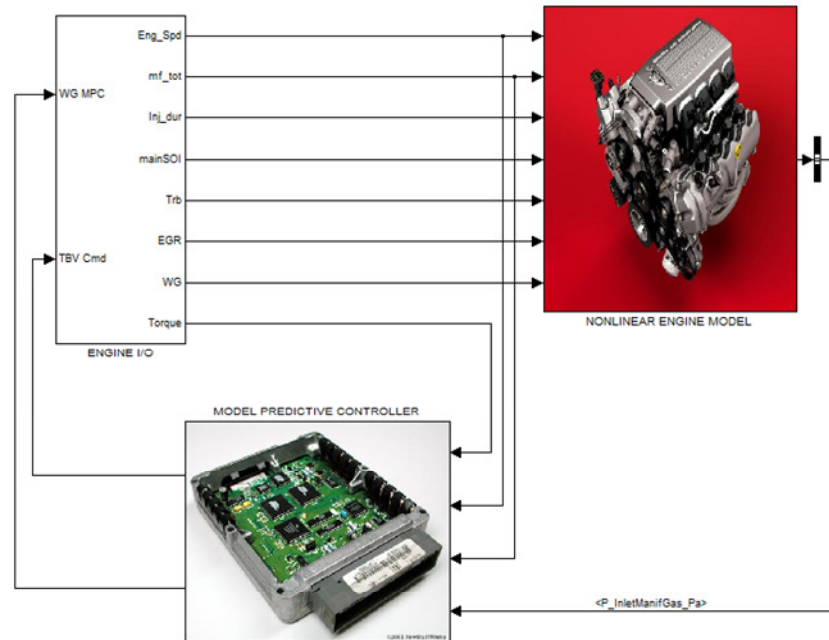


Figure 5.1 : Overview of MATLAB-SIMULINK simulation model.

Simulations for were performed for SISO and MIMO cases seperately. For both of the cases, offline simulations are performed in 4 different groups shown below

- Step response simulations in fixed engine speeds

Step signal is applied to boost pressure according to small, medium and large step signal steps as shown in Tables 4.3 and 4.5. During simulations engine speed is

fixed. Small, medium and large setpoints are applied at 1500, 2000 and 2500 rpms respectively. Controller's disturbance rejection capability is also observed during offline simulations.

- Simulations with mixed transient cycle in fixed engine speed

A mixed transient cycle are generated by combining ramp and step load responses. Mixed cycles includes small, medium and large steps.

Please note that, load signal applied for setpoint signal rather than imposing boost pressure signal directly. This means, fuel and air setpoints are changed together. This allows to test controller similar to the structure used in real time ECUs.

5.1 Offline Simulations with SISO Controller

5.1.1 Step Response Simulations with fixed engine speed

Figure 5.2 shows the small step response performed at 1500 rpm. First 7 seconds of simulation is neglected as model is initialized during that duration. At 10 seconds, load step applied which corresponds to 200 hPa boost pressure and 15 mg/stk main injection quantity.

The rise time of system is calculated as 1.53 seconds. This satisfies the controller objectives shown in Table 4.5. The maximum overshoot is below %1 which is also satisfactory in terms of target requirement which is %7 for small step responses. Figure 5.2 also shows the changes in the controller partition regions, which are mentioned in section 4.4.2.4. There is no change in the explicit controller and always one controller is active. Please note that this should not be confused with local linear regions. During this simulation, controller related to local linear region 2 is used due to engine speed and torque changes.

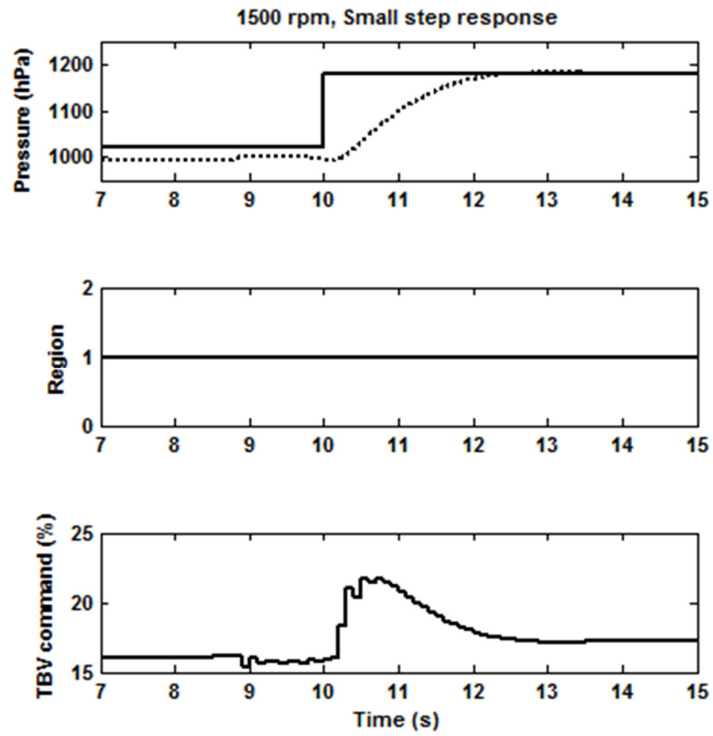


Figure 5.2 : SISO small step response at 1500 rpm.

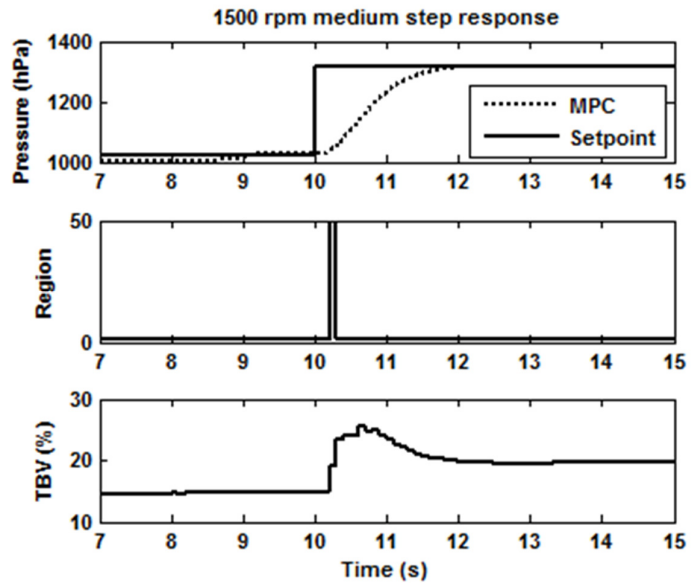


Figure 5.3 : SISO medium step response at 1500 rpm.

Figure 5.3 shows the medium step response at 1500 rpm. The rise time of system is calculated as 1.3 seconds, which is below than the target requirement shown in Table 4.5. Controller region is changed to 50 once during boost pressure build-up when the

step set point is applied. There is no overshoot observed in system response. Kalman filter contributes to the system that it shows zero steady state tracking error.

In order to assess controller's disturbance rejection capability, simulation is performed with medium step boost pressure signal applied with disturbance applied at steady state. In order to replicate real conditions, disturbance is generated by triggering EGR valve at time 25 seconds by %20 opening. This allows exhaust flowing through EGR valve, which would require boost pressure declines. As shown in Figure 5.4, the amount of decline in boost pressure is not more than 100 hPa, which would not create any drivability and performance concerns in real world conditions.

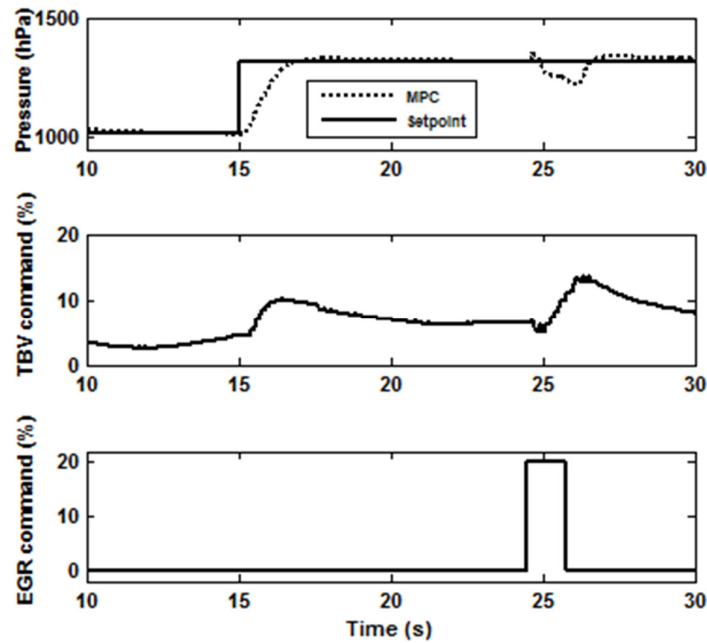


Figure 5.4 : SISO disturbance rejection with medium step setpoint applied at 1500 rpm.

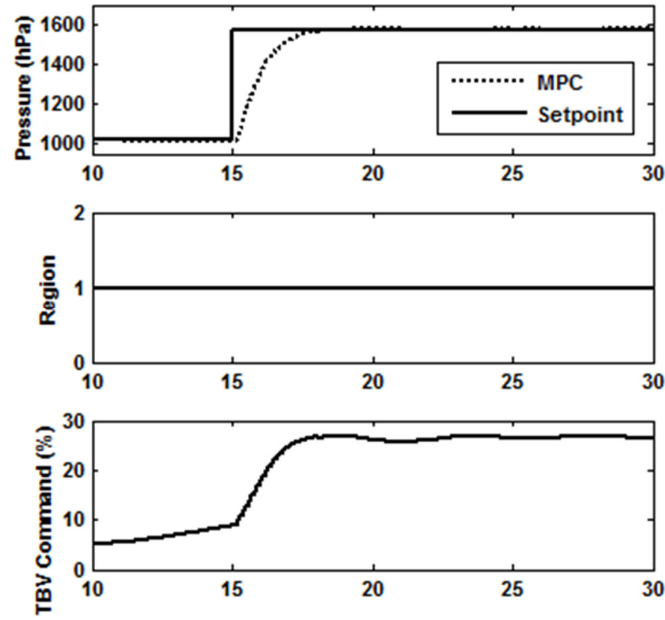


Figure 5.5 : SISO large step response at 1500 rpm.

Figure 5.4 shows the large step response of the system. During large step simulation, an injection quantity of 27.95 mg/stk step demand is applied as desired injection quantity with step boost pressure demand 530 hPa. The rise time of the step response is calculated as 1.75 seconds. The target requirement is 2.7 seconds as shown in Table 4.5. Maximum overshoot is calculated as %0.7 which can be neglected. Controller region is not changing similar to small and medium step responses.

Figure 5.6 shows the simulations results of medium step response performed at 2000 rpm. The rise time is approximately 2 seconds with maximum overshoot of 0.01% which satisfies the controller objectives. Controller region is not changing during simulation and only single controller is active.

The disturbance rejection simulation has been performed with large step signal applied. However, disturbance is applied with a step injection quantity signal rather than applying EGR. This is because in real conditions EGR is operational only in low loads and speed conditions. Using EGR at high load speed point would create excessive engine soot generation thus particulate emissions will be affected.

During simulations, 5 mg/stk injection quantity is applied at time 30 seconds. Injection quantity disturbance is much more realistic in high load speed points. 5 mg/stk disturbance value is realistic as higher values might create damage to the cylinder and the probability of occurrence is rare.

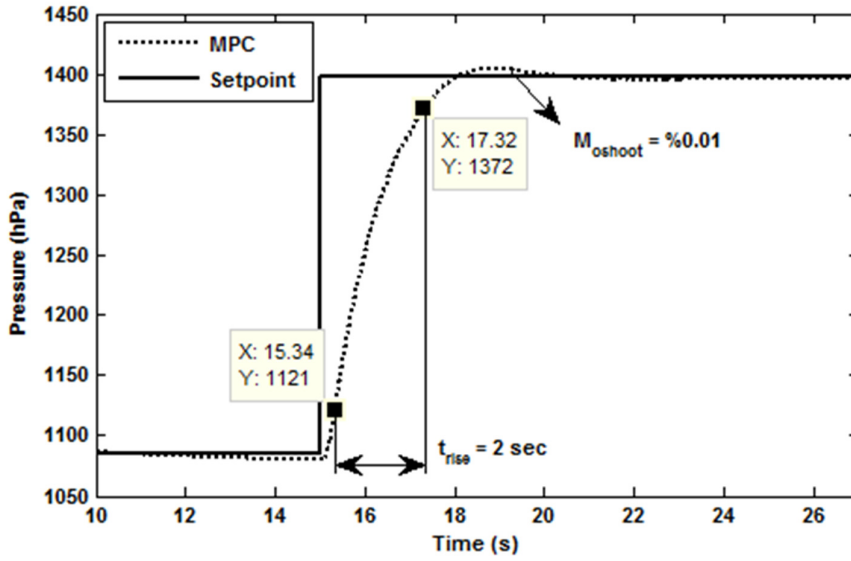


Figure 5.6 : SISO medium step response at 2000 rpm.

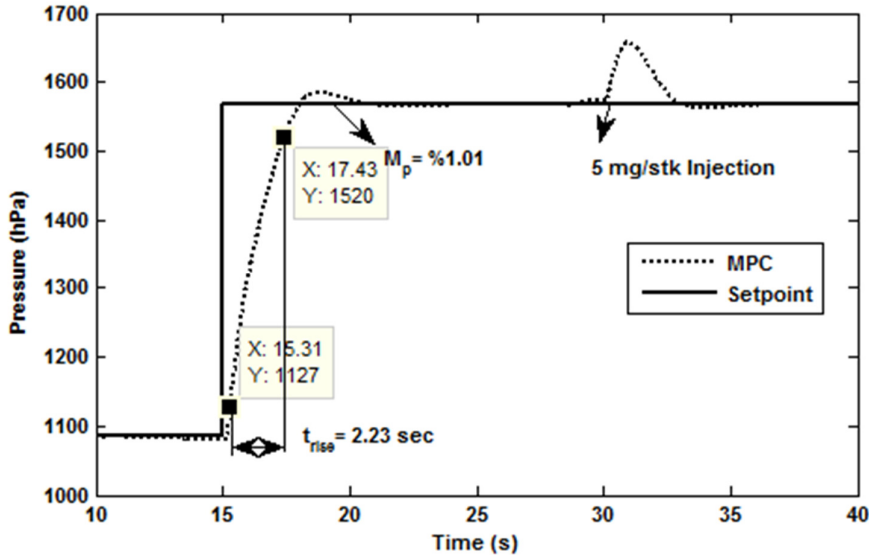


Figure 5.7 : SISO large step response at 2000 rpm with injection disturbance.

The rise time of large step response shown in Figure 5.7 is 2.23 seconds, which satisfies the controller objectives in addition to maximum percent overshoot of %1.01. The deviation caused by injection quantity is not exceeding 100 hPa.

Figure 5.8 shows large step responses results of the simulations performed at 2500 rpm. 5 mg/stk injection quantity is applied as disturbance signal. Maximum percent overshoot is close to %1 and the rise time is found as 1.76. Both of the values are satisfying target requirements. Figure 5.8 also shows the acceleration of two sequential turbochargers and their dynamics behavior.

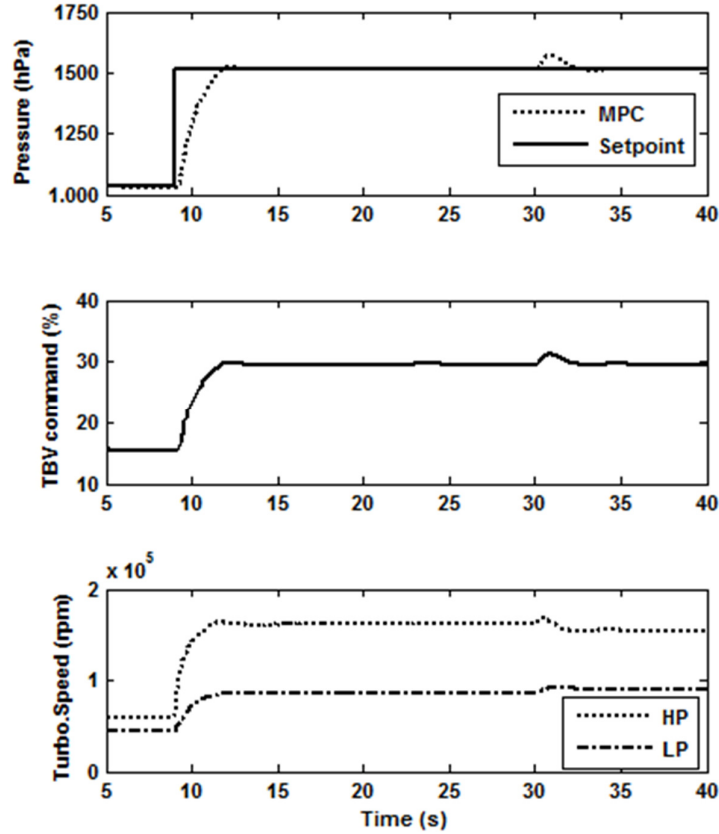


Figure 5.8 : SISO large step simulation at 2500 rpm with injection disturbance.

Not all simulations results are presented here. Entire simulation results are found in Appendix B.

5.1.2 Simulations with mixed transient cycle in fixed engine speed

As controller performance is tested with step signal and various disturbance signals, we can extend the offline simulations by applying series of different step and ramp inputs. During mixed step transient cycle simulations, fine-tuning of Kalman filter gain has been performed. Simulations were performed with a mixed transient cycle different engine speeds (1500, 2000 and 2500 rpm). Figure 5.9 shows the simulation result performed at 1500 rpm. As mentioned in section 4, the effect of Kalman filter gain is especially on the system rise time. The Kalman filter gain is shown in Figure 5.9 is the multiplier used to change Kalman filter gain vector M mentioned in section 4. The transient cycle used in this simulation includes small to large steps as well as ramp inputs. The controller is tuned in order to cancel steady state error as well as minimizing rise time and maximum percent overshoot. The minimum rise time

observed during simulation is 2.46 seconds, which well below the target requirements in addition to maximum percent overshoot of %0.5.

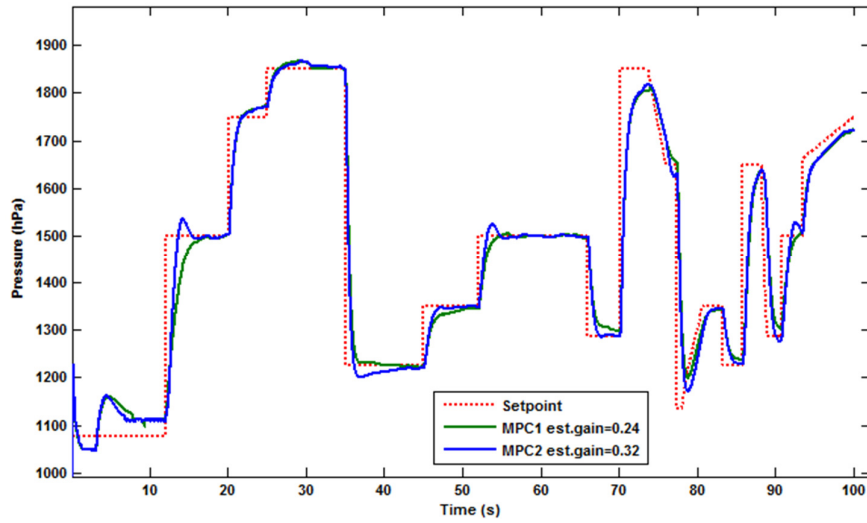


Figure 5.9 : Effect of Kalman filter gain on mixed transient cycle simulation at 1500 rpm.

Kalman estimator multiplier has been chosen as 0.24 in order to minimize overshoots. This results in increase in the rise time but as there is already margin to target requirements. As fine-tuning of Kalman filter has been performed, same cycle is also used to assess the effect of prediction horizon when using non-linear model simulations. Figure 5.10 shows how the system response is changed when Prediction horizon is changed from 30 steps to 10 steps. Simulations were performed with modified Kalman filter gain as mentioned above. When the prediction horizon is decreased the rise time of the system also decreases.

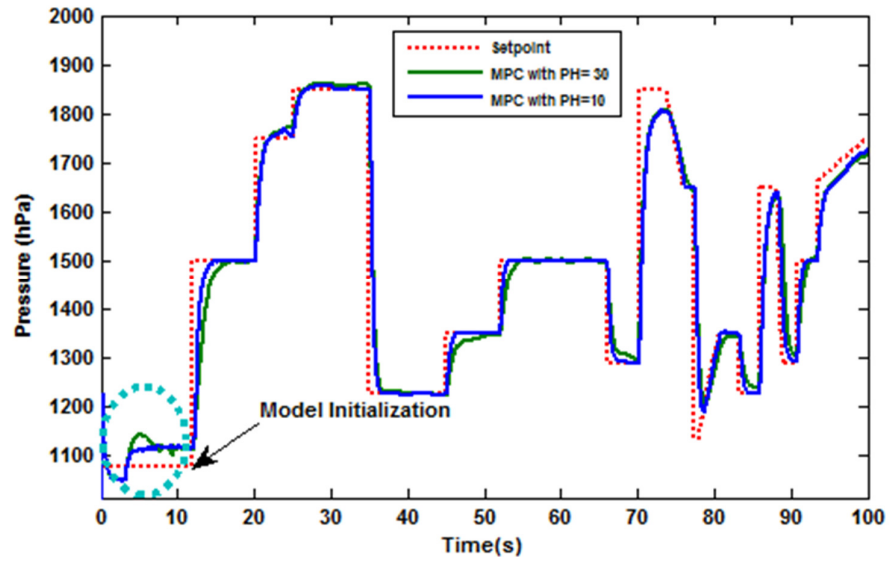


Figure 5.10 : Effect of Prediction horizon on mixed transient cycle simulation at 1500 rpm.

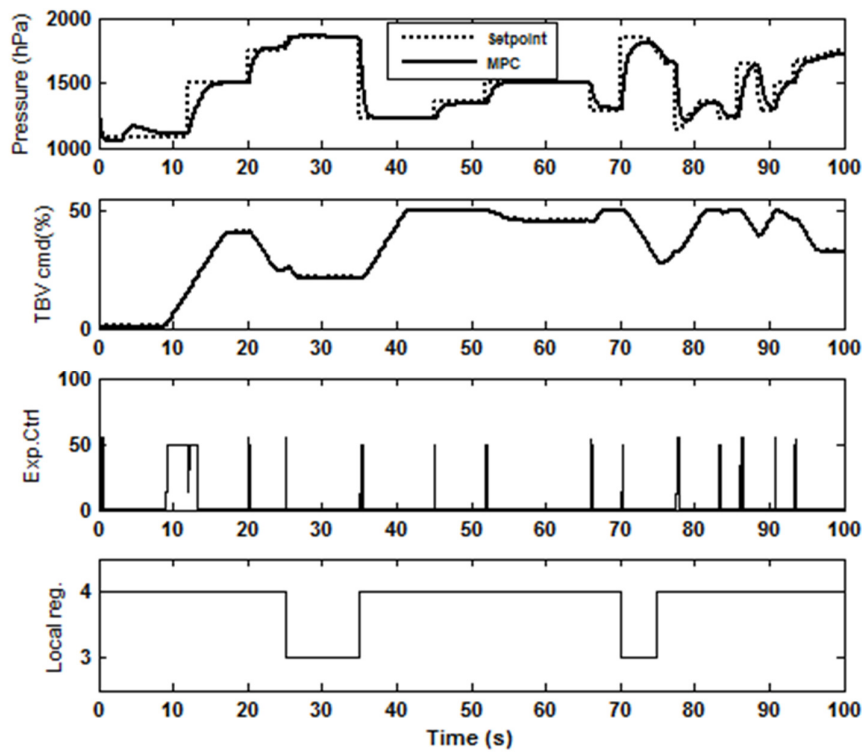


Figure 5.11 : Mixed transient simulation at 1500 rpm

During mixed transient cycle simulations, MPC is switched between local linear controller for region 3 and 4 as well as explicit controller change between various controllers. In order to provide smooth transitions, all controllers update their internal state observers regardless of being active or inactive. This phenomenon is shown in Figure 5.11 above.

5.2 Offline Simulations with MIMO Controller

5.2.1 Step Response Simulations with fixed engine speed

Step response simulations are performed also with MIMO controller. Figure 5.12 and Figure 5.13 shows the results of large and small step responses simulation performed at 1500 rpm.

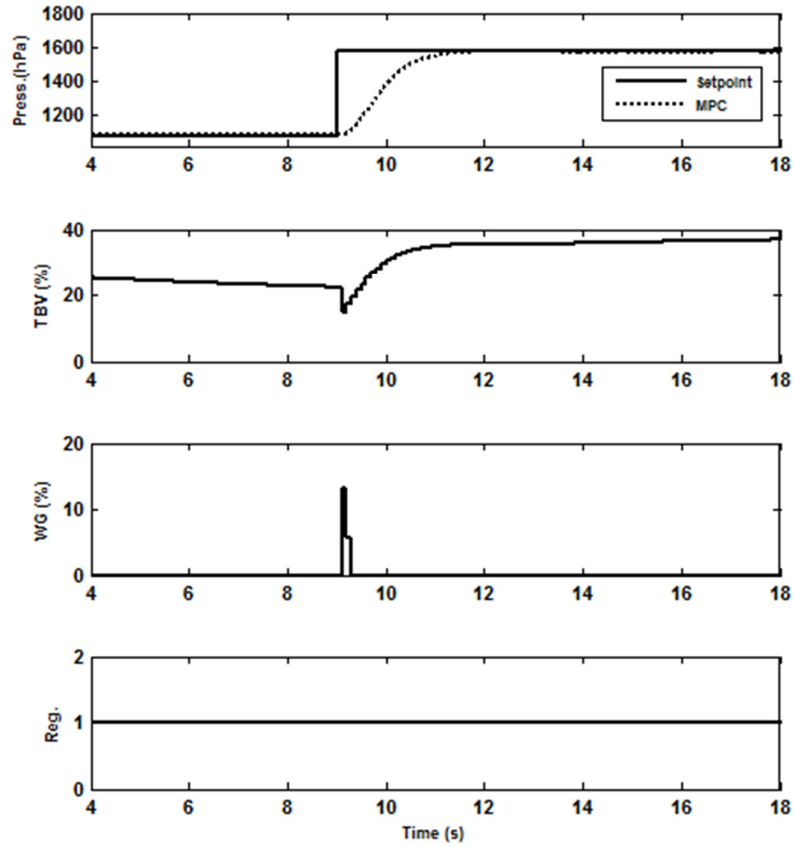


Figure 5.12 : Large step simulation performed at 1500 rpm with MIMO controller.

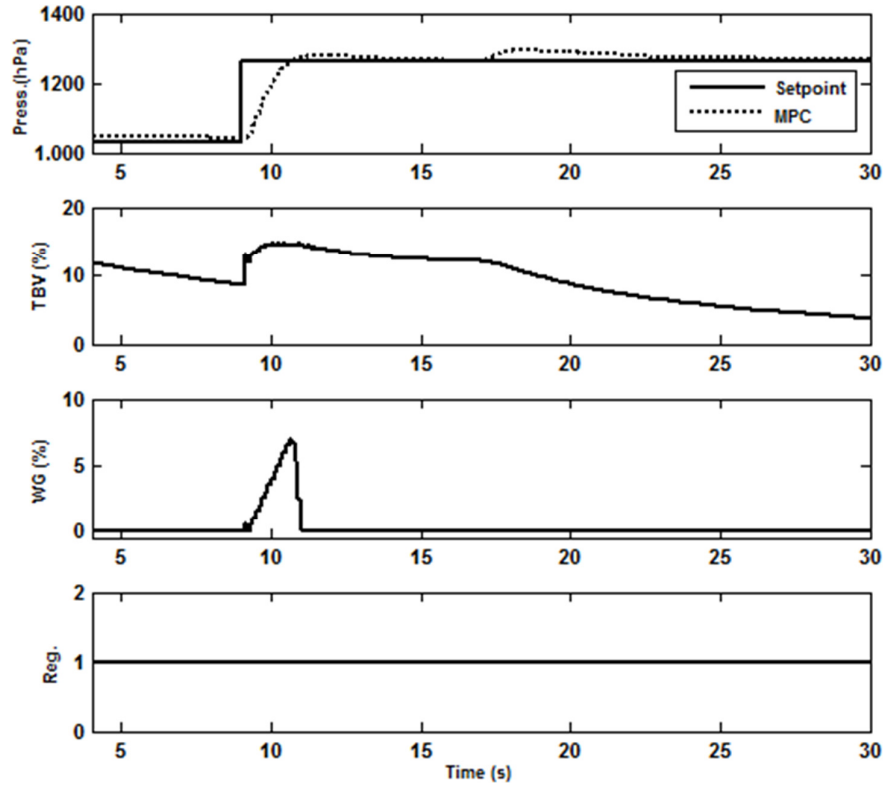


Figure 5.13 : Small step simulation performed at 1500 rpm with MIMO controller.

It is clearly visible that during boost pressure build-up, waste gate valve is tending towards fully closed position in order to increase boost pressure rise time. The rise time of the system is calculated as 1.57 seconds compared to 2.23 seconds in SISO controller when large step response applied. The maximum overshoot is calculated as %1.02 which can be neglected. For small step response, the rise time is calculated as 1.17 seconds where overshoot is increase to %3.

As WG valve tends to behave in fully closed position, simulations were performed by fully closing the waste gate valve and providing boost pressure control only by TBV. This is accomplished by manually setting WG signal as fully closed while MIMO controller is still calculating the WG signal. Figure 5.14 shows the results of two simulations and the difference in boost pressure error. The difference in rise time of two simulations is calculated as 0.12 seconds. The importance of this phenomenon is under specific engine speed and load points, WG is set as fully closed in order reduce controller energy and operation.

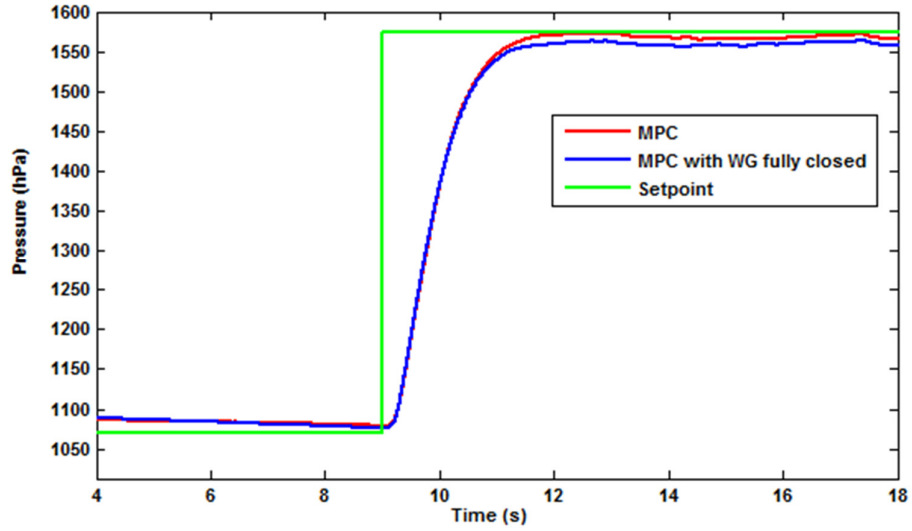


Figure 5.14 : Comparison of MIMO MPC with WG control and WG fully closed setting.

Figure 5.15 shows large step response simulation performed at 2500 rpm with disturbance applied at time 17 seconds. The disturbance is applied in terms of 5 mg/stk step injection signal due to the reasons outlined in section 5.1.1. The rise time of the system is calculated as 1.82 seconds where maximum overshoot is calculated as %3.05. The disturbance rejection capability is worse than SISO control. Although, maximum deviation from set point is close to 100 hPa, the settling time is longer than SISO control.

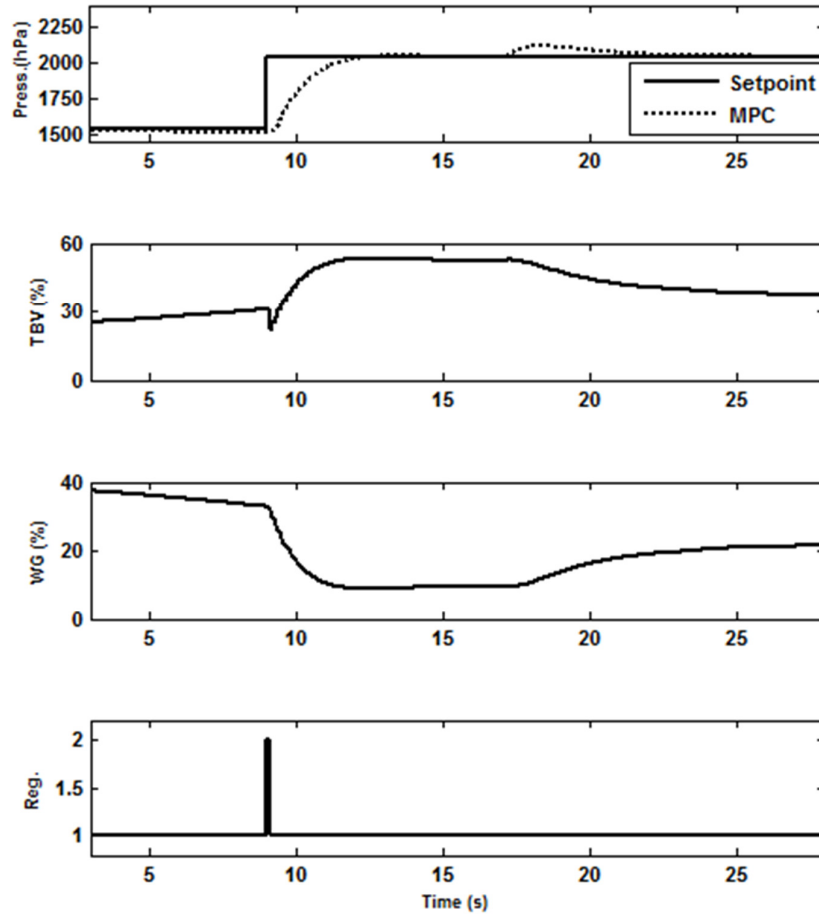


Figure 5.15 : Large step simulation performed at 2500 rpm with MIMO controller.

Figure 5.16 shows the medium step simulation result at 2000 rpm with injection disturbance applied. In contrast to large step simulations performed at 2500 rpm, duration in which WG is demanded as fully closed, is higher. The disturbance rejection capability is improved at 2000 rpm and settling time is decreased. The amount of boost pressure increase during disturbance is under 100 hPa limit. Disturbance rejection is accomplished by means TBV only operation. WG valve is fixed as constant. The rise time of the controller is calculated as 1.2 seconds in contrast to increased overshoot as %6 which is borderline according to the target requirements.

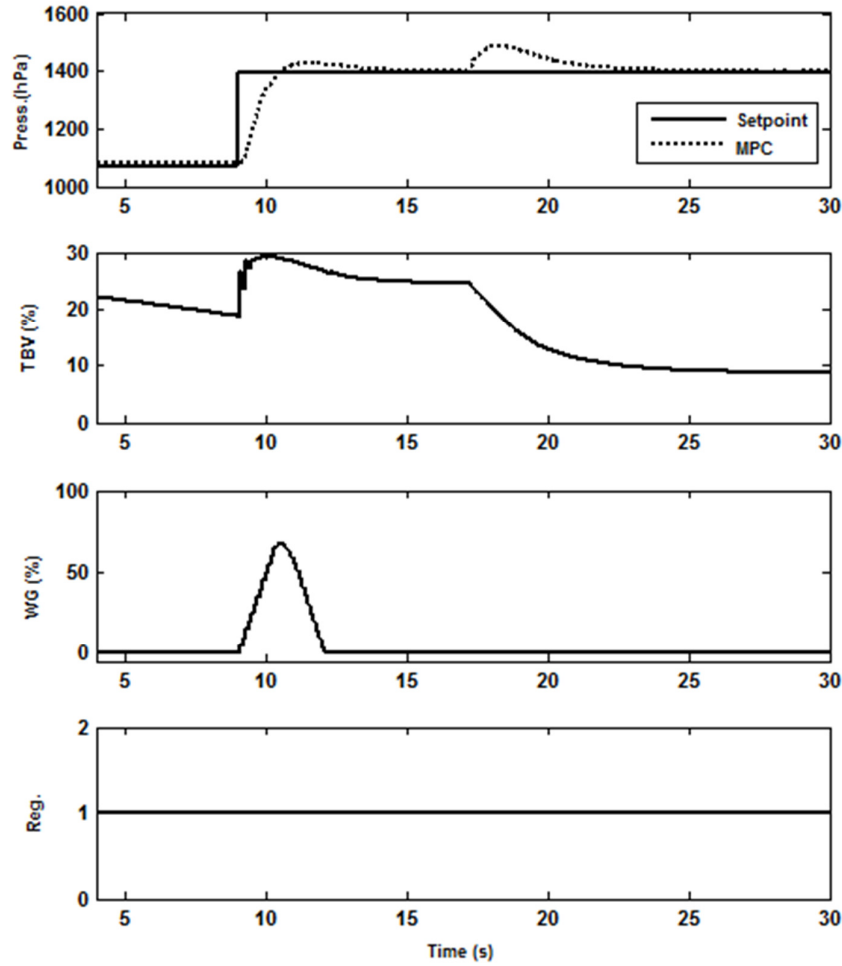


Figure 5.16 : Medium step simulation performed at 2000 rpm with MIMO control.

Figure 5.17 shows much more detailed simulation result related to medium step response simulation performed at 2500 rpm with disturbance applied. The maximum overshoot is calculated as %6.5 which is close to the target requirements. The rise time is calculated as 1.17 seconds which faster than SISO controller. Waste gate is regulated but most of the time, is working close to fully closed position. Figure 5.17 also shows the changes in the turbo speeds of the two turbochargers. During boost pressure build-up, TBV is set to fully closed position therefore; airflow is flowing through high Pressure stage turbocharger which leads to more turbocharger acceleration. On the other hand, WG is regulated to enable partial flow flowing through low-pressure turbocharger that leads to less acceleration in shaft speed.

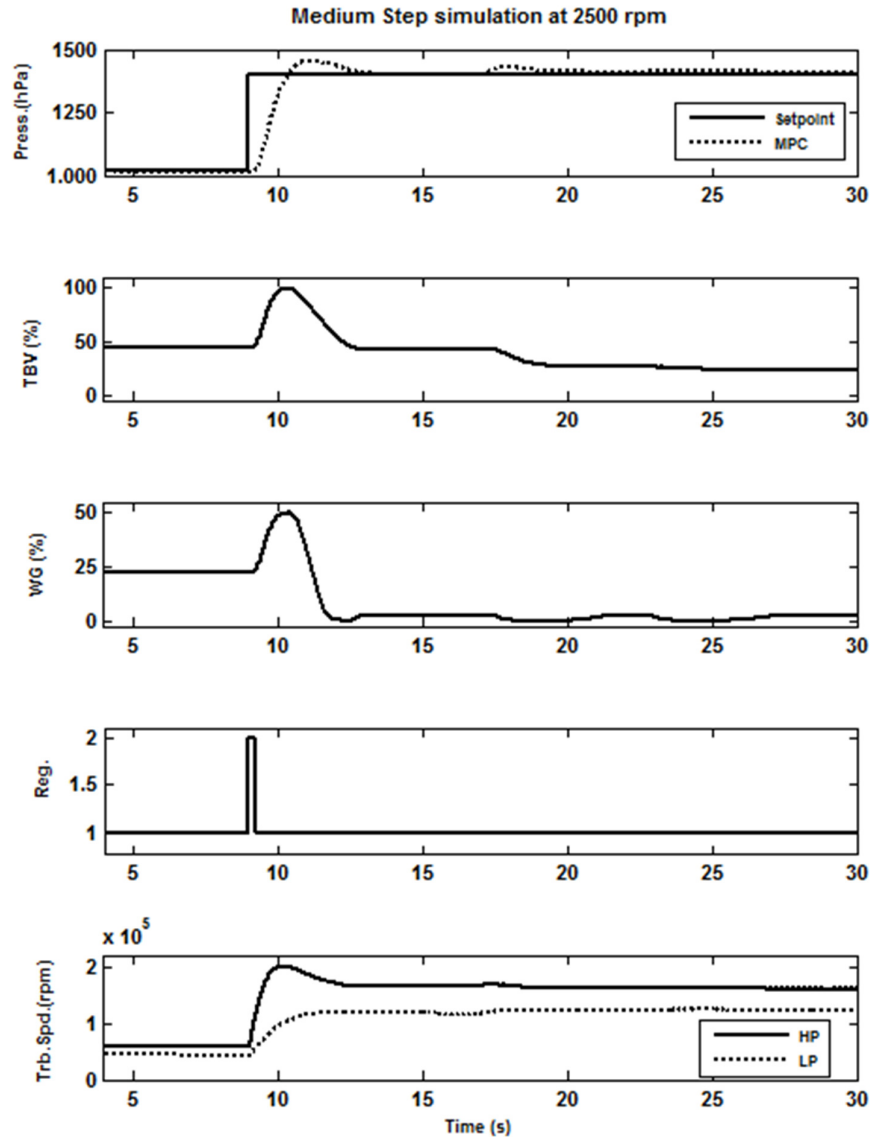


Figure 5.17 : Medium step simulation performed at 2500 rpm.

5.2.2 Simulations in mixed transient cycle at fixed engine speed

Transient cycle mentioned in section 5.1.2 is used during simulations with MIMO controller. First simulation is performed at 1500 rpm. It is observed that initial Kalman gain configuration results in non-zero steady state tracking error. Therefore, Kalman gain has been fine tuned. Observer tuning desensitize the controller and increases the rise time.

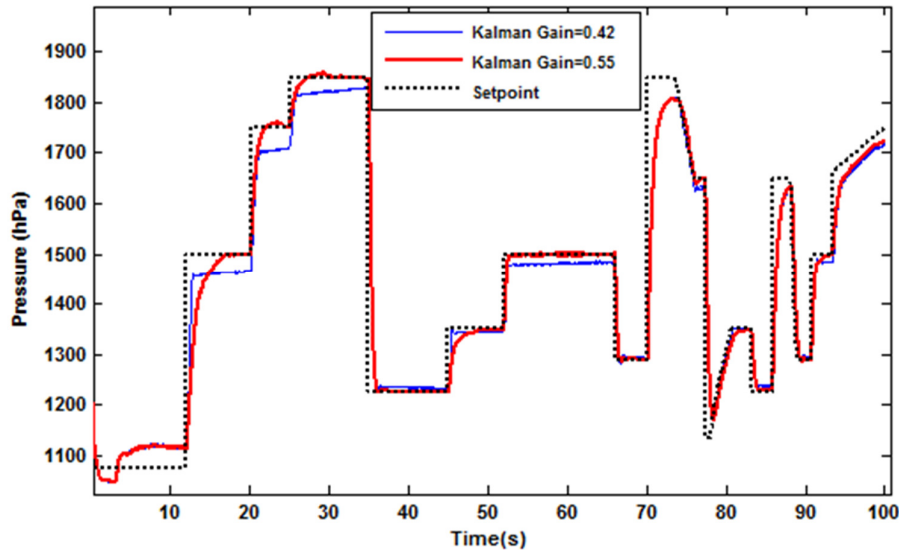


Figure 5.18 : Fine tuning of Kalman gain for MIMO controller at 1500 rpm.

Overall system performance is very similar to SISO case due to minimal activation WG. Further validation of the MIMO controller is repeated with the same mixed transient cycle at 2500 rpm.

Figure 5.19 shows the simulation results including the change in the local linear region as well as the change in the explicit controller region.

Unlike SISO case, explicit controller does not change often. During local linear region 3, only one explicit controller is active. During transition to local region 4 at time 35 seconds, the explicit controller number 3 of the region 4 has been switched.

It is observed that boost pressure regulation is obtained mostly by TBV actuation rather than WG. Similar to step response simulations, WG valve is operating very close to fully closed position. Unlike simulation at 1500 rpm, excessive overshoots are observed especially at high boost pressure setpoint close to 3000 hPa.

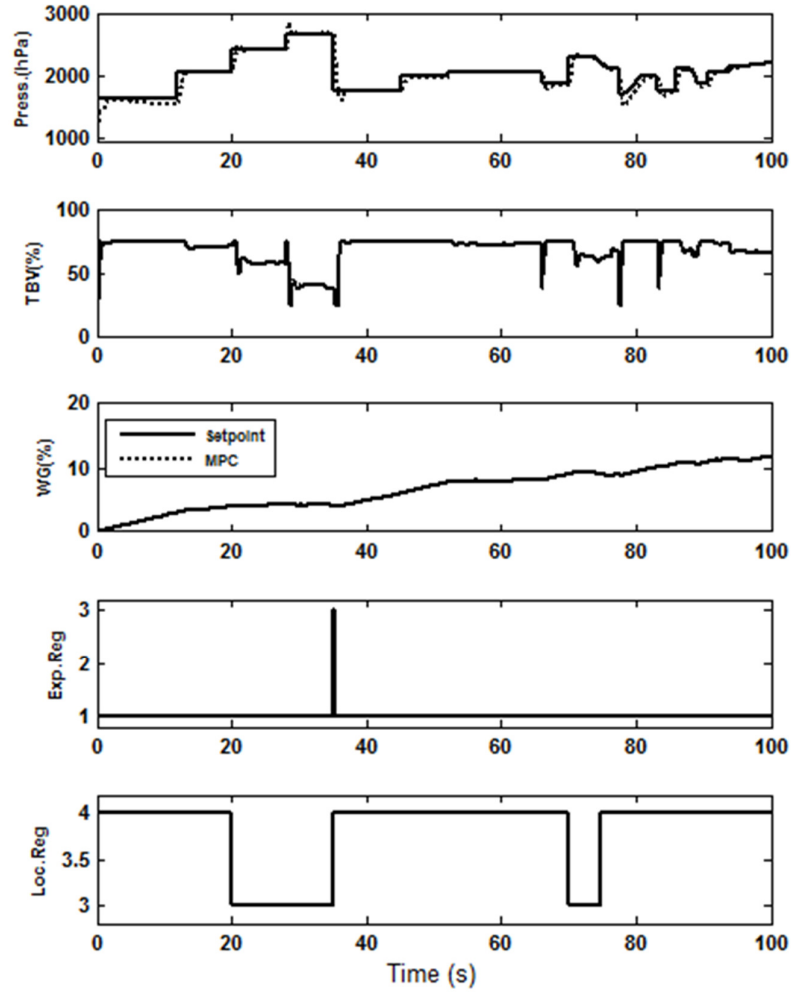


Figure 5.19 : MIMO simulation performed at 2500 rpm.

This results can also be viewed from Figure 5.20 by looking at the turbocharger speed gradients. Due to more activation in TBV, HP turbo speed gradient are larger than LP turbo speed gradients. The other critical effect of high gradients is that due to the low inertia of the HP turbocharger the acceleration is higher than LP turbo.

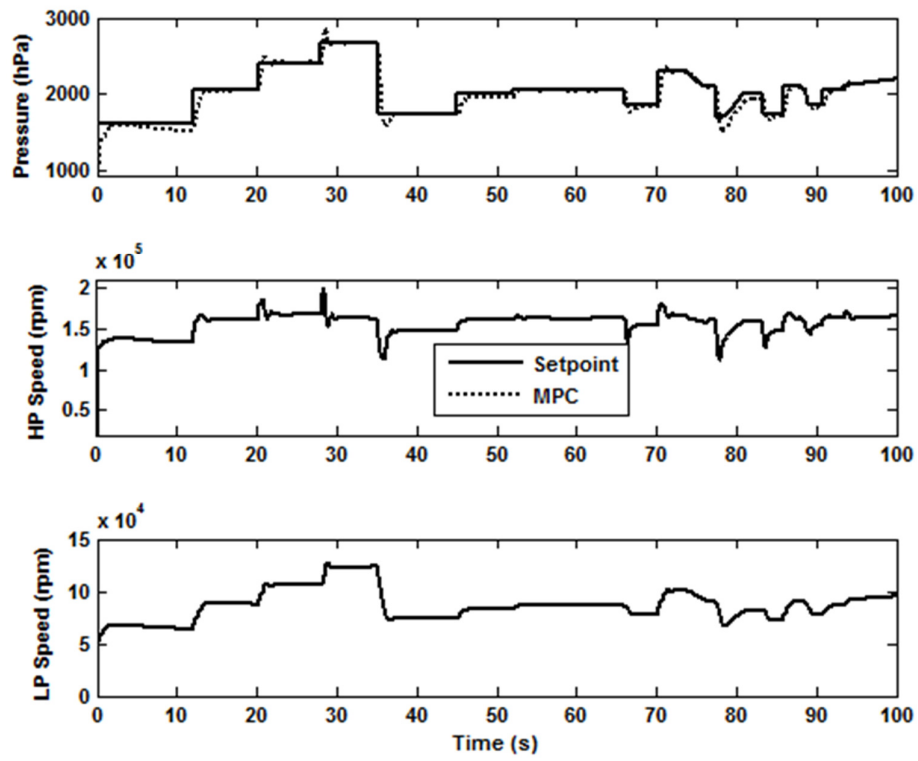


Figure 5.20 : MIMO simulation performed at 2500 rpm.

6. REAL TIME TESTS

Although nonlinear simulations are a convenient method for controller performance assessment, validation of controllers in real time justifies the controller's performance in case of real constraints and hardware. In addition, although 1D gas dynamics based nonlinear engine model offers great advantages in terms of accuracy, not all nonlinearities can be represented. Real time tests offers to observe controller reaction to unmodeled nonlinearities. During this study, real time tests have been performed in terms of vehicle and engine dynamometer testing. Vehicle testing includes real time tests performed on road. Engine dynamometer testing consists of transient test cycles performed on engine dynamometer.

6.1 Vehicle Testing

Controller performance has been assessed by means of series of vehicle testing. During vehicle testing, controller is tested by using the API communication interface between VISION and MATLAB. VISION API is based component object model feature of Microsoft Windows, which offers a communication protocol between software components. TBV and WG control signals are calculated in MATLAB and overwritten to ECU variables via API connection in host PC. Control signals are applied as PWM signal via ECU's power stages. Figure 6.1 shows the layout of the test setup used in vehicle testing. VISION is communicating with Engine ECU in either by using Can Calibration Protocol (CCP) or A7 emulation method.

Test vehicle is a prototype vehicle which is Compact-D car platform based SUV. The engine is equipped with emulated ECU. This enables to change the calibration via CCP or A7 as mentioned above.

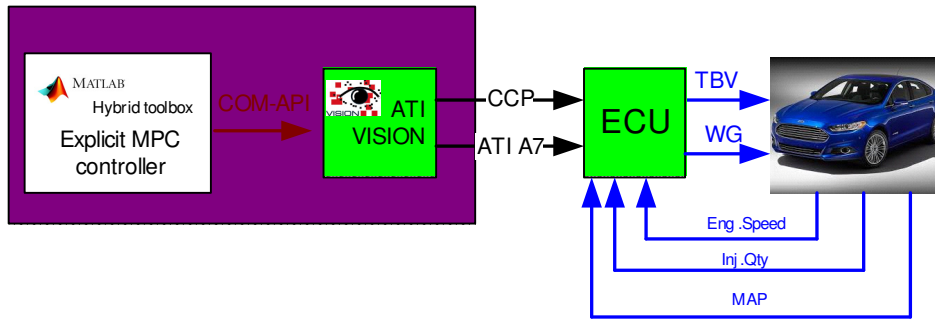


Figure 6.1 : Vehicle testing setup.

Vehicle tests are carried in terms of both on-road testing and chassis dynamometer. On-road testing includes several maneuvers, which includes mostly transient acceleration and deceleration, as well as accelerator pedal tip-in maneuvers. In addition, step input applied to accelerator pedal when working in idle.

Chassis dynamometer testing includes specific customer drive cycles and emissions (NEDC) cycle replicated in chassis rolls. This enables to compare the performance of conventional controllers and designed controllers.

Figure 6.2 shows the on-road driving result. The test is standard launch maneuver which includes medium and small tip-ins in which the gradient of accelerator pedal position is small.

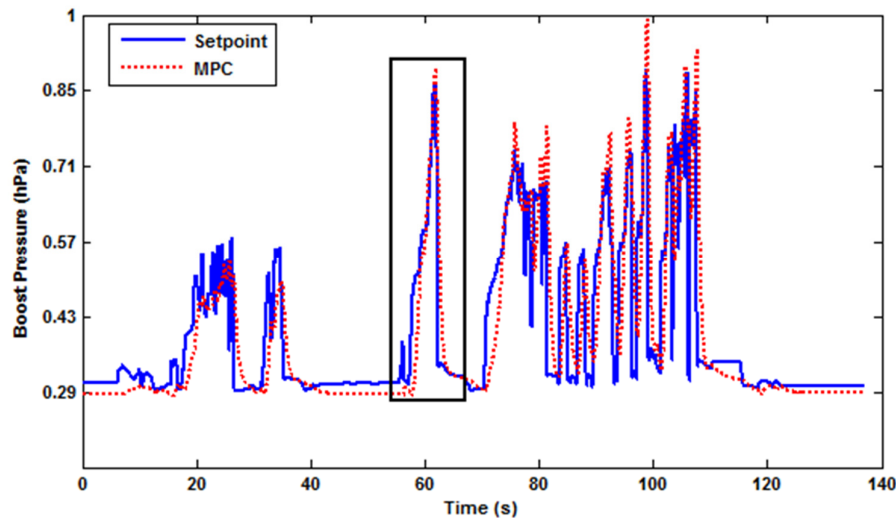


Figure 6.2 : On Road vehicle testing results.

Overall tracking performance of boost pressure controller is satisfactory only where the overshoots might be improved although they are still maximum allowed over boost limits defined by engine's durability limits. The boost pressure set points are

directly set by ECU, which are similar to production level ECU. Therefore, the y-axis of the figure has been normalized due to confidentiality of the data. Figure 6.2 shows the zoom view of the test results between 56 and 68 seconds as shown with black rectangular in Figure 6.1. The system response employs pure time delay. This is combination of actuator delay as well as transport delay. Actuator delay consists of EVRV actuation and formation of vacuum pressure to actuate bypass valve. Transport delay consists of the communication delays between VISION and ECU.

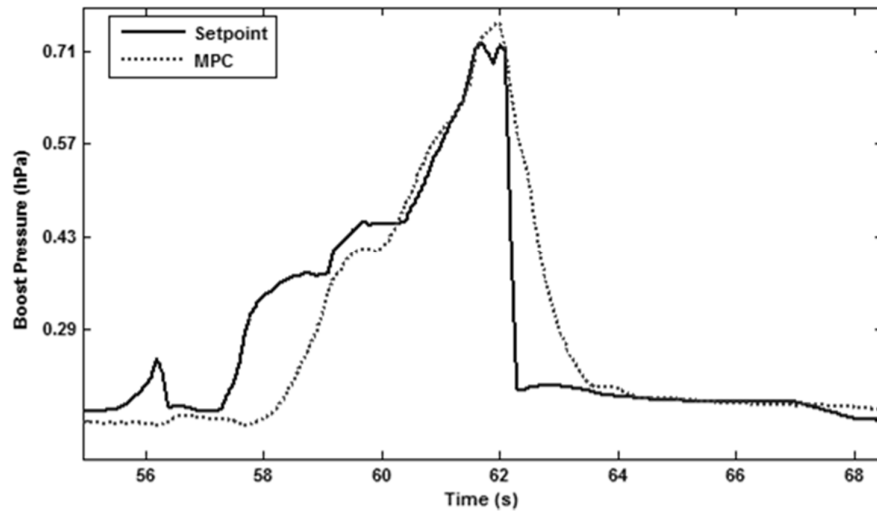


Figure 6.3 : On Road Vehicle Testing-Zoom.

Figure 6.4 shows the details on Controller operation. The optimal control signal for WG is calculated as zero which means no control applied to WG and it is assumed to be fully closed. Boost is regulated via TBV actuation. During controller switchover, there is a bumpless transfer in which the drop in boost pressure is negligible. All 4 of the local linear regions are active. This is due to automatic transmission which limits the usable engine operating region to match with automatic transmission scheduling.

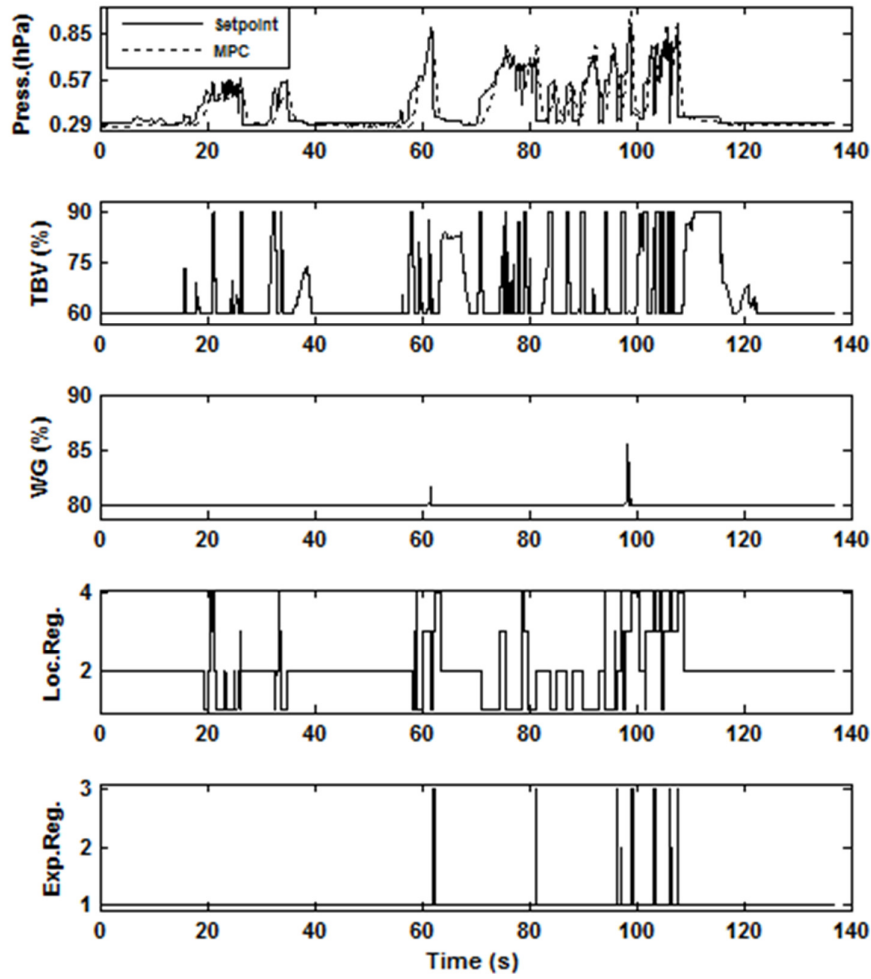


Figure 6.4 : On-Road test results-controller operation.

It would worthwhile to check turbocharger operation on compressor phase planes as they would indicate how effective turbocharger are working during operation as well as the margin to surge and choke. Figure 6.5 and 6.6 shows the engine operation on the HP and LP compressor maps. As mentioned in section 2, it is clearly visible that low flow-pressure ratio region is used in both of the compressor maps.

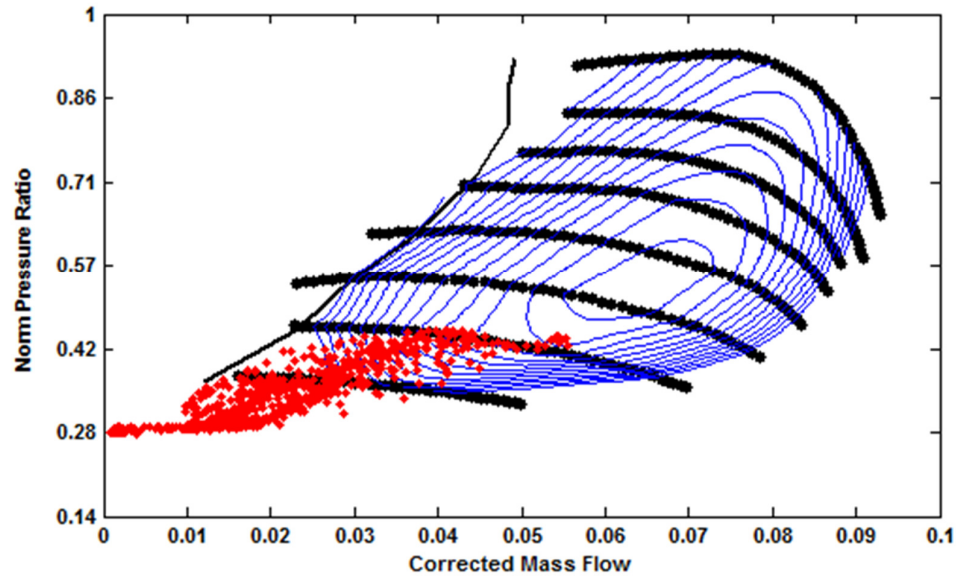


Figure 6.5 : HP Compressor operation during On-Road vehicle testing.

HP compressor is over speeding at some points. As MPC prediction model does not have turbocharger speeds as output or states, there are no constraints over compressor speeds.

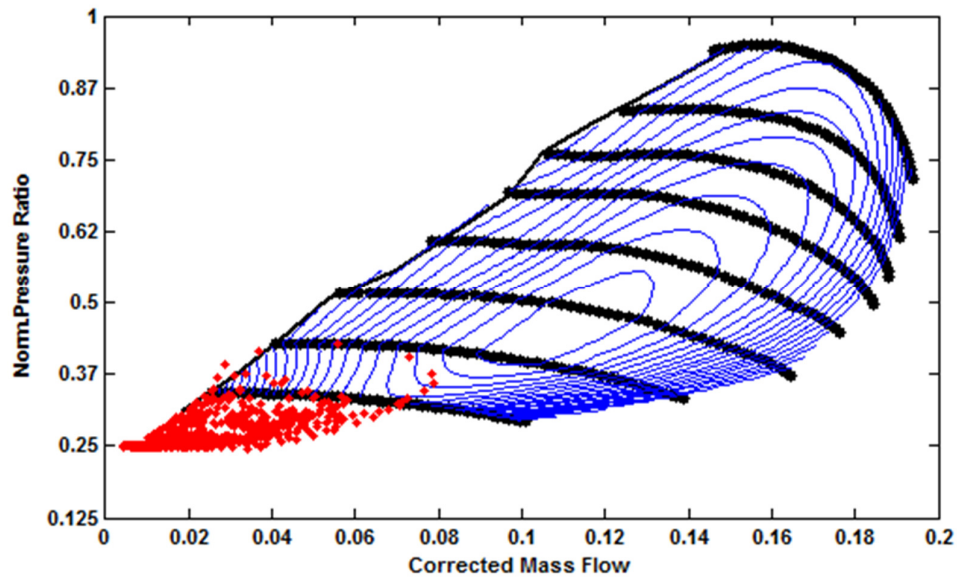


Figure 6.6 : HP Compressor operation during On-Road vehicle testing.

6.2 Engine Dynamometer Testing

Boost pressure controller has been validated on engine dynamometer by means of transient test cycles. Figure 6.7 shows the general outline of the test bench setup and real time control system.

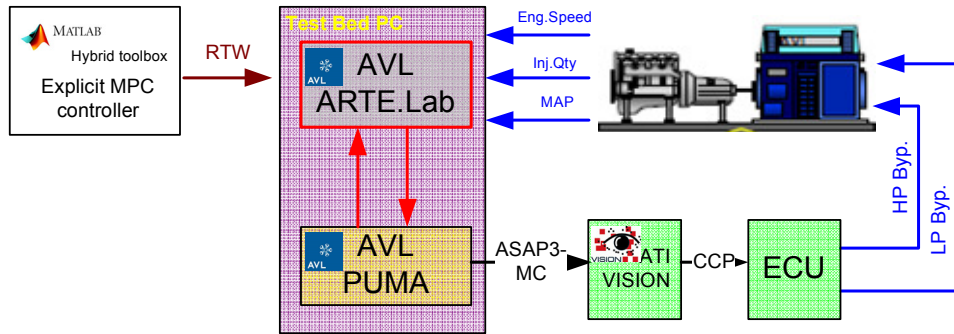


Figure 6.7 : Engine Dynamometer test setup.

TestBed PC is used as Real time processor in which Controller code is executed in real time. Real time workshop module of MATLAB-SIMULINK has been used to auto-generate application code. Auto-generated code has been uploaded to TestBed PC via AVL ARTELab. ARTELAB integrates MATLAB-SIMULINK models open-simulation environment which is fully capable of communication with AVL PUMA dyno operating system. ARTELAB support SIMULINK model library which has specific input and output blocks used to define the inputs and outputs from PUMA. Input and outputs naming should be aligned with PUMA normnames.

As a engine calibration and measurement software ATI VISION has been used. During this study, Boost pressure control of Engine ECU has been bypassed via calibration switches. Constant control values are changed via ASAP3-MC communication protocol between PUMA and VISION. Finally, VISION sends the control signals for bypass valves via CCP to Engine ECU. ECU drives the bypass valves. On the other hand, engine speed, injection quantity and Boost pressure values are sent to PUMA testbed PC to enable processing in real time MPC controller.

The engine used in dynamometer is aged engine in which total operating time has been completed 1000 hrs. This would be beneficial in terms of testing controller robustness where all valves, sensors and turbochargers are subjected to aging and wear to some extent and inside supplier tolerances. During the testing production

intent ECU calibration is used in which injection patterns includes several modes (several pre and main injections).

During engine dynamometer testing, 2 different test cycles have been performed. The boost pressure step response have been analyzed by applying load steps at fixed engine speeds. Second, boost pressure controller setpoint tracking performance have been observed by transient sweep tests in which load and engine speed is changed simultaneously. Figure 6.8 shows the test points in engine operating region.

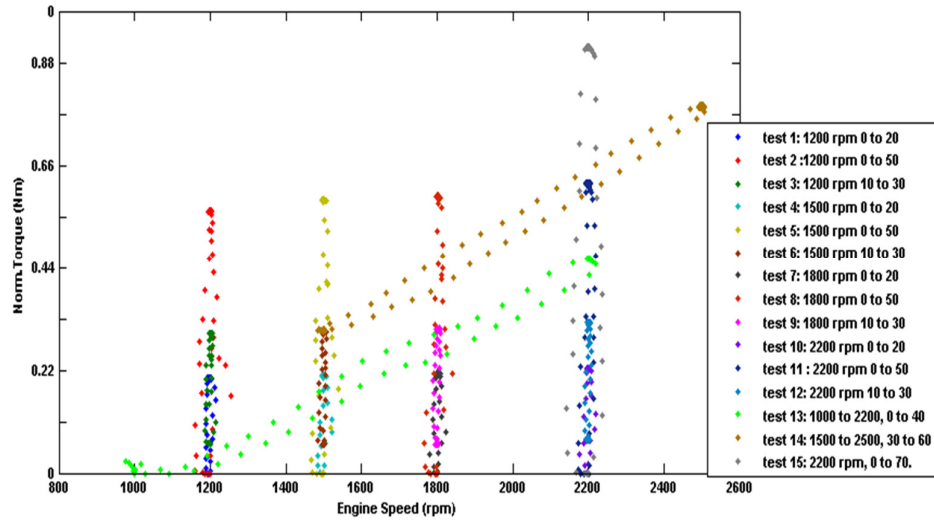


Figure 6.8 : Transient test points.

Load steps are applied at 1200, 1500, 1800 and 2200 rpms with varying loads. The step signal amplitudes are changing from %0 to %20, %0 to %50, %10 to %30 and %0 to %70. These steps corresponds to small, medium and large step boost pressure setpoints. Transient sweep tests includes two different cycles. First cycle includes engine speed sweeping from 1000 rpm to 2200 rpm with load is changing from %0 to %40. This cycle is especially used to observe part load acceleration behaviour of controller. Second transient cycle is starting from 1500 rpm to 2500 rpm with load is changing from %30 to %60.

During testing, boost pressure setpoint are directly used from ECU calibration. Figure 6.9 shows the test results of the fixed engine speed testing performed at 1800 rpm where the load is changing from %0 to %50. The rise time of the boost pressure response in case of MPC controller is improved in tradeoff with overshoot. However the maximum overshoot is %1.5 which satisfies the controller performance

objectives. Rise time is improved as approximately %20. In addition, The fall time is improved slightly compared to conventional controller.

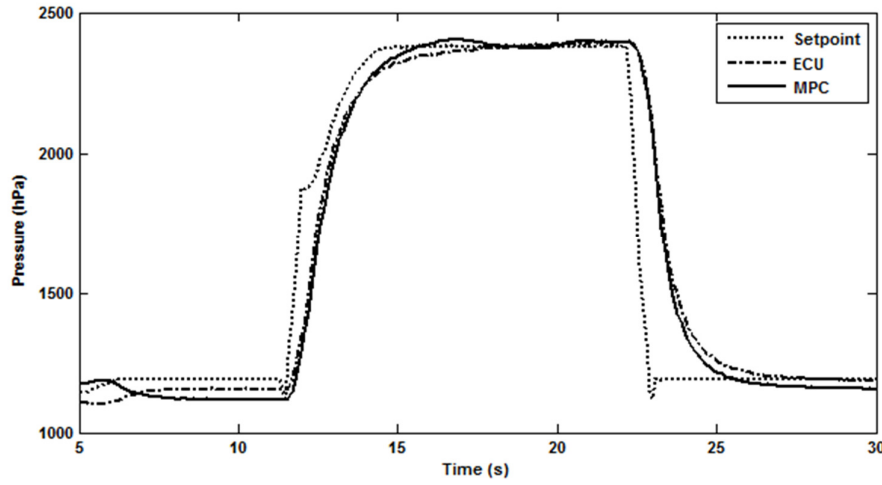


Figure 6.9 : Test results at 1800 rpm from %0 to %50.

Figure 6.10 shows the actuator operation of the testing performed at 1800 rpm from %0 to %50 load step. As expected from nonlinear simulation, TBV is acting as main boost pressure actuator where optimal WG signal calculated by MPC is limited in narrow range. TBV and WG control signals are clipped to %50 and %88 due to ECU driver PWM Duty cycle range.

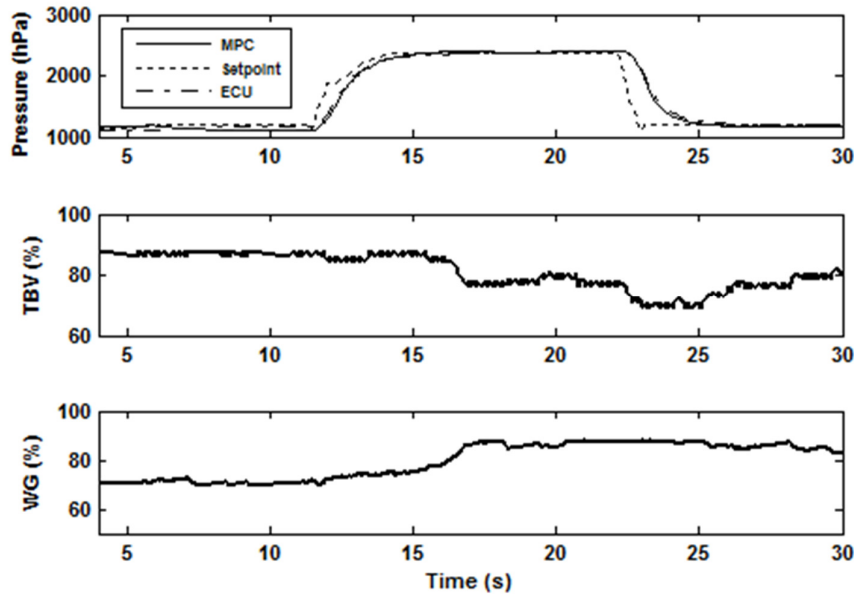


Figure 6.10 : Test results at 1800 rpm from %0 to %50-Actuator operation.

Figure 6.11 shows the behaviour of HP compressor at compressor phase plane. MPC controller and ECU controller shows similar pressure ratio where MPC controller

accelerates HP turbocharger to higher speed. The red dashed line is the compressor speed limit which is defined by turbocharger supplier. Continuous operation above this limit would result in turbocharger failure due to ineffective lubrication.

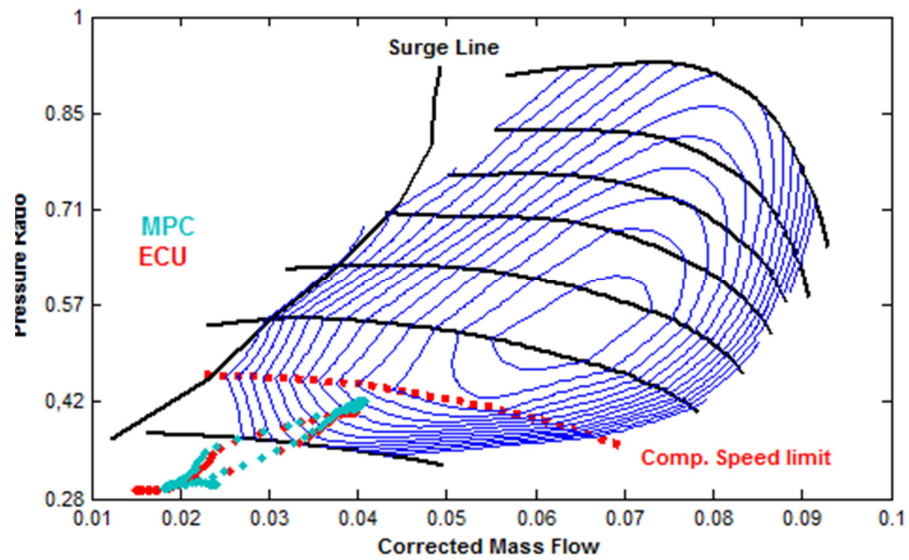


Figure 6.11 : HP compressor map trace at 1800 rpm %0 to %50 load.

Figure 6.12 shows the results of testing performed at 2200 rpm with load steps from %0 to %70. Setpoint tracking of MPC is superior to ECU controller. MPC exhibits 1.4 seconds rise time where ECU controller has 2.1 seconds. System response has a maximum overshoot of %3.5 which satisfies the controller objectives. This cycle represents the aggressive part load acceleration. Therefore, one shall investigate the overboost behaviour of system being controlled. The output constraint is 3500 hPa, therefore MPC is calculating the optimal control signals based on the constraints.

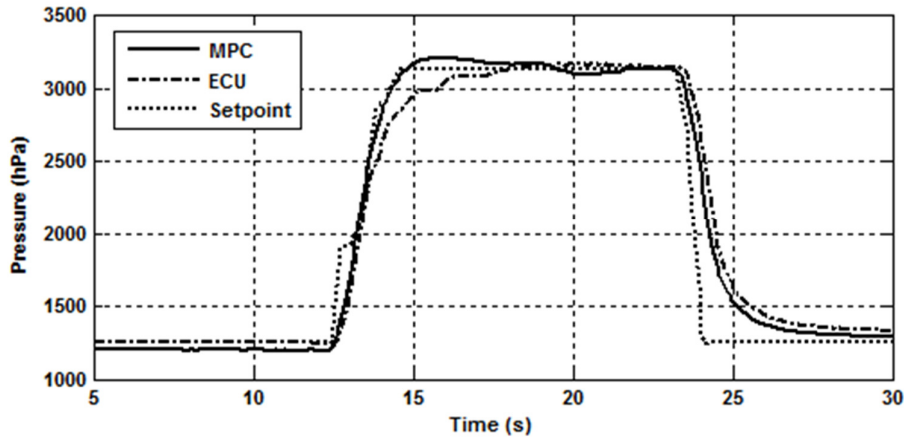


Figure 6.12 : Test results at 2200 rpm from %0 load to %70 load.

Figure 6.13 shows the actuator operation for 2200 rpm %0 to %70 test. Simultaneous control of TBV and WG results in better transient in MPC controller. The local linear regions are switched from region 3 to region 4. The amount of boost pressure fluctuation is minimal although WG and TBV control signal are changed slightly.

Figure 6.15 shows the distribution of the boost pressure deviations both for ECU and MPC controller. MPC controller shows better 3-sigma separation statistically which means boost pressure deviation is distributed close to zero-mean. This would have some advantages for On-Board Diagnostics (OBD) monitoring calibration as the system nominal limits is narrower, OBD thresholds can be selected smaller to.

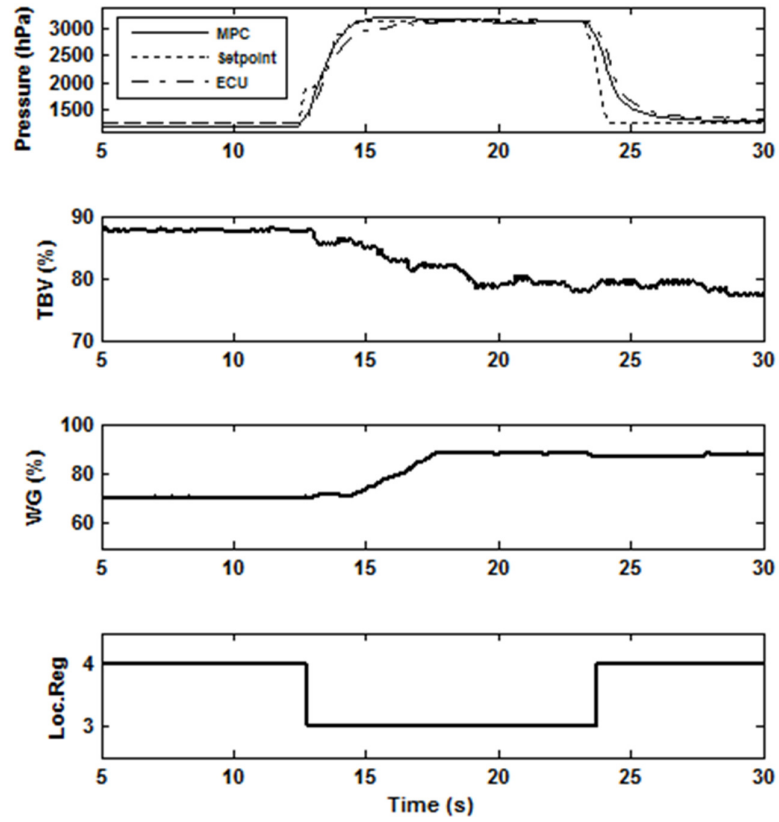


Figure 6.13 : Test results at 2200 rpm from %0 load to %70 load-actuator operation.

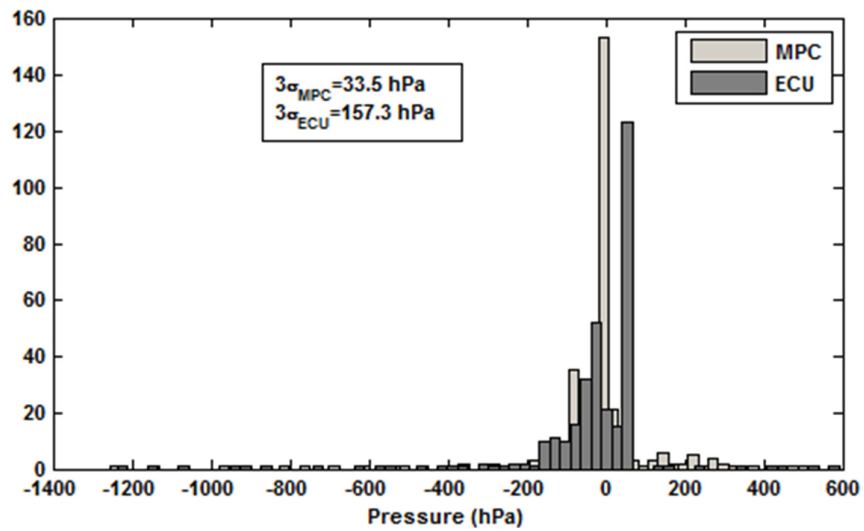


Figure 6.14 : Boost pressure deviation distribution for 2200 rpm %0 to %70 testing.

Figure 6.15 indicates the performance comparison of MPC and ECU controllers in test performed at 2200 rpm and %50 load step. The rise time of the system in case of MPC controller is 2.1 seconds where, Conventional ECU controller results in 2.8 seconds. This improvement results in more acceleration in HP turbocharger operation as mentioned in Figure 6.16.

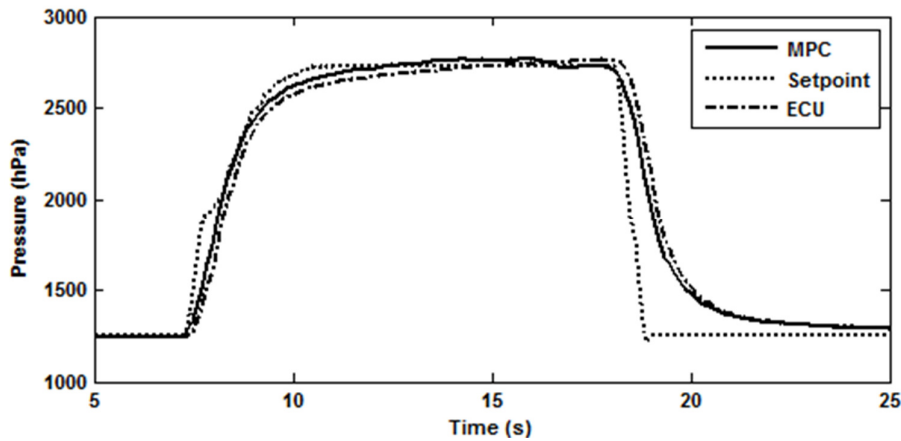


Figure 6.15 : Test results at 2200 rpm from %0 to %50 load.

The turbo speed is on the limit borderline where the behavior is similar to the ECU controller case. LP turbocharger operation is much more limited. Although the WG signal is calculated, WG valve is regulated around fully closed position. This phenomenon is clearly visible on LP compressor phase plot as shown in Figure 6.17.

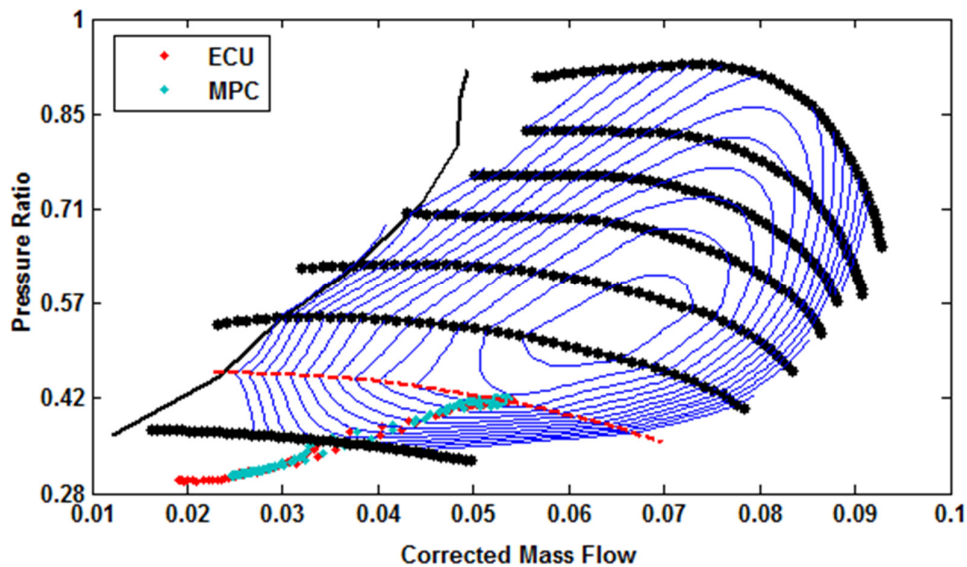


Figure 6.16 : HP compressor map trace at 2200 rpm %0 to %50 load.

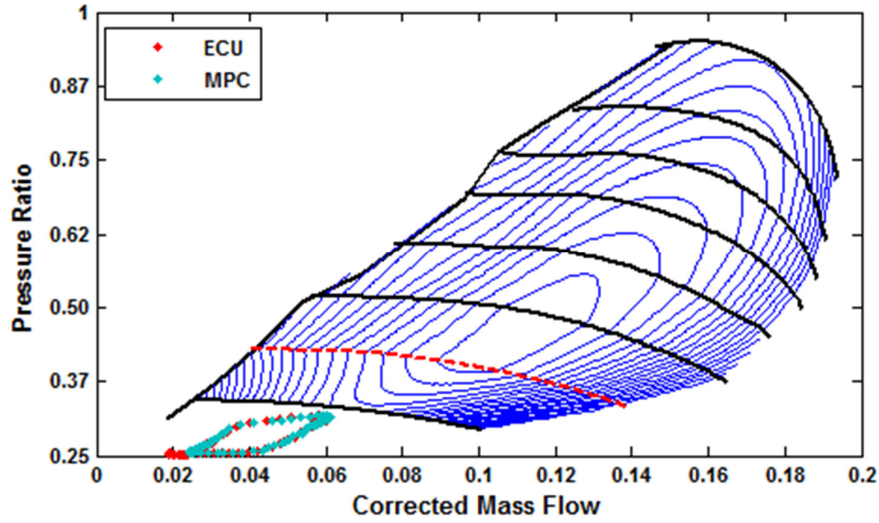


Figure 6.17 : LP compressor map trace at 2200 rpm %0 to %50 load.

The LP turbocharger operation is very similar in case of ECU and MPC cases. Due to having relatively high inertia, the turbospeeds are not close to LP turbocharger overspeed border.

During real time testing it was observed that, MPC and ECU performances are very similar at low speed load points as 1500 and 1200 rpms. This is due to high boost pressure setpoints at ECU calibration. Controllers are saturated at fully closed TBV and WG valves to achieve high setpoints.

Fixed engine speed tests represents the general idea about MPC controller behaviour in comparison with ECU controller. However, real conditions can be better replicated by using sweep tests. During this study, 2 different sweep tests have been performed. First test includes the engine speed from 1000 rpm to 2200 rpm with the load changing from %0 to %40. Second test includes engine speed from 1500 rpm to 2500 rpm with load is changed from %30 to %60.

Figure 6.18 shows the test result of the first sweep test. The rise time of the MPC controller is improved 0.7 seconds compared to ECU controller. MPC controller exhibits more overshoot than the ECU controller which is still below the objectives (%4.5).

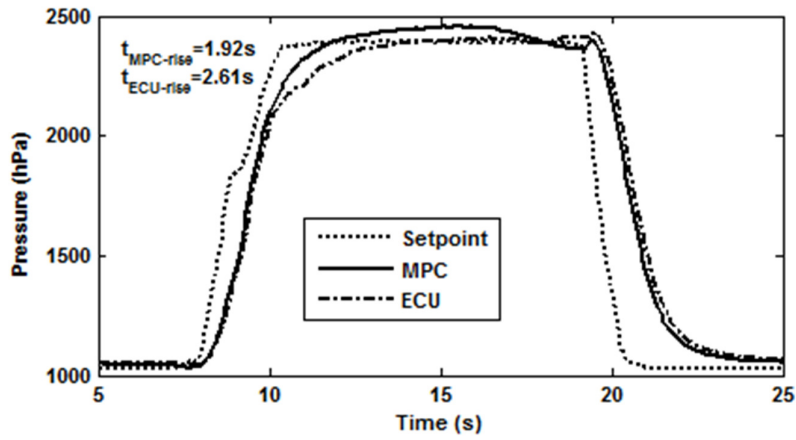


Figure 6.18 : Sweep test (1000-2200 rpm) test results.

Number of regions activated during sweep test is 3. As shown in figure 6.20, the local region transition is smooth. WG valve control signal is regulated around fully closed position.

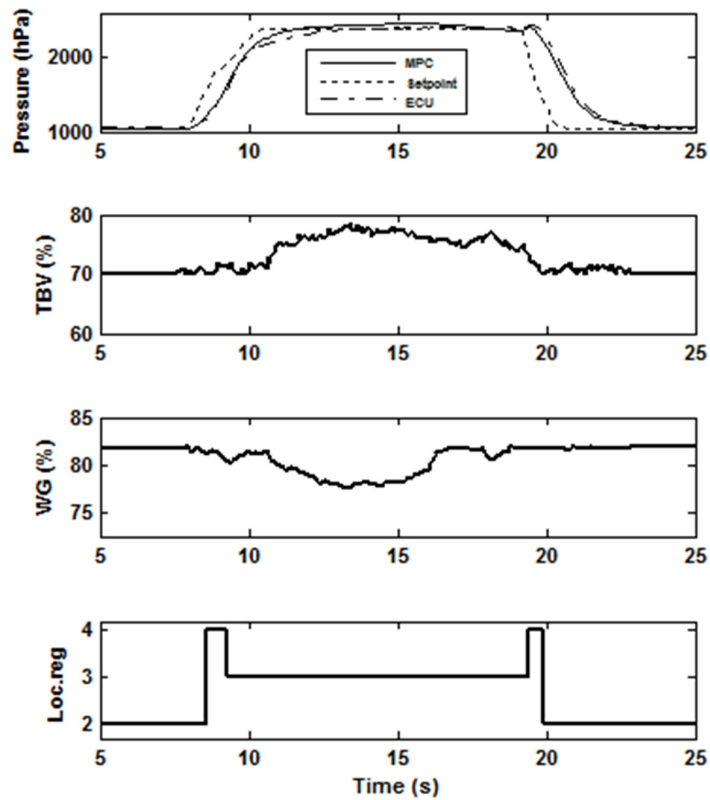


Figure 6.19 : Sweep test (1000-2200) rpm detailed test results.

As shown in Figure 6.20, HP turbocharger speed range is wider in case of MPC controller as the speed values are higher than ECU controller. This concludes the relationship between boost pressure rise time and turbocharger acceleration. Better utilization of Control valves results in higher turbocharger acceleration and rapid boost pressure build-up.

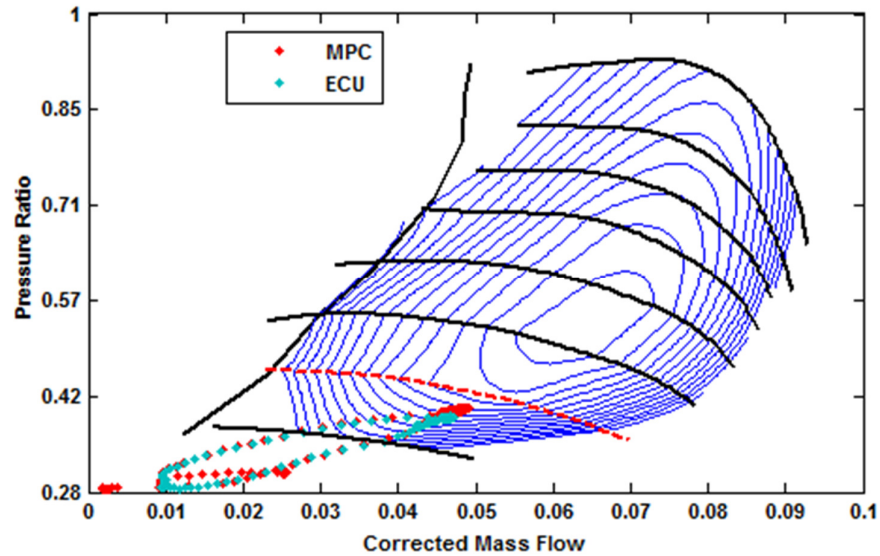


Figure 6.20 : HP compressor map trace for sweep test(1000-2200 rpm).

Figure 6.21 to 6.23 shows the test results of sweep test 2. This test consists of engine speed ranging from 1500 to 2500 rpm and the load value from %30 to %60 load. This dataset is representing the part load acceleration.

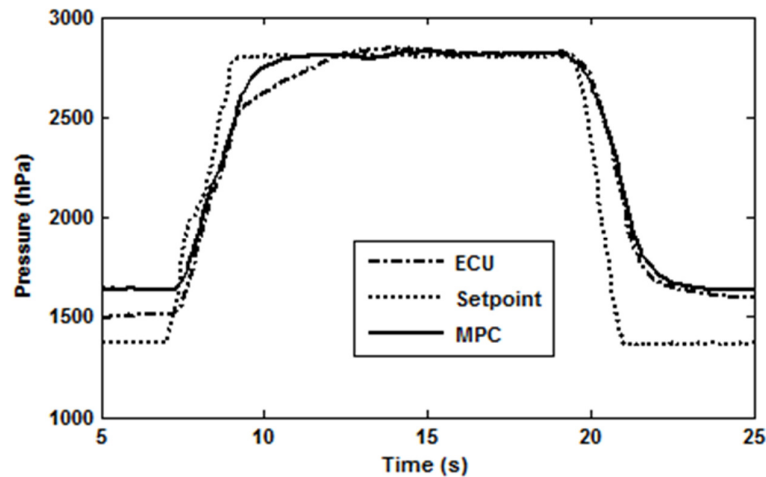


Figure 6.21 : Sweep test 2 (1500-2500 rpm) test results.

The general trend of MPC controller does not change in this test. Optimal WG input is fluctuating around fully closed position where main boost regulation is handled via TBV. The rise time improved as %20 percent. Maximum overshoot is also improved as %30 percent where both of controllers have overshoots below the targets.

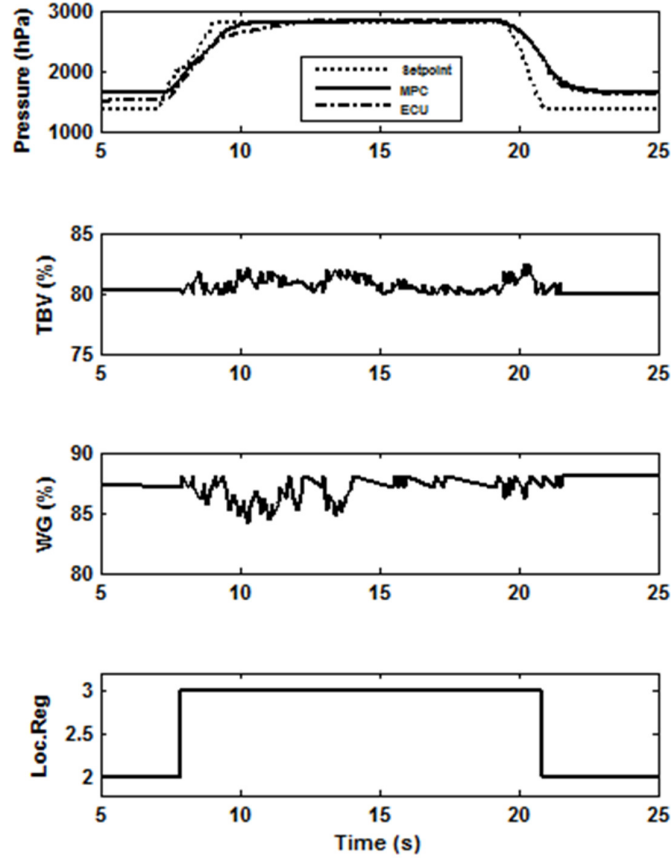


Figure 6.22 : Sweep test 2 (1500-2500 rpm) detailed test results.

During testing, it was observed that HP-LP turbine out temperatures are relatively higher when MPC controller is used. This can be explained by activation of WG valve more aggressive TBV valve. Figure 6.23 shows the plots for compressor outlet and turbine outlet temperatures for sweep test 1. Compressor outlet temperatures are greater than ECU controlled case but still satisfied the component protection limits.

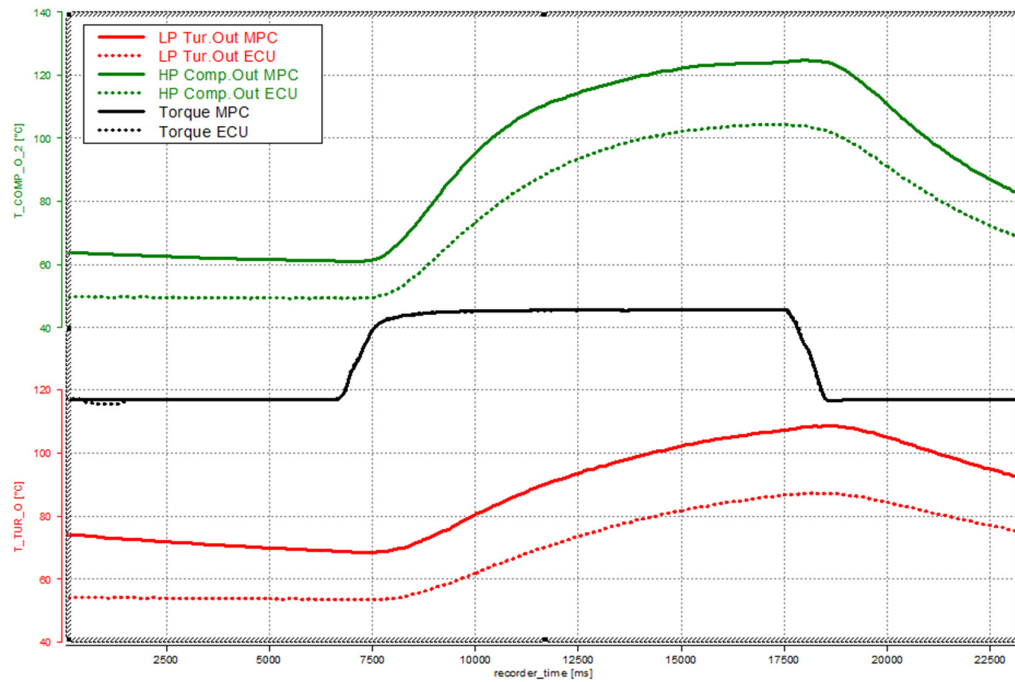


Figure 6.23 : HP compressor outlet temperature and LP turbine outlet temperatures at sweep test 1.

Increase in LP turbine outlet temperatures will result in more rapid catalyst heat-up thus leading to Diesel Oxidation catalyst and Nox adsorber catalyst activation quicker. This would lead to decrease in HC-CO emissions as well as better Nox conversion.

7. CONCLUSIONS

A new application of controller concept of a boost pressure control of a series sequential turbocharged diesel engine was implemented in this study. During this research, MPC is selected a intelligent controller which is well-documented and theoritized but not applied to boost pressure control of two-stage turbocharged diesel engine before. During the MPC design process, first step is selected as construction of nonlinear engine model for offline simulations. 1D model methodology has been used in order to provide high fidelity simulation environment. A linear prediction model for MPC is facilitated by utilizing black-box system identification methods. During MPC design, main factors were examined separately such as effect of prediction and control horizons, Kalman filter, Constraint handling as well as sampling time and polyhedral partitions. Before controller simulations, objectives were defined for better assesment of controller performance. Objective were defined as a time domain specific parameters (rise time, maximum overshoot, settling time) which are carried over from a signoff criteria of conventional industrial ECU controllers. Offline simulations were performed on 1D engine model combined with MPC controllers. At the final step of the study, real time tests were performed bith in vehicle and engine dynamometer for subjective analysis and comparison with ECU controller

The highlights of the contribution in this thesis are listed as follows;

- Proposed a 1D engine model based high fidelity simulation environment usd for control synthesis
- Develop a multi-linear black box model that supports engine operating regions
- Implement Model Predictive Control framework to series sequential boosting controls
- Implement explicit MPC real time tests on real engine and dynomometer.

7.1 Conclusions

The research was targeted to implement a controller algorithm which would be feasible against conventional ECU controllers. The feasibility study includes the real time implementation and comparison with conventional controller by a series of real time tests. Some conclusion from the contribution of this thesis are highlighted below.

- Nonlinear engine model satisfies at least %10 accuracy band with respect to real engine data both for transient and steady state validation results.
- Thanks to high WAVE RT high fidelity simulation environment, model parametrization times are reduced compared to MVEM. This had resulted in more accurate models in less development durations. Moreover, it is capable of control design and verification.
- Single blackbox model is not feasible to represent entire engine operating region. Partition into local linear regions improved the linear model prediction accuracy which is a key input to MPC. The linear model accuracy is verified with engine dyno testing.
- Design of MPC controller based on industrially proven objectives and signoff criteria made the acceptance of overall process more reliable.
- MPC proves effective tool itself an effective tool for boost pressure control of series sequential turbocharged diesel engine. Simulation results showed that the step response tracking as well mixed transient cycle responses are well below the targets defined by design objectives. Due to computational issues, explicit MPC formulation is used both in offline simulations as well as real time tests.
- Real time dyno tests performed on transient engine dyno are those similar to acceptance tests performed for conventional ECU controllers. MPC showed better dynamic behaviour where more controller activity was a key factor. Introducing WG and TBV actuation simultenaously resulted in better setpoint tracking.

- In vehicle tests showed more subjective analysis, in which the driveability effect of MPC was assessed. During the vehicle maneuvers, torque fluctuations as well as launch performance of the vehicle was satisfactory.

7.2 Recommendations

Although this research contributes a new controller application to series sequential turbocharged boost pressure controls, due to the wide-range applicability of this topic there are still remaining items for further research and development. Below are the potential subjects that are candidates for such applications:

- Application of nonlinear MPC design for two stage turbocharged diesel engine.
- Investigation of detailed interactions between boosting system and EGR-Throttle for a series sequential turbocharged system.
- Investigation of emissions effect of controller especially for heavy duty applications.
- Fault-diagnosis and fault-tolerant control for series sequential boosting system.

REFERENCES

- Bemporad, A.** (2004). Hybrid Toolbox. Retrieved May 5, 2014. Available from <http://cse.lab.imtlucca.it/~bemporad/hybrid/toolbox/>
- Bemporad, A.** (2006). Model Predictive Control Design: New trends and Tools, *Proceedings of the 45th IEEE Conference on Decision & Control*, (pp.6678-6683), San Diego, CA, USA, December 13-15.
- Bemporad, A.** (2013). *Model Predictive Control* [PowerPoint slides]. Retrieved from <http://cse.lab.imtlucca.it/~bemporad/teaching/mpc/imt/1-mpc.pdf>
- Bemporad, A., Morari, M., Dua, V., & Pistikopoulos, E. N.** (2002). The explicit linear quadratic regulator for constrained systems, *Automatica*, 38, 3-20.
- Bemporad, A., Morari, M., & Ricker, N. L.** (2004). *Model Predictive Control Toolbox for Matlab-User's Guide*. Retrieved April 13, 2014, from <http://www.mathworks.com/access/helpdesk/help/toolbox/mpc/>.
- Boyd, S. & Vandenberghe, L.** (2009). *Convex Optimization*. Cambridge, UK: Cambridge University Press.
- Byungchan, L.** (2009). *Dual-Stage Boosting systems: Modeling of configurations, Matching and Boost Control options* (Doctoral dissertation). The University of Michigan, MI.
- Camacho, E. & Bordons, C.** (1999). *Model Predictive Control*, London: Springer Verlag,
- Canova, M., Chiara, F., Rizzoni, G., & Wang, Y.** (2010). Model-based characterization and analysis of diesel engines with two-stage turbochargers. *SAE Technical Paper*. 2010-01-1220, doi: 10.4271/2010-01-1220
- Challen, B. & Baranescu, R.** (1999). *Diesel Engine Reference Book*. Woburn, MA: Butterworth-Heinemann.
- Chiuso, A. & Pucci, G.** (2005). Prediction error vs subspace methods in closed loop identification, *Proceedings of IFAC 16th World Congress*, (pp. 84-94).Prague, Czech Republic: July 03-08.
- Eriksson, L.** (2007). Modeling and Control of turbocharged SI and DI engines, *Oil & Gas Science and Technology-IFP*, 62(4), 523-538. doi: 10.2516/ogst:2007042
- Eriksson, L., Wahlström, J., & Klein, M.** (2010). Physical modeling of turbocharged engines and parameter identification, *Automotive Model Predictive Control: Lecture Notes in Control and Information Sciences* (Vol.402, pp.53-71), Berlin-Heidelberg: Springer Verlag.

- Ferreau, H. J., Ortner, P., Langthaler, P., Del Re, L., & Diehl, M.** (2007). Predictive control of a real world Diesel engine using an extended online active set strategy. *Elsevier Annual Reviews in Control*, 31, 293-301. doi:10.1016/j.arcontrol.2007.09.001
- Findensen, R. & Allgöwer, F.** (2002). An Introduction to Nonlinear Model Predictive Control, *Proceedings of the 21th Benelux Meeting on Systems and Control*, (pp.1-23). The Netherlands: Velkoven, March 19-21.
- Findensen, R., Allgöwer, F., & Biegler, L.** (2007). *Assessment and Future Directions of Nonlinear Model Predictive Control*. Berlin-Heidelberg: Springer-Verlag.
- Greitzer, E. M.** (1976). Surge and rotating stall in axial flow compressors: part 1: theoretical compression system model. *ASME Journal of Engineering Power*, 98, 190-198.
- Guzzella, L. & Onder, H. C.** (2010). *Introduction to Modeling and Control of Internal Combustion Engine Systems*. Berlin-Heidelberg: Springer-Verlag.
- Haverkamp, L. R. J.** (2001). *State Space Identification: Theory and Practice*. Delft: TU Delft.
- Hendricks, E.** (2001). Isothermal vs. adiabatic mean value SI engine models. *Proceedings of the Third IFAC Workshop on Advances in Automotive Control*, (pp. 373-378). Germany: Karlsruhe, March 28-30.
- Herceg, M., Kvasnica, M., Jones, C. N., & Morari, M.** (2013). Multi-Parametric Toolbox 3.0. *Proceedings of the 2013 European Control Conference*, (pp.502-510). Switzerland: Zurich, July 17-19.
- Heywood, J. G.** (1988). *Internal Combustion Engine Fundamentals*. New York: McGraw-Hill.
- Hiereth, H. & Prenninger, P.** (2007). *Charging the Internal Combustion Engine*. Wien-New York: Springer-Verlag.
- Houska, B., Logist, P., Diehl, M., & Van Impe, J.** (2012). A Tutorial on Numerical Methods for State and Parameter Estimation in Nonlinear Dynamic Systems. In D. Alberer, H. Hjalmarsson, L.del Re (Eds.), *Identification of Automotive Systems* (Vol.418, pp.67-88). London: Springer-Verlag.
- Isermann, R. & Münchhof, M.** (2011). *Identification of Dynamic Systems*. Berlin-Heidelberg: Springer-Verlag.
- Jankovic, M., & Kolmanovsky, I.** (1998). Robust nonlinear controller for turbocharged diesel engine. *Proceedings of American Control conference*, (pp.1389-1394). Philadelphia, June 24-26.
- Jensen, J., Kristensen, A. F., Sorenson, S. C., Houbak, N., & Hendricks, E.** (1991). Mean Value modeling of a small-turbocharged diesel engine. *SAE Technical Paper*. 910070. doi:10.4271/910070
- Keesman, K. J.** (2011). *System Identification: an Introduction*. London: Springer-Verlag.

- Kotmann, P., Bitzer, M. M., & Kugi, A.** (2010). Flatness based Feed forward Control of a two-stage turbocharged Diesel Air system with EGR. *Proceedings of the 2010 IEEE International Conference on Systems and Control*, (pp.979-984). Yokohama, September 08-10.
- Kouvaritakis, B. & Cannon, M.** (2008). *Nonlinear Predictive Control theory and Practice*. Herts-UK: IET.
- Kristofferson, I.** (2006). *Model Predictive Control of a Turbocharged Engine*. (Master's thesis). Royal Institute of Technology, Stockholm.
- Kwon, W. & H., Han, S.** (2005). *Receding Horizon Control*. London: Springer Verlag.
- Leith, DJ. & Leithhead, WE.** (2012). Survey of gain-scheduling analysis and design, *International Journal of Control*,73(11), 1001-1025.
- Lezhnev, L., Kolmanovsky, I. & Buckland, J.** (2002). Boosted gasoline direct injection engines: Comparison of throttle and VGT controllers for homogenous charge operation. *SAE Technical Paper*, 2002-01-0709. doi:10.4271/2002-01-0709
- Liuping, W.** (2009). *Model Predictive Control System Design and Implementation using MATLAB®*. London: Springer Verlag.
- Ljung, L.** (1999). *System Identification- Theory for the User*. Upper Saddle River: Prentice-Hall Inc.
- Ljung, L.** (2001). *Prediction error estimation methods* (Report No: LiTH-ISY-R-2365). Linköping, Sweden: Linköping University Department of Electrical Engineering.
- Mattarelli, E., Rinaldini, C. A., Mazza, A., & Oliva, M.** (2009). Development of a 2-Stage Supercharging System for a HSDI Diesel Engine, *SAE Technical Paper*. 2009-01-2757. doi: 10.4271/2009-01-2757
- Mollenhauer, K. & Tschoeke, H.** (2010). *Handbook of Diesel Engines*. Berlin-Heidelberg: Springer.
- Moraal, P. & Kolmanovsky, I.** (1999). Turbocharger Modeling for Automotive control applications. *SAE Technical Paper*. 1999-01-0908. doi:10.4271/1999-01-0908
- Moulin, P.** (2010). *Modelisation et commande des Systemes d'Air des Moteurs Suralimentes*. (Doctoral dissertation). Paris Tech, Paris, France.
- Moulin, P., Grondin, O., & Fontvieille, L.** (2009). Control of a two stage turbocharger on Diesel Engine. *Proceedings of IEEE Conference on Decision and Control* (pp.5200-5206). Shanghai, December 15-18.
- Ortner, P. & Del Re, L.** (2007). Predictive control of a Diesel engine air path. *IEEE Transactions on Control systems Technology*,15(2), 449-456.
- Perez, E., Blasco, X., Garcia-Nieto, S., & Sanchis, J.** (2006). Diesel engine identification and predictive control using Wiener and Hammerstein models. *Proceedings of the 2006 IEEE International Conference on Control Applications*, (pp.2417-2423). Munich, October 04-06.

- Plianos, A. & Stobart, R. K.** (2008). Modeling and Control of Diesel Engines equipped with a two-stage turbo-system. *SAE Technical Paper*, 2008-01-1018. doi: 10.4271/2008-01-1018
- Plianos, A. & Stobart, R. K.** (2010). Nonlinear airpath control of modern diesel powertrains: a fuzzy systems approach. *International Journal of Systems Science*, 42 (2), 263-275.
- Qin, S. J.** (2006). An Overview of subspace identification, *Computers & Chemical Engineering*, 30, 1502-1513.
- Rakopoulos, C. D. & Giakournis, E. G.** (2009). *Diesel Engine Transient Operation: Principles of Operation and Simulation Analysis*. London: Springer.
- Renberg, U.** (2008). *1D engine simulation of a turbocharged SI engine with CFD computation on components*. (Licentiate Thesis). Royal Institute of Technology, Stockholm.
- Ricardo Wave** (2013) [Computer software]. Warwickshire, UK: Ricardo UK.
- Schmitt, F. & Sweetland, P.** (2004). Regulated 2-stage charging systems for Future Diesel applications. *2004 Diesel Engine Emissions Reduction (DEER) Conference*, Coronado, CA.
- Schwarzmann, D., Nitsche, R., Lunze, J., & Schanz A.** (2006). Pressure control of a two stage turbocharged diesel engine using a novel nonlinear IMC approach, *Proceedings of 2006 IEEE International Conference on Control Applications*, (pp.2399-2404). Munich, Germany, October 04-06.
- Shridhar, R. & Douglas, J. C.** (1997). A Tuning strategy for unconstrained SISO model predictive control, *Ind.Eng.Chem.Res.* 36, 729-746.
- Shu, Y. & Van Nieuwstadt, M.** (2007). Two stage turbocharger modeling for engine control and estimation, *Proceedings of IMECE2007*, (pp.243-257). Seattle, USA, November 11-15.
- Stefanopoulou, A. G., Kolmanovsky, I., & Freudenberg, J. S.** (2000). Control of variable geometry turbocharged diesel engine for reduced emissions. *IEEE Transactions on Control systems Technology*, 8, 733-745.
- Sung, S. W. & Lee, J. H.** (2003). Pseudo-random binary sequence design for finite impulse response identification. *Control Engineering Practice*, 11(8), 935-947.
- Swamee, P. K. & Jain, A. K.** (1976). Explicit equations for pipe-flow problems. *Journal of Hydraulics Division ASCE*, 102(5), 657-664.
- Thomasson, A., Eriksson, L., Leufven, O., & Andersson, P.** (2009). Waste gate Actuator Modeling and Model-based Boost Pressure Control, *IFAC workshop on Engine and Powertrain Control, Simulation and Modeling*, (pp. 87-94). Rueil-Malmaison, France, December 01-02.
- Tondel, P., Johansen, T., A., & Bemporad, A.** (2001). An algorithm for multi-parametric quadratic programming and explicit MPC solutions. *Proceedings of the 40th IEEE Conference on Decision & Control*, (pp.1199-1204). Orlando-Florida, CA, December 04-07.

- Regulated 2-stage turbocharging (R2S®).** (n.d.). Retrieved August 31, 2014, from <http://www.turbos.bwauto.com/products/r2s.aspx>
- Viberg, M.** (1995). Subspace-based methods for the identification of linear time-invariant systems, *Automatica*, 31(17), 1835-1851.
- Wahlström, J. & Eriksson, L.** (2011). Modeling of a Diesel Engine with VGT and EGR capturing sign reversal and non-minimum phase behaviors. *Proceedings of IMECH Journal of Automobile Engineering*, 225. 960-986.
- Wahlström, J., Eriksson, L., Nielsen, L., & Petterson, M.** (2005). PID controllers and their tuning for EGR and VGT control in Diesel engines, *Proceedings of the 16th IFAC World Congress*, (pp.1922-1928), Prague, Czech Republic: July 03-08.
- Wu, H.** (2011). *Performance Simulation and control design for diesel engine NOx emission reduction technologies* .(Doctoral Dissertation). University of Illinois at Urbana-Champaign, Urbana, Illinois
- Yang, X., and Zhu, G.** (2010). A Mixed mean-value and crank-based model of a dual-stage turbocharged SI engine for Hardware-in-the-loop simulation, *American Control Conference*, (pp.3791-3796). Baltimore, USA, June 30-July 02.
- Zhu, Y.** (2001). *Multivariable System Identification for Process Control*. Kidlington-Oxford: Elsevier Science.

APPENDICES

APPENDIX A: Nonlinear Engine model validation plots

APPENDIX B: Simulation results of SISO and MIMO MPC controllers

APPENDIX A: Nonlinear Engine model validation plots

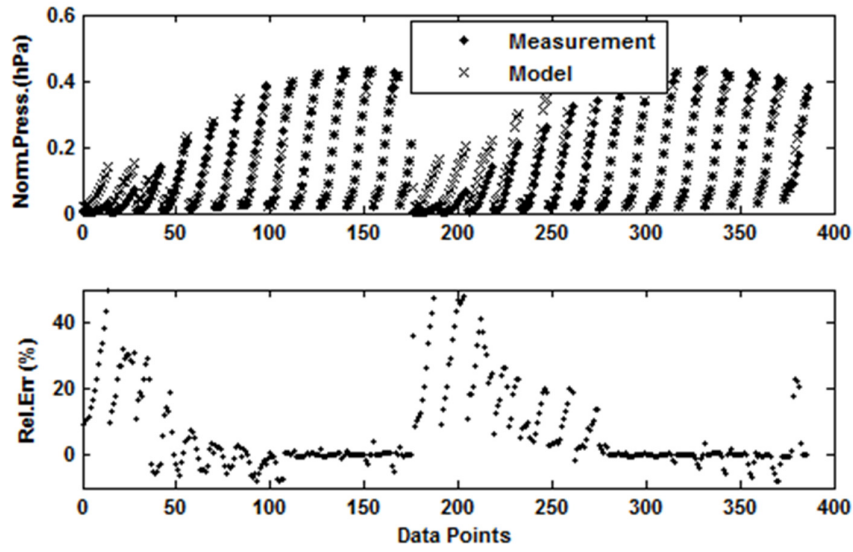


Figure A.1 : HP compressor inlet pressure.

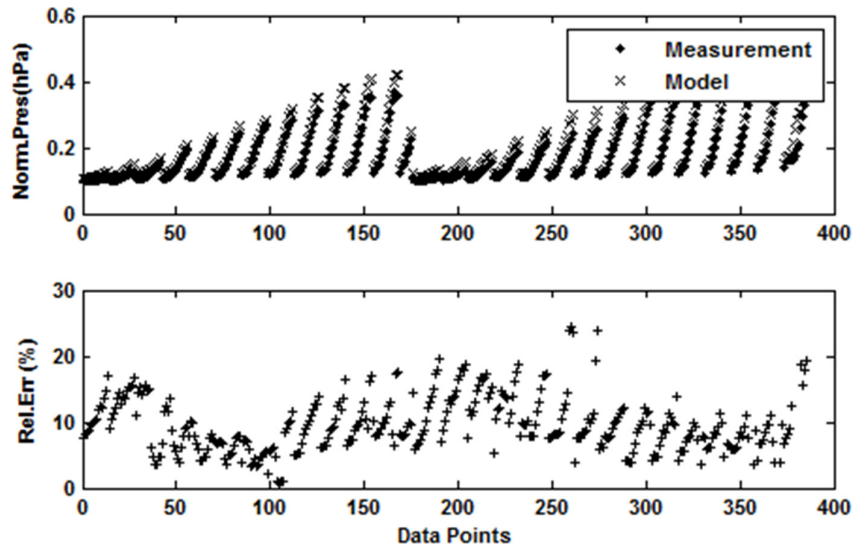


Figure A.2 : LP turbine inlet Pressure.

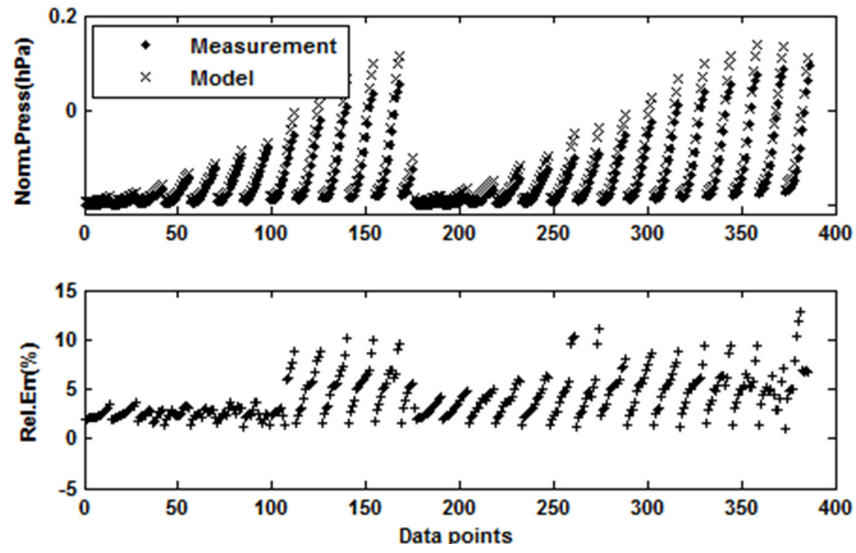


Figure A.3 : LP turbine outlet pressure.

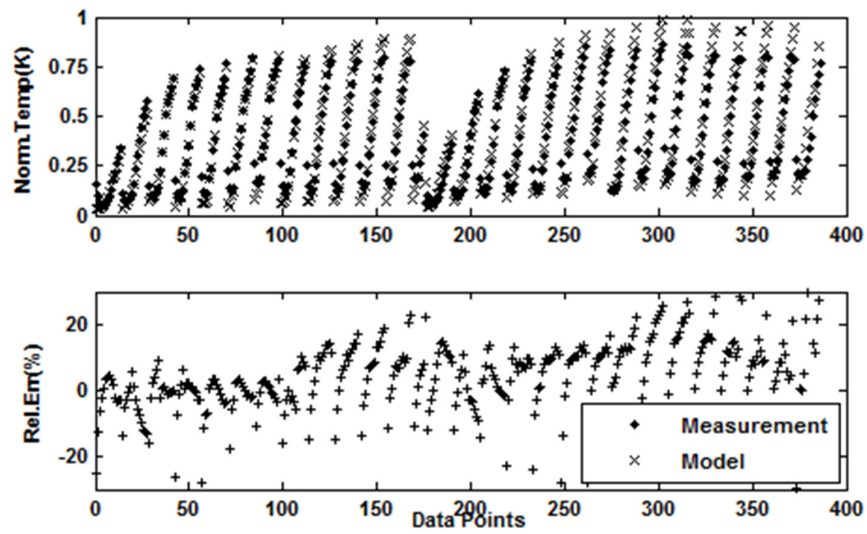


Figure A.4 : HP compressor outlet temperature.

APPENDIX B : Simulation results of SISO and MIMO MPC controllers

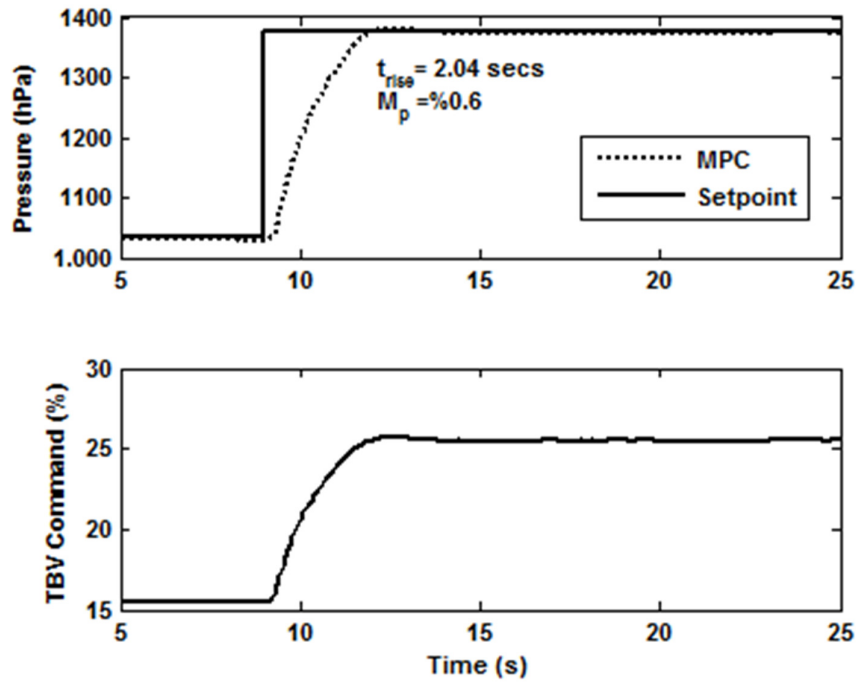


Figure B.1 : SISO medium step response at 2500 rpm.

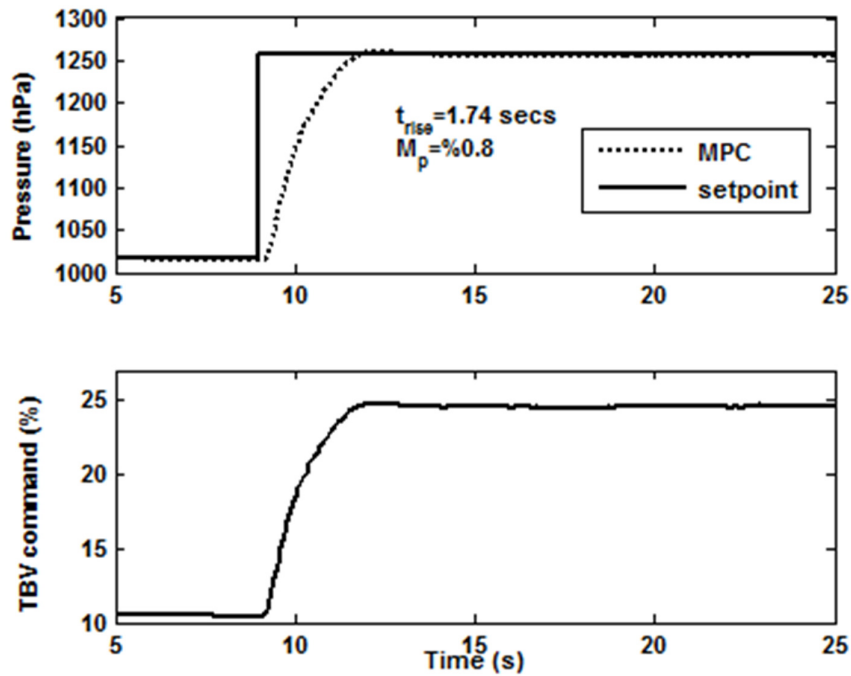


Figure B.2 : SISO small step response at 2500 rpm.

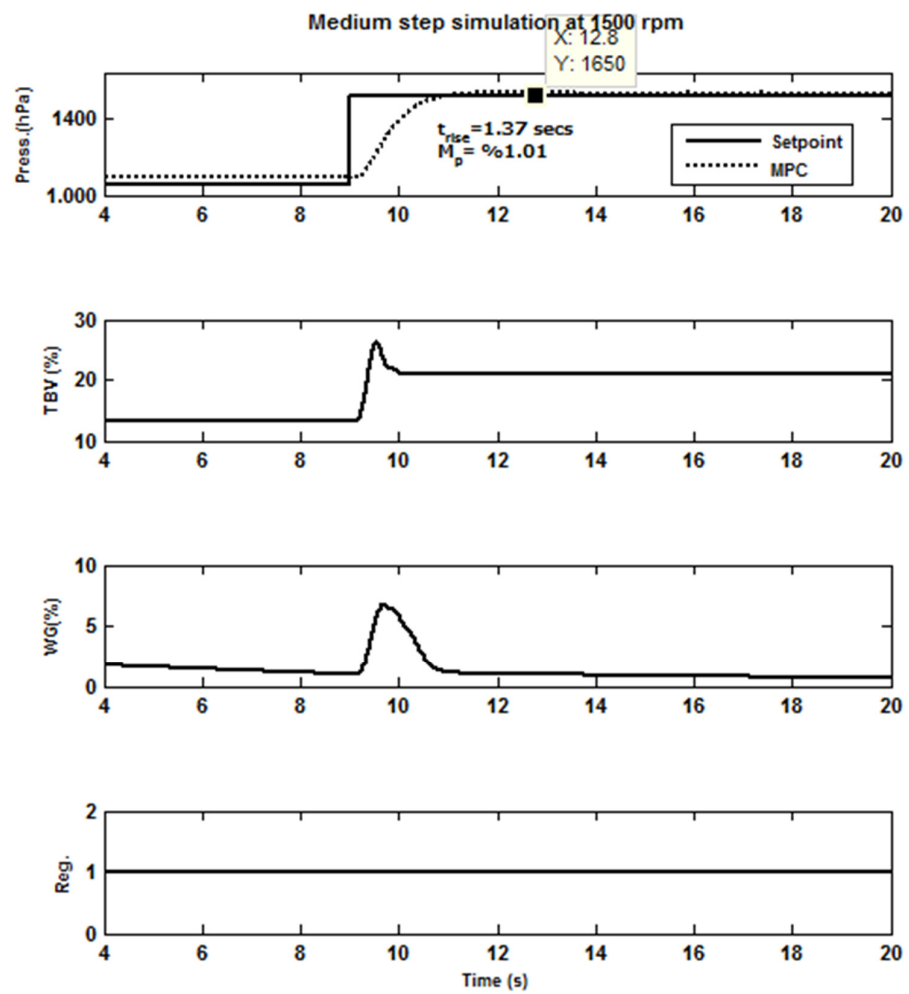


Figure B.3 : MIMO small step response at 1500 rpm.

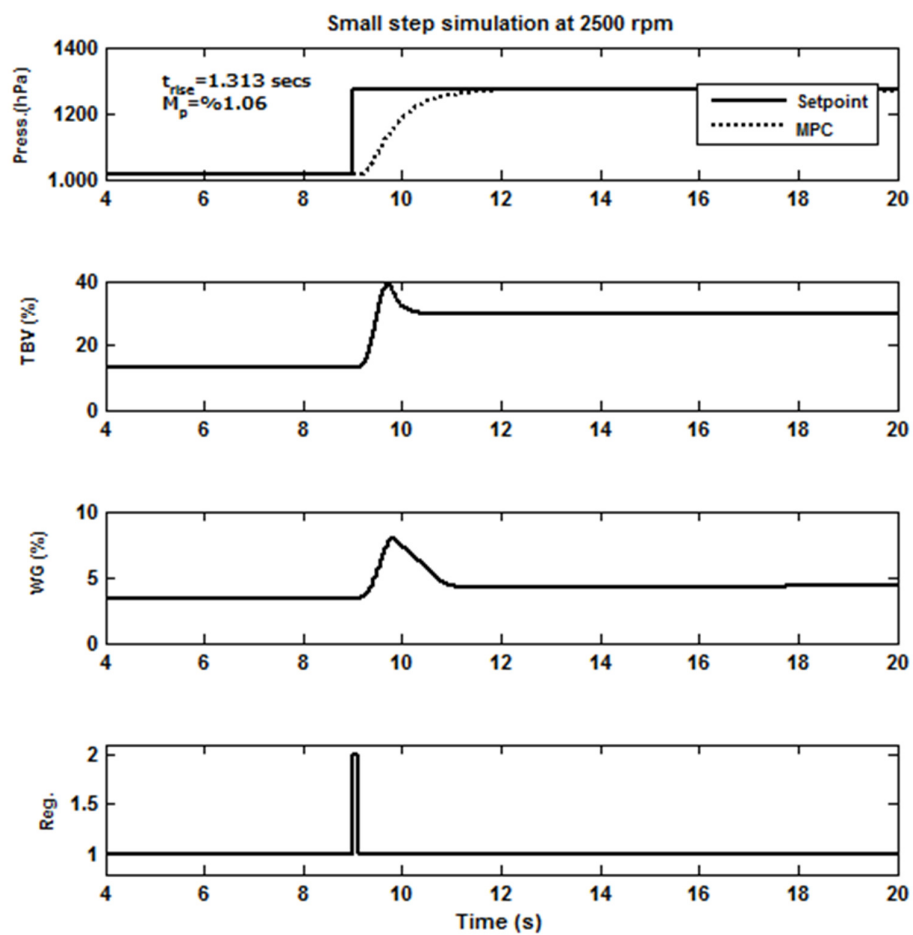


Figure B.4 : MIMO small step response at 2500 rpm.

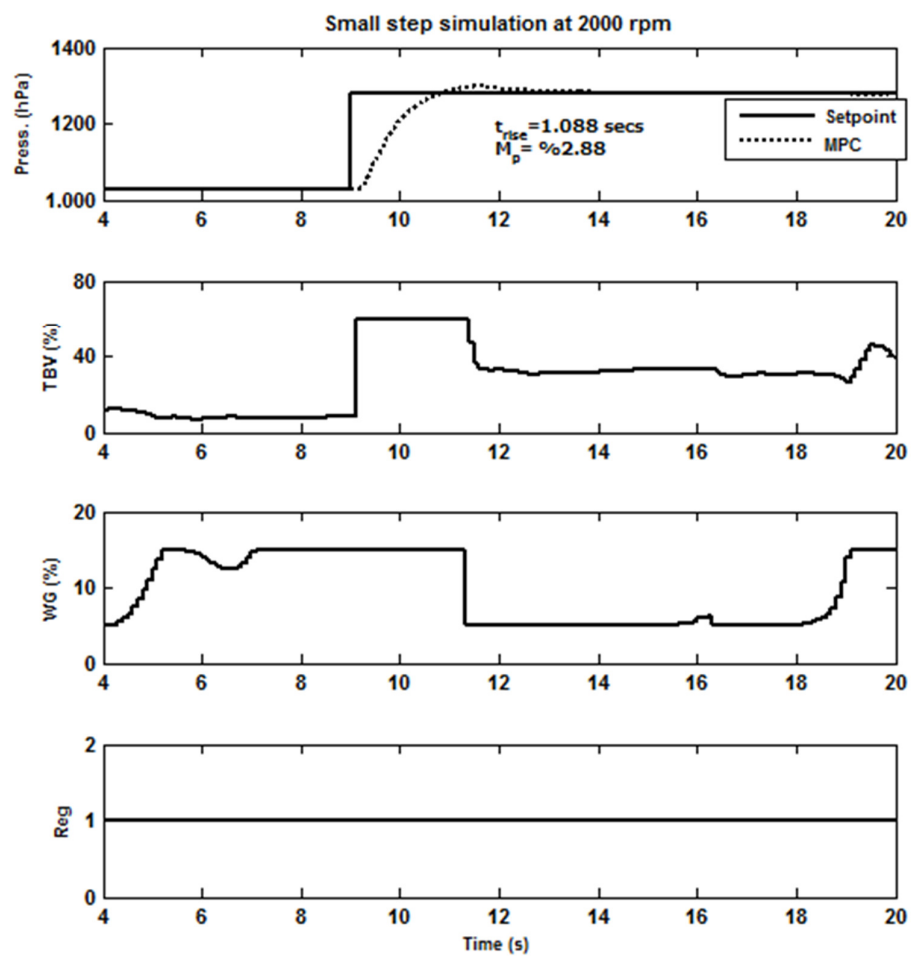


Figure B.5 : MIMO small step response at 2000 rpm.

CURRICULUM VITAE



Name Surname: Mustafa Engin Emekli

Place and Date of Birth: Bursa, 01/02/1984

E-Mail: enginemekli@gmail.com

B.Sc.: İTÜ-Mechanical Engineering

M.Sc.: İTÜ-Mechatronics

Professional Experience and Rewards:

2007-2011 Powertrain Calibration Engineer- Ford Otomotiv Sanayi A.Ş

2011-... Product Development Supervisor-Ford Otomotiv Sanayi A.Ş

List of Publications and Patents:

PUBLICATIONS/PRESENTATIONS ON THE THESIS

- **Emekli M. E.**, and Güvenç, B. A., 2014: Design and Implementation of Linear Model Predictive SISO Boost Pressure Controller for a Series Sequential Diesel Engine. *Gazi University Journal of Polytechnic*, Accepted for Publication on October 8th
- **Emekli M. E.**, Özgül, E., and Güvenç, B. A., 2014: Explicit Model Predictive Controller Design for Boost Pressure Control of Two Stage Turbocharged Diesel Engine. *7th OTEKON Automotive Technologies Congress*, May 26-27, Bursa, Turkey
- **Emekli M. E.**, and Özgül, E., 2014: Motor Kontrolü Uygulamaları için Çift Kademeli Aşırı Doldurma Sistemine Sahip bir Dizel Motorun Modellenmesi. *Mühendis-Makina, MMO*, Accepted for publication on November 19th.